Performance Evaluation of a Combined Floating Offshore Energy System (CFOES) in Operational and Extreme Conditions

Joshua Cutler

A thesis submitted in partial fulfilment of the requirements of Liverpool John Moores University for the degree of Doctor of Philosophy

August 2023

Declaration

I hereby declare that that no portion of the work referred to in the thesis has been submitted in support of an application for another degree or qualification of this or any other university or other institute of learning.

Abstract

The holistic aim of this thesis is to broaden knowledge on the coupled behaviour of a combined floating offshore energy system (CFOES) that supports three different offshore renewable energy (ORE) systems. In this work, a CFOES concept is innovated and tested using numerical simulation under typical design load cases. The three systems include a catamaran-type floating wind turbine, a wave energy converter system, and a tidal turbine system. Currently, no numerical tools exist explicitly for the design and analysis of such a system. Thus, numerical tools used purposed for pure ORE systems are integrated together in order to create a sophisticated numerical model of the CFOES. The numerical model is built within FAST2AQWA (F2A). F2A is an aero-hydro-servo-elastic tool used for the design and analysis of floating wind turbines. The tool is based on the integration of a commercial wind turbine simulator, FAST, into a commercial hydrodynamic analysis software tool, ANSYS AQWA. AQWA is effective at studying multibody hydrodynamics and has modelling features such as fenders and joints which allow the simulation of linear WEC PTO systems. AQWA also provides a built-in DLL capability which is used for external force calculations. This function permits the calculation of the aerodynamic forces of the wind turbine and hydrodynamic forces of the tidal turbines. Together, the combination of these capabilities enables the construction of an integrated numerical model of a triple CFOES. The numerical model is used to perform integrated loads analysis for operational and extreme conditions. It was found in rated and above rated conditions, the performance of the wind turbine in the CFOES improves compared to a floating wind turbine. The power output is greater and smoother and there is less variability in aerodynamic thrust, rotor torque and blade pitch. The WEC system significantly reduces platform rolling and pitching in more energetic sea states. For certain conditions, the WEC system reduces the roll motion of the platform by 66%. Consequently, the side-side tower-base bending moment of the wind turbine is reduced. A reduction of 35% and 40% in the maximum

and minimum was observed. When the tidal turbines are in operation a hydrodynamic thrust is produced. As a result of this, the global surge response is increased and so is mooring line tension. However, the variability about the mean surge is reduced because of added hydrodynamic damping. Finally, the mean additional power that could be generated by the tidal and wave energy systems was up to 30%. The numerical results demonstrated several important advantages in ORE hybridization including increased energy yield, reduced structural loading, and improved floating platform stability. This work provides a solid basis for future study involving advanced design and analysis of CFOESs that are comprised of three or more ORE systems.

Acknowledgements

I would like to state my sincerest gratitude to my supervisory team which was formed of Dr Musa Bashir, Professor Jin Wang, and Dr Sean Loughney. I am deeply indebted to them for their invaluable support and guidance during this project. It has been a great honour to have collaborated towards this monumental achievement.

I would also like to thank my family, who include my mother, father, grandparents, and surprisingly even my brothers (Sam, James, and Zach), for their continuous motivation throughout this project for me to complete my education.

Finally, I would like to thank my friends for distracting me too many times to count during the busy periods. However, it was with the best intentions and without them I could not have completed this thesis.

Contents

List of Figures

List of Tables

Abbreviations

BCFOES	Braceless Combined Floating Offshore Energy System
BEM	Boundary Element Method
BEMT	Blade Element Momentum Theory
CFD	Computational Fluid Dynamics
CFOES	Combined Floating Offshore Energy System
CTT	Catamaran floating wind turbine integrated with tidal energy system concept
CWS	Catamaran floating wind turbine integrated with wave energy conversion system concept
DOF	Degree Of Freedom
EL	Euler-Langrange
F2A	FAST2AQWA
FEM	Finite Element Model
FOWT	Floating Offshore Wind Turbine
F-A	Fore-Aft
GDWT	Generalized Dynamic Wake Theory
HWNC	Hywind-Wavebob-NACA 638xx Combination
IEC	International Electrotechnical Commission
JONSWAP	Joint North Sea Wave Project
LC	Load Case
LCOE	Levelized Cost of Energy
NE	Newton-Euler
O-o-P	Out-of-Plane

ORE	Offshore Renewable Energy
ORPC	Ocean Renewable Power Company
OWC	Oscillating Water Column
OWSC	Oscillating Wave Surge Converter
PM	Pierson-Moskowitz
PSD	Power Spectral Density
PTO	Power Take-Off
RAO	Response Amplitude Operator
RNA	Rotor-Nacelle Assembly
S-S	Side-Side
SFC	Semisubmersible Flap Combination
STC	Spar-Torus Concept
TEC	Tidal Energy Converter
TLP	Tension-Leg Platform
TRL	Technology Readiness Level
WEC	Wave Energy Converter

Nomenclature

A	Area
A	Axial stiffness
B_{ext}	Linear damping coefficient
B_{PTO}	PTO damping coefficient
$B_{Pot}(\omega)$	Potential damping for distinct wave frequency
B_2	Quadratic damping coefficient
C_a	Added mass coefficient
C_D	Drag coefficient
C_L	Lift coefficient
C_m	Inertia coefficient
C_p	Power coefficient
C_T	Thrust coefficient
D	Diameter
E	Young's modules
F	Force
F_B	Buoyancy force
H	Wave height
I	Turbulence intensity
I_{xx}	Second moment of area
K_{PTO}	Linear spring stiffness coefficient
L	Length
L_K	Integral scale parameter
M	Moment

M_R	Restoring moment
P	Power
Q	Torque
$S(\omega)$	Spectral ordinate at wave frequency
T	Tension
T	Thrust
T	Wave period
T_Z	Mean zero crossing period
T_0	Peak period
T_1	Mean wave period
V	Velocity
W	Relative wind speed
a	Acceleration
c	Chord length
c	Hydrostatic stiffness
c	Wave celerity
d	Water depth
d_r	Demi-hull separation
f	Cyclic frequency
g	Gravity
$h(t)$	Radiation impulse function
k	Wavenumber
m	Mass
p_s	Hydrostatic pressure

r	Radius
t	Time
$\bar{u}$	Mean flow speed
v	Wave steepness
x	Displacement
z_{CB}	Vertical position of centre of buoyancy
z_{CG}	Vertical position of centre of gravity
Λ_U	Turbulence scale parameter
θ	Angle
$\dot{\theta}$	Angular velocity
γ	Peak enhancement factor
ε	Axial strain
λ	Wavelength
ρ	Density
σ	Standard deviation
ϕ	Velocity potential
ϕ_D	Diffraction wave potential
ϕ_I	Incident wave potential
ϕ_R	Radiation potential
ω	Wave frequency
∇	Displacement

Chapter 1.   Introduction

1.1   Background

The dependence on energy in human society to function is enormous. The finite reserves of fossil fuels are continuously depleting. The consequences of climate change are growing in severity. These are some of the most difficult challenges energy companies worldwide face today. The current agenda to mitigate the impact of climate change is to maintain the global temperature within $+2°$ since the pre-industrial era. To achieve this, the emission of greenhouse gases must be reduced. Approximately one quarter of global greenhouse gas emissions are produced from the power sector with coal being the greatest emitter (UK Government 2021). This large contribution from the power sector depicts the urgency to replace fossil fuels with renewable energy resources. In the pursuit of low-carbon electricity generation, the offshore environment is being recognised as a viable solution, and as a result, is witnessing increased exploitation.

The offshore environment represents an untapped and enormous energy source. It is abundant in both variety and quantity of renewable energy. Different forms of Offshore Renewable Energy (ORE) include offshore wind, waves, marine currents, tides, ocean thermal energy and salinity gradients (Pérez-Collazo et al. 2015). Out of all forms of ORE, only the offshore wind industry is an established energy industry. Since 2015, the deployment of offshore wind turbines has increased significantly across the globe. This is because of maturing technology, rapidly developing supply chains, increased market competition, and experience gained from utility-scale installations. By the end of 2020, the cumulative global offshore wind installed capacity increased by 5.52GW to reach 32.91GW from 200 operating projects (Walter et al. 2021). Much of this added global capacity has come from European and Asian markets. Conversely, all the other forms of ORE, or ocean energy, is far from commercialisation. Tidal

and wave are showing the greatest potential considering technological readiness and project development. Even then, these markets significantly lag behind offshore wind with the most advanced concepts only in the demonstration phase. High capital investment and low rated power capacities of current installations are the main factors for slow maturity (Lerch et al. 2019).

The latest technological innovation in the offshore wind industry is Floating Offshore Wind Turbine (FOWT) technology. Approximately 80% of the world's offshore wind resource potential is in waters deeper than 60m (Equinor 2020a). From an economic perspective, bottom-fixed foundations e.g., monopile, do not represent worthwhile solutions for wind turbine applications in water depths greater than 60 m (Goupee et al. 2014). As such, alternative support structures for wind turbines which have better economics are required for application in deep waters. This is a primary reason for the major focus in research on FOWT technology in recent years (Yang et al. 2021). Offshore wind farms in deeper water also have additional advantages including exposure to better quality wind resources, wind farm space availability and reduced noise and visual constraints (Bae 2013). In a short space of time, the floating wind industry has evolved quickly with 15 units currently online representing 9 projects globally including demonstrators (Quest Floating Wind Energy 2021). However, despite this rapid development of floating wind, the industry is still nascent; only 0.08GW (0.25 %) of the 32.91GW cumulative global offshore wind installed capacity can be attributed to floating installations (Walter et al. 2021).

A major design challenge prohibiting the commercialisation of FOWTs is cost-effective concepts which are capable of penetrating a competitive energy market. Some issues which need to be addressed are increasing understanding on coupled dynamic characteristics, economic viability, and acceptable motion and stability assessment criteria (Le et al. 2020). In relation to these issues, concepts need to demonstrate manufacturability and installation on a

utility-scale and water depth applicability. FOWTs can be classified into one of four types depending on how they achieve static stability. Spars are long cylindrical structures with excellent hydrodynamic stability owing to its deep draught and low centre of gravity (Meng et al. 2020). On the other hand, the draught of the spar is a constraint whereby the assembly of the structure must be completed inshore and there is a minimum water depth for application (Zheng et al. 2020). A Tension-Leg Platform (TLP) uses a system of taut vertical tendons to keep the platform in upright and in position. The platform has excessive positive buoyancy which keeps the mooring system constantly in tension. Currently, the costs and risks of TLP application remain unknown unless full-scale sea testing is conducted (Murfet and Abdussamie 2019). Semisubmersibles and barge platforms are stabilized by buoyancy by taking advantage of their large waterplane areas. Semisubmersibles are usually composed of several columns connected to each other through braces. The hydrodynamic behaviour of the platform subject to wind load excitations is considered particularly good. However, in contrast to other FOWTs, the construction of them is more difficult even though it can be fabricated on the dockside. Furthermore, the design of semisubmersibles is far more challenging due to complexity in their dynamic responses, caused by the combined effects of wind-wave coupled loads (Liu et al. 2016). Barge platforms possess good advantages in their fabrication, assembly, deployment and anchoring when compared to other platform types. However, the uptake of barge platforms for intermediate and deep water application is limited by problems that include its sensitivity to pitch stability in waves and complex requirements for its operational control (Olondriz et al. 2018).

It is evident then that there is no FOWT class that has advantages in all aspects over the other classes. As such, innovative design solutions are still required for floating wind and ocean energy technologies to achieve cost reductions in order to be competitive energy technologies in the future. Thus, this is where an opportunity presents itself:

"*Can hybridization of floating offshore wind with marine energy be achieved so that collectively offshore renewable energy applications can accelerate towards commercialisation through innovating integrated infrastructure?*".

The concept of an offshore floating platform that facilitates more than one ORE asset is referred to in this thesis as a Combined Floating Offshore Energy System (CFOES). A CFOES offers a multitude of benefits. Considering power generation, the energy yield can be substantially enhanced, and the power output is smoother with reduced intermittency. Considering physical integration, major cost reductions can be achieved by eliminating the need for multiples of the same component for example floaters, mooring systems and electrical infrastructure such as power cables. A floating platform which can host multiple energy systems creates other synergies that exist in installation, transportation, operation and maintenance, decommissioning, legislation, and surveying. This is because the cost of these processes can be spread over multiple assets (Skene et al. 2021). Specifically, for wind-wave systems, with proper design, integration could improve platform dynamics by reducing wave loads or introducing positive damping or extra restoring moments to the system (Si et al. 2021). For wind-tidal systems, a tidal turbine system can introduce additional hydrodynamic damping and reduce variability in mooring line tension (Yang et al. 2020b). Considering the environmental impact of offshore energy parks, integrated applications optimize the usage of marine space enabling full sustainable exploitation of the offshore environment.

However, the integration of ORE technologies in a single floating platform is not fully understood. There is extremely limited research on floating power plants which facilitate more than two different types of ORE system. Incorporating multiple dynamic systems into a single floating platform increases the structural complexity significantly. Each dynamic system influences the dynamics of the global structure, and it is vital that they function in harmony rather than disruptively. As such, there is a need for further research in this area in order to gain

knowledge on the complex coupling effects between floating wind and marine energy hybridization. Moreover, research is often conducted using sophisticated numerical tools which allow engineers to perform detailed design and analysis. Another problem arises in that there are no numerical tools explicitly for the design and analysis of CFOESs. If no tools currently exist, then the process is not trivial. Therefore, additional research is necessary in order to build a numerical model of a CFOES which can accurately predict the coupled dynamics of the integrated structure. Finally, Technology Readiness Levels (TRL) are a type of measurement system used to assess the maturity level of a particular technology. Therefore, any research in the field of CFOESs is classed as fundamental research which is categorised by TRL 1-3.

1.2 Aim, objectives, and project novelty

Based on the above introduction, the aim of this research is to innovate a CFOES concept which can exploit three different forms of ORE using technology based on latest trends and to develop a numerical model of this concept so that the performance can be evaluated under typical design load cases.

Within the framework of this aim, the work has been split into seven objectives which are summarised as follows:

1. To review the current state of knowledge on the topics of ORE and CFOESs, focussing specifically on the floating wind, wave, and tidal energy industries.

2. To innovate a CFOES concept based on latest technology trends which can exploit wind, wave, and tidal energy resources through systematic engineering design approach.

3. To review current numerical modelling methods of ORE systems and to devise a methodology that can be implemented in order to study the CFOES concept.

4. To build a sophisticated numerical model of the CFOES concept within a comprehensive simulation tool.

5. To validate the numerical model against either published experimental and/or numerical data where possible.

6. To use the numerical model to perform integrated loads analysis on the CFOES concept in the context of normal operation and extreme conditions.

7. To critically analyse the outputs of the numerical model in order to evaluate the performance of the CFOES and to determine if the hybridization of ORE technologies is beneficial and the CFOES concept has merit.

The novelty of the conducted research is achieved from the completion of these seven objectives. The main novelty of this work is the development of a numerical model of a CFOES that can extract power from three different ORE types (objective 4). To achieve this main objective, supplementary numerical models are developed which start simpler and increase in the level of complexity. In other words, the first numerical model built is of a pure FOWT system (**Figure 1-1**). The design of the support platform for the FOWT is based on a catamaran vessel, which is unique and provides first insights into the viability of a twin-hull platform to function as a support platform for floating wind energy application. This unique design further adds to the novelty of this work. The second and third numerical models developed are of a Wave Energy Converter (WEC) system and tidal turbine system. The fourth and fifth numerical models are of the FOWT and WEC system and the FOWT and tidal turbine system. These numerical models can be used independently to better understand the coupling of the FOWT concept with two different marine renewable energy systems. Equally, the research will be the first study into a twin-hull support platform combined with marine renewable energy technologies. Finally, the sixth and most novel numerical model is of the FOWT/WEC system and tidal turbine system. The numerical model can be used to improve scientific understanding

into the coupled dynamic behaviour of CFOESs that combine three or more systems. This is a research area with extremely limited knowledge and any research would be a contribution to this field. Furthermore, to the author's knowledge, only one other numerical model of a CFOES that integrates three different energy system has been publicly presented (Li et al. 2018). However, in this numerical model, the elasticity of flexible elements including the blades and tower of the wind turbine were neglected. Furthermore, no blade pitch or rotor speed control was applied in the numerical model. This means that the power performance cannot be sufficiently assessed. The presented work aims to build upon these shortfalls by including structural flexibility of the wind turbine and include a servo-control scheme in the model to adequately evaluate the performance of the wind turbine. Finally, the literature survey which was carried out in the initial stages of this project can be used as a strong reference for future work in this scientific area.
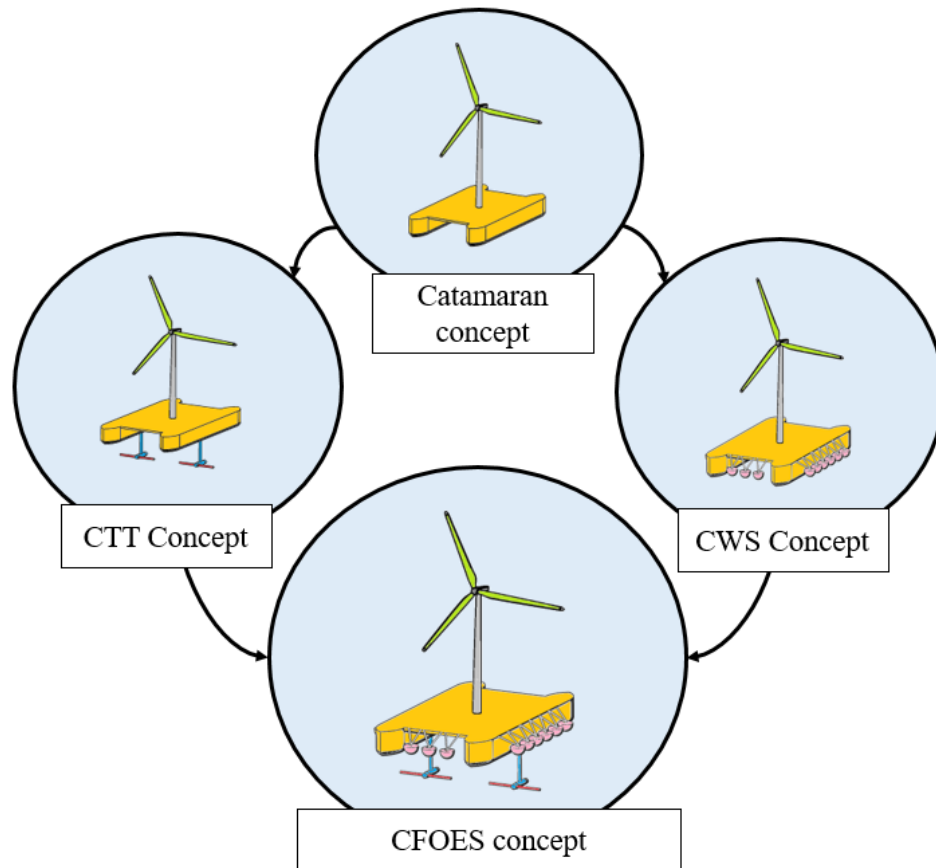
Figure 1-1. Numerical model development of a CFOES concept.

1.3 Thesis structure

This thesis is structured into 7 chapters which are described as follows:

Chapter 1 provides an overview to the project and states the engineering challenge addressed by this research. The overview provides background on the scientific topics of ORE and CFOESs. This chapter also delivers the aims and objectives of the project, the novelty, the structure of the thesis, and notable publications generated from the project.

Chapter 2 is a state-of-the-art literature survey on the current state of ORE and CFOESs. The survey focuses on the floating wind, wave and tidal energy industries, and there is strong emphasis of market and technology for each ORE industry and CFOESs.

Chapter 3 considers the main numerical modelling methods available to simulate and analyse ORE systems. Initially, mathematical models of environment conditions within engineering tools are discussed. The mathematical models within engineering tools used to capture the dynamic behaviour in the different physics domains are reviewed. Finally, a strategy on adapting common engineering tools for pure ORE systems for the purpose of designing and analysing a CFOES is provided.

Chapter 4 introduces an innovative FOWT concept which is the central system to the CFOES concept presented in Chapter 6. The chapter shows the development of the numerical model in a comprehensive engineering tool of the FOWT concept. Next, the numerical model is used to perform coupled analysis on the FOWT concept, and the results and discussion are presented in the chapter.

Chapter 5 is dedicated to the development and integration of numerical models of the WEC system and tidal turbine system into the numerical model of the FOWT separately. The chapter begins with the development of the numerical models of the pure marine renewable energy systems. The coupling of these numerical models with the FOWT numerical model is presented. Both models are used to perform further coupled analysis on the FOWT concept integrated now with a marine renewable energy system. The results from the numerical models are compared to the pure FOWT concept presented in Chapter 4 to gain insight into the consequences of integration.

Chapter 6 couples together the three numerical models of three different types of ORE systems to create one numerical model of the CFOES. The numerical model is then used to perform the final coupled analysis for common design load cases which reflect operational and extreme conditions. Another CFOES concept is also presented in the second part of this chapter

which aims to reinforce the methodology derived from this work of coupling numerical models of ORE systems.

Chapter 7 summarises the work completed in the project, presents conclusions and suggestions for future work.

1.4   Publications generated

Notable publications generated as a result of this research include:

1. Cutler, J., Bashir, M., Yang, Yang., Wang, J., Loughney, S., 2021. Assessment of dynamic responses of 5 MW floating offshore wind turbine platforms in intermediate water depth. In: *CORE 2021 Conference Proceedings (5th International Conference on Offshore Renewable Energy*, 26th-27th August 2021, Virtual Event).

2. Cutler, J., Bashir, M., Yang, Yang., Wang, J., Loughney, S., 2022. Preliminary development of a novel catamaran floating offshore wind turbine platform and assessment of dynamic behaviours for intermediate water depth application. *Ocean Engineering*, 258. ISSN 0029-8018

Chapter 2. Combined floating offshore energy systems

This chapter presents a literature survey on the scientific topics of ORE and CFOESs. To completely understand the concept of a CFOES, knowledge is required on the pure ORE technologies which comprise these integrated systems. The ORE types reviewed in-depth include floating offshore wind, wave, and tidal energy. The presented literature aims to provide a solid background on these ORE forms in terms of market and technology.

Therefore, the chapter is organised into the following sections: Section 2.1 is an introduction to ORE. Sections 2.2, 2.3, and 2.4 present a review of floating offshore wind, wave, and tidal energy, respectively. Section 2.5 introduces the main topic of this work, CFOESs. In this section both commercial and academic CFOES concepts and synergies of hybridization are critically discussed. Section 2.6 presents chapter conclusions highlighting a summary of key findings from the survey of literature on the chosen topics.

2.1   Offshore renewable energy

Water makes up approximately 71% of the Earth's surface as oceans and seas (U.S. Geological Survey (USGS) Water Science School 2019). The offshore environment is a vast natural deposit of renewable energy. ORE encompasses all renewable energy resources found in the offshore environment. The different energy forms can be grouped into two: offshore wind energy (bottom-fixed and floating) and ocean energy (Pérez-Collazo et al. 2015). Ocean energy includes all renewable energy forms present in oceans and seas. These energy forms make use of the kinetic, potential, chemical, or thermal properties of seawater. The energy forms include ocean waves, ocean currents, tidal currents, tidal range, thermal gradients, and changes in salinity. Each resource can be exploited using different technologies which convert the energy into a useful form, electricity (Mofor et al. 2014).

One of the most active solutions to reducing carbon emissions and the rate of climate change is to increase the development of renewable energy systems. ORE is now considered a viable and attractive branch of renewable energy which can significantly contribute to the growing demand of green energy development (European Commission 2023). The rapid growth of ORE is mainly attributable to bottom-fixed offshore wind energy. However, the last decade has witnessed the conceptualization and commercial application of a number of floating platforms for wind energy conversion (Equinor 2020b) (Principle Power 2020) (Ideol 2020a) (Murfet and Abdussamie 2019). The success of demonstrators and pre-commercial scale projects has placed floating platform technology for wind turbine application at the forefront of academic research and industry innovation (Jonkman 2010) (Robertson and Jonkman 2011) (Robertson et al. 2014a).

In contrast to offshore wind, ocean energy industries collectively have struggled to gain traction and reach commercialisation. The fundamental problem is the high initial costs associated with concept development and demonstrator installation. The power ratings of ocean energy technologies create an unattractive payback period, which can be as long as decades. This deters investors and hinders the necessary optimised development of ocean energy technology. For ocean energy to reach commercial status and become competitive, significant scalability needs to be demonstrated (Mofor et al. 2014) (Uihlein and Magagna 2016). On the other hand, due to the success of floating wind, questions have arisen concerning the possibility of ORE hybridization. In sites where offshore wind and ocean energy resources coexist, an offshore floating platform that can support multiple renewable energy systems is a bright solution to reducing the LCOE for all integrated ORE assets. Amongst other factors, the reduction in the LCOE can be achieved through increasing power production and the sharing of expensive infrastructure. This includes the support platform, mooring system, and electrical

infrastructure. ORE hybridization is the next natural step to developing an optimized and sustainable offshore environment.

Therefore, this chapter presents a state-of-the-art literature review on ORE hybridization. The first part of this chapter will separately review floating wind energy, wave energy, and tidal energy in terms of the resource, market, and technology. The second part of this chapter will review CFOESs, synergies of hybridization, and review previously proposed pre-commercial concepts and concepts from key academic groups within the field. The discussion will also highlight why the present research is novel and how it is relevant in improving scientific understanding on the chosen topics.

2.2   Floating offshore wind energy

The offshore wind industry is rapidly growing which has been stimulated by the urgent need to produce electricity from renewable energy sources. The offshore environment offers attractive advantages over the onshore environment for wind power generation. These advantages include resource availability and stability, optimum wind speeds, relatively low wind shear and turbulence intensity, and increased probability of higher energy density (Liu et al. 2021). As defined in the International Electrical Commission (IEC) 61400-3 standard, a wind turbine is classed as an offshore wind turbine, if the support structure is subject to hydrodynamic loading (International Electrotechnical Commission (IEC) 2009).

2.2.1   Offshore wind market

In 2017, Europe recorded an upswing in investment in offshore wind that approximately reached 7.5billion Euros. As a result of this investment, 560 offshore wind turbines were successfully connected to the grid. This increased Europe's wind generated electricity by 3.15GW (Shi et al. 2019). Two years later, a further 502 offshore wind turbine installations were completed. This provided an additional capacity of 3.63GW to bring the overall capacity

in Europe to 22.1GW (Wind Europe 2020). Although fewer offshore wind turbines were installed in 2019 compared to 2017, a 15% increase in installed capacity was reported. This increase was achieved because of improvements in blade, drivetrain, and control technologies. It enabled the deployment of larger wind turbines with higher power ratings (IRENA 2019). By the end of 2020, the cumulative global offshore wind installed capacity increased by 5.52GW to reach 32.91GW from 200 operating projects (Walter et al. 2021).

The offshore wind industry has two markets which are separated by the foundation used to support the wind turbine. The foundation simply can be fixed to the seabed or floating. Most existing offshore wind farms employ bottom-fixed foundation technology to support wind turbines in shallow waters (< 50m). However, viable nearshore sites are becoming exhausted. Inevitably, the development of wind farms will have to move further from shore into deeper waters (Loughney et al. 2021). On the other hand, approximately 80% of the world's offshore wind resource potential is located in waters deeper than 60m (Equinor 2020a). The engineering problem is that bottom-fixed foundations are not viable economic solutions for wind turbine applications in water depths greater than 60m (Goupee et al. 2014). Consequently, floating platforms have become the favoured option for supporting wind turbines in deeper waters (Yang et al. 2021).

The floating wind industry is nascent with only three operational wind farms worldwide. These are Hywind Scotland (29km off Peterhead, Scotland), Windfloat Atlantic (off the coast of Viana do Castelo, Portugal) and Windfloat Kincardine (15km off the coast of Aberdeen, Scotland). The contribution of the installed capacity of floating wind with respect to the cumulative global offshore wind installed capacity is only 0.08GW (0.25%) of the 32.906GW (Walter et al. 2021). Nonetheless, FOWTs are the next generation of offshore wind turbines. The technology was inspired by offshore platforms purposed for use in the oil and gas industry to harvest the fuel reserves in deep-water fields. The offshore wind industry is now following

suit and utilizing floating platform technology to exploit the abundant wind resource available out at sea. FOWTs can be placed kilometres away from shore in depths well over 1,000m where they can benefit from much higher quality wind resources (Wind Europe 2017). FOWTs will create new markets and unlock acres of marine space where depth and poor bathymetry previously constrained bottom-fixed offshore wind farms.

2.2.2 *Wind turbine technology*

A wind turbine is a complex system of many structural components (**Figure 2-1**). The main components include the blades and hub (which together form the rotor), nacelle, and tower. In the case of offshore wind turbines, a substructure can be considered a main component. The nacelle is located at the top of the tower and connects all the parts used to generate electricity which include the rotor, drivetrain, and generator. The drivetrain is a system of mechanical components such as gears, bearings, and shafts that connects the primary converter (rotor) to the secondary converter (generator). The first component in a drivetrain is typically the low-speed shaft, or main shaft. One end of the shaft is connected to the rotor whilst the other end is connected to the slow-rotating side of the gearbox. When the wind blows over the blades, they are lifted causing the rotor to spin. The function of the gearbox is to increase the rotational speed in order to drive a generator that is situated at the other end of the drivetrain. A generator converts the mechanical energy of the wind turbine rotor into electricity. A large brake disc is also attached to the drivetrain which keeps the turbine in stand-still when required or when the turbine needs to be shut down in an emergency. There are also a series of sensors that measure the incoming wind speed and direction so that the turbine can be positioned accordingly to optimise power generation (Madvar et al. 2019).
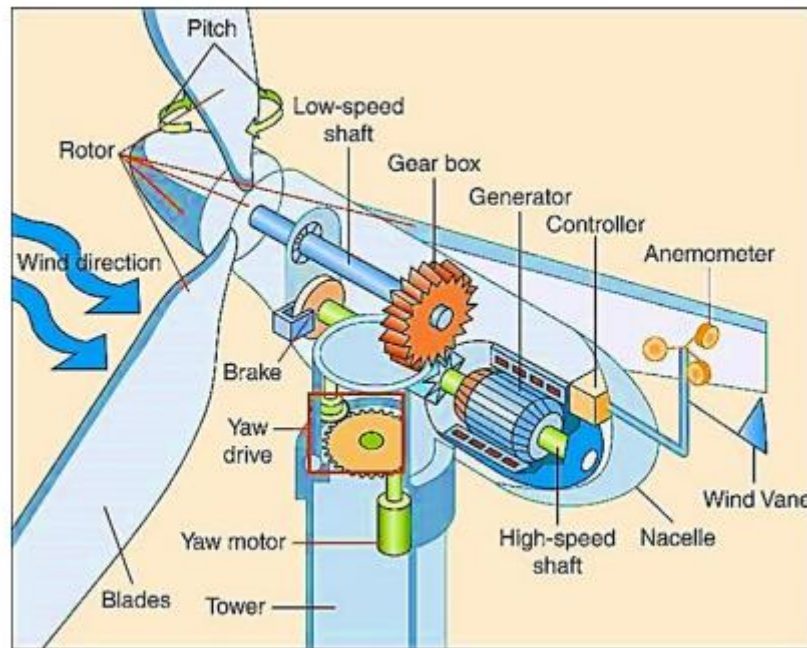
Figure 2-1. The internal system of a wind turbine (Madvar et al., 2019).

The generated power from a wind turbine can be calculated using the following equation:

$$P = \frac{1}{2}\rho_{air}C_pA_sV_{rel}^3 \qquad [1]$$

where ρ_{air} is the density of air; C_p is the power coefficient; A_s is the swept area of the rotor; and V_{rel} is the relative wind velocity.

Modern wind turbines are variable-speed and pitch-controlled. Blade pitch control continuously adjusts the blade pitch angle to optimize the angle of attack to the wind speed. By doing so, maximum lift force is generated, and maximum power is produced. The hub component is what permits the pitching of the blades. The blades are mounted on to special bearings within the hub. The blades can produce maximum lift force for a range of wind speeds without stalling. Fast pitching of the blades to zero degrees (feathering) provides an effective means to stop the turbine in emergencies (Karimirad 2014).

2.2.3   Support platforms

A wind turbine is exposed to a new range of motions when mounted on to a floating platform (Hall et al. 2014). This creates a modern design problem involving complex coupled aero-hydro-elastic dynamics. Specifically, two modes of motion introduced by the floating platform can increase critical structural loads of a wind turbine. The two motions correspond to fore-aft translation (surge) and fore-aft rotation (pitch) of the platform. These motions can induce large bending moments in the tower and blades. Motions mainly occur due to wave excitation or by the aerodynamic forces acting on the wind turbine. To reduce motions resulting from hydrodynamic loading is to design a structure that is "hydrodynamically transparent". In other words, a floating structure with a small waterplane area and moment of inertia to minimize loading from waves. Conversely, the simplest way to resist an overturning moment as a result of aerodynamic thrust is by using a large waterplane area and moment of inertia. The waterplane area and moment of inertia properties directly affect the floating platform's ability to resist hydro- and aerodynamic loading. The difficulty in floating wind turbine design becomes apparent when considering these properties. If the waterplane area and moment of inertia is large, then the platform has better aerodynamic resistance, but the hydrodynamic loading is greater. If the waterplane area and moment of inertia is small, then the platform is more transparent hydrodynamically but is more susceptible to aerodynamic loading (Hall et al. 2014).

FOWTs are classified based on their rotational (pitch and roll) hydrostatic stability characteristics (Jonkman and Matha 2011) (Thiagarajan and Dagher 2014). These platform characteristics govern how the floating platform counteracts the overturning moment mainly due to the hydrodynamic forces acting on the platform and aerodynamic forces acting on the

wind turbine. The total restoring moment counteracting the overturning moment in roll ($M_{R,44}$) and pitch ($M_{R,55}$) can be calculated as the sum of three contributions:

$$M_{R,44} = \left(\underbrace{\rho g I_{xx}}_{\alpha} + \underbrace{F_B \cdot z_{CB} - mg \cdot z_{CG}}_{\beta} + \underbrace{C_{44,moor}}_{\gamma} \right) \sin \phi \qquad [2]$$

$$M_{R,55} = \left(\underbrace{\rho g I_{yy}}_{\alpha} + \underbrace{F_B \cdot z_{CB} - mg \cdot z_{CG}}_{\beta} + \underbrace{C_{55,moor}}_{\gamma} \right) \sin \theta \qquad [3]$$

where α is the 'buoyancy' contribution from the waterplane area, proportional to ρ, the density of seawater; g, the gravitational acceleration constant; and I_{xx} or I_{yy} , the second moment of the waterplane area. β is commonly referred to as the 'ballast' contribution which results from the relative position of the centre of gravity (z_{CG}) and the centre of buoyancy (z_{CB}); F_B is the buoyancy force; and m, is the total mass of the support structure. γ is the contribution due to the mooring system. While this contribution can be considered negligible for catenary mooring systems, it can be the main roll/pitch restoring mechanism for Tension Leg Platform (TLP) systems. If the main contribution is α to the total restoring moment, the support structure is said to be 'buoyancy stabilized'. If β is the main contribution, the support structure is considered as 'ballast stabilized'. Finally, if γ is the main contribution, the structure is said to be 'mooring stabilized' (Collu and Borg 2016) (**Figure 2-2**).
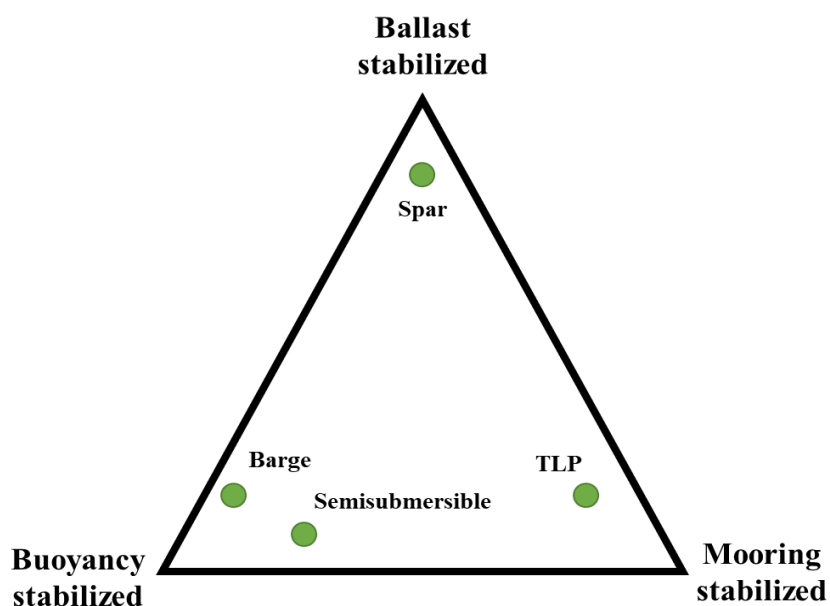
Figure 2-2. Stability triangle with annotation of common floating offshore wind types (Thiagarajan and Dagher, 2014).

Within the stability triangle, there are four main groups of FOWTs (**Figure 2-3**). Spars are simple cylindrical structures with excellent hydrodynamic stability owing to its deep draught and low centre of gravity (Meng et al. 2020). On the other hand, the draught of the spar is a constraint whereby the minimum water depth for application is restricted (Zheng et al. 2020). Hywind in Scotland, developed by Statoil (now Equinor) (Equinor 2020b) is the world's first fully operational floating offshore wind farm. The farm consists of five 6 MW wind turbines using spar platforms.

A TLP uses a system of taut vertical tendons to keep the platform in upright and in position. The platform has excessive positive buoyancy which keeps the mooring system constantly in tension. TLPs are typically smaller structures geometrically compared to the other types (Taboada 2016). This platform type has good potentials for application due to its limited motions derived from the use of restraint tendons (Murfet and Abdussamie 2019). Despite these

positives, the costs, and risks of application of a TLP remain unknown unless full-scale sea testing is conducted.

Semisubmersibles and barge platforms are stabilized by buoyancy by taking advantage of their large waterplane areas. Semisubmersibles are usually composed of several columns connected to each other through braces. The hydrodynamic behaviour of the platform subject to wind load excitations is considered particularly good. Application of semisubmersible platforms is regarded more achievable due to ease in their installation and tendency to have lower costs of installation (Shi et al. 2019). However, in contrast to other FOWTs, the construction of them is more difficult even though it can be fabricated on the dockside. Furthermore, the design of semisubmersibles is far more challenging due to complexity in their dynamic responses, caused by the combined effects of wind-wave coupled loads. In addition, the heave response of the platform is also another source of concern because of its influence on general platform stability (Liu et al. 2016). Currently, there are three 8.4 MW semisubmersible FOWTs developed by Principle Power (Principle Power 2020), as part of the WindFloat Atlantic project in full operation off the coast of Portugal. These platforms are currently the largest FOWTs in the world with power generated capacity that is capable of supplying up to 60,000 users each year.

Barge platforms possess good advantages in their fabrication, assembly, deployment and anchoring when compared to other platform types. However, the uptake of barge platforms for intermediate water application is limited by problems that include its sensitivity to pitch stability in waves and complex requirements for its operational control (Olondriz et al. 2018). Although the ITI Energy barge concept has been around for a while, the only high-capacity barge FOWTs in operation are the Ideol demonstrators of its Damping Pool concept, Floatgen (Ideol 2020a) and Hibiki (Ideol 2020b), off the coasts of France and Japan, respectively.
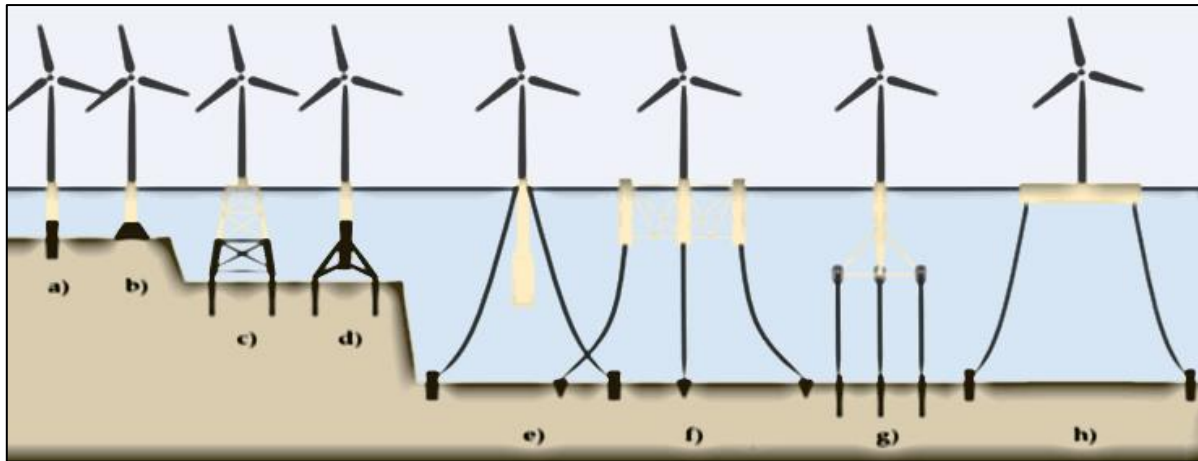
Figure 2-3. Foundation types of offshore wind turbines: a) monopile b) gravity-based c) jacket d) tripod e) spar f) semisubmersible g) tension-leg platform h) barge.

2.3 Wave energy

2.3.1 Resource

Converting wave energy into electricity has been an idea for centuries (Falnes 2007). Wave energy is a powerful ORE resource which is considered as a derivative of solar and wind energy. The natural rotation of the earth results in differential heating by the sun. Consequently, an uneven distribution of high- and low-pressure regions exist in the atmosphere. Air moves between these pressure fields in the form of wind. When wind blows over the oceans and seas, waves are generated through friction between the wind and water's surface and the progressive transfer of energy (Mattiazzo 2019). Some distinct advantages of this physical phenomena include high energy density (defined as the available resource power per meter), the ability of travelling large distances with minimal energy losses, and a high degree of predictability. Despite these positives, the wave energy industry has found it difficult to develop a technology that is cost efficient and reliable (Sandberg et al. 2016).

2.3.1.1 Quantification of wave energy resource

An important initial step towards investor confidence and market deployment of wave energy technology is the characterization and mapping of the resource. Such assessments include identification of geographical areas with high wave energy, the quantification of energy (e.g., total annual wave energy), and the description of the resource using design parameters such as significant wave height, wave energy period and mean wave direction. Governments, private organisations, and researchers have all conducted studies to estimate the wave energy resource at global and regional scales. The European Commission (2015a) quantified the global potential wave energy to be 29500TWh/year. Gunn and Stock-Williams (2012) estimated the world's theoretical wave power resource to be 2.11 ± 0.05TW to 95% confidence using the tool WAVEWATCH-III. Perez-Collazo et al. (2015) stated the best wave conditions for harvesting as an energy resource are found in medium-high latitudes and on deep waters (> 40m), with maximum power densities between 60-70kW/m. Rusa and Onea (2018) suggested the most attractive areas from an energy aspect are found between $30 - 60°$ latitudes in both hemispheres, a similar finding to the previous study. They estimated the total theoretical energy potential to be around 32,000TWh/year. This estimation is slightly higher than others but is in the same order of magnitude. Aderinto and Li (2018) provide a general overview for the theoretical potential of the wave energy resource in different regions of the world, see **Table 2-1.**

Table 2-1. Theoretical potential of wave energy resource in different regions of the world (Aderinto and Li 2018).

Regions	Wave Energy Potential (TWh/yr)
Africa	3,500
Europe	4,100
South America	4,600
North America and Greenland (inc. Central America)	5,500

Oceania	5,600
Asia	6,200
TOTAL	29,500

Carbon Trust (2011) and the Crown Estate (2012) estimated the total recoverable wave energy resource in the UK to be 50TWh/yr and 69TWh/yr, respectively. Weiss et al. (2018) conducted a wave and wind global resource assessment and identified that Brazil and New Zealand were the countries with the highest estimated extractable wave power in the world with an output exceeding 250TWh/month. Moreover, Weiss et al. (2018) additionally assessed the combined estimated extractable power of both resources for the two sites. They found that the combined power output exceeded 345TWh/month for each site. Arinaga et al. (2012) found monthly median significant wave heights mirror the spatial pattern and seasonal trends of winds and that significant wave heights are generated as a result of strong westerlies in mid latitudes. The importance of the frequency content of oceans waves in relation to available power was also highlighted. Essentially, longer wave periods increase wave power. Furthermore, it was reported that wave periods increase in magnitude generally from west to east in each basin. This is because of the mid-latitude swells generated in the northwest and southwest parts of the northern and southern hemispheres respectively, propagating east.

2.3.2 *Wave energy converter technology*

Devices used to convert wave energy into electricity are known as WECs. No commercial WEC concepts currently exist, however, some companies are testing their concepts at sea which deliver small amounts of power to the grid. Engineers and researchers over time have continuously innovated and developed WEC concepts. This has amounted to a large number of them. The lack of design convergence is primary factor to why the industry has staggered. Significant technological progress can only be made once a concept is mutually recognised (Gao et al. 2016).

A WEC is designed to harvest wave energy for a range of sea states defined by wave periods and wave heights. According to the law of conservation of energy, a device which extracts energy through the interaction with ocean waves, must reduce the amount of wave energy that is otherwise present in the ocean (Falnes 2007). In other words, wave energy absorption should principally be understood as wave interference. To absorb the energy from a wave, the device must be capable of generating a wave that interferes destructively with the incident wave (Todalshaug 2017).

WECs can be classified based on distinctive characteristics such as shape and size, working principles and installation location (Ding et al. 2015) (**Figure 2-4**). The most common classification is based on working principles. Drew et al. (2009) classified WECs into three main classes: attenuators, terminators, and point absorbers.
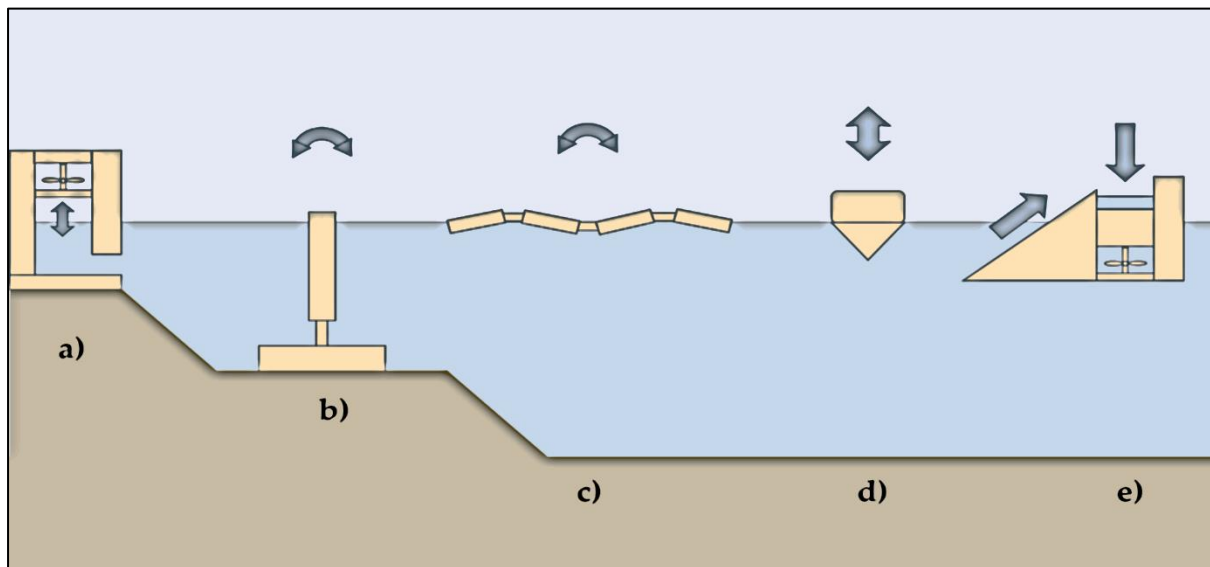
Figure 2-4. WEC types: a) oscillating water column b) oscillating wave surge converter c) attenuator d) point absorber e) overtopping device/terminator.

Attenuators are long structures with their principal axis positioned parallel to the incident wave. The structure typically comprises multiple floating segments connected together by hinges which 'flex' with the rise and fall of waves. This flexing motion drives a Power Take-

Off (PTO) system. PTO systems connect the primary converter and electrical generator; it is the system which converts the captured wave energy into useful electricity. A disadvantage of attenuators is that if positioned incorrectly, their efficiency can be adversely affected. Pelamis (Henderson 2006) was a famous example of an attenuator WEC.

Terminators have their principal axis positioned perpendicular to the incident wave, so these WEC types physically intercept ocean waves. Overtopping devices and oscillating wave surge converters (OWSCs) can be considered terminator WECs. Overtopping devices collect seawater in a reservoir situated above the mean water level and release the seawater back out through a chamber at the bottom of the reservoir. Within the chamber are hydro turbines which generate electricity as the seawater flows through. OWSCs are typically large, hinged deflectors which rotate about a fixed point exploiting the horizontal water wave particle velocity. It is this rotary motion which drives a generator to produce electricity.

Point absorbers are small in dimension relative to the other two WEC classes and the wavelengths of the incident waves. This enables a strong advantage of being able to exploit wave energy from all directions. Point absorbers generate electricity through the relative motion between a body that heaves up and down on the water's surface and a fixed point. Submerged pressure differentials can be considered point absorbers except that the difference between the two is that they are fully submerged devices. They exploit the pressure differential above the device as a result of passing wave crests and troughs.

Oscillating Water Columns (OWCs) are another type of WEC which can be classed as both a point absorber and terminator class. An OWC consists of a column with an opening below the water's surface. As waves interact with the device, water is forced up and down the column. This forces air in the column upwards and downwards as the waves rise and fall. Within the column is a turbine which generates electricity from the airflow. Bi-directional

turbines are typically installed in OWCs which can take advantage of the oscillating airflow in both directions.

2.3.3 *Power take-off system*

The PTO system is the mechanism that transforms energy absorbed from the primary converter into electricity. The primary converter is the working principle to capture energy e.g., a point absorber. The importance of a PTO system is significant as it strongly influences the efficiency of energy conversion of the WEC. Moreover, the PTO system contributes to the mass, size, and structural dynamics of the WEC. The PTO system can be anywhere between 20-30% of the total cost of the WEC which means it has a direct impact on the LCOE. This highlights the important relationship between the PTO system and WEC economics (Erselcan and Kükner 2014) (Têtu 2017). Designing a cost-effective PTO system is one of the main challenges in developing a WEC concept. The PTO system must be durable and reliable enough to survive extreme sea state conditions whilst operating smoothly on a day-to-day basis.

The type of PTO system selected for WEC is often governed by the primary converter. The types of PTO systems are as follows:

- Hydro turbine

- Air turbine

- Hydraulic system

- Direct mechanical drive system

- Direct electrical drive system

Hydro turbines for power generation have been around for decades and are a mature technology which are used in overtopping devices. Kaplin and Francis turbines are common types of hydro turbine and the main difference between them is the design of the runner which

is either axial or radial. Kaplan turbines have preference in wave energy devices because the design allows for sufficient head and flow for the turbine to be economical. Hydro turbines have the capability to operate at 90% efficiency or higher and require little maintenance (Escaler et al. 2006). Air turbines are used in OWCs; the challenge for this PTO system is the bi-directional airflow. Self-rectifying air turbines are one solution that converts energy from the alternating air flow into mechanical unidirectional rotational energy. There are numerous types of self-rectifying air turbines with the most common being the Wells air turbine (Falcão et al. 2014). Others include impulse turbines and Dennis-Auld turbines. Hydraulic PTO systems are typically used in WECs which have a working principle of oscillatory movement. Hydraulic converters are designed to absorb energy when dealing with large forces at low frequencies. The movement of the WEC creates the linear/rotary motion of the hydraulic motor which subsequently drives an electrical generator. Direct mechanical drive systems transfer the mechanical energy of an oscillating body to an electrical generator via an additional mechanical system such as a gearbox. If the direct mechanical drive system is rotary then flywheels can be added to in order to store rotational energy, thus smoothing power output. These types of systems are usually very efficient as transmission losses are minimal due to a simplistic design. However, reliability of these types of PTO systems are in question. Direct electrical drive PTO systems use the principles of electromagnetic induction to generate electricity. The mechanical energy captured by the primary converter is directly coupled to the moving part of a linear electrical generator. This is encompassed by magnets creating a magnetic field. The movement of the primary converter cuts the magnetic flux thereby inducing an alternating current (Têtu 2017).

2.3.4   Wave energy market

This section presents reviews WEC technologies being developed across the globe at the time of authoring this thesis. Irish WEC company Seapower has designed an attenuator called the Seapower Platform (Sea Power 2022) (**Figure 2-5**). The concept consists of hollow pontoons making up two separate bodies connected via a hinge. The concept has good cost efficiency due to its straightforward design and it makes for easier manufacturing and installation. The PTO system is a mechanical direct drive, and the concept has a 1MW rated power capacity.

Figure 2-5. Seapower Platform (Sea Power 2022).

Mocean Energy (Mocean Energy 2022) is another WEC company with an attenuator concept. The Blue Horizon concept (**Figure 2-6**) is a hinged raft that features 'digger bucket-like' fore and aft. This means that the system can dive through the largest waves easily. The concept has undergone extensive experimental and numerical testing and secured funding from Wave Energy Scotland to test a scaled prototype.

Figure 2-6. Mocean Energy Blue Horizon concept (Mocean Energy 2022).

Finnish company AW-Energy have pioneered an OWSC called WaveRoller (AW-Energy 2022) (**Figure 2-7**). The machine operates nearshore in shallow waters (8 – 20m) and its submerged and anchored to the seabed. The back-and-forth movement of water driven by wave surge puts WaveRoller into motion. A single WaveRoller unit is rated up to 1MW power capacity with a capacity factor of 25 – 50% depending on site conditions.

Figure 2-7. AW-Energy WaveRoller (AW-Energy 2022).

Australian firm Carnegie Clean Energy (Carnegie 2022) are developing a fully submerged pressure differential WEC (**Figure 2-8**). CETO technology has completed thousands of hours of sea testing. Some advantages of CETO include adaptability to ocean depth, swell directions and seabed conditions and great storm survivability due to full submergence of device.

Figure 2-8. Carnegie CETO 6 (Carnegie 2022).

Swedish company CorPower Ocean (CorPower Ocean 2022) is also developing a point absorber WEC. However, this design is more traditional featuring a heaving buoy on the water's surface connected to the seafloor using a tensioned mooring system (**Figure 2-9**). A unique phase control system that makes the device oscillate in resonance with incident waves is used. Usually, resonance wants to be avoided as WECs have limited maximum offset and if the device exceeds this limit, great stress can be put on the system. However, CorPower have developed their WEC with high structural efficiency to allow operation with strongly amplified motion; the benefit is greater quantity of energy available (up to five times more energy per ton of device). Furthermore, the concept has improved storm survivability; the system can cope with large wave amplitudes.

Figure 2-9. CorPower WEC (CorPower Ocean 2022).

Wavestar (Wavestar 2016) and Eco Wave Power (Eco Wave Power 2022) developed similar WEC concepts (**Figure 2-10**). The systems harvest wave energy by a row of partially submerged buoys which rise and fall in sequence as the wave propagates through the system. The buoys are attached to a main structure via an arm which rotates about a fixed point. Each individual buoy produces a small amount of power, but the cumulative power can total sizeable, rated power capacities. Both concepts were initially developed for nearshore application, however with new research, possibilities are being explored of combining these WEC concepts with offshore wind.
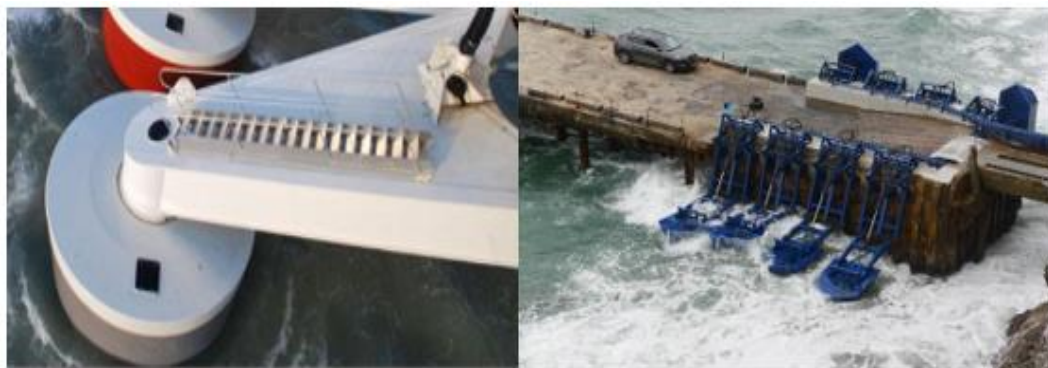
Figure 2-10. Wavestar (Wavestar 2016) (left) and Eco Wave Power (Eco Wave Power 2022) (right).

OceanEnergy (OceanEnergy 2022) is another Irish WEC company which have developed an OWC, namely OE Buoy (**Figure 2-11**). Recently, the company have just completed their demonstrator which will be deployed off the coast of Hawaii. The floating structure is exceptionally large (826ton) and has a potential power capacity of 1.25MW. Because it is an OWC, the turbine is the only moving part of the system which means that OE Buoy has particularly good reliability and can easily be maintained offshore.

Figure 2-11. OE Buoy (OceanEnergy 2022).

2.4 Tidal energy

2.4.1 Resource

Tidal energy is another form of ocean energy with good potential to contribute to global power generation. Tidal energy can be separated into two categories: tidal current energy and tidal potential energy. Tidal current energy exploits the kinetic energy of tidal currents. Tidal potential energy exploits the potential energy associated with the water-level difference during ebb and flood (typically exploited using dams or barrages) (Soleimani et al. 2015). Tidal currents have excellent long-term predictability; it is possible to predict tidal currents to 98% accuracy for many years ahead. Thus, it is one of the most reliable forms of renewable energy available. The predictability of renewable energy sources is critical to the successful integration into the electrical grid (Ben Elghali et al. 2007). The underlying driving mechanism of tidal currents are gravitational forces of the moon and sun. The strength of these gravitational forces depends on distance rather than mass which means the moon has much greater influence (the impact of the moon is 2.6 times more than the sun) (Khan et al. 2017). Tides move around the earth as "bulges" in a cyclical pattern. High tides are created as the ocean bulges toward the moon.

The available tidal current power in the world and Europe is estimated about 75GW and 11GW, respectively (Zhou et al. 2017). The total power extracted by a tidal turbine is similar to a wind turbine:

$$P = \frac{1}{2}\rho A V^3 \qquad\qquad [4]$$

where ρ is seawater density; A is cross-sectional area of the turbine and V is fluid velocity. Just like wind turbines, only a certain fraction of power can be harvested due to losses during conversion into electricity. Thus, the above equation becomes:

$$P = \frac{1}{2}C_p\rho A V^3 \qquad\qquad [5]$$

where C_p is the power coefficient. For wind turbines, C_p is generally between 0.25 – 0.3 but some wind turbines can reach up to 0.4. For tidal turbines, C_p is estimated to be in the range of 0.35 – 0.5 (Ben Elghali et al. 2007).

The UK has around 50% of Europe's tidal energy resource, yet as of 2019 the installed capacity was 35.5MW (Walker and Thies 2021). Primary factors for limited deployment include high initial cost of projects and difficulty with operation and maintenance. Tidal power plants have few optimal locations where the plant can be set up. The installations have been challenged with reliability issues resulting in lower-than-expected power generation, shortened deployments or even failure. Consequently, the investment landscape is challenging as investor risk is high. As such tidal energy has a high LCOE compared to other forms of renewable energy which reduces its overall competitiveness.

2.4.2   Tidal energy technology and market

Technology used to generate electricity from tidal currents can be referred to as Tidal Energy Converters (TECs). TECs are typically one of the following technologies: axial-flow turbine, crossflow turbine, oscillating hydrofoil (Laws and Epps 2016) (Khan et al. 2009), or tidal kite (**Figure 2-12**).

The majority of TEC concepts are axial-flow turbines with rotation axis parallel to the current flow direction akin to conventional wind turbines. Similarly, active control can be used to yaw the turbine to the flow direction, and to pitch the blades based on flow conditions to optimise hydrodynamic performance and maximise power generation. Furthermore, axial-flow turbines can be open or ducted (venturi) and can be positioned anywhere in the water column (fixed to the seabed or floating). Floating tidal turbines are used to exploit tidal energy in deep waters. Additionally, tidal flows are stronger near the water's surface so more power can be generated by a floating tidal turbine compared to a traditional tidal turbine fixed to the seabed at the same location (Sanchez et al. 2014).
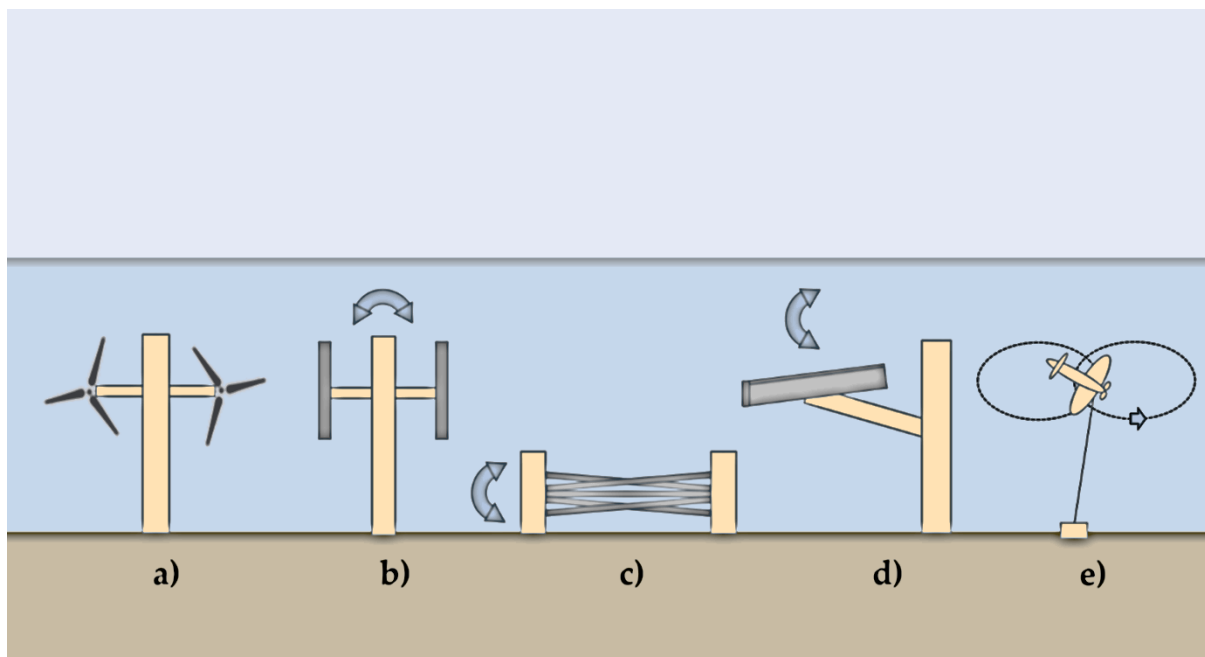
Figure 2-12. TEC types: a) axial-flow turbine b) vertical-mounted crossflow turbine c) horizontal-mounted crossflow turbine d) oscillating hydrofoil e) tidal kite.

Other advantages of floating tidal turbines include no bathymetric or subsurface topography requirements, and ease in accessibility and maintenance because all the electrical components can be set inside the floater. On the other hand, floating tidal turbines are exposed to the harshness of the ocean surface's which requires rigorous designs to be able to deal with

waves and turbulent current inflows. Floater motions are another new design challenge as they could induce dynamic loads on the turbines potentially resulting in unexpected structural failure (Guo et al. 2018).

SIMEC ATLANTIS ENERGY are currently developing the MeyGen project which is the largest tidal farm project in the world and is the only commercial multi-turbine array to have commenced construction. The first phase of the project is a 6MW demonstration array comprising four 1.5MW turbines which are fully submerged and installed on gravity-base foundations resting on the seabed (**Figure 2-13**). They are all upstream, three-bladed, horizontal-axis machines with a rated power capacity of 1.5MW at 3.0m/s and a rotor diameter of 18m. Only two of the four turbines are installed and since 2017 have exported more than 25.5GWh of electricity to the grid. SAE have now secured £2.5million from Scottish Enterprise, which will enable completion of the demonstration array within the next year (SIMEC ATLANTIS ENERGY 2022).

Figure 2-13. SIMEC ATLANTIS ENERGY tidal turbine (SIMEC ATLANTIS ENERGY 2022).

Verdant Power (Verdant Power, 2021) are another TEC developer who have designed their turbines to sit on the seabed. Their concept the Free Flow System (FFS) is three tidal turbines

mounted to a triangular structure which for a single unit array (**Figure 2-14**). The turbines in the FFS are conventional horizontal-axis turbines. They consist of three fixed-pitch blades that rotate slowly capturing the energy from fast underwater currents (+1.8m/s), a rotor and nacelle assembly typical of that of a wind turbine, and the drivetrain and generator that is enclosed within the nacelle that converts the captured energy by the turbine into electricity.

Figure 2-14. Verdant power free flow system (FFS) turbine (Verdant Power, 2021).

Orbital Marine Power (Orbital Marine Power 2022), at present, have developed the world's most powerful floating tidal turbine called the O2 (**Figure 2-15**). The concept features two bi-directional two-bladed turbines mounted on a unique 74m floating platform which is moored via anchors to the seabed where the underwater rotors capture the kinetic energy of seawater. The turbines have a diameter of 20m and a total rated capacity of 2MW. Orbital Marine Power are leading a consortium to deliver the FORWARD2030 project. The project aim is to accelerate the commercial deployment of floating tidal energy.

Figure 2-15. Orbital Marine Power, Orbital O2 (Orbital Marine Power 2022).

Crossflow turbines are alike to vertical-axis wind turbines meaning their axis of rotation is oriented perpendicular to the flow direction. They can be installed vertically or horizontally, can be open or ducted, and installed anywhere in the water column. Generally, crossflow turbines are less efficient compared to axial-flow turbines. They do possess certain advantages over their counterparts. They can generate power from any flow direction that is perpendicular to axis of rotation. Also, arrays of crossflow turbines can be more efficiently grouped due to the blades having a rectangular cross-section. However, the working principle of crossflow turbines mean they are inherently subject to cyclic loading. Cyclic loading increases fatigue on the structure or structural components, which in this case is the turbine blades. Although, if the turbine blades are of a helical shape, then cyclic loading can be reduced. Ocean Renewable Power Company's (ORPC) RivGen Power System (Ocean Power Renewable Company (ORPC) 2022) is an example of horizontal mounted crossflow turbine (**Figure 2-16**).

Figure 2-16. ORPC RivGen Power System (Ocean Power Renewable Company (ORPC) 2022).

There are other unconventional types of tidal turbines which include oscillating hydrofoils and tidal kites. Oscillating hydrofoils comprise of one or more hydrofoils that rotate about a fixed point. They oscillate due to induced lift and drag forces caused by the fluid flow over the hydrofoil (Dahmani and Sohn 2020), (Esmaeilifar et al. 2017), (Kinsey and Dumas 2010). Tidal kites consist of a turbine mounted to a hydrodynamic wing and tethered by a cable to a fixed point that leverages flow to lift the wing. As the kite follows a distinct shaped trajectory sweeping a large area, the relative speed of the kite can reach several times the actual speed of the underwater current. At certain points this increases the generated power significantly. Electricity production is typically via a generator coupled to the turbine. Minesto's Dragon Class (Minesto 2022) is a pre-commercial tidal kite concept that has completed a 0.5MW demonstrator phase and Minesto now plan to expand to a 10MW commercial demonstrator (**Figure 2-17**).

Figure 2-17. Minesto Dragon Class tidal kite concept (Minesto 2022).

2.5   Combined floating offshore energy systems

This section begins the second part of this chapter which is dedicated to the main subject of this thesis, CFOESs. The chapter is organised into the following sections: (1) the concept of a CFOES; (2) the benefits of hybridization; (3) a market review; and (4) a review of the literature.

2.5.1   Concept of CFOES

Holistically, the development of ORE parks is restricted by cost. This is mainly because deploying a power generation system offshore requires sophisticated and robust designs which typically come at high expense. In deep sea areas, where multiple ORE resources are available in good quantities for power generation, a CFOES is a unique solution to reducing the LCOE.

Before exploring different concepts of CFOESs, it is important to first understand the motives for combining ORE systems (floating wind and ocean energy) into a single infrastructure. Floating offshore wind has an established "parent" industry in bottom-fixed offshore wind. This means the nascent industry can take advantage of existing supply chains and infrastructure, and grid connections (Mofor et al. 2014). For ocean energy technologies,

no specific supply chains are readily available. This means that developers often have to take on more roles than initially expected which can be costly and time consuming. Thus, development is hindered as ocean energy technology developers often have limited resources (International Renewable Energy Agency (IRENA) 2020). The existence of a parent industry has proven to boost momentum concerning deployment and the maturity rate of technology. Floating wind has overtaken ocean energy in terms of installed capacity even though these industries have been established for much longer. Therefore, this accelerated success of floating offshore wind has prompted companies, academics, and researchers alike to question the possibility of ORE hybridization. The motives include: (1) ORE developers share the same goal which is to produce electricity for the cheapest price possible; (2) all ORE systems operate and must survive in the same environment, thus share the same design challenges (Pérez-Collazo et al. 2015); (3) is there a possibility that ocean energy can effectively "piggyback" on floating wind's growth by using the existing supply chains in place (Mofor et al. 2014); and (4) marine space is becoming increasingly congested with users including established industries such as fishing and shipping as well as emerging industries such as offshore aquaculture, seabed mining, and marine biomass cultivation (Schupp et al. 2019). In relation to these factors, the incentive to explore and research the feasibility of CFOESs is warranted.

2.5.2 Synergies of hybridization

The main objective of a CFOES is to increase power production at the same location by exploiting more than one ORE source compared to a pure system which can only exploit one. However, with proper design there is an array of other synergies associated with CFOESs. These include: (1) intermittency, an inherent characteristic of most renewable energy sources, can be reduced resulting in a smoother, more reliable power output; (2) this enables the creation of an integrated energy mix; (3) significant cost reductions can be achieved through the sharing

of a common substructure, grid infrastructure and mooring system, shared logistics, installation, transportation vessels and operation & maintenance; (4) in the context of combining floating wind turbines with WECs, it has been discovered that some WEC devices can dampen the platform motions of floating wind turbines thereby improving the stability and thus the performance of the wind turbine (Zhu and Hu 2016); (5) similarly, tidal turbines can introduce additional hydrodynamic damping resulting in reduced variability of platform motions and mooring line tensions (Yang et al. 2020b); and (6) sustainable development, the optimization of marine space can prevent conflicts amongst offshore users and alleviate pressure on fragile ecosystems (Karimirad 2014). The potential advantages gained from floating wind and ocean energy hybridization has led to this scientific field becoming a hot research topic in recent years. Now, there are even a few concepts undergoing prototype development and open sea testing.

2.5.3   *Pre-commercial concepts and demonstrators*

Floating Power Plant's (Floating Power Plant 2022) FPP platform is the world's first successfully offshore-tested combined wind and wave device (**Figure 2-18**). The substructure is a semisubmersible platform which can support a single wind turbine (4 – 15MW) and up to 4MW of wave power depending on the available resource. The platform is kept in position by a single-point mooring system which permits platform weathervaning (the platform can passively rotate to face incoming wind and waves). The WEC system can absorb between 60 – 80% of incident wave energy and creates a safe landing zone in the wake of the platform which eases operation and maintenance. Floating power plant aims to operate the first commercial plant by 2022, followed by a number of plants that accumulates to a capacity of 50MW by 2030.

Marine Power Systems (MPS) (Marine Power Systems 2022) have devised a flexible solution called PelaFlex. It can be configured to harness wind and wave energy in deep water, either as a combined solution or on their own. Their concept has been tested through a series of scale prototypes and they have proved it can generate grid compatible electricity. MPS are currently in progress of deploying a commercial megawatt-scale device at Biscay Marine Energy Platform, Spain. They also plan for a multi-megawatt array at European Marine Energy Centre, Scotland.

Figure 2-18. Floating Power Plant's FPP platform (Floating Power Plant 2022) (left) and Marine Power Systems' PelaFlex floating platform and wave energy converter (Marine Power Systems 2022) (right).

Excipio Energy (Excipio Energy 2022) conceptualised a platform capable of integrating a full spectrum of ORE technologies called Excibuoy. The concept hosts wind turbines, WECs, tidal turbines and ocean thermal energy converters giving a total projected rated power capacity of 29MW (**Figure 2-19**). This is equivalent to multi-unit floating wind farms e.g., Hywind Scotland. The concept is ambitious, but it potentially symbolizes the future of optimised renewable power generation in the offshore environment. The Excibuoy platform for now remains in the conceptual design phase as Excipio Energy pursue funding to support

experimental tank testing and computer modelling required to confirm the integrated power output.

Figure 2-19. Excipio Energy's Excibuoy platform (Excipio Energy 2022).

German company Sinn Power (Sinn Power 2022) have installed an 80kW demonstrator of their floating hybrid multipurpose platform concept, SOcean (**Figure 2-20**), in Heraklion. The concept extracts energy from three different renewable energy sources; wave, wind, and solar energy. A novelty of the concept is that it is designed to be used in a modular approach to build large floating solar plants with a combined capacity of up to 10MW at full scale. Additional electricity can be produced by small wind turbines at each of the corner points of the solar panel arrays. The system can also be powered by WECs, depending on the maritime conditions and power demand. Sinn Power has successfully carried out testing in Heraklion and is actively marketing its solutions to project developers worldwide.

Figure 2-20. Sinn Power's Ocean Hybrid Platform (Sinn Power 2022).

Principle Power is a major floating wind platform developer who explored the integration of WECs into their semisubmersible FOWT concept, WindFloat. The project, WindWaveFloat (Roddier and Banister 2012), assessed the technical and economic viability of three different WEC concepts installed on WindFloat with a focus on maximizing power output and reducing the overall LCOE. The three WECs selected for assessment were point absorber, OWC and OWSC (**Figure 2-21**). The WECs were chosen to represent promising concepts in line with current developments at the time of the project. The performance of the CFOESs were evaluated in terms of dynamic responses and power output. Considering dynamic responses, all three concepts had minimal effect on the overall platform motion. The OWSCs had the most significant impact increasing the surge motion amplitude of the WindFloat platform. Calculations from Principle Power showed a maximum average power of 150kW/m^2 could be extracted in these configurations. Several of the resulting system designs demonstrated technical feasibility, however, the size and design constraints of the WECs (technical and economic) meant the WindWaveFloat concept was economically unfeasible at this time. Not enough additional power was generated to cover the additional expense associated with wave energy integration to make WindWaveFloat worthwhile.

Figure 2-21. From left to right: WindFloat, WindFloat and two OWCs, WindFloat and point absorber and WindFloat and three OWSCs (Roddier and Banister 2012).

2.5.4 *Funded research programmes*

In the past some EU funded projects focused on researching sustainable solutions for the advanced development of the offshore sector. In particular, five projects H2OCEAN (H2OCEAN (European Commission 2014a), MARINA (European Commission 2014b), MERMAID (European Commission 2015b), ORECCA (European Commission 2011), and TROPOS (European Commission 2015c) had a common theme of integration of various user functions into a single infrastructure. Functions could include energy generation, hydrogen generation, offshore aquaculture, shipping, tourism, and leisure.

2.5.4.1 *Project MARINA*

Project MARINA is aimed specifically at accelerating ORE applications to utility-scale through hybridization. Three combined concepts (**Figure 2-22**) were selected to have their feasibility assessed through physical modelling and numerical simulation. The concepts were the Spar-Torus Combination (STC), the Semisubmersible Flap Combination (SFC), and the larger floater with multiple oscillating water columns and one wind turbine (OWC array).

a)   **b)**   **c)**
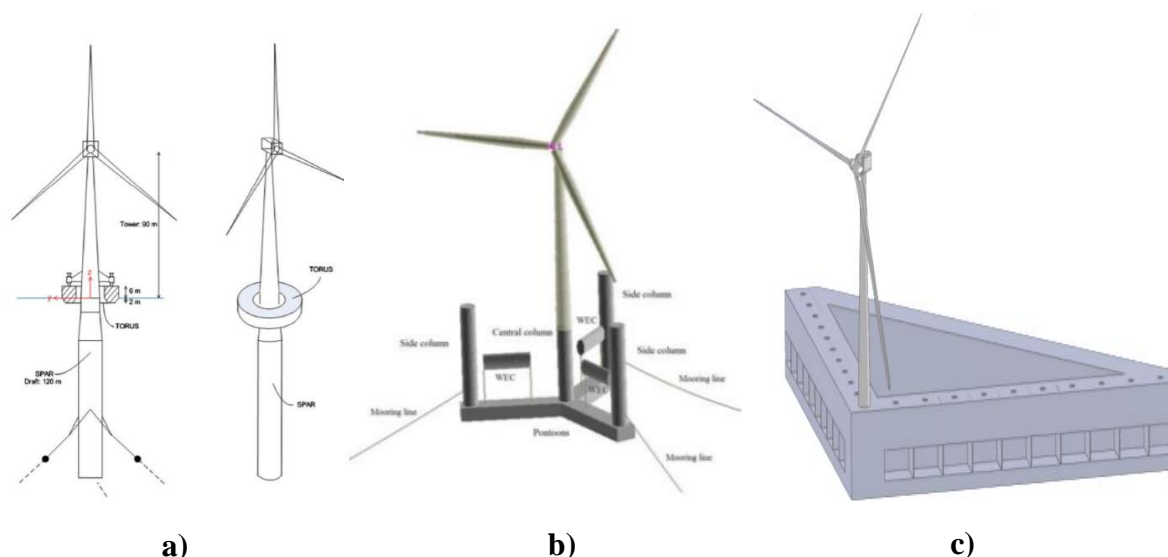
Figure 2-22. a) STC concept **b)** SFC concept **c)** OWC array concept (European Commission 2014b).

The STC concept combines a spar FOWT with a point absorber WEC inspired by the models 'Hywind' and 'Wavebob', respectively. The WEC is a large donut-shape buoy which is known as a torus and surrounds the body of the spar FOWT. Power is generated from two ORE sources: (1) the incident waves by the WEC, through the relative heave motion between the WEC and FOWT platform, and (2) the wind by the wind turbine supported by the spar substructure. Muliawan et al. (2013) performed a time-domain coupled analysis to study the dynamic responses and estimate the power production of STC concept. A 15% enhancement in power output could be achieved and the variability of platform motions decreased compared to a pure spar FOWT. Wan et al. (2015) studied the STC concept experimentally and investigated the concept subject to extreme conditions in order to fully assess concept feasibility. Several nonlinear phenomena were observed during the experimental campaign including vortex-induced motion, Mathieu instability and wave slamming.

The SFC concept is a semisubmersible FOWT which is made up of a central column, which supports the wind turbine, three side columns which provide restoring stiffness, and

three pontoons which connect the side columns to the central column. Mounted onto the pontoons are three flap-type WECs with elliptical cylinders which exploit the horizontal water wave particle velocity. Luan et al. (2014) presented a numerical modelling method for the SFC concept and carried out a sensitivity study on the PTO damping coefficients and mass of the elliptical cylinders. Michailides et al. (2014) investigated the effect of the flap-type WECs on the dynamic responses of the semisubmersible FOWT. Two different layouts were considered and comparisons of responses in terms of stability, motions and internals loads were made. Michailides et al. (2016) experimentally investigated the functionality of the SFC concept. Results showed produced power increased without significant impact on platform motions and there was a good agreement between experimental and numerical results.

Gao et al. (2016) numerically and experimentally compared the dynamic responses of STC and SFC concepts. Based on a preliminary comparison of dynamic responses including motions, power generation, and the WEC PTO systems, they found the STC concept had a lower cost of energy compared to the SFC concept. However, whilst the results showed that the numerical models can reasonably predict the responses of the CFOESs, for most cases, the linear hydrodynamic model was not adequate for the STC concept in extreme wave conditions, due to the occurrence of slamming. On the other hand, the results found that compared to a pure wind energy concept, the combined concepts were more expensive due to the immaturity of wave energy technology, a similar finding to that of Principle Power.

The OWC array concept is large floater supporting an array of OWCs and a wind turbine. In contrast to the previous two concepts, the displacement of the structure is ten times larger in order to accommodate for the array of OWCs. One purpose of this concept was to investigate the viability of extremely large floating platforms. It was found that the power performance of the WECs was comparable to that of wind turbines i.e., MW scale, however, it came at a much

higher cost of energy as a result of the enormous structure despite the significantly increased power production. Moreover, the size of the structure meant it was subject to extreme structural loadings. Further details can be found here (Sojo and Auer 2014).

2.5.5 *Academic research*

There is a good quantity of journal publications on the topic of CFOESs. However, most of these publications are within the context of floating wind and wave hybridization with only a small number of publications focussing on floating wind and tidal hybridization. There is extremely limited research on CFOESs with more than two energy systems integrated within the same platform/structure. Most studies concentrate on the power production capabilities of the energy systems as well as the resultant dynamics of the CFOES.

2.5.5.1 *Academic reviews of CFOESs*

Ding et al. (2015) presented an overview of hybrid wind-wave energy systems; WEC technology and FOWT platform technology were briefly described. Two CFOES concepts were discussed including the STC concept and WindWaveFloat to provide insight into the flexibility of combining FOWTs with WECs. McTiernan and Sharman (2020) published a concise review on the types of hybrid floating offshore wind and wave energy systems, their advantages and design challenges. Compared to these two works, Perez-Collazo et al. (2015) conducted a comprehensive review of offshore wind and wave energy hybridization. An overarching analysis was presented on the most relevant aspects related to hybridization such as resource, synergies, possibilities, and suitable technology (substructures and WEC technology). A novel classification was also proposed based on how the technologies are integrated. The classification distinguishes co-located, hybrid, and island systems. Dong et al. (2022) have published the most recent state-of-the-art review on hybrid wind-wave energy converters. The review follows a similar structure to the work of Perez-Collazo et al. (2015),

providing up-to-date information on joint wind and wave energy resources, and suitable offshore wind foundation types including floating foundations. The paper reviews the most recent concepts and devices within the context of combined wind and wave exploitation, and a preliminary assessment of synergies is made. Existing methods to study such systems are summarized and this work provides a comprehensive guide for future developments of combined wind-wave systems.

2.5.5.2 Barge FOWT and WEC

Aboutalebi et al. (2021) developed a numerical model of a novel platform design to investigate if undesired oscillating motions of a barge floating platform, particularly in rotational modes, can be reduced with the integration of OWC WECs. The academic group focused on RAOs of platform motions to understand the behaviour of the system in the frequency-domain. Then, from the RAOs four periods were chosen to analyse the system in the time-domain. A comparison between the CFOES and a generic barge FOWT was made to assess the performance of the CFOES. The results showed that the proposed concept could efficiently decrease oscillations for low wave periods (6 – 12s), however for larger wave periods (12 – 20s) the pure barge system displayed better performance. To improve the performance of the CFOES in larger wave periods, Aboutalebi et al. (2021) recommend the implementation of a specific control strategy for the WECs in future studies.

2.5.5.3 TLP FOWT and WEC

Bachynski and Moan (2013) examined the resultant responses of a TLP FOWT combined with three point absorbers, in terms of structural loads, platform motions and WEC PTO system, for operational and 50-year extreme environmental conditions. Zhou et al. (2016) and Ren et al. (2020) analysed the performance of a CFOES integrating a torus-shaped heave-type WEC onto a TLP FOWT. They explored different PTO parameters and wave periods on WEC

performance to determine preliminary optimal values for the WEC PTO. Time-domain simulations were conducted to assess the main dynamic characteristics of the CFOES under typical operational combined wind-wave loads.

Konispoliatis et al. (2022) performed a coupled analysis in both time- and frequency-domain on a CFOES exploiting wind and wave energy. The concept is a TLP FOWT encompassed by an array of hydrodynamically interacting OWC WECs. The concept was assessed for two offshore sites: a Mediterranean site and a North Sea site. Fundamental hydrodynamic properties such as hydrodynamic coefficients and RAOs of platform motions, as well as the ultimate and fatigue loads from several load cases are presented. As expected, the time-domain analysis found that the concept had increased tower and tendon DELs (50% and 59%, respectively) at the North Sea site. There was a slight increase in the blade moment DELs (2% in edgewise and 14% in flapwise direction). Under normal sea state conditions however, the tower and blade loads remained almost unaffected.

2.5.5.4 Semisubmersible and WEC

Hallak et al. (2018) proposed a novel CFOES concept made up of an unconventional semisubmersible platform (a larger number of columns) and point absorbers. In this numerical study, only the platform's hull was considered in this first analysis and the platform stability and seakeeping performance was assessed and compared. Experiments were conducted in a wave basin were conducted and results were compared to the numerical ones. It was discovered the CFOES would benefit with stronger and smoother power output, and stability enhancement compared to a pure semisubmersible system. Lee et al. (2018) developed a numerical model to investigate the hydrodynamic interaction of a CFOES containing 24 point-absorber WECs in the frequency-domain. Hu et al. (2020) conducted an optimization study and performance analysis of a semisubmersible FOWT combined with multiple point absorber WECs. The

results provide guidance for the optimized design of WECs in the context of floating wind and wave hybridization. Wang et al. (2020) proposed a CFOES comprising a braceless semisubmersible FOWT and point absorber WEC. The effects of different PTO parameters on hydrodynamic performance and wave energy production were investigated. On the same concept, Li et al. (2021) used a newly developed numerical tool FAST2AQWA (F2A) (this numerical tool is used as the foundation tool for this present work), which is an open-source aero-hydro-servo-elastic framework, coupling numerical tools FAST and AQWA, to examine the power performance and fully coupled dynamic responses of the CFOES, subject to operational and extreme conditions.

Chen et al. (2022) also using F2A, conducted a dynamic response analysis of a CFOES (FWWP), which is a semisubmersible FOWT and a point absorber WEC. To thoroughly investigate the performance of the FWWP, three numerical models are developed of the single point absorber, the pure FOWT and the combined system, to compare results and observe the performance of the FWWP system. The model of the FWWP is system is validated by comparing results with OpenFAST. Fully coupled analyses of the FWWP is carried out for regular and irregular waves in the operational sea-states.

2.5.5.5   *Spar and WEC*

Karimirad and Koushan (2017) studied the feasibility of combining a spar FOWT with a WEC system, inspired by Hywind and Wavestar, respectively. The results showed the WEC system did not impact the power performance of the FOWT and there was an increase in power production, albeit only 6%. Ghafari et al. (2021) investigated a novel Wavestar-Hywind combined system. The effect of WEC unit addition on produced wave power and platform responses was investigated in the frequency- and time-domains. Skene et al. (2021) developed a generalised study for combining a FOWT with a point absorber WEC. In the concept/early

development phase, research on CFOESs focuses on a specific design instead of a more general perspective. This is because designs can vary significantly, for instance, floating platform can be of barge, semisubmersible, or spar type, and for WECs there are point absorber, OWC, OWSC and other WECs to select from. There is a small convergence towards using point absorber WECs for the purpose of floating wind and wave energy hybridization because of its breadth of possibilities when integrating its structure with a FOWT. Therefore, the work of Skene et al. (2021) explored the integration of floating wind and wave using general established designs and investigated the overall general consequences. Sai et al. (2020) carried out a comparative response analysis of three different CFOES concepts. The concepts were STC concept, a semisubmersible platform with conical-cylinder point absorbers mounted on the columns, and a TLP platform integrated with a torus-shaped point absorber. Time-domain aero-hydro-servo-elastic simulations was used to study the motion behaviour of the CFOESs. Considering all the structural parameters and coupled dynamics responses, they concluded that the STC concept has better stability and performance compared to the other two concepts.

2.5.5.6 Floating wind and tidal

Only a few notable publications exist on the topic of floating wind and tidal hybridization. Ma et al. (2019) proposed a concept which mounted two vertical-axis tidal turbines on the underside of the top deck of a twin-hull semisubmersible platform, which supported a wind turbine (**Figure 2-23**), and conducted a hydrodynamic analysis of the concept in ANSYS AQWA. The platform motion Response Amplitude Operators (RAOs) and hydrodynamic coefficients of the platform were obtained from a hydrodynamic diffraction analysis (frequency-domain). The results indicated the concept had good hydrodynamic performance based on all modes of motion. A hydrodynamic response analysis (time-domain) was subsequently carried out in which the platform motions and mooring line tensions were studied.

The time-domain simulations showed the concept had good hydrodynamic performance as the platform motion responses were well within acceptable limits under all design load cases. Ashglaf (2019) published a thesis on the development of hybridization concept for horizontal-axis wind and tidal systems using functional similarities and advanced real-time emulation methods. Yang et al. (2020b) conducted a performance evaluation of a CFOES consisting of a spar FOWT and two tidal turbines installed approximately 46 m below the water's surface. FAST2AQWA (F2A) was used to investigate the power performance and dynamic responses in operational conditions. It was found that power output increased by 3.84% to 6.46%, transient behaviour improved, and mooring line tension fluctuation was reduced due to hydrodynamic damping provided by tidal turbines. In addition, the tidal turbines had no negative affect on the aero-elastic responses or power performance of the wind turbine.
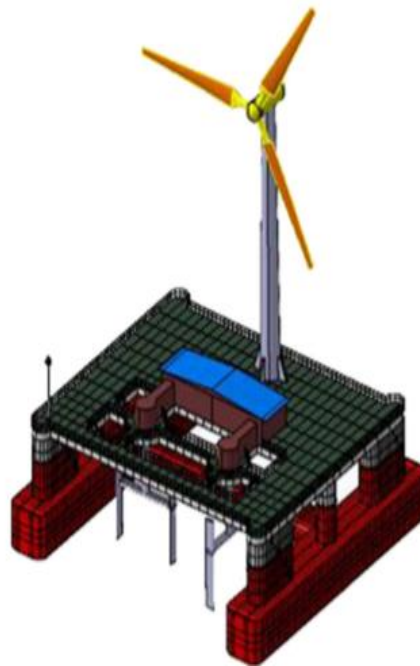
Figure 2-23. Combined wind-tidal floating power generation platform (Ma et al. (2019)).

2.5.5.7   Floating wind, wave energy and tidal energy systems

To the author's knowledge at the present time, only one publication presented the development of a numerical model combining three ORE systems into a single floating structure. Li et al. (2018), investigated the dynamic responses of a novel floating platform consisting of a spar FOWT, a point absorber WEC and two tidal turbines (**Figure 2-24**). The CFOES is referred to as 'Hywind-Wavebob-NACA 638xx Combination (HWNC)', which expands on the STC concept by including the additional tidal turbines. A numerical model was developed to assess the power production capabilities of this CFOES in addition to other dynamic responses such as platform motions and mooring line tensions. Results indicated pitch and surge motions of the HWNC were reduced in three operational conditions which is attributed to the damping force produced by the underwater turbines. The reduced motions proved beneficial to wind turbine power output enhancing quality. The overall power production increased between 22 – 45% depending on environmental conditions. Mean mooring line tensions also increased due to forces acting on underwater turbines. However, the numerical model only considered the aerodynamics, hydrodynamics, and mooring line dynamics. The model excluded the elasticity of flexible elements, and no blade-pitch or rotor speed control was applied. In essence, the adequacy of the study is limited as a result of these exclusions. Therefore, an opportunity is presented whereby any new research on the topic of ORE hybridization in this particular area, i.e., when three or more systems are involved, would be new and contributing research. Thus, the work in this thesis is intended to provide greater insight into the coupled dynamics of a CFOES when considering the structural dynamics of flexible components and the implementation of a wind turbine controller within the numerical model.
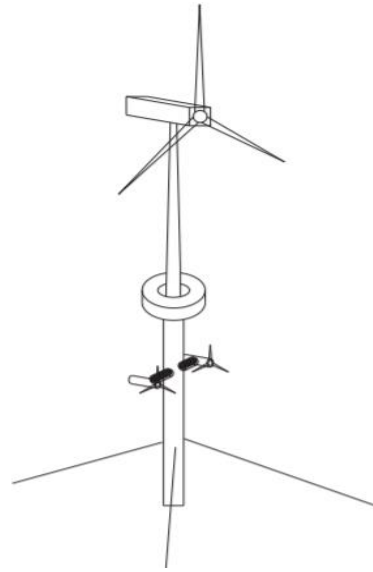
Figure 2-24. HWNC concept (Li et al. (2018)).

2.6 Chapter summary

A summary of this chapter is given through consideration of two parts: (1) a literature survey on ORE, specifically on floating wind, wave, and tidal energy industries, and with a focus on market and technology, and (2) a literature survey on CFOESs, with emphasis on combined concepts composed of floating wind turbine integrated with either a WEC or a tidal turbine system or both. Initially, the first part of this chapter is a review on the current state of ORE. Then, surveyed literature establishes reasoning for ORE hybridization which is the focus of the present research. Before the main subject of this thesis is introduced, it is important to have a thorough understanding of what comprises a CFOES, hence the critical review on the individual ORE industries. For each ORE industry, the literature survey reviews information on the resource, the types of machines used to convert the energy form into electricity, or in the case of floating wind the platform technology, and the latest market developments within the industries. The second part of this chapter is dedicated to a state-of-the-art literature survey on CFOESs. The second part begins by definition of a CFOES and the discussion of synergies

of hybridization. Then, an in-depth review of pre-commercial concepts and demonstrators, funded research programmes, and academic research on CFOESs is presented.

The survey of literature concluded the following points:

- Floating wind turbines have 4 main types: barge, semisubmersible, spar and TLP. Barge-type floaters have advantages in construction and deployment, which could ease utility-scale production providing excessive pitching motion can be mitigated.

- WECs have a large spread of technologies but there is some industry consolidation towards the point absorber concept. This technology can absorb wave energy from all directions, and they have much smaller structural size compared to other concepts.

- Tidal turbine systems follow suit to the wind turbine industry with axial flow turbines as the most advanced technology.

- CFOES concepts that comprise FOWT combined with wave energy technology are more prevalent than CFOES concepts made up of FOWT combined with tidal energy technology. There are even some prototypes in development such as Floating Power Plant.

- Only one numerical model of, no experimental data for, and only one conceptualised commercial concept of a CFOES which integrates three or more ORE systems exist. There is an opportunity for research to significantly contribute to knowledge in the scientific area.

Chapter 3.   Theory, numerical modelling, and simulation

Engineers must setup the numerical environment within engineering tools in order to simulate ORE systems in a range of operational and survival scenarios. A knowledge of the different environment condition models is required so that the correct environment can be calibrated. Specifically, to offshore structures, environment conditions are often referred to as 'Metocean conditions', which means the combined effect of the meteorology and oceanography (wind, ocean waves and current) (Subrata K. Chakrabarti 2005). Once the numerical environment has been configured, the environment condition kinematics are used as input into dynamic models which solve the equations of motion in order to calculate the dynamic responses of the ORE system. The dynamic response outputs are usually in terms of forces and moments and motions of important structural components, and generated power (Gao et al. 2016). Similarly, different models are available within numerical tools to predict the loads and responses for an ORE system for each physical domain e.g., aerodynamic and hydrodynamic. The engineer must have a strong understanding of the theory, governing assumptions, and differences between models in order to develop a sophisticated numerical model of an ORE system that can produce reliable results.

Therefore, this chapter is organised into the following sections: Section 3.1 provides a comprehensive summary to modelling the offshore environment within an engineering tool for ORE system design and analysis. Sections 3.1.1, 3.1.2, and 3.1.3 are dedicated to modelling the wind, ocean waves, and current, respectively. Section 3.2 is a critical discussion on the mathematical models used for modelling the structure(s) in ORE system design and analysis. Section 3.2 begins with an overview of current numerical tools which is presented in Section 3.2.1. Sections 3.2.2 – 3.2.6 present the theory and modelling techniques concerning the different physics domains e.g., aerodynamic, hydrodynamic. Sections 3.2.7 describes how the

mathematical equations are solved in order to obtain the dynamic responses of the ORE system. Section 3.2.8 presents the theory to modelling and integrating the WEC and tidal turbine systems. The importance of validating and verifying numerical models is presented in Section 3.2.9 and a chapter summary is provided in Section 3.2.10.

3.1 Modelling the offshore environment

An offshore structure will be subject to many different types of loading and the corresponding load effects. The structure must survive in the hostile offshore environment throughout its service life. It needs to be able to withstand extreme conditions without compromising performance during operation. Loads can be broadly categorised into static and dynamic loads. Static loads are constant loads which include loads such as gravity, hydrostatic pressure, and loads from the structure itself including equipment. Dynamic loads are of consequence of variable environment loads such as wind, ocean waves, and currents (Karimirad 2014). A schematic of the offshore environment is shown in **Figure 3-1** illustrating the important environment loads.
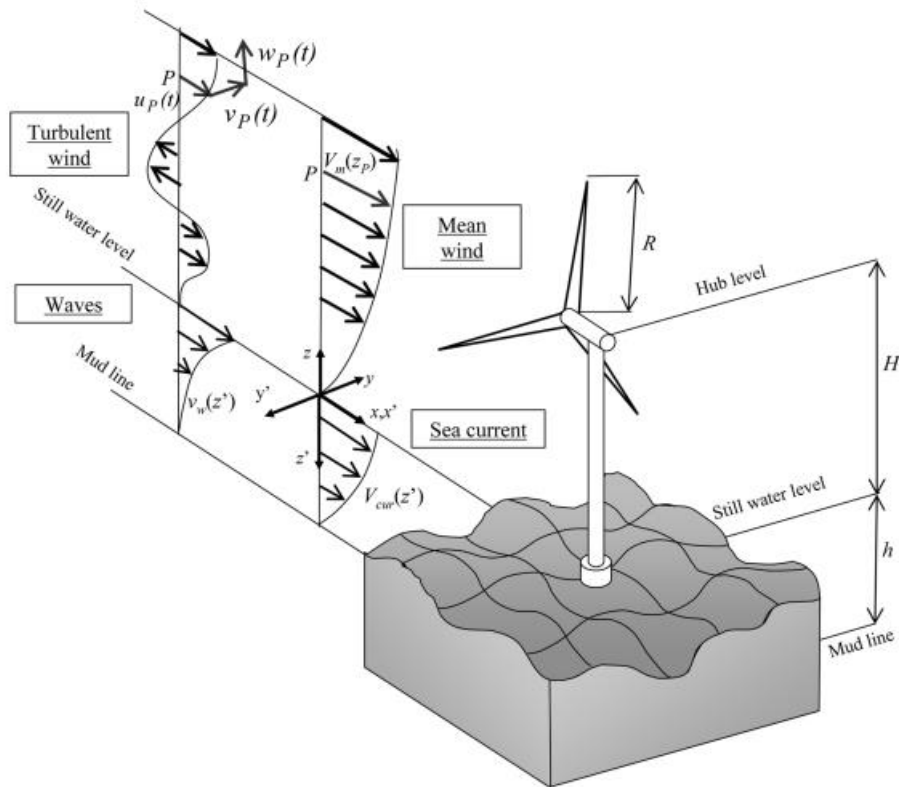
Figure 3-1. Schematic of the offshore environment (Petrini et al. 2010).

Other environment loads include tsunamis, earthquakes, and ice (**Figure 3-2**). In practice, all these need to be considered in ORE system design. However, often for preliminary concept development only the driving loads (aerodynamic and hydrodynamic) need to be considered (Petrini et al. 2010).
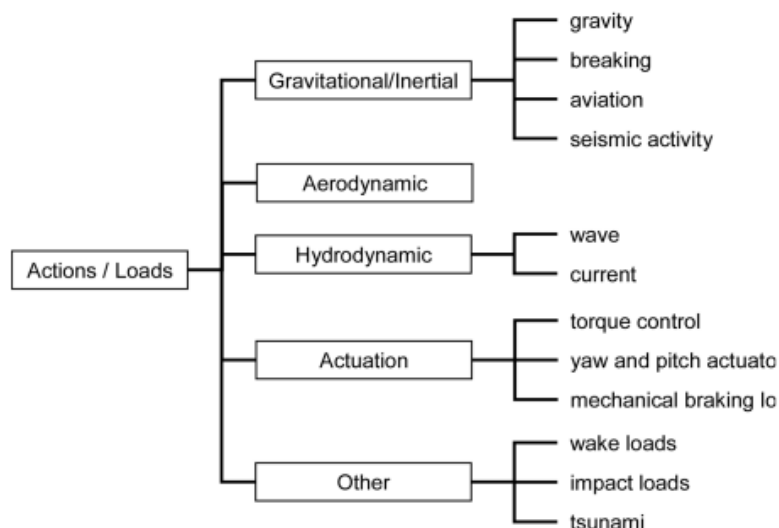
Figure 3-2. Categorisation of loads (Petrini et al. 2010).

3.1.1 Wind

The foundation to calculating the aerodynamic loads is formulating a representation of wind velocities. Typically, wind velocities are not constant, but vary over time. These variations can be annual or seasonal variations, synoptic or diurnal variations, or changes over seconds and minutes often referred to as turbulence (Karimirad 2014).
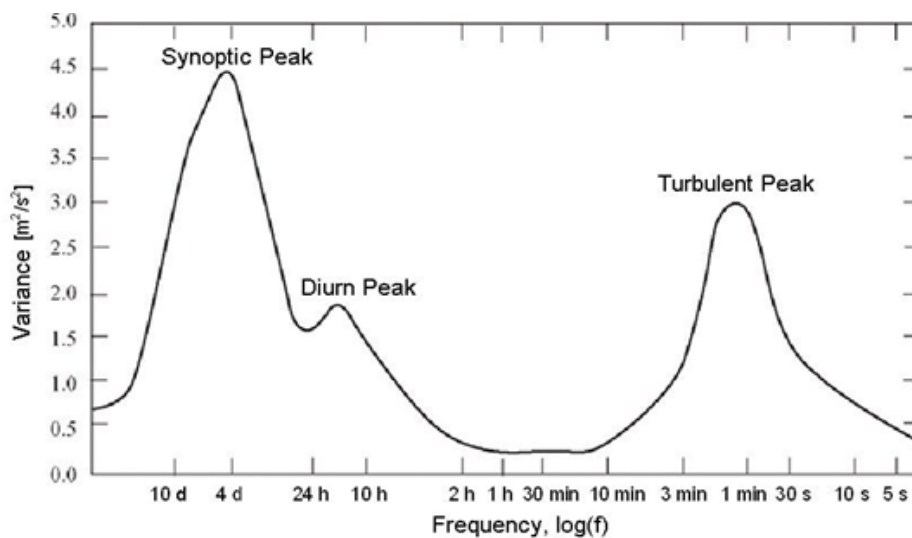
Figure 3-3. Spectral wind density (Karimirad 2014).

Figure 3-3 shows how wind energy concentrates around two distinct frequency ranges separated by a spectral gap (Van der Hoven 1957). The low-frequency peaks represent quasi-static wind, $\bar{u}$ (mean wind speed). The high-frequency peak represents dynamic wind, $u_0(t)$ (turbulent wind). A quasi-static load is a load that can be assumed as time independent. Thus, time-varying wind speed, $u(t)$, consists of a steady value, $\bar{u}$, and fluctuations about the steady value, $u_0(t)$. By assuming the steady part of the time-varying wind as quasi-static, numerical modelling and simulation of wind are simplified.

A dynamic load is time dependent for which inertial effects cannot be neglected. These wind speed variations can be described by a turbulence intensity and a Power Spectral Density

(PSD). The turbulence intensity (I) is a characterization of the overall level of turbulence and is defined as:

$$I = \frac{\sigma}{\bar{u}}$$

[6]

where σ is the standard deviation of the variation of wind speed about $\bar{u}$, the mean wind speed (taken as 10-minute average). This turbulence intensity only captures non temporal information. The temporal information of the turbulence i.e., the frequency of wind speed fluctuations is captured in the turbulence PSD from which a time series can then be constructed. Typical wind spectrums include von Karman, Kaimal, and Mann.

3.1.1.1 TurbSim

TurbSim is a stochastic, full-field, turbulent-wind simulator. It employs a statistical model to simulate the time series of three-component wind-speed vectors at points in a two-dimensional vertical rectangular grid that is fixed in space. Spectra of velocity components and spatial coherence are defined in the frequency domain and an inverse Fourier transform produces the time series (Jonkman 2009). TurbSim is used to create the turbulent wind fields which are used as input into the numerical models developed later on in this thesis. The IEC Kaimal model and power law model were selected as the models to generate the wind fields in the turbulent wind simulator.

3.1.1.1.1 IEC Kaimal model

The Kaimal model is defined in IEC 61400-1-3 and assumes neutral atmospheric stability. The spectra for the three wind components, $K = u, v, w$ are given by

$$S_K(f) = \frac{\frac{4\sigma_k^2 L_K}{\bar{u}_{hub}}}{\left(1 + 6f\frac{L_K}{\bar{u}_{hub}}\right)^{\frac{5}{3}}} \tag{7}$$

where $\bar{u}_{hub}$ is the steady state wind speed at hub height, f is the cyclic frequency, and L_K is an integral scale parameter. The IEC 61400-1 standard defines the integral scale parameter to be

$$L_K = \begin{cases} 8.10\Lambda_U, & K = u \\ 2.70\Lambda_U, & K = v \\ 0.66\Lambda_U, & K = w \end{cases} \tag{8}$$

where the turbulence scale parameter, Λ_U, is

$$\Lambda_U = 0.7 \cdot \min\,(60m, HubHt) \tag{9}$$

From this spectrum a wind velocity time series is constructed, and it is this time history of wind speed that is fed into simulation so that the aerodynamic loads acting can be determined.

3.1.1.1.2 Wind speed profile

The wind speed profile determines the mean u-component wind speeds at each height for the length of the simulation. The power-law wind profile calculates the average wind speed at height z using the equation

$$Mean\ wind\ speed, \quad \bar{u}(z) = \bar{u}(z_{ref})\left(\frac{z}{z_{ref}}\right)^{\alpha} \tag{10}$$

where α is power law exponent; $\bar{u}(z)$ is the mean wind speed at height z; and z_{ref} is a reference height above ground where the mean wind speed $\bar{u}(z_{ref})$ is known (typically $10\ m$).

3.1.2   Ocean waves

Oceans waves form due to perturbations of the free surface and propagate due to gravity. Several types of ocean waves exist which can be characterised by wave height and wave period (**Figure 3-4**).
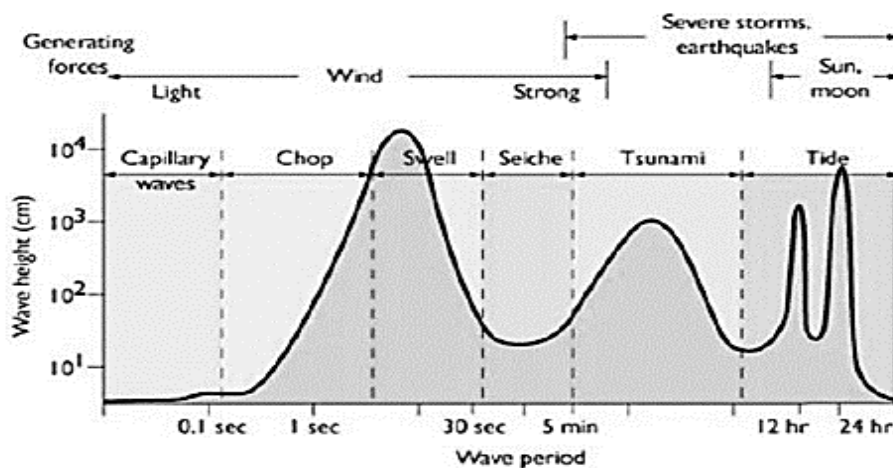
Figure 3-4. Types of ocean waves (Folley 2017).

The most common disturbance of the ocean's surface is from wind. **Figure 3-5** illustrates how perturbations of the ocean's surface from wind form into ocean waves. Waves begin as small ripples and grow due to sustained energy input from the wind. At some point waves reach a limit beyond which they cannot grow. This is because the energy being transferred in is balanced out by the losses due to gravity. Waves that have reached this condition are considered fully developed. For a sea to be fully developed, it is dependent on the wind speed and the fetch (distance) over which the wind blows. After the wind ceases to blow, the formed oceans waves will continue to exist and can travel for exceptionally large distances with minimal energy losses; these waves are referred to as swell waves. It is a common representation to separate ocean waves into wind waves (waves created by local winds) and swell waves (waves created by winds that are no longer blowing that have typically travelled from another area). This can be useful for describing the conditions of a particular sea state; however, it must be noted, this

is simply an abstraction and there is no fundamental difference in the hydrodynamics of wind and swell waves (Folley 2017).
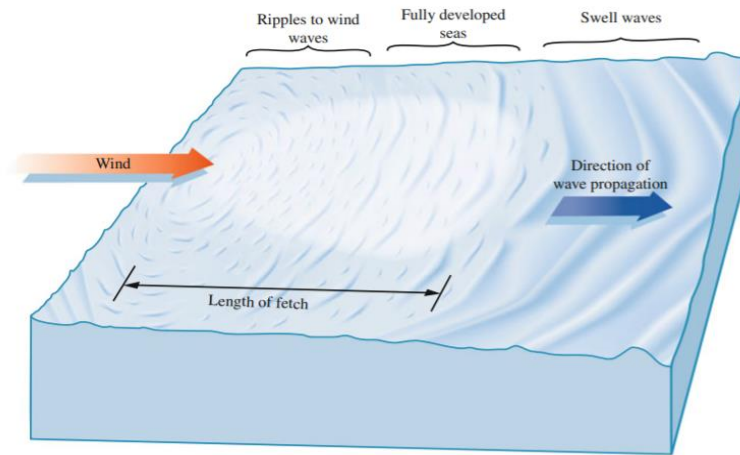
Figure 3-5. Formation of ocean waves by wind (Folley 2017).

3.1.2.1   *Modelling ocean waves*

3.1.2.1.1   Regular wave

Linear wave theory (or Airy theory) is the simplest mathematical representation of an ocean wave. It is the core theory for modelling ocean surface waves in offshore engineering and other similar fields. An ocean wave is represented by a sine (or cosine) function; this is termed a 'regular wave'. A regular wave can be defined by three parameters (**Figure 3-6**):

- Wave height (H)

- Wave period (T)

- Wavelength (λ)
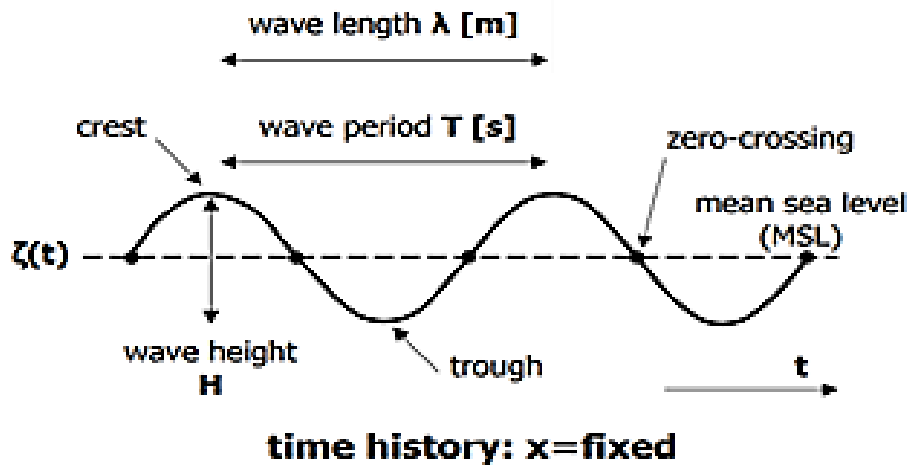
Figure 3-6. Regular wave definition.

The wave height is the vertical distance from the wave trough to the wave crest; the wave period is the time taken for the wave to repeat cycles; and the wavelength is the distance between two similar points of the wave i.e., two peaks. A regular wave is defined by Equation 11 (Karimirad 2012):

$$\eta(x,t) = \frac{H}{2}\sin(\omega t - kx) \qquad [11]$$

where $\eta(x,t)$ is the space- and time-dependent wave elevation.

Regular waves have a characteristic of having a period of the same form for every cycle. This means regular waves properties can be described in one cycle with properties invariant from cycle to cycle. There are other useful parameters used to describe ocean waves which are derivatives of the three main parameters defined above. They include wave frequency (ω), wave celerity (c), wavenumber (k, the number of wave cycles, in radians, that exist per m), and wave steepness (s):

$$Wave\ frequency, \omega = 2\pi/T \qquad [12]$$

$$Wavenumber, k = 2\pi/\lambda \tag{13}$$

$$Wave\ celerity, c = \omega/k \tag{14}$$

$$Wave\ steepness, s = H/\lambda \tag{15}$$

Ocean waves are governed by water depth as the seabed influences the water particle motion. (**Figure 3-7**). Water particle motion from ocean waves does not occur at depths greater than half a wavelength. Therefore, in deep waters the water particles move in an orbital shape and the seabed does not affect the waves. However, as depth decreases the seabed causes a change in the pattern of motion of the water particle from orbital shape into elliptical shape.
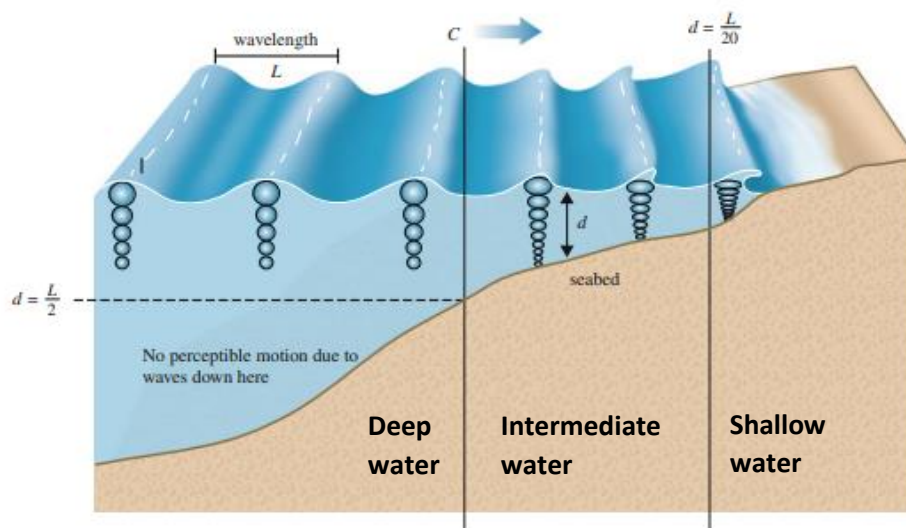
Figure 3-7. Motion of water particles in waters of varying depth (Folley 2017).

Another important characteristic of ocean waves is that they are dispersive. This means that for a given depth, waves of different frequencies travel at different speeds. Therefore, for a given frequency, the wavelength, and hence wave speed, must change with depth. This phenomenon is known as dispersion and the importance of this phenomenon is discussed after the theory of a regular wave which is presented next.

Regular waves can be modelled by different theories; **Figure 3-8** shows the applicability of different wave theories which are determined by relative water depth and wave steepness. Linear wave theory is valid for a wave steepness below 0.001. Above this value the theory begins to lose accuracy and higher-order wave models such as 2nd order Stokes theory become more appropriate. On the other hand, the application of higher-order wave models when analysing anything other than regular waves is extremely strenuous. As of consequence, linear wave theory is widely used for modelling ocean waves beyond its bound, even when wave steepness exceeds 0.001. It needs to be recognized though that this is not entirely correct and is a limitation of wave theory applicability (Folley 2017).

The main purpose of modelling ocean waves is to obtain the dynamic and kinematic properties such as dynamic pressure, velocities, and accelerations which are used to calculate the hydrodynamic loads. Linear wave theory can be used to represent wave kinematics and is based on the assumptions of homogenous, incompressible, inviscid fluid and irrotational flow. With such assumptions, a velocity potential exists which satisfies the Laplace equations. The velocity potential and wave kinematics can be found by applying the kinematic boundary conditions and the dynamic free-surface conditions. A derivation is not provided here, however more information can be found in most offshore engineering or fluid mechanics textbooks. Before the kinematics are calculated, the effect of water depth must be considered; this is known as the dispersion relation.
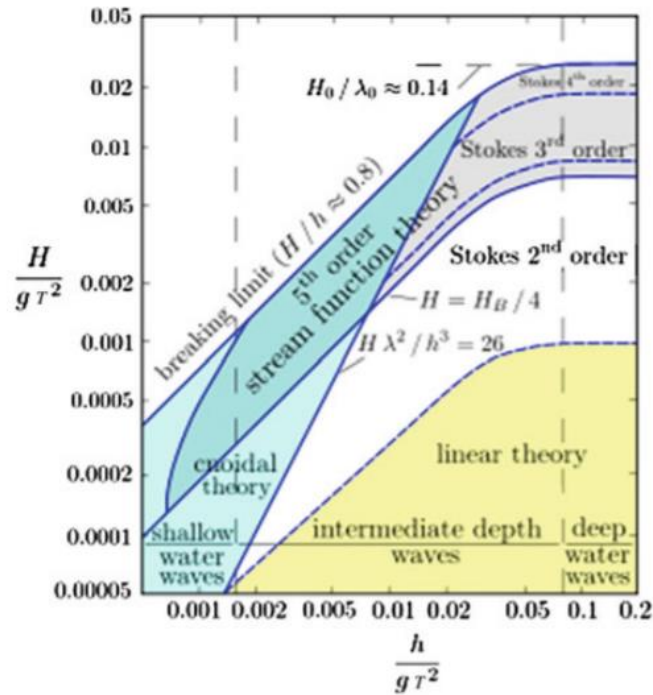
Figure 3-8. Chart of wave model suitability.

The wavenumber k is equal to $2\pi/\lambda$ where λ is the wavelength; the angular frequency, ω is equal to $2\pi/T$ where T is the period. The dispersion relation relates wavelength and period:

$$\omega^2 = gk\tanh(kd) \tag{16}$$

where d is the water depth. Depending on the classification of water depth in relation to the wavelength, simplified versions of the dispersion relation may be adopted, for example, if the water is deep ($d > 0.5\lambda$):

$$\omega^2 = gk$$

$$\lambda = 1.56T^2 \tag{17}$$

and if the water is shallow ($d < \lambda/20$):

$$\omega = \sqrt{gd}\,k$$

[18]

$$\lambda = T\sqrt{gd}$$

Once the water depth has been classified considering the wavelength, the wave kinematics can be calculated using the appropriate formula.

3.1.2.1.2 Irregular wave

In reality an ocean's surface is a composition of waves with different frequencies and directions. The interaction of waves from different directions creates difficulty when mathematically modelling wave conditions. A significant development in the representation of the ocean's surface is definition by a spectrum. The practical way of modelling ocean waves assumes the ocean surface forms a stochastic wave field that can be assumed to be stationary in a short-term period. The stationary assumption of the wave is site-dependent, and this assumption works well for most offshore engineering applications and gives good agreement with full-scale measurements. To understand the concept of the wave spectrum it is first necessary to accept that the variation in water surface can be represented as the linear superposition of sinusoidal waves (regular waves) of different frequencies, amplitudes, directions, and phases (**Figure 3-9**). The wave spectrum is generally used to fully define any

sea-state, with the assumption that there is a random phase between all the individual wave components, a natural consequence of the assumption of linear superposition.
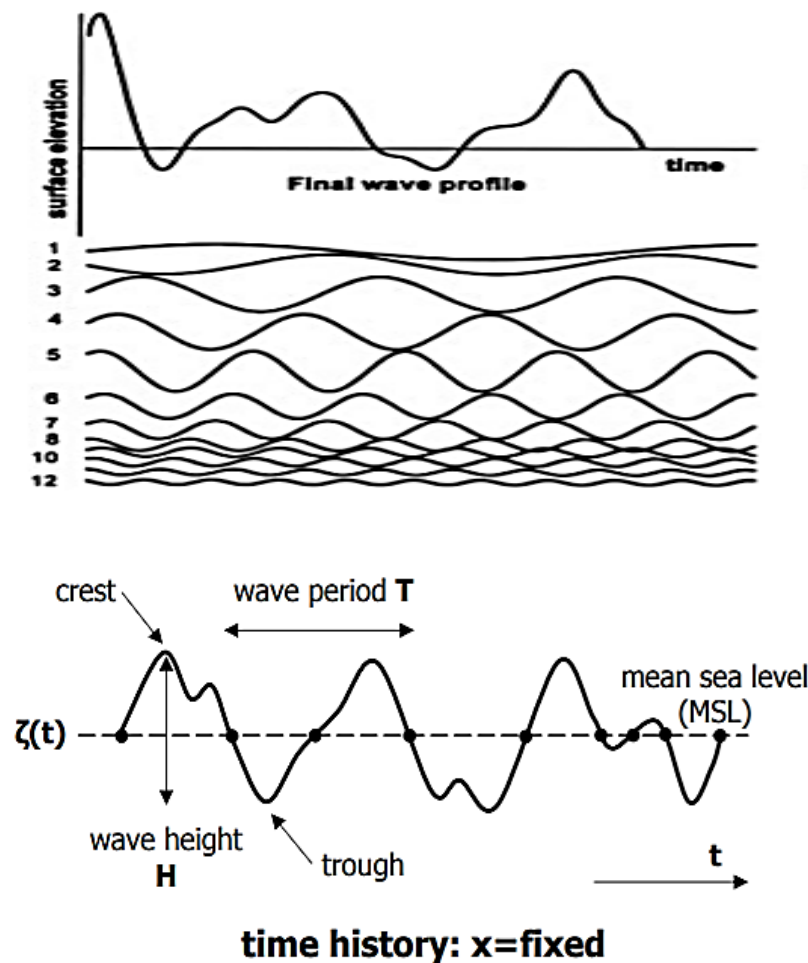
Figure 3-9. Superpositioning of waves to create water surface elevation and irregular wave definition.

The most applied mathematical models to represent the ocean wave spectrum include the Pierson-Moskowitz (PM) and Joint North Sea Wave Project (JONSWAP) spectra. The PM spectrum is used for a fully developed sea and assumes that the wind has been blowing across a sufficiently large expanse of water for an extended period that the waves are in equilibrium with the wind i.e., the sea state is fully developed and so that the spectrum is dependent only on wind speed. The JONSWAP spectrum is commonly applied to represent sea states that are not fully developed, or a growing wind sea. The Torsethaugen spectrum (two-peaked wave

spectrum) is used to define seas comprising wind-generated waves and swells (Karimirad 2012).

3.1.2.1.2.1 Pierson-Moskowitz spectrum

The PM spectrum is formulated in terms of two parameters: the significant wave height and the average (mean zero-crossing) wave period. The form of the PM spectrum used here is considered of more direct use compared to the classic form (in terms of the single parameter wind speed), and the form involving peak frequency. The spectral ordinate at a frequency (in rad/s) is given by:

$$S(\omega) = 4\pi^3 \frac{H_s^2}{T_Z^4} \frac{1}{\omega^5} \exp(-\frac{16\pi^3}{T_Z^4} \frac{1}{\omega^4}) \qquad [19]$$

where H_s is the significant wave height; T_z is mean zero crossing period; ω is wave frequency in rad/s. It was found that a good estimate of the significant wave height, H_s, was given using the average height of the third highest waves. The following relationships exist between T_Z, T_1, and T_0:

$$T_0 = 1.408T_Z$$

$$[20]$$

$$T_1 = 1.086T_Z$$

where T_0 is the peak period and T_1 is the mean wave period. Furthermore, the start and end frequencies of the PM spectrum can be specified using the following definitions:

Start frequency (in rad/s):

$$\omega_s = 0.58 \frac{2\pi}{T_Z} \qquad [21]$$

End frequency (in rad/s):

$$\omega_f = 5.1101 \frac{2\pi}{T_z} \qquad [22]$$

3.1.2.1.2.2 JONSWAP Spectrum

The JONSWAP spectrum can account for the imbalance of energy flow in the wave system, for instance when the seas are not fully developed. Energy imbalance is nearly always the case when there is a high wind speed. The spectral ordinate at a frequency is given by:

$$S(\omega) = \frac{\alpha g^2 \gamma^a}{\omega^5} \exp\left(-\frac{5\omega_p^4}{4\omega^4}\right) \qquad [23]$$

where ω is the wave frequency (rad/s); ω_p is peak frequency; α is a constant that relates to the peak frequency of the wave spectrum and wind speed; γ is the peak enhancement factor (this parameter defines the shape of the peak of the spectrum. When the peak enhancement factor equals 1.0, the spectral shapes of both the JONSWAP and PM spectra are identical. Thus, it can be inferred that the bandwidth of the spectrum is dependent on its state development with new and developing seas having a narrower bandwidth so that the wave components are all at similar frequencies and fully developed seas having a broader bandwidth, with the wave energy spread over a larger range of frequencies.); and

$$a = \exp\left(-\frac{\left(\omega - \omega_p\right)^2}{2\sigma^2 \omega_p^2}\right)$$

$$\qquad [24]$$

$$\sigma = \begin{cases} 0.07 & where \ \omega \leq \omega_p \\ 0.09 & where \ \omega > \omega_p \end{cases}$$

3.1.3 Current

Currents can be driven by several factors including tides, wind, and thermohaline circulation. The rise and fall of tides create currents in the oceans, near the shore, and in bays and estuaries. Modelling current is typically done by defining a uniform current velocity and/or a current profile with depth (which is similar to a wind profile with height):

- Uniform current is defined by a current velocity U_0 and a heading θ_0 (in degrees) in a fixed reference axis. Uniform current is constant from the seabed to the water surface.

- Current profile is defined by a series of current velocities with an amplitude (U_z) and direction (θ_z) at specific depths (z).

The change in current speed with depth normally follows a 1/7 power law decay. The total current velocity at a specified position (z-axis) is the sum of uniform current and the profiled current velocity:

$$\vec{U}_c(z) = (U_0 \cos \theta_0 , U_0 \sin \theta_0 , 0) + (U_z \cos \theta_z , U_z \sin \theta_z , 0) \qquad [25]$$

3.1.4 Wave-current interaction

The interaction between waves and currents is important in the simulation of offshore structures. The fluid drag force on slender members of a floating structure can be significantly increased from the combined fluid particle velocity of currents and waves. In addition, currents also affect the diffraction and radiation forces on the floating structure. Under the assumptions of constant water depth and steady current with depth, a regular wave propagating on the current can be modelled by linear wave theory, except the wave period relative to a stationary observer should be shifted as:

$$\frac{\lambda}{T_e} = \frac{\lambda}{T} + U_c \cos\theta \qquad\qquad [26]$$

where λ is the wavelength; T_e is the wave period relative to stationary observer; T is the wave period relative to current; U_c is the current speed amplitude; and θ is the angle between the waves and current (ANSYS 2020).

3.2 Theory, modelling, and simulation of a CFOES

Sophisticated numerical tools are required for the detailed design and analysis of ORE systems. Mathematical models and simulation code are the foundations to a numerical tool, and a comprehensive understanding of these is required in order to build numerical models of complex systems, which can produce representative results. Additionally, in numerical model development, a range of modelling approaches exist so it is important to know the differences between these approaches to ensure adequate model fidelity. Finally, to ensure the predictions made by the numerical model are credible, validation and verification of numerical models is compulsory. Thus, this section explains the numerical tools available to perform concept modelling, the underlying mathematical models and simulation code of these numerical tools, and the modelling approaches which can be used to develop models within them, in the context of a CFOES. The section concludes with a discussion on how to validate and verify numerical models.

3.2.1 Numerical tools

Several numerical tools are available for the advanced design and analysis of pure ORE systems such as wind turbines or WECs. On the other hand, no tools exist explicitly for the design and analysis of CFOESs. To develop a numerical model of a CFOES, will require modifying the tools purposed specifically for the analysis of the pure ORE systems, in a way

which can predict the fully coupled responses of a CFOES. A FOWT can be considered the central system of a CFOES due to its rated power capacity and structural size, and the other renewable energy systems are an addition which make up the CFOES. This idea translates through to numerical modelling: at the centre of the numerical model will be the computational modules representing the different dynamic domains of a FOWT, then, to incorporate other energy generation systems into the model, either some of these modules will be expanded, or an additional module will be needed and coupled to the main numerical model. As such, this section, and the subsequent sections, describe the mathematical models underlying the core computational modules within the numerical tools available for a FOWT. Time-domain methods are almost exclusively used for wind turbine calculations today. This is because of the ready availability of computing power which means the superior efficiency of frequency-domain methods is no longer an important consideration (Burton et al. 2011).

Within each numerical tool are various modelling options to choose from which represent certain aspects of the structure or environment. Generally, making a decision on a numerical modelling method is a trade-off between model fidelity, accuracy, and computational efficiency (Otter et al. 2022). Model fidelity describes the level of detail that a numerical model can represent the physics. Accuracy is the difference between the measured physical responses from experimentation and the predicted responses from the numerical model. Computational efficiency refers to the amount of time required for a numerical simulation to complete. Typically, numerical models can have three levels of fidelity: low-, mid-, and high-fidelity. The level of fidelity is chosen based on the objective function of the simulation and the accuracy that is required. In the design of ORE structures, low-fidelity models are typically used for preliminary concept design, sizing analysis and optimization. Mid-fidelity models, or engineering-level tools, are used for loads analysis to examine the concept design in operational and extreme environment conditions. High-fidelity models are used for detailed and specific

investigations. High-fidelity models provide a level of confidence that a certain degree of accuracy is achieved during simulation which comes at the expense of computational resources. Moreover, higher fidelity tools may also be used to tune lower fidelity ones.

Engineering tools, or mid-fidelity software, are typically used for global dynamics and loads analyses of FOWTs. Some popular options include:

- Bladed

- HAWC2

- OpenFAST

- Orcaflex

- SIMA

Most engineering tools follow a similar approach to model a FOWT which is the coupling of different computational codes, or "modules", representing the different dynamic domains to form the numerical tool. Models built within these engineering tools are typically referred to as aero-hydro-servo-elastic models. The term 'aero-hydro-servo-elastic' implies there is a coupling between the codes: at each time step, the model simultaneously calculates the aerodynamic loads and responses (aero), the hydrodynamic loads and responses (hydro), the control system responses (servo) and the deformation response of the structure due to elasticity (elastic) (National Renewable Energy Laboratory (NREL) 2022). A typical interface scheme for an aero-hydro-servo-elastic numerical tool is depicted in **Figure 3-10**. Simulations within these tools use numerical techniques to integrate the equations of motion over time, by subdividing the time into short time steps. In this way, all nonlinearities and non-stationary aspects of the system can be dealt with to any desired level of accuracy. In terms of integrating the equations of motion, there are a number of different algorithms or solvers. Some use a fixed time step (which has to be short enough to account for all modal frequencies which are

considered important), while others use a variable time step which is continually adjusted during the simulation, keeping it as long as possible to maximise simulation speed while still keeping all the integrated states within a certain error tolerance. The use of variable time step methods also allows accurate modelling of discontinuities because close to a discontinuity the time step can be adjusted to find the exact moment when the characteristics of the system change (Burton et al. 2011).
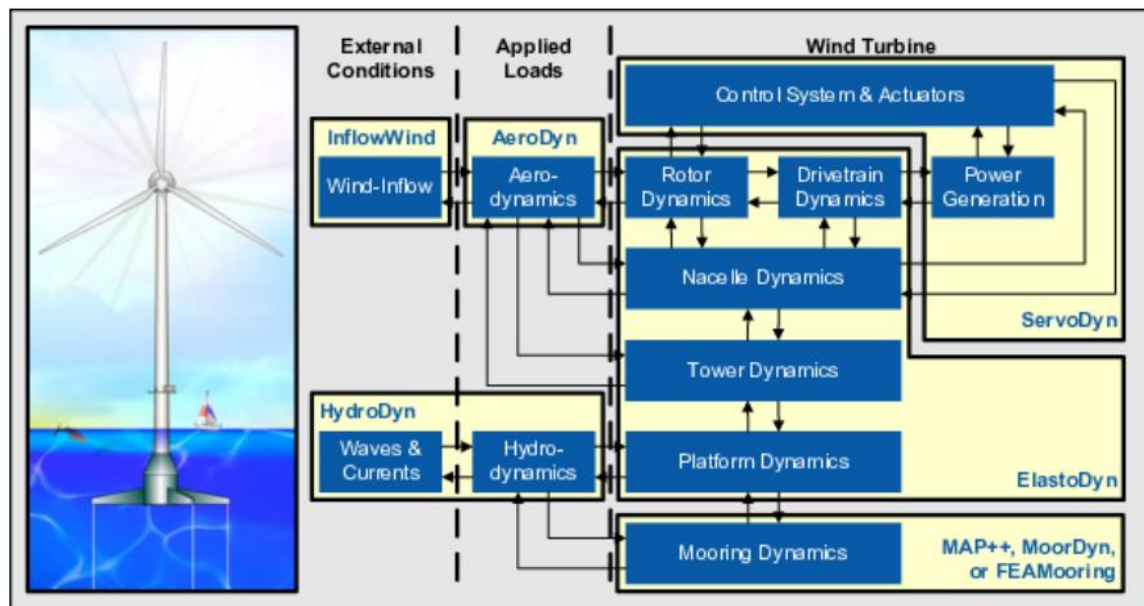
Figure 3-10. OpenFAST schematic (National Renewable Energy Laboratory (NREL) 2022).

For each domain, different modelling approaches are available to represent the environment phenomena such as the wind, or the dynamics of the different structural components of a FOWT. However, often there is a "most common" modelling approach for each. However, because of such differences, discrepancies between engineering tools arise which is why it is imperative that there is validation and verification of numerical models and tools. **Table 3-1** details some engineering tools and the modelling approaches used (Borg and Bredmodes 2015). For FOWTs, most engineering tools will require input from a frequency-domain potential flow solver such as AQWA, Nemoh, WAMIT, or Wadam. The potential flow solvers will calculate the hydrodynamic coefficients which are subsequently used to solve the

hydrodynamic radiation/diffraction problems during simulation. The next sections will discuss the dynamic domains in detail individually, reviewing the modelling approaches, and their advantages and disadvantages.

Table 3-1. Examples of engineering tools and modelling methods.

Engineering tool	Aerodynamics	Hydrodynamics	Structural dynamics	Mooring line dynamics	Controller modelling
AQWA	-	PF + MD or ME	RB or FEM	GSM or QSM or FEM	-
WAMIT	-	PF	RB or Modal	GSM	-
Bladed	BEMT + DI + DS	PF + MD or ME	Modal or MBS	GSM or QSM or FEM	DLL
HAWC2	BEMT + DI + DS	PF + MD or ME	MBS/FEM	GSM or QSM or FEM	DLL or UD
OpenFAST	BEMT + DI + DS or GDW	PF + MD or ME	Modal or MBS	GSM or QSM or FEM	DLL, UD, or SM
Orcaflex	Coupled to FAST	PF + MD or ME	Coupled to FAST	GSM or QSM or FEM	Coupled to FAST
SIMA (SIMO/RIFLEX)	BEMT + DI + DS	PF + MD or ME	MBS	GSM or QSM or FEM	DLL or UD

3.2.2 Aerodynamic modelling

There are numerous methods available for computing the aerodynamic loads on a wind turbine rotor which vary in simulation fidelity. They include Blade Element Momentum Theory (BEMT), Generalized Dynamic Wake Theory (GDWT), Computational Fluid Dynamics (CFD) and free vortex wake methods (Yu et al. 2020). For the aerodynamics, all these codes generally use BEMT, as this is currently the only way to achieve rapid enough simulations for the standard sets of load calculations which are normally needed. More advanced aerodynamic methods such as vortex wake and panel methods are starting to be used to examine specific

cases where BEM is not sufficiently accurate. Such cases might include flexible rotors, dynamic wakes, and skewed flows. At the top-level are CFD methods based on direct solution of the Navier-Stokes equation which could be used, and some general commercial CFD codes are now available such as STAR-CCM+, but the downside to these methods is the computational cost and in practice, the number of simulations that can be performed are limited meaning application of these methods is only used for specific detailed case studies (Shaler et al. 2020).

3.2.2.1   *Blade element momentum theory*

BEMT is the most employed method for calculating the wind turbine rotor aerodynamic loads. The computational requirement is low, and it is proven to give reliable results for steady-state operating conditions which is why in the wind turbine industry it is the main method for aerodynamic load analysis (Bangga 2018). BEMT originates from two other theories: blade element theory and momentum theory.

3.2.2.1.1   Blade element theory

Blade element theory assumes that the turbine blades can be discretized into a finite number of small elements that each act independently of one another and work aerodynamically as two-dimensional aerofoils so that the elemental aerodynamic forces can be calculated based on the local flow conditions. Each of the blade's elements will experience a slightly different flow as they have different rotational speed (Ωr), chord length (c), and twist angle (γ). These elemental forces are integrated across the blade span to determine the overall performance of each blade and the total forces and moments applied on the rotor. From blade element theory, the thrust distributed around an annulus of width dr is equivalent to:

$$dT = \frac{1}{2} \rho W^2 (C_L cos\varphi + C_D sin\varphi) cdr \tag{27}$$

where W is the relative velocity; C_L is the lift coefficient; and C_D is the drag coefficient. The torque produced by the elements in the annulus is equal to:

$$dQ = \frac{1}{2} \rho W^2 (C_L sin\varphi - C_D cos\varphi) crdr \tag{28}$$

3.2.2.1.2   Momentum theory

Momentum theory assumes that the pressure differential across the rotor plane is attributed to the work done by the airflow passing through the rotor. As air nears the rotor it slows down gradually, resulting in an increase in static pressure in the region in front of the turbine. As air flows through the rotor, static pressure is reduced which causes the fluid in the region behind the rotor to have a reduction in pressure compared to the free stream conditions. As the fluid proceeds downstream, the pressure climbs back to the free stream resulting in a further slowing down of the flow. Consequently, there is a reduction in the kinetic energy of the flow, some of which is converted into useful energy by the turbine. To understand this further, consider the relation between flow velocity at the rotor disk U_d and the upstream wind velocity U_0:

$$U_d = (1 - a)U_0 \tag{29}$$

The reduced flow velocity at the rotor is dependent on a, the axial flow induction factor. By applying Bernoulli's equation and assuming uniform and incompressible flow, the thrust T acting on the rotor disk can be derived to give:

$$T = 2\rho A U_0^2 a(1 - a) \tag{30}$$

where A is rotor swept area and ρ is fluid density.

Similarly, the power P_{WT} generated by the wind turbine, can be found:

$$P_{WT} = 2\rho A U_0^3 a(1-a)^2 \qquad [31]$$

The total wind power available is:

$$P = \frac{1}{2} A \rho U_0{}^3 \qquad [32]$$

The efficiency of a wind turbine η_{WT} can then be given in terms of the axial induction factor:

$$\eta_{WT} = C_p = \frac{P_{WT}}{P} = \frac{2\rho A U_0^3 a(1-a)^2}{\frac{1}{2} A \rho U_0^3} = 4a(1-a)^2 \qquad [33]$$

and

$$C_T = \frac{2\rho A U_0^2 a(1-a)}{\frac{1}{2} A \rho U_0^2} = 4a(1-a) \qquad [34]$$

The value of a that maximizes wind turbine efficiency is determined by setting the derivative of η_{WT} with respect to *an* equal to zero and solving for a. It gives $a = \frac{1}{3}$. Substituting this value of a into the wind turbine efficiency relation gives an efficiency of 59.3% (Hansen 2008). This is known as the Betz limit and is the theoretical upper limit for the efficiency of turbines. The axial induction factor describes how well the wind turbine affects the wind velocity. An induction factor of 1 means that the wind turbine does not affect the upwind velocity at all, whereas a value of 0 means that the turbine completely blocks/stops the wind. The thrust coefficient C_T has a maximum value of 1 when a is $\frac{1}{2}$. In practice, turbines typically operate at an efficiency between $30 - 40\%$ with a maximum limit of 50%.

The theory above provides an estimate of the energy extracted from the wind flow without considering that the power absorbed by the rotor is the product of torque Q and angular velocity

Ω of the rotor. The torque developed by the rotor must impart an equal and opposite rate of change of angular momentum to the flow and therefore induces a tangential velocity to the flow. The change in tangential velocity is expressed in terms of an angular induction factor a'. If the conservation of angular momentum is applied to this annular stream tube, an equation for the tangential force on an annular element of fluid can be derived. The blade wake rotates with an angular velocity ω and the blades rotate with an angular velocity Ω. For a small element, the corresponding torque will be:

$$Q = \frac{dI\omega}{dt} = \frac{d(mr^2\omega)}{dt} = \frac{dm}{dt}r^2\omega \qquad [35]$$

$$dT = d\dot{m}\omega r^2 \qquad [36]$$

For a rotating annular element:

$$d\dot{m} = \rho A U_d \qquad [37]$$

$$dm = \rho 2\dot{\pi} r dr U_d \qquad [38]$$

$$dQ = \rho 2\pi r dr U_d \omega r^2 = \rho U_d \omega r^2 2\pi r dr \qquad [39]$$

Define angular induction factor, *a'*:

$$a' = \frac{\omega}{2\Omega} \qquad [40]$$

Recall that $U_d = U_0(1 - a)$:

$$dQ = 4a'(1 - a)\rho U_0 \Omega r^3 \pi dr \qquad [41]$$

Momentum theory has therefore yielded equations for axial (Equation 30) and tangential (Equation 36) force on an annular element of fluid. The axial and tangential induced velocities can be calculated from the momentum lost in the flow, and these affect the inflow and therefore

also the forces calculated by blade element theory. Relating the induced velocities in the rotor plane to the elemental forces, the thrust extracted by each rotor annulus is equal to:

$$dT = 4\pi r \rho U_\infty^2 (1 - a) a \, dr \qquad [42]$$

and the torque extracted from each annular section is equivalent to:

$$dQ = 4\pi r^3 \rho U_\infty \Omega (1 - a) a' \, dr \qquad [43]$$

Equations 27 – 28 and 42 – 43 form BEMT and when the two-dimensional aerofoil tables of lift and drag coefficients as a function of angle of attack are included, an iterative process has been set up to determine the aerodynamic forces and induced velocities on each blade element. However, before solving the system of equations, corrections need to be applied to consider other aerodynamic effects. These corrections include Prandtl hub- and tip-loss models which account for vortices shed at these locations, Pitt and Peters skewed wake correction to model the effects of incoming flow that is not perpendicular to the rotor plane and Beddoes-Leishman dynamic stall model to consider unsteady aerodynamics (Zhao et al. 2021).

3.2.3   Hydrodynamic modelling

A floating structure is subject to hydrostatic and hydrodynamic loads which both require modelling. Hydrostatic loads are the fluid loads acting on a body when placed in still water. Hydrodynamic loading is mainly the result of kinematics of water particles in waves, interactions between waves and the structure, and motions of the structure (ANSYS 2020).

3.2.3.1   Hydrostatic loads

The volume of water displaced by a body which is partially or fully submerged can be calculated by integrating over the wetted surface area of the body:

$$\nabla = \int_{S_0} Z n_3 \, dS \qquad [44]$$

where S_0 is the wetted surface of the body in still water; $\vec{n} = (n_1, n_2, n_3)$ is the unit normal vector of the body surface pointing outwards; and Z is the vertical coordinate of a wetted surface point.

The buoyancy force is the vertical upthrust as a result of this displaced water by the structure:

$$F_B = \rho g \nabla \qquad [45]$$

where ρ is density of seawater.

The hydrostatic force and moment can be determined by integrating the hydrostatic pressure over the submerged area of the body:

$$\vec{F}_{hys} = -\int_{S_0} p_s \vec{n} \, dS$$

$$\vec{M}_{hys} = -\int_{S_0} p_s (\vec{r} \times \vec{n}) \, dS \qquad [46]$$

where $p_s = -\rho g Z$ and represents the hydrostatic pressure and $\vec{r} = \vec{X} - \overrightarrow{X_g}$ represents the position vector of a point on the hull surface.

3.2.3.2 Hydrodynamic loads

Among all the environmental loads, the dynamic wave-induced load is the one of the most significant and plays a critical role in ORE structural design. Hydrodynamic loading is primarily wave-induced with main contributions coming from water particle kinematics, the interaction between waves and the structure, and motions of the structure. In other words, wave

loading can be loosely separated into three load types: a diffraction load, an inertia load, and a drag load. The diffraction load arises from the existence of the structure which modifies the ambient fluid flow and pressure field, the inertia load is exerted by disturbed waves induced by the structure motions, and viscosity gives rise to drag (Barltrop 1988). Wave-induced loads can be further subdivided into different frequency ranges depending on the dynamic behaviour and flexibility of the structure. The low frequency loads are the second order wave exciting force which are relatively small in magnitude but results in free drifting motions to unrestrained structures or slowly varying rigid body motions to moored structures. Responses at wave-frequencies are the first order rigid body motions and accelerations. Loads in this case are due to first order hydrodynamic pressures around the hull which induce local loads, and when integrated results in global loads. High frequency loads arise from impact type of localized hydrodynamic pressures that the structure experiences during events such as slamming. These high frequency loads are for example the springing and whipping loads inducing dynamic and transient vibratory responses on the hull. Among these three broad classes of loads in the three frequency ranges, the global loads induced by the first order wave-frequency hydrodynamic pressure remain the most significant for overall ORE structural design (Computation of wave-induced motions and loads on catamaran hulls with forward speed (Sen and Negi)).

Two main methods can be used for modelling these hydrodynamic loads: Morison's equation and potential flow theory. The applicability of these two theories is dependent on the size of the structure being modelled and the water flow regime (Robertson et al. 2014b), and can be assessed through three dimensionless parameters: (1) the Keulegan-Carpenter number; (2) the Reynolds number; and (3) the diameter-to-wavelength ratio. These parameters define the relative importance of inertia, diffraction, and drag for different flow regimes. For codes which enable using a combined-theory approach such as AQWA, the potential-flow solution is used to model the radiation and diffraction loads of large-volume components by diffracting

panels, while Morison's equation is used to model the viscous-drag loads of small cross-sectional components by Morison elements (Offshore Code Comparison Collaboration Continuation Within IEA Wind Task 30: Phase II Results Regarding a Floating Semisubmersible Wind System). **Figure 3-11** graphically shows the validity of each hydrodynamic loading model and when is most appropriate depending on the design case. It can be seen as the diameter-to-wavelength ratio increases viscous effects become less important and vice versa. In some cases, it is possible to combined both theories where potential flow theory is used to model the radiation and diffraction loads, while Morison's equation is used to model the viscous drag loads. This is often the approach used for semisubmersibles which have a combination of slender components as well as large volume components comprising its floater.
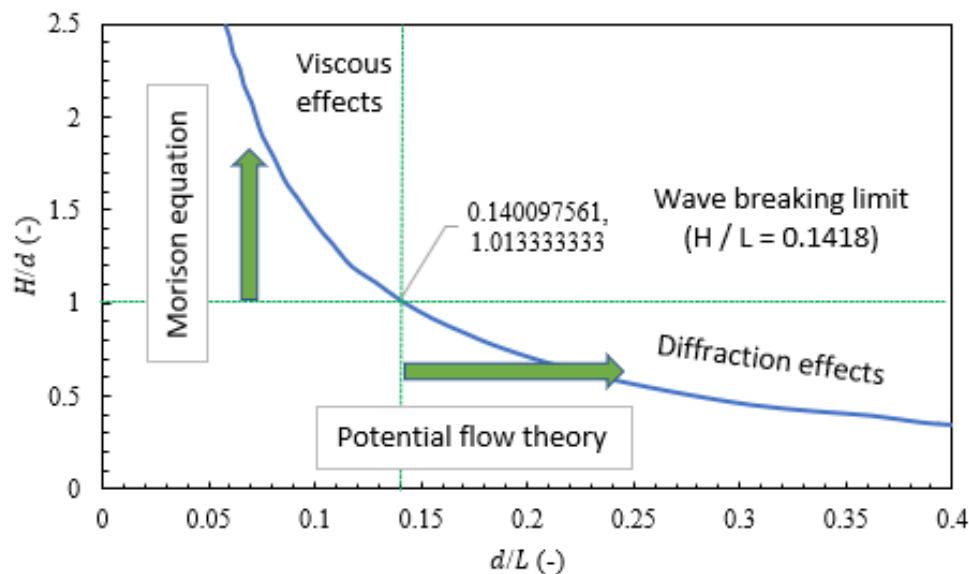
Figure 3-11. Regions of validity of Morison's equation and potential flow theory.

3.2.3.2.1 Morison's equation

In offshore hydrodynamics, Morison's equation is commonly employed to calculate the hydrodynamic loads on slender structures when flow separation occurs, and the viscous effects

are prevalent. Morison's equation is an empirically derived hydrodynamic loading model that includes excitation from waves (with a long wavelength approximation), added mass effects, and viscous forces. The theory can be enhanced by integrating the Morison forces up to the instantaneous water surface elevation using a wave stretching approach such as Wheeler stretching (reference) and/or by applying the forces at the instantaneous position of the displaced body in the water. The inclusion of these methods results in higher order loads (including a mean-drift force) on the structure. The relative form of Morisons equation can be broken down into 3 contributions:

$$F = \underbrace{(C_m - 1)\rho \frac{\pi D^2}{4} L(\dot{u} - \dot{v})}_{Added\ mass} + \underbrace{\rho \frac{\pi D^2}{4} L\dot{u}}_{Froude-Krylov} + \underbrace{\frac{1}{2} C_d \rho DL |u - v|(u - v)}_{Viscous\ drag} \qquad [47]$$

where C_m is the inertia coefficient ($C_m = C_a + 1$); $\boldsymbol{u}$ is the velocity vector of water particle and $\boldsymbol{v}$ is the structural velocity vector.

The added mass contribution accounts for the additional mass of water surrounding a body that must be accelerated with the relative movement of the body to the fluid. This force is applied onto the body through the action of pressure and is frequency dependent. Generally, added mass coefficients can be found in literature to inform simulation predictions. The Froude-Krylov contribution is analogous to hydrostatic pressure and arises due to a pressure gradient in the fluid inducing the acceleration in the wave. As such this is only a function of the acceleration of the fluid and is independent of the movement of any body and cross-sectional shape i.e., a circle with the same cross-sectional area as a square will have the same Froude-Krylov force. The viscous drag contribution arises as a result of a drag force as the fluid flows past the structure. Most structural elements are cylindrical, although this is certainly not always the case, and so the drag on the member in steady flow is highly dependent on Reynolds number. In oscillatory flow the perceived drag coefficient is also dependent on KC number

with relations for drag coefficients found in literature. Both numbers have applicable ranges where they can be applied. Furthermore, the quadratic model of drag is a simplification whereby the loading is actually unsteady in reality and therefore does not include effects that could be important such as vortex shedding and resulting structural resonance.

3.2.3.2.2 Linear potential flow theory

When the size of the structure in the water is large compared to the incident wavelength, the water will remain attached as it flows past the structure which means diffraction/radiation effects become significant. This means a different approach must be used to the Morison equation as this model is no longer valid. Linear potential flow theory can be used to represent external flows around bodies which do not separate. Often, only the linear portion of the potential flow solution is used in offshore wind simulations. Some codes, offer the option of including second order terms but generally these are neglected except for specific analyses. For a bluff body in waves, its radiation and diffraction problems must be solved to obtain the hydrodynamic coefficients required for subsequent analysis of its dynamic behaviours. Three-dimensional panel methods, or Boundary Element Methods (BEM) are the most common numerical tools to analyse the hydrodynamic behaviour of large volume structures in waves such as AQWA and WAMIT. These methods are based on potential flow theory and represent the structure surface by a series of diffraction panels. In general, BEM apply source or dipole functions on the surfaces of submerged bodies and solve for their strength so that all boundary conditions are met. Once these velocity potential fields have been solved, excitation forces, added mass and damping matrices in addition to wave field pressure, velocity and surface elevation can be found (Bosma et al. 2012). The computations may be performed directly in the time domain, or they may provide frequency-domain transfer functions to be used in another time domain simulation code using the Cummins equation for example OpenFAST.

Application of potential flow theory is done based on the assumption that the fluid is irrotational (without vorticity), incompressible (constant density), and inviscid (zero viscosity). The fluid field velocity around the floating body is calculated once the velocity potential, ϕ, as a function of spatial displacement x, y, z and time, t and the relevant boundary conditions satisfy the conservation of mass and momentum conditions, or known better as the Laplace equation (Equation 48):

$$\nabla^2 \phi = 0 \qquad\qquad [48]$$

In addition, the total velocity potential induced by fluid flow around the body can be expressed as a combination of incident wave, diffraction (incoming waves would scatter due to existence of floating body) and radiation (waves are radiated due to structure motions). This is represented by Equation 49:

$$\phi(x, y, z; t) = \phi_I(x, y, z; t) + \phi_D(x, y, z; t) + \phi_R(x, y, z; t) \qquad\qquad [49]$$

$$\phi_R(x, y, z; t) = \sum_{j=1}^{6} \zeta_j \phi_{R_j}(x, y, z; t) \qquad\qquad [50]$$

where $\phi_I(x, y, z; t)$ is the incident wave component of velocity potential in space and time, $\phi_D(x, y, z; t)$ is the spatial diffraction wave potential as a function of time, $\phi_R(x, y, z; t)$ is the radiation potential also in space and time. $\phi_{R_j}(x, y, z; t)$ is the radiation potential of the floating body induced by the platform movement in the j-th mode, ζ_j represents the platform's displacement in the j mode under the action of a unit wave amplitude, and $j = 1,2 \ldots, 6$ represents the floating body's six degrees of freedom (surge, sway, heave, roll, pitch and yaw).

Detailed representation of the incident wave potential $\phi_I(x, y, z, t)$ is given in equation (Equation 51) as:

$$\phi_I(x,y,z,t) = \frac{-iga}{\omega_0} e^{k_0 z} e^{i(k_0 x \cos\theta + k_0 y \sin\theta - \omega_0 t)} \qquad [51]$$

where i is the imaginary unit component of the incident wave, a is the unit incident wave amplitude, gravitational acceleration is represented by g, while k_0 is the wave number, and θ is the incident wave angle.

When the wave velocity potentials are known, the first-order hydrodynamic pressure distribution may be calculated using the linearized Bernoulli equation given in Equation 52.

$$p = -\rho \cdot \frac{\partial \phi(x,y,z,t)}{\partial t} \qquad [52]$$

Following the prediction of the water pressure distribution, the various fluid forces may be obtained by integrating the pressure over the wetted surface of the body.

The first order hydrodynamic force and moment components can be represented in a generalized form:

$$F(x,y,z;t) = \iint_S p \cdot n_j(x,y,z;t) dS =$$
$$= -i\omega\rho \iint_S [\phi(x,y,z;t)] \cdot n_j(x,y,z;t) dS \qquad [53]$$

where ρ is the seawater density (kg/m^3), S is the floating body's wetted body surface area (m^2) and n_i is the wetted body surface's normal vector in the j-th mode.

From Equation 49 and 50, the total first order hydrodynamic wave force can be written as:

$$F_j = \left[\left(F_{I_j} + F_{D_j} \right) + \sum_{k=1}^{6} \zeta_k F_{R_{jk}} \right] \text{ where } j = 1,6 \qquad [54]$$

where Equation 55 defines the jth Froude-Krylov force, F_{I_j}, due to incident wave:

$$F_{I_j} = -i\omega\rho \iint_S [\phi_I(x,y,z;t)] \cdot n_j(x,y,z;t)dS \qquad [55]$$

Equation 56 defines the diffracting force, F_{D_j}, due to diffraction:

$$F_{D_j} = -i\omega\rho \iint_S [\phi_D(x,y,z;t)] \cdot n_j(x,y,z;t)dS \qquad [56]$$

Equation 57 defines the radiation force, $F_{R_{jk}}$, due to the radiation wave induced by the kth unit amplitude body rigid motion:

$$F_{R_{jk}} = -i\omega\rho \iint_S [\phi_{R_k}(x,y,z;t)] \cdot n_j(x,y,z;t)dS \qquad [57]$$

The hydrodynamic wave force can be further characterized in terms of active and reactive components. The active force, or the exciting force, is the combination of the Froude-Krylov force and diffraction force. The reactive force is the radiation force due to the radiated waves induced by body motions.

If the radiation wave potential is expressed in terms of real (Re) and imaginary parts (Im), then the added mass and radiation damping coefficients can be obtained:

$$
\begin{aligned}
F_{R_{jk}} &= -i\omega\rho \iint_S \{Re[\phi_{R_k}(x,y,z;t)] + iIm[\phi_{R_k}(x,y,z;t)]\} \cdot n_j(x,y,z;t)dS \\
&= \omega\rho \iint_S Im[\phi_{R_k}(x,y,z;t)] \cdot n_j(x,y,z;t)dS \\
&\quad - i\omega\rho \iint_S Re[\phi_{R_k}(x,y,z;t)] \cdot n_j(x,y,z;t)dS \\
&= \omega^2 A_{jk} + i\omega B_{jk}
\end{aligned}
\qquad [58]
$$

$$A_{jk} = \frac{\rho}{\omega} \iint_S Im[\phi_{R_k}(x, y, z; t)] \cdot n_j(x, y, z; t) dS \qquad [59]$$

$$B_{jk} = -\rho \iint_S Re[\phi_{R_k}(x, y, z; t)] \cdot n_j(x, y, z; t) dS \qquad [60]$$

where A_{jk} is the added mass coefficient and B_{jk} is the damping coefficient (Lin and Yang 2020).

A potential-flow model will capture excitation from waves (including diffraction) and radiation (including added mass and damping effects) but does not capture the viscous drag on the structure resulting from flow separation. Global damping coefficients are commonly applied in floating offshore industry to add damping to the global motions of the floater in order to match tank test results. Regardless of whether Morison's equation or potential flow theory is used, the represented wave loads will not be fully correct. When using Morison's equation, the wave radiation effect is disregarded, and when using potential flow theory, the viscous drag is missing. Therefore, a combination of the methods is sometimes used: potential theory plus viscous effects from Morison's equation. Often a slender model is used together with a panel method to introduce the effect of viscosity by drag forces on the Morison elements.

3.2.3.2.3 Other methods

It has become increasingly common to apply CFD when solving strongly nonlinear fluid-structure interaction problems. Examples of such problems are wave impact (slamming) and ringing loads in steep waves. CFD methods solve the Navier-Stokes equations in time domain by various numerical schemes, offering a more correct way to compute strongly nonlinear wave loads as well as dealing more properly with viscosity than other methods. CFD is also the most appropriate tool if one is to study vortex induced motions numerically.

3.2.4   *Structural dynamic modelling*

With the development of larger rotors and more powerful generators, the rated power capacity of modern wind turbines is growing. MingYang Smart Energy, a Chinese wind turbine manufacturer, currently holds the record for the biggest wind turbine in the world. The MySE 16.0-242 is an offshore hybrid drive wind turbine with 118 m long blades and a total rotor diameter of 242 m. For machines of this size to remain cost-effective, typically, the weight of the turbine is reduced which increases the flexibility of the structure and makes them more dynamically active (van der Tempel and Molenaar 2002). In this circumstance amongst, integrated structural design is required to ensure the additional flexibility of critical wind turbine components does not have a negative impact on the wind turbine performance. Just like aerodynamic and hydrodynamic modelling, structural dynamic models vary in sophistication.

In statics and dynamics, the simplest representation of a structure is to assume it is a single rigid body with a point mass and corresponding inertial characteristics. A rigid body model restricts deformation other than rigid body motions which are six modes of motion, three translational and three rotational. This model type is suitable for structures with low flexibility e.g., wind turbine hub and nacelle, and some types of floating platforms and WECs.

To improve on the accuracy and fidelity of a rigid body model would be to split a single rigid body representing a global system into a finite number of smaller rigid bodies, for example, to divide a FOWT system represented as a single rigid body into three smaller rigid bodies representing the Rotor-Nacelle Assembly (RNA), tower, and floater. Forces acting on the connections between these rigid bodies could then be investigated. For parts of a wind turbine that have significantly greater flexibility e.g., blades and tower, more sophisticated models are required. For these slender components flexibility can be introduced through a linear modal representation. This means a flexible structural component is represented by a

finite number of nodes, each able to move in six degrees of freedom. In linear modal representation small local deflection is assumed and the response of each node is determined from mass, stiffness, and damping matrices. The limitations of these models are that they are not strictly valid for large-amplitude displacements and deflections, often experienced by larger wind turbines.

The two principal approaches to the modelling of the structural dynamics of a FOWT in time-domain simulation packages is Finite Element Models (FEM) and the modal analysis method. These methods have been widely applied in commercial aero-elastic codes and proven to provide reliable results. FEM decomposes the structural component into small elements and the equations of motion are solved for each element with the boundary conditions matched at the interfaces between the elements. This can be computationally intensive since it results in thousands of equations to be solved simultaneously, but depending on applied formulation, this method can consider structural nonlinearities and large deformations.

To reduce this large computational requirement, modal models, or reduced order models, may be implemented to represent the wind turbine structural components. They apply a modal reduction scheme to reduce the number of degrees of freedom and predict just the first few modes of vibration of the main components, such as the blades and tower. The equations of motion are derived for the entire coupled system which is traditionally done by constructing the Lagrangian for the system including all degrees of freedom. Whilst modal models are computationally efficient, they are not suited to handle effects such as nonlinearities occurring at large deflections within each body.

More recently, modal reduction models combined with a multibody model have been used. A multibody formulation divides the model into a specified number of different bodies that are coupled using algebraic equations as constraints. Each of the bodies is modelled with a finite

element model or a finite element with a modal reduction model. This provides a powerful technique which is capable of handling nonlinear deflections and other nonlinearities, because the flexible components have been subdivided into a number of bodies. Large rotations are accounted for by the coupling interfaces while small deflections are assumed within the bodies. To model the motion and flexible behaviour, the multibody formulation introduces a moving frame of reference to each body. This allows for elastic deformations of each component to be solved linearly since the relative displacements (to the moving reference frame) are small (Borg et al. 2014). However, the structural component must be divided into a sufficient number of bodies so that small-angle assumption holds true and increasing the number of bodies comes at an expense of computational resources.

One example of a widely used commercial code based on the component mode approach is Bladed. Originally built using a Lagrangian approach, this code has been converted to use a multibody approach. Beam elements models for the blades and tower are combined with elements representing other components of the transmission system, the yaw and pitch actuators etc. The control system, which has major influence on the performance as well as the loads, can be modelled in full detail. By using a limited number of modes, the modal approach results in rapid calculations, so that a complete set of design or certification load cases, typically amounting to several hundred load cases each consisting of a ten-minute simulation, can be run in a few hours on a standard computer. A small number of modes is generally adequate for predicting the loads as the higher frequency modes generally have negligible effect. However, to model the deflections accurately it would be necessary to model more modes, because the modelled deflection is a linear combination of the mode shapes used, and a small number of mode shapes may not be sufficient to model the actual deflected shape (wind turbine handbook reference).

Another example of a wind turbine time-domain simulator is OpenFAST which is an open-source code and employs a combined modal and multibody formulation. OpenFAST has two structural dynamics codes: ElastoDyn and BeamDyn. In ElastoDyn, blade and tower flexibility are characterised using a linear modal representation and by specifying distributed mass and stiffness properties that flexibility characteristics can be determined along the length of the component. In addition, ElastoDyn requires mode shapes to be prescribed as equivalent polynomials. ElastoDyn permits two flapwise and one edgewise bending mode DOFs per blade and two fore-aft and two side-side bending mode DOFs in the tower. Even though there is a limited number of structural degrees of freedom, most conventional wind turbine configurations can be modelled (Jonkman 2007).

3.2.5   Mooring system modelling

Floating structures must be kept in position at all times which is the function of the mooring system. A mooring system is made up of multiple mooring lines, anchors, and fairleads (connectors to the platform). The mooring system provides restoring forces against external loads caused by wind, currents, and nonlinear hydrodynamics. There are variety of variety of mooring line types and systems. Chain and wire are the most popular materials currently available; chain provides weight and the catenary effect whilst wire rope provides greater elasticity and significantly reduced cost per unit length. There are six types of mooring systems which include catenary, taut leg, semi-taut, spread, single-point and dynamic positioning.

Figure 3-12 illustrates a typical single-point turret moored ship and a spread moored semisubmersible. All mooring lines connect to the vessel at the turret base. The kink in the catenary shape shows that a midwater buoy is present in each of the lines. The advantage of single-point mooring systems is generally the structure is able to weathervane by rotating about the turret. This can reduce the environmental loads by streamlining the structure into the wind

and waves. In the context of wind power production, this can also optimize production by aligning better with the incoming wind. The spread moored system comprises mooring lines emanating from the four corner columns of the semisubmersible. The mooring lines follow the shape of a catenary, and the mooring lines are guided through fairleads which could either be sheaves (pulleys) or of bending shoe type (curved guides).
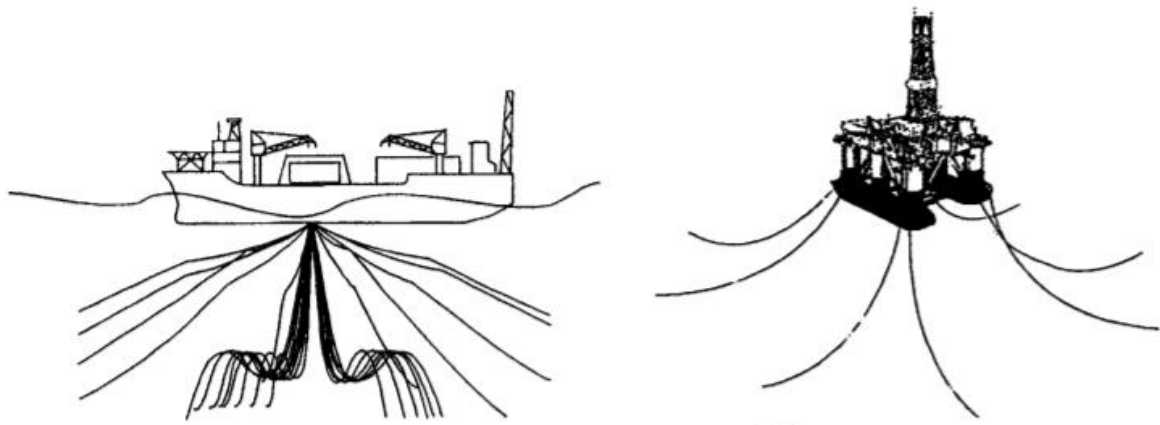
Figure 3-12. Turret moored ship (left) and spread moored semisubmersible (right) (Subrata K. Chakrabarti 2005).

Global platform motions are directly impacted by the design of the mooring system which subsequently effect the loads on the other structural components such as the turbine. There the design of a mooring system is critical (Azcona and Vittori 2019). Additionally, in view of economics it is important to keep limit mooring systems costs whilst ensuring drift constraints and mooring line break strength limits are met (Brommundt et al. 2012). This requires modelling techniques so that mooring system configurations can be studied and optimised. Three main modelling methods are used for a mooring system during the preliminary design of an offshore floating structure: (1) static; (2) quasi-static; or (3) dynamic (Davidson and Ringwood 2017).

3.2.5.1 Static mooring line model

Static modelling of mooring lines is typically performed at the early design stages and can be used as a sanity check before taking the configuration further for study in a time-consuming dynamic analysis. A mooring line is defined by its end points i.e., location of anchor and fairlead, its line length, diameter, weight, and axial stiffness. A static model considers constant loads only and determines the equilibrium between the loads and the restoring force of all the mooring lines in the system. Then a relationship between mooring line tension and displacement is calculated by displacing the platform through prescribed horizontal distances. An example of this relationship is represented in **Figure 3-13** (Subrata K. Chakrabarti 2005).
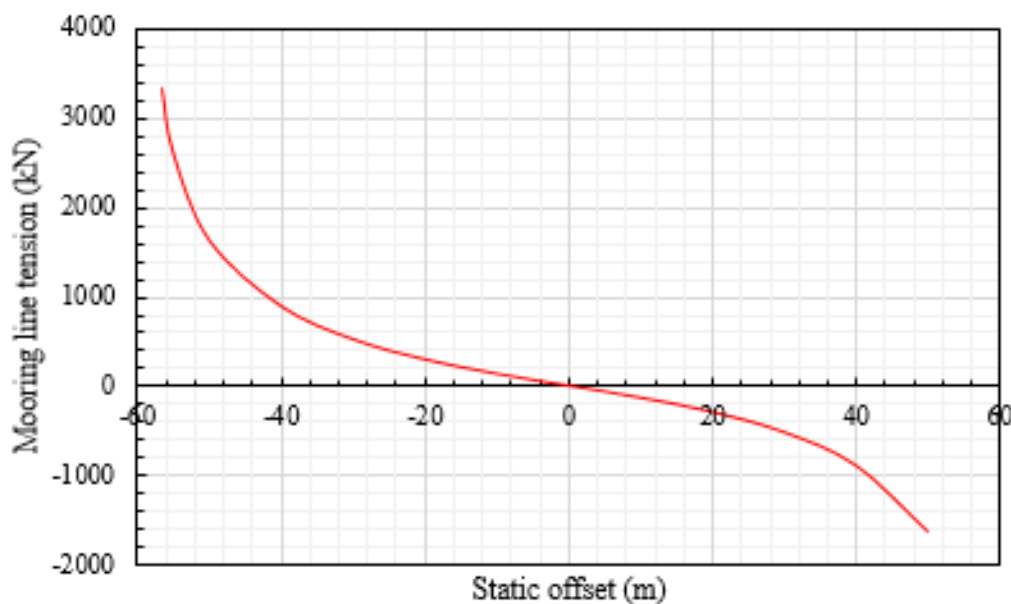
Figure 3-13. Example of static design: force-displacement graph.

3.2.5.2 Quasi-static model

Quasi-static methods are the next tier of mooring line models in terms of fidelity. The quasi-static model permits multi-segment elastic catenary lines. Each catenary segment is defined by its length, weight, diameter, and axial stiffness properties. An iterative procedure is involved in simulation based on the catenary segment solution with either linear or nonlinear

axial elasticity. However, quasi-static methods ignore current drag and inertia forces on the line itself; this can sometimes produce inadequate results when predicting mooring line tensions.

A standard schematic of a mooring line is presented in **Figure 3-14**. For any single line of a mooring system, the catenary equations can be used to derive the shape and line tensions. A summary of the catenary equations is presented next which has been adapted from (Subrata K. Chakrabarti 2005). In the development that follows, some assumptions are made:

- The seabed is horizontal.

- Cable is in the vertical plane coinciding with the X-Z plane.

- Bending stiffness of cable line is ignored.

- Dynamic effects are ignored.
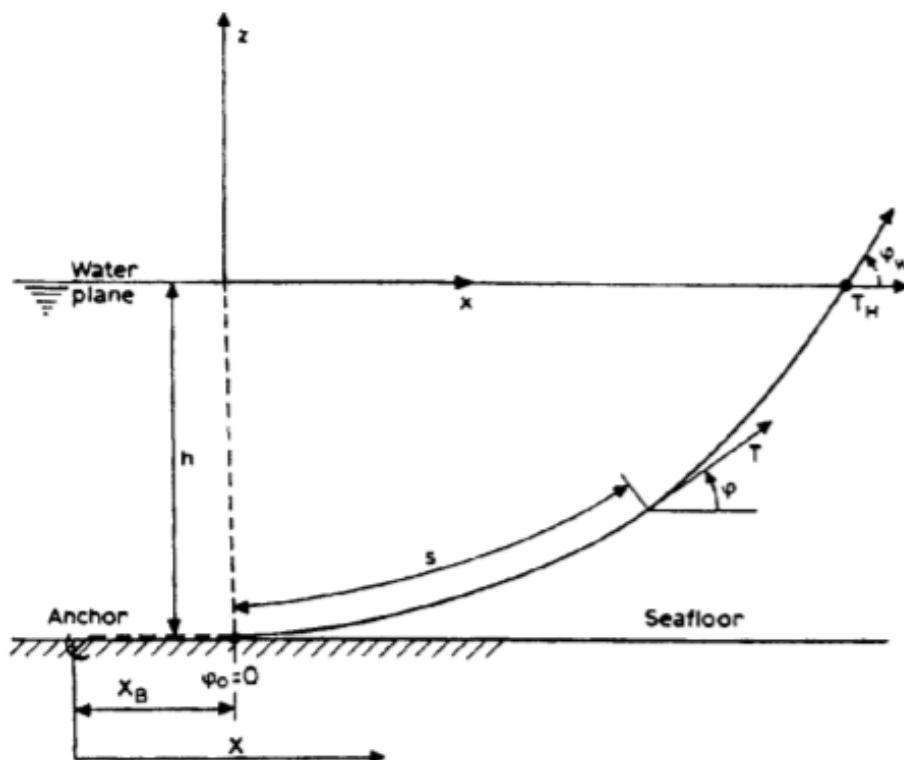
Figure 3-14. Schematic of a mooring line.

Figure 3-15 is a diagram of a single mooring line element. In this schematic representation w defines the submerged weight per unit length of the mooring line; T is the line tension; A is the cross-sectional area; and E is the elastic modulus. The mean hydrodynamic forces on the element are given by D and F per unit length.
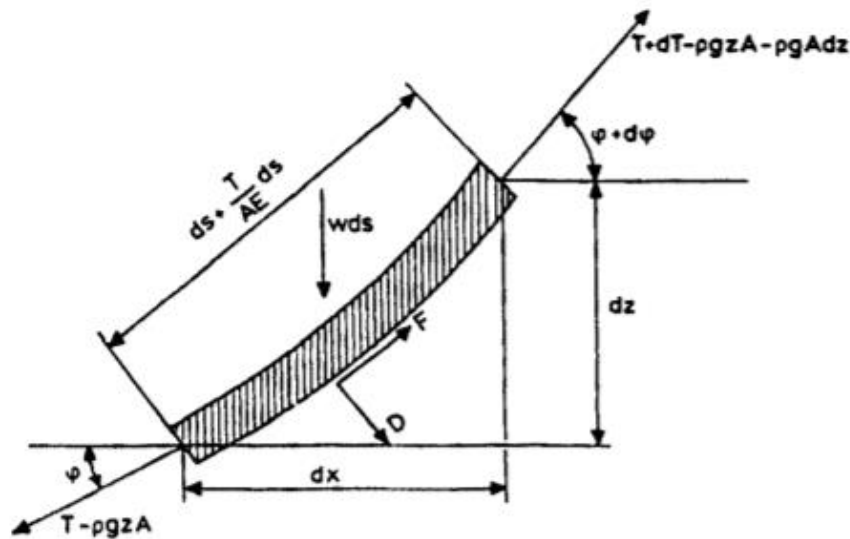
Figure 3-15. Forces acting on a single mooring line element.

Considering tangential and normal forces, two equations can be derived:

$$dT - \rho g A dz = \left[w \sin \phi - F \left(\frac{T}{EA} \right) \right] ds \qquad [61]$$

$$T d\phi - \rho g A z d\phi = \left[w \cos \phi + D \left(1 + \frac{T}{EA} \right) \right] ds \qquad [62]$$

Considering line elasticity ($AE = \infty$) and ignoring the hydrodynamic forces can simplify the two equations. It is noted for large values of w or deep waters, elastic stretch can be especially important and needs to be considered under such circumstances. With these assumptions, and applying boundary conditions at the seabed and the top connection, formula for the suspended line length s and vertical height h can be obtained:

$$s = \left(\frac{T_H}{w}\right) \sin h \left(\frac{wx}{T_H}\right) \qquad [63]$$

$$h = \left(\frac{T_H}{w}\right) \left[\cos h \left(\frac{wx}{T_H}\right) - 1\right] \qquad [64]$$

These equations are the recognised solutions to the catenary equation. Using these two equations, a mooring line profile for any single mooring line can be plotted (**Figure 3-16**). The mooring line system is compared for different lengths. A change in length means that the pre-tension can be increased or decreased. As tension increases and line length reduces, more length of line is lifted off the seabed. The higher the pre-tension, the stiffer the system i.e., less excursion for the same amount of force. However, higher stiffness also means higher line forces and a risk of breaking of highest loaded lines. Therefore, a balance between platform stiffness vs. excursion must be found to ensure safe mooring design.
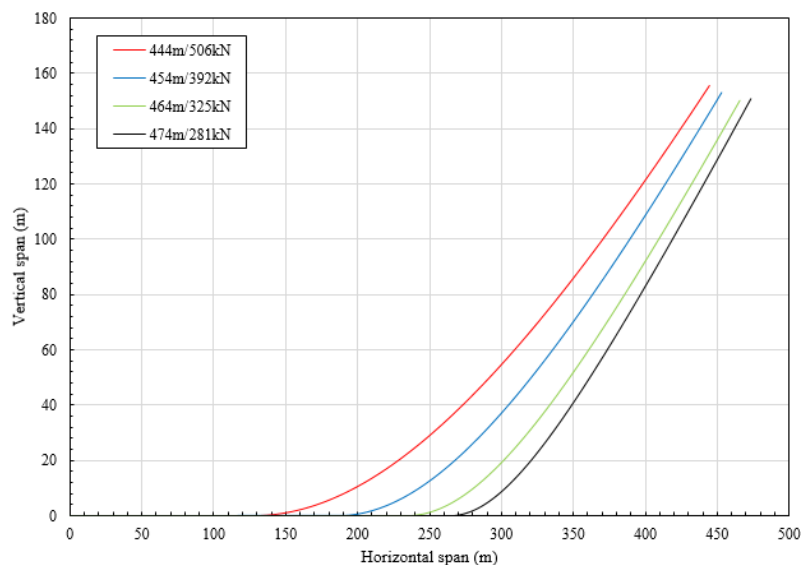
Figure 3-16. Example of quasi-static analysis.

3.2.5.3 Dynamic model

The need for a dynamic mooring line model depends on the importance of drag and inertia forces on the mooring lines. The magnitude of the dynamic effects increases with larger

transverse velocities and accelerations of the mooring line integrated over the line length which means dynamic effects are typically more important for catenary systems in deep waters. In a dynamic analysis, the mooring lines are modelled as slender elements so that mass and drag forces acting along the length of the line may be included. A discretization along the mooring line length is used and the solution is fully coupled i.e., the motions of the floating structure and cable tensions are considered to be mutually interactive, where motions affect cable tension and vice versa. In a dynamic analysis the forces on the mooring line will vary in time, and the mooring line will typically exhibit nonlinear behaviour. To find total mooring line tension, the elemental mass and forces are determined and assembled for integration. **Figure 3-17** shows the configuration of a dynamic mooring line: $\hat{a}_j = (a_1, a_2, a_3)$ denotes the unit axial vector from the j-th node to the $(j+1)$-th node and S_j is the unstretched mooring line length from anchor point to the j-th node. The seabed is assumed horizontal and flat.
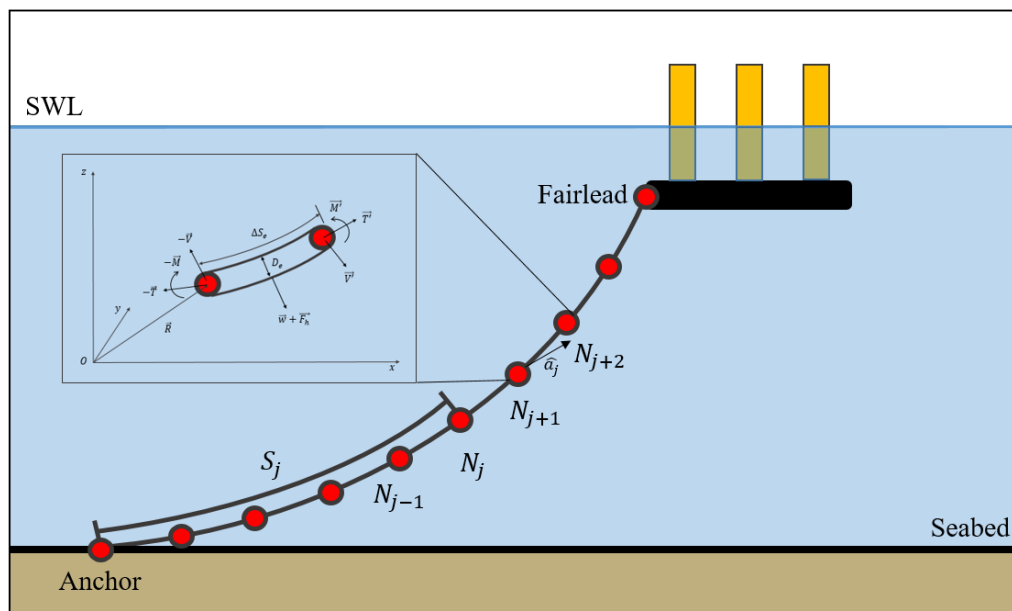
Figure 3-17. Dynamic modelling of a mooring line.

A single mooring line element subject to external hydrodynamic loadings and structural inertial loading is also shown in **Figure 3-17**. Each mooring line element is Morison-type, and

each mooring line is modelled as a chain of Morison elements. The equation of motion of an arbitrating mooring line element is:

$$\frac{\partial \vec{T}}{\partial S_e} + \frac{\partial \vec{V}}{\partial S_e} + \vec{w} + \vec{F_h} = m\frac{\partial^2 \vec{R}}{\partial t^2}$$

$$\frac{\partial \vec{M}}{\partial S_e} + \frac{\partial \vec{R}}{\partial S_e} \times \vec{V} = -\vec{q}$$

[65]

where m is structural mass per unit length; $\vec{V}$ is shear force vector; $\vec{T}$ is the tension force vector; $\vec{M}$ is the bending moment vector; $\vec{R}$ is the position vector all at the first node of the mooring line element; $\vec{w}$ is element weight per unit length; $\vec{F_h}$ is the external hydrodynamic loading vector per unit length; $\vec{q}$ is distributed moment loading per unit length; and S_e is element length.

Tension is related to the axial stiffness EA of the mooring line material through the following relation:

$$T = EA\varepsilon$$

[66]

and bending moment related to the bending stiffness EI:

$$M = \varepsilon I \frac{\partial \vec{R}}{\partial S_e} \times \frac{\partial^2 \vec{R}}{\partial S_e^2}$$

[67]

where ε is the axial strain of the element. The Lump-Mass model is used in AQWA to numerically solve the dynamic responses of the mooring lines with bending governed by the above equations. The solution is an extensive procedure which shall not be detailed here but can be viewed in (ANSYS 2020). In a mooring analysis, it is sufficient to consider the anchor points as being prescribed and fixed.

3.2.6 Control modelling

The control system on a wind turbine processes inputs to generate outputs which will affect the performance of the wind turbine. The control system usually consists of a computer or micro-processor-based controller which carries out the normal control functions needed to operate the turbine. The main control system is supplemented by a reliable hard-wired safety system in case of malfunctions. The safety system must be capable of overriding the normal controller in order to bring the turbine to a safe state if a severe problem occurs.

3.2.6.1 The power curve

Before discussing some control features of a wind turbine, it is important to understand the relationship between power produced by the turbine and wind speed so that control methods, optimisation, or limitation can be determined. A power curve specifies how much power you can extract from the incoming wind (**Figure 3-18**).
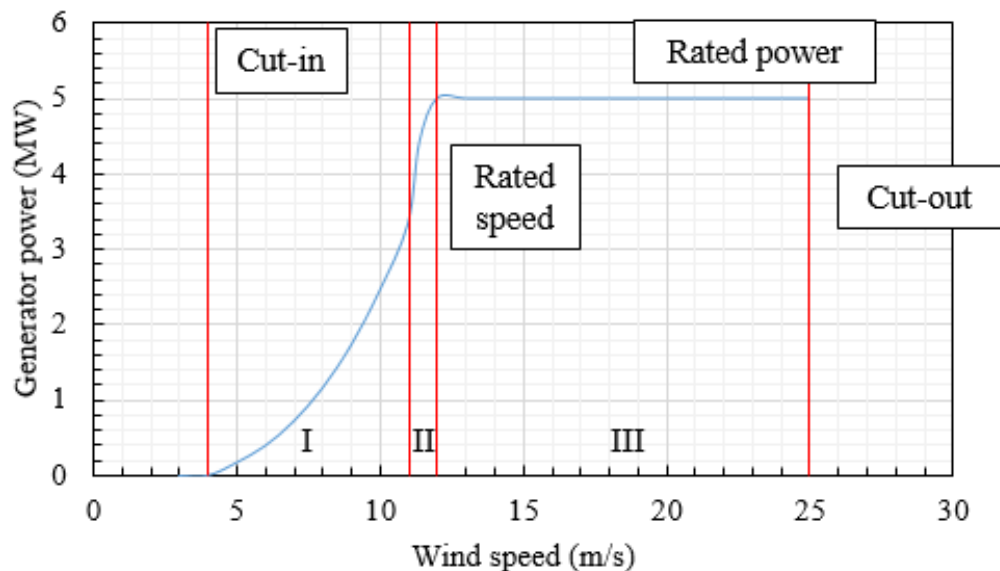
Figure 3-18. Wind turbine power curve for a 5MW turbine.

The cut-in/out speeds are the operating limits of the wind turbine. Within this operating window, it is ensured that the available energy is above the minimum threshold and structural health is maintained. The rated speed and power are provided by the turbine manufacturer. In the graph, the power curve is split into three regions. Region I is called the below-rated region; the turbine is run at maximum efficiency to extract as much power as possible from low wind speeds. Region II is a transition region between low wind speed and high wind speed regions. In this region, rotor torque is maintained, and noise is kept low. Region III is the above-rated wind speed region whilst maintaining rated power. Once a wind turbine hits its rated power, control is used to maintain this power up to the point of cut-out. Blade pitch control is one such method to maintain rated power as wind speed increases.

3.2.6.2   Functions of a controller

The main functions of a wind turbine controller can be broadly grouped into three: (1) supervisory control, (2) closed-loop control, and (3) the safety system (Burton et al. 2011).

3.2.6.2.1   Supervisory control

Supervisory control can be considered as the means whereby the turbine is brought from one operational state to another. The operational states include:

1. Standby, when the turbine is available to run if external conditions permit.

2. Start-up.

3. Power production.

4. Shut down.

5. Stopped with a fault.

As an example, the sequence control for start-up of a pitch regulated wind turbine may consist of the following steps.

1. Power up the pitch actuators and other subsystems.

2. Release the shaft brake.

3. Ramp the pitch position demand at a fixed rate to some starting pitch.

4. Wait until the rotor speed exceeds a certain small value.

5. Engage the closed loop pitch control of speed.

6. Ramp the speed demand up to the generator minimum speed.

7. Wait until speed has been close to the target speed for a specified time.

8. Close the generator contractors.

9. Engage power or torque controller.

10. Ramp the power/torque/speed set points to the rated level.

The supervisory controller must check that each stage is completed successfully before moving on to the next. If any stage is not completed within a specified time limit or if faults are detected, then controller should initiate shut-down mode.

3.2.6.2.2 Closed loop controller

The closed loop controller is usually a software-based system that automatically adjusts the operational state of the turbine in order to keep it on some predefined operating curve or characteristic. Examples include:

- Control of blade pitch in order to regular power output or rotational speed of the turbine to a fixed slowly varying set point (e.g., the rated level in above rated wind speeds).

- Control of generator torque in order to regulate rotational speed of a variable speed turbine.

- Control of yaw motors in order to minimise yaw tracking error.

3.2.6.2.3 The safety system

The safety system function is to bring the turbine to a safe condition in the event of a serious or potentially severe problem This usually means bringing the turbine to rest or to a slow idling speed with blades feathered and generator switched off.

The normal supervisory controller should be capable of starting and stopping the turbine safely in all foreseeable "normal" circumstances, including extreme winds, loss of electrical network, and most fault conditions which are detected by the controller. The safety system acts as backup to main control system, which takes over if main system appears to be failing to do this. It can also be activated by operator-controlled emergency stop bottom.

Thus, safety system must be independent from main control system as far as possible and must be designed to be fail-safe and reliable. Rather than utilising any form of computer or microprocessor-based logic, the safety system would normally consist of a hard-wired fail-safe circuit linking a number of normally open relay contacts that are held closed when all is healthy. Then if any one of the contacts is lost, the safety system trips, causing the appropriate fail-safe actions to operate. This might include disconnecting all electrical systems from the supply and allowing fail-safe pitching to pitch position. The safety system might, for example, be tripped if:

- Rotor overspeed reaching hardware overspeed limit – this is set higher than the software overspeed limit, which would cause the normal supervisory controller to initiate a shut-down.

- Vibration sensor trip, which may indicate major structural failure.

- Controller watchdog has expired.

- Emergency stop pressed by operator.

- Other faults that indicate main controller cannot control turbine.

3.2.6.3   Modelling the controller

To incorporate a wind turbine control system within a numerical model, either a simple algorithm can be implemented, or most tools provide interfaces to include a controller Dynamic-Link Library (DLL). Some engineering tools can provide interfaces for control design software such as Matlab. OpenFAST for example allow analysts to include control system logic for actively controlling nacelle yaw, generator torque, and blade pitch, among other actuators. The controller outputs can be based on inputs that can be developed from the feedback of any number of previously calculated model states or other derived parameters (Jonkman 2007).

3.2.7   Equations of motion and coupled dynamic modelling.

The structural components of a FOWT such as the turbine blades, hub, nacelle, tower, and support platform can be considered as separate entities which are mechanically connected to create a multibody system. Compared to onshore and bottom-fixed offshore turbines, the addition of the support platform creates six new Degrees of Freedom (DOF) in the system as a result of the support platform motions. For wind turbines with fixed foundations, the tower-base reference frame is the inertial frame which means as an example the kinematics expression for the position, velocity, and acceleration vectors of a point in the nacelle, depends only on the tower bending-mode, and nacelle-yaw DOF. For floating wind turbines, the tower-base reference frame now moves with the support platform which affects the kinematics expressions for all points and reference frames in the system (Jonkman 2007). As such, a dynamic coupling is introduced between the motions of the wind turbine and the motions of the support platform which needs to be captured in the numerical model. To simulate the coupled dynamics motions, two conventional analytical methods are typically employed which are the Newton-Euler (NE)

equations or Euler-Lagrange (EL) equations (Wang and Sweetman 2012). These equations model the motion of every structural component within the system and collectively formulate an equation of motion for the entire system. This equation can then be solved to calculate the time history of displacement, velocity and acceleration of the FOWT system under the actions of wind, waves, and current, and external forces such as mooring cable forces (Salehyar et al. 2017). The coupling between the different dynamic domains is usually represented by loads and moments at the tower-base (interface with the support platform) (Cottura et al. 2021).

The NE equations are conventionally established by separating the free-body diagrams of each rigid body in the system. Matsukuma and Utsunomiya (2008) use the NE equations together with constraint conditions representative of the joints connecting the rigid bodies, to evaluate the dynamic responses of a 2MW downwind turbine supported by a spar floating platform, for pitch amplitudes up to 10°. The EL equations apply energy methods to establish the equations of motion for generalized degrees of freedom. This method is efficient for the solution of motion, however, the derivation of partial derivatives of energy about related generalized DOFs is laborious. Kane's method combines the advantages of both methods which was used by Jonkman (2007) within the numerical tool FAST, to derive the equations of motion for the complete floating wind turbine system with maximum platform rotations of 20°.

The nonlinear equations of motion are derived & implemented using Kane's method as follows:

$$\boldsymbol{F}_r^* + \boldsymbol{F}_r = 0 \qquad [68]$$

where $\boldsymbol{F}_r^*$ is the generalized inertia force vector and $\boldsymbol{F}_r$ is the generalized active force vector.

Kane's method allows the complexity of a rigid subsystem to be minimized leading to simpler equations of motion when a choice is made for motion variables. This is carried out for all rigid subsystems such as the hub and nacelle. As an example, the nacelle has a yaw DOF with respect to the tower-top and so the generalized inertia can be represented using the following formula:

$$\boldsymbol{F}^*_{r,nac} = \sum_{i=1}^{N} v_{i,nac}(-m_{nac} \cdot a_{nac}) + \omega_i(-\dot{H}_{nac}) \qquad [69]$$

where N is the total number of DOFs examined; $v_{i,nac}$ and ω_i are the partial velocity and angular velocity of the nacelle contributed by the ith DOF of the wind turbine, respectively; m_{nac} and a_{nac} are the mass and acceleration of the nacelle, respectively; and $\dot{H}_{nac}$ is the time derivative of angular momentum of the nacelle about its mass centre.

The flexible components such as the blades and tower, are represented by geometrically exact, mixed, beam finite elements derived from formulation. As an example, the mixed formulation leads to compact equations of motion for the nonlinear structural behaviour of the blades. The blade equations are coupled to the rigid-body equations via connection points, i.e., the boundary conditions. The generalized active forces are composed of aerodynamic, elastic restoring, gravity, and damping loads:

$$F_r = F_{r,aero} + F_{r,elastic} + F_{r,gravity} + F_{r,damping} \qquad [70]$$

As an example, the generalized active aerodynamic force acting on a blade $F_{r,aero}$ is denoted as:

$$F_{r,aero} = \sum_{i=1}^{N} \int_{0}^{R-R_{hub}} v_{i,bld}(r) \cdot F_{aero}(r) \cdot dr \qquad [71]$$

where R and R_{hub} are the radii of the rotor and hub, respectively; $v_{i,bld}(r)$ is the partial velocity of the local blade section contributed by the ith DOF of the wind turbine; $F_{aero}(r)$ is the total force acting on the local blade section. A full development of all these local generalized inertia force and active force vectors is out of the scope of this thesis. However, further information is presented in the publication by Lee et al. (Lee et al. 2002).

In conjunction with the generalized active and inertia forces, the partial velocity vectors are established from the derived kinematics expressions which formulate the complete nonlinear time-domain equations of motion of the coupled wind turbine and support platform system. This results in a general form of the complete nonlinear time-domain equation of motion of the coupled wind turbine and support platform system:

$$M_{ij}(q,u,t)\ddot{q}_j = f_i(q,\dot{q},u,t) \qquad [72]$$

where M_{ij} is the inertia mass matrix as a function of the system DOFs (q), control inputs (u), and time (t); $\ddot{q}_j$ is the second time derivative of DOF j; and f_i is the component of the forcing function associated with DOF i.

3.2.7.1   FAST2AQWA

In this work, the numerical models are built within a newly developed tool called FAST2AQWA (F2A). F2A is an aero-hydro-servo-elastic coupled tool which can predict the coupled dynamic responses of FOWTs in the time-domain. F2A has a unique approach to modelling the dynamics of a FOWT; the tool is based on the integration of FAST (Jonkman

and Buhl Jr 2005) into a commercial hydrodynamic analysis software tool, AQWA (ANSYS 2012). The new tool operates by implementing the FAST aero-servo-elastic modules only into AQWA, removing the need for the FAST hydrodynamic module, known as HydroDyn. HydroDyn is replaced by AQWA to calculate the hydrodynamic loads of a FOWT. The justification for the choice of F2A is that it uses the superior predictive capabilities of AQWA to calculate the hydrodynamic loads acting on the FOWT. FAST aero-servo-elastic simulation capabilities are implemented within F2A via a coupling framework to synchronously calculate the effects of wind induced loads and hydrodynamic forces. The coupling of F2A is achieved through the user_force64.dll interface, which is a built-in DLL of AQWA for external force calculation. The coupling framework is represented by a flowchart presented in **Figure 3-19** (Yang 2020).
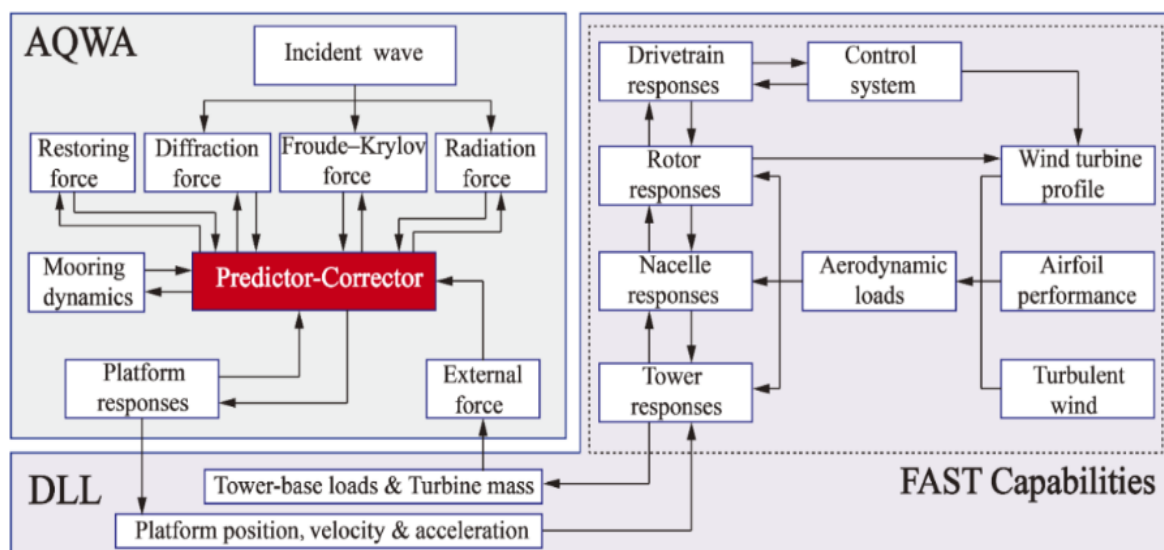
Figure 3-19. Flowchart of F2A (Yang, 2020).

The flowchart illustrates how the dynamic responses of a FOWT are predicted within different modules. More explicitly, the upper structure of the wind turbine (tower, rotor, and nacelle) is modelled in FAST, and the coupled dynamic responses are predicted within the DLL using the platform kinematics calculated by AQWA as input. The terms within both AQWA

and FAST are transformed to coincide with the platform's local coordinate system from their respective inertial coordinate systems. This transformation becomes necessary to enable FAST to correct the kinematics of FOWT's upper structures in relation to the platform responses calculated in reference to its local coordinate system. Therefore, a transformation is needed as the platform responses predicted by AQWA are referred to its inertial coordinate system. Following successful transformation of the coordinate system, the platform's tower-base loads are subsequently calculated by FAST subroutines. The lower structure of the FOWT, which consists of the platform and mooring lines, is modelled in AQWA. The resulting dynamic responses, mainly hydrodynamic, are calculated in AQWA by solving the equation of motion of the platform using the calculated tower-base loads as an external force. The governing equation of motion of the platform is defined in Equation 73:

$$(\boldsymbol{M} + \boldsymbol{A})\ddot{x} + \boldsymbol{B}_{ext}\dot{x} + \boldsymbol{B}_2\dot{x}|\dot{x}| + \int_0^t \boldsymbol{h}(t - \tau)\dot{x}(\tau)d\tau + \boldsymbol{C}x = \boldsymbol{F}_{ext} \qquad [73]$$

where $\boldsymbol{M}$ is the inertial mass matrix, $\boldsymbol{A}$ is the added mass matrix, and $x, \dot{x}, \ddot{x}$ are the unknown FOWT platform's displacement, velocity, and acceleration vectors, respectively, for each degree of freedom. $\boldsymbol{B}_{ext}$ and $\boldsymbol{B}_2$ are the linear and quadratic viscous damping coefficients respectively, typically obtained from model tests, $\boldsymbol{h}(t)$ is the radiation impulse function defined by:

$$\boldsymbol{h}(t) = \frac{2}{\pi}\int_0^\infty \boldsymbol{B}_{Pot}(\omega)\cos(\omega t)\,d\omega \qquad [74]$$

where $\boldsymbol{B}_{Pot}(\omega)$ is the potential damping matrix corresponding to the wave frequency of ω, and $\boldsymbol{C}$ is the stiffness matrix with contributions from hydrostatic and the mooring line restoring forces. Matrix $\boldsymbol{A}$ and $\boldsymbol{B}_{Pot}$ can be computed numerically using the potential theory-based solver. in AQWA. This, in turn, can provide the total external force vector denoted by $\boldsymbol{F}_{ext}$.

For more information on the F2A coupling framework and coordinate system transformations refer to (Yang et al. 2020a).

3.2.8 *Additional systems*

3.2.8.1   Tidal turbine

To predict the rotor forces and power of the tidal turbines, AeroDyn has been integrated into F2A numerical tool (Yang et al. 2020b). **Figure 3-20** illustrates this integration; in this instance AeroDyn is a standalone module used to compute the rotor force and power of the tidal turbines. The coupling between F2A and AeroDyn happens through the interaction of the platform and the tidal turbines in terms of platform motion and the inflowing current velocity. At each time step the platform response calculated by the AQWA solver in conjunction with the instantaneous relative current speed are used as input into AeroDyn to return the tidal turbine rotor force and power, which are fed back into F2A and included in the external force term.
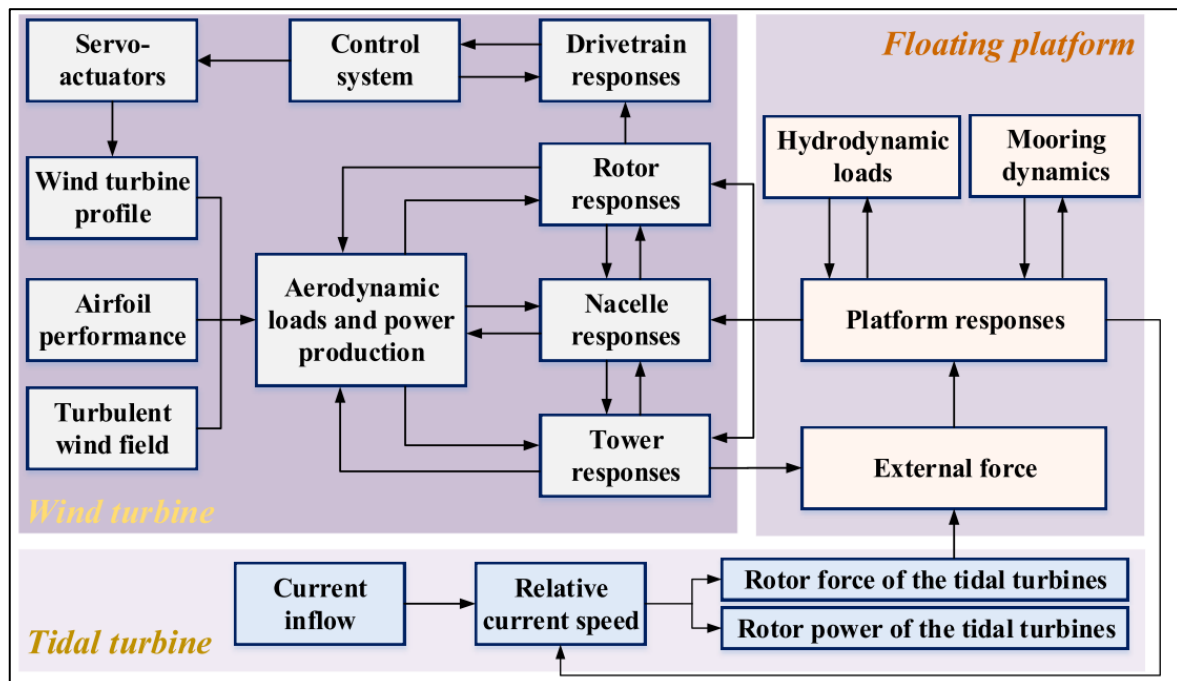
Figure 3-20. F2A with tidal turbine module (Yang et al. 2020b).

The platform motions (surge, pitch, and yaw) affect the relative inflow current velocity, therefore, a correction must be applied to the relative inflow velocity, $U_{curr,rel}$, to consider the effects due to platform motions. At each time step, U_{curr} is calculated according to the hub depth and instantaneous current velocity at the MSL. Thus, assuming small-angle approximation for platform rotations:

$$U_{curr,rel} = U_{curr} - (X_{TTCM} - X_{PCM})U_{11} - (Z_{TTCM} - Z_{PCM})U_{15} + (Y_{TTCM} - Y_{PCM})U_{16} \quad [75]$$

where U_{curr} is the inflow current velocity at tidal turbine hub depth. U_{11}, U_{15}, U_{16} is body 1 (platform) surge, pitch, and yaw velocities, respectively. X_{TTCM} and X_{PCM} are the x-coordinates, Y_{TTCM} and Y_{PCM} are the y-coordinates, and Z_{TTCM} Z_{PCM} are the z-coordinates of the CMs of the tidal turbine and platform respectively. At each time step, U_{curr} is calculated according to the hub depth and instantaneous current velocity at the MSL. The current profile follows a power law distribution with an exponent of 1/7.

3.2.8.2   Wave energy converter

It was briefly stated that ANSYS AQWA has superior capabilities calculating hydrodynamic loads. This is particularly true when modelling the hydrodynamic interaction between multiple bodies. In AQWA, approaches based on three-dimensional potential flow theory are employed for hydrodynamic analyses of complex multibody systems. Hydrodynamic interaction concerns the influence of one body's flow field on another's. The importance of interaction will depend on both the body separation distances and the relative size of the bodies. The hydrodynamic interaction includes the radiation coupling and shielding effects.

In the multiple structure hydrodynamic interaction, the total DOFs of rigid body motions are $6 \times M$, where M is the number of structures; the total unsteady potential is expressed as a superposition by Equation 49:

$$\phi_R(x, y, z; t) = \sum_{m=1}^{M} \sum_{j=1}^{6} \zeta_{jm} \phi_{R_{jm}}(x, y, z; t) \qquad [76]$$

where ζ_{jm} is the amplitude of motion of the j-th degree of freedom of the m-th structure and $\phi_{R_{km}}(x, y, z; t)$ is the radiation potential due to the unit j-th motion of the m-th structure while other structures remain stationary. Once the unsteady potential is calculated, the wave exciting forces and radiation force related added mass and damping coefficients are expressed as:

$$F_{jm} = F_{I_{jm}} + F_{D_{jm}} = -i\omega\rho \iint_{S_m} \left(\phi_I(x, y, z; t) + \phi_D(x, y, z; t)\right) \cdot n_{jm}(x, y, z; t) dS \qquad [77]$$

$$A_{jm,kn} + \frac{i}{\omega} B_{jm,kn} = -\frac{i\rho}{\omega} \iint_{S_m} [\phi_{R_{kn}}(x, y, z; t)] \cdot n_{jm}(x, y, z; t) dS \qquad [78]$$

where the subscripts m, n correspond to the m-th and n-th structures, and the subscripts j, k refer to the motion modes.

Additionally, the time domain equations of multiple floating bodies, considering their hydrodynamic interaction, is expressed by:

$$\begin{aligned}
&\begin{bmatrix} (M+A)_{11} & \cdots & A_{1N} \\ \vdots & \ddots & \vdots \\ A_{N1} & \cdots & (M+A)_{NN} \end{bmatrix} \begin{bmatrix} \ddot{x}_1(t) \\ \vdots \\ \ddot{x}_N(t) \end{bmatrix} + \begin{bmatrix} (B_L)_{11} & \cdots & 0 \\ \vdots & \ddots & \vdots \\ 0 & \cdots & (B_L)_{NN} \end{bmatrix} \begin{bmatrix} \dot{x}_1(t) \\ \vdots \\ \dot{x}_N(t) \end{bmatrix} + \begin{bmatrix} (B_Q)_{11} & \cdots & 0 \\ \vdots & \ddots & \vdots \\ 0 & \cdots & (B_Q)_{NN} \end{bmatrix} \begin{bmatrix} \dot{x}_1(t)|\dot{x}_1(t)| \\ \vdots \\ \dot{x}_N(t)|\dot{x}_N(t)| \end{bmatrix} \\
&+ \int_0^t \begin{bmatrix} h_{11}(t-\tau) & \cdots & h_{1N}(t-\tau) \\ \vdots & \ddots & \vdots \\ h_{N1}(t-\tau) & \cdots & h_{NN}(t-\tau) \end{bmatrix} \begin{bmatrix} \dot{x}_1(\tau) \\ \vdots \\ \dot{x}_N(\tau) \end{bmatrix} d\tau + \begin{bmatrix} C_{11} & \cdots & 0 \\ \vdots & \ddots & \vdots \\ 0 & \cdots & C_{NN} \end{bmatrix} \begin{bmatrix} x_1(t) \\ \vdots \\ x_N(t) \end{bmatrix} = \begin{bmatrix} F_1(t) \\ \vdots \\ F_2(t) \end{bmatrix}
\end{aligned} \qquad [79]$$

where M_{ij} are the inertial mass matrices, A_{ij} are the added mass matrices, and $x(t), \dot{x}(t), \ddot{x}(t)$ are the displacement, velocity, and acceleration matrices of the floating bodies. The subscripts 1 and 11 denote variables of body 1 (platform), subscripts N and NN denote variables of body N (WEC), and subscripts $1N$ and $N1$ denote the coupling terms, or hydrodynamic interaction, between the two bodies. $(B_L)_{ij}$ and $(B_Q)_{ij}$ are the linear and quadratic damping matrices, $h_{ij}(t)$ is the radiation impulse response function defined by

$$h_{ij}(t) = \frac{2}{\pi} \int_0^\infty B_{ij}(\omega) \cos(\omega t) \, d\omega \qquad [80]$$

where $B_{ij}(\omega)$ is the radiation damping matrix corresponding to the wave frequency ω, and C_{ij} are the restoring matrices with contributions from hydrostatic and mooring line forces. Matrix A_{ij} and B_{ij} can be computed by a numerical code based on the potential flow theory in the frequency-domain, in this case AQWA, which are later used to calculate the total external force in the time-domain denoted by $F_i(t)$:

$$\begin{bmatrix} F_1(t) \\ \vdots \\ F_N(t) \end{bmatrix} = \begin{bmatrix} F_1^{Hyd}(t) \\ \vdots \\ F_N^{Hyd}(t) \end{bmatrix} + \begin{bmatrix} F^{moor}(t) \\ \vdots \\ 0 \end{bmatrix} + \begin{bmatrix} F_1^{PTO}(t)) \\ \vdots \\ F_N^{PTO}(t) \end{bmatrix} + \begin{bmatrix} F^{(W+T)_{ext}}(t) \\ \vdots \\ 0 \end{bmatrix} \qquad [81]$$

where $F_i^{Hyd}(t)$ represents the hydrodynamic loads of the respective floating body, a breakdown of hydrodynamic loads is presented in the previous sections; $F^{moor}(t)$ is the mooring line loads; $F_i^{PTO}(t)$ are the PTO forces; and $F^{(W+T)ext}(t)$ is the external force received from the DLL, including forces from the wind turbine and tidal turbines. Therefore, as a result of the additional systems into the numerical model the updated workflow for F2A is presented in **Figure 3-21**.
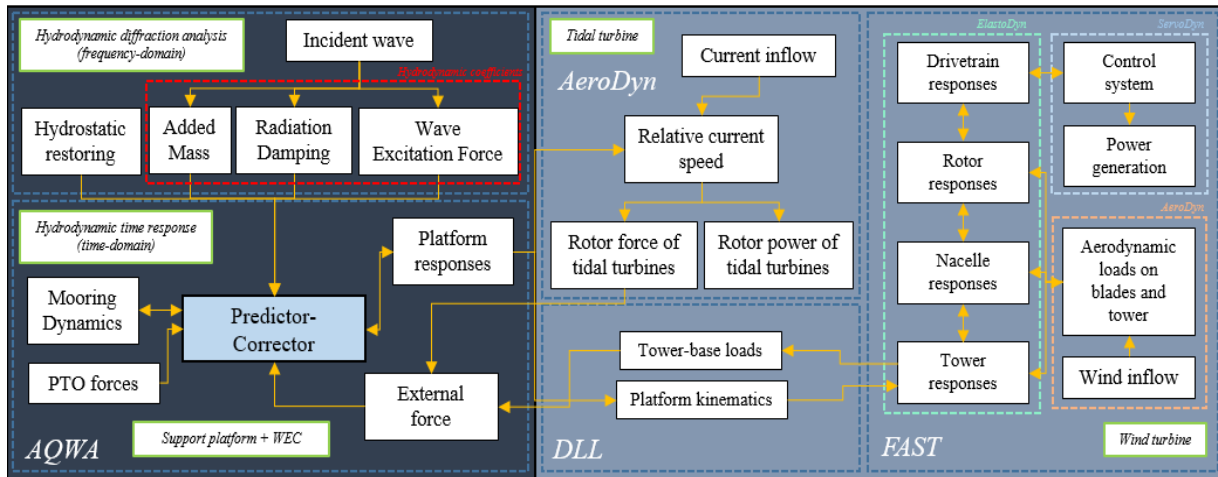
Figure 3-21. Workflow of F2A for a combined floating offshore energy system.

3.2.9   Model validation

Numerical modelling allows for quantitative representation of physical systems which make complex analyses and sound design practices possible. However, using different assumptions and idealizations, such representations are rarely perfect when comparing to the actual physical system. Therefore, numerical models are required to be validated and verified. (Coulling et al. 2013). Model validation and verification is an enabling methodology for the development of numerical models that can be used to make engineering predictions with quantified confidence. However, the scarcity of publicly available test data creates difficulty in accomplishing numerical code validation for ORE systems with low technical maturity (Stewart and Muskulus 2016). To address this issue there have been some international research projects organised such as the Offshore Code Comparison Collaboration projects (Jonkman and Musial 2010), (Robertson et al. 2014a), (Wendt et al. 2019). These focused on validation and verification of numerical codes for analysis of FOWTs through comparison against tank test data and other codes. In 2016, Phase II of the International Energy Agency Wind Task 30 Project, also known as OC5, used data from a test campaign in 2013 of a 1:50-

scale model of a semisubmersible FOWT. This model was subsequently used to compare simulation results with coupled response test data.

3.2.10 Chapter summary

A summary of this chapter is provided in this section and the findings are listed as followed:

- At present, no numerical tools exist explicitly for modelling CFOES. This resulted in the integration of numerical tools that could model the independent ORE systems. The floating wind turbine is considered the central system (in terms of rated power capacity and structural size), so this was the basis for the numerical tool coupling i.e., numerical models of the marine renewable energy systems would be integrated into a numerical model of the FOWT.

- Software used to design and analyse FOWTs can be categorised based on the level of fidelity required by the numerical model. Engineering tools are considered mid-fidelity and are commonly used for loads analysis to examine concept designs for operational and extreme conditions. Thus, F2A was used to construct a numerical model of a CFOES.

- Engineering tools are comprised of computational modules that can numerically represent the offshore environment and structure. Offshore structures are exposed to a wide variety of external conditions. The main external conditions relevant to offshores structures are wind, ocean waves, and currents. Different mathematical models can be selected to represent the offshore environment to suit the needs of the analysis e.g., regular wave or wave spectrums which represent fully developed or developing seas.

- For each physical domain, similarly a range of models can be implemented to represent the applied load or system responses of a FOWT. The aerodynamics is commonly computed within engineering tools using BEMT theory. Corrections can be added to this model to capture other aerodynamic effects such as tip- and hub-losses, skewed wakes, and dynamic stall. Morison's equation or potential flow theory can be used to calculate the wave loading within engineering tools. The choice of model is dependent on size of the structure relative to incident wavelength. For commercial aero-elastic codes, FEM models and modal analysis methods are employed to model the structural dynamics of a FOWT. There are also multiple modelling options for the controller and mooring system. To simulate the coupled dynamics motion, Kane's method is employed in FAST to formulate an equation of motion for the entire system.

- WECs can be modelled in ANSYS AQWA owing to the software's excellent capabilities of calculating hydrodynamic loads and modelling complex multibody systems. Additionally, AQWA has 'joint' features which can be used to model the PTO system of some WECs. F2A uses AQWA as its core hydrodynamic module which meant coupling of FOWT numerical model and WEC numerical could be achieved. To model the tidal turbines, a module for calculating aerodynamic loads in FAST is repurposed to calculate the hydrodynamic loads of tidal turbines and integrated within the F2A via the external.dll.

Chapter 4.   Development of catamaran FOWT numerical model

To meet the objective of developing a fully coupled model of a CFOES, this project is split into three key stages. This chapter presents the first of the three stages which is the development of a numerical model in F2A of a catamaran-type FOWT.

Therefore, the chapter is organised into the following sections: Sections 4.1 and 4.2 present the inspiration behind the research and the reasoning for the choice of a catamaran for use as a support platform for a FOWT. The novel concept and development of the numerical model is presented after in Section 4.3. A number of considered design load cases are simulated to comprehensively assess the concept which are described in Section 4.4. A detailed explanation of the hydrodynamic pre-processing calculations is provided. Typical performance indicators of a FOWT are used to examine the concept including platform motions, blade-root, and tower-base bending moments, and generated power. The results are presented in Sections 4.5 – 4.7 and a chapter summary and conclusions are presented at the end of this chapter in Section 4.8.

4.1   Introduction

A major design challenge prohibiting the commercialisation of FOWTs is cost-effective concepts which are capable of penetrating a competitive energy market. Some issues which need to be addressed are increasing understanding on coupled dynamic characteristics, economic viability, and acceptable motion and stability assessment criteria (Le et al. 2020). Considering economic viability, concepts need to demonstrate significant potential for utility-scale production. Barge-type platforms have advantages over other FOWT types in terms of easy fabrication, fast deployment, and installation. The simple geometry of a barge allows for

uncomplicated platform construction, similarly, a wind turbine can be easily mounted onto a barge at quayside. The transportation process is also simple as tugboats can be used to tow the entire assembly to the offshore site. This operation can eliminate any need for specialist vessels. Such operations mean that barge-type FOWTs have lower overall costs of fabrication, transportation, and installation compared to others and show good suitability for utility-scale production. However, the uptake of barge-type platforms is restricted by stability problems mainly related to the pitch degree of freedom. This can result in complex requirements for its operational control (Olondriz et al. 2018). Therefore, if a new barge-type platform concept could be innovated, which had uncomplicated design so that the aforementioned advantages in fabrication, transportation, and installation could be maintained, and improve upon platform pitch stability of conventional barge-type platforms, then this FOWT concept would hold some worth.

The use of catamarans in the maritime transportation and leisure industries has been on the rise since the turn of the century (Fang et al. 1997). This vessel type was selected to build the largest construction vessel in the world (Allseas 2021) (**Figure 4-1**) and green power boats such as ECO SLIM (Drassanes Dalmau 2021). A catamaran is a type of vessel comprised of two demi-hulls connected by a beam, often referred to as a cross-structure (Bashir 2014).

Figure 4-1. The Pioneering Spirit (formerly the Pieter Schelte), an offshore (multi-purpose)

catamaran support vessel constructed by Allseas (Allseas 2021).

This upward trend can be attributed to the good hydrodynamic performance and the large

usable deck area that catamarans offer (enabled by the cross-structure). Both of these factors

would also be beneficial for ORE platforms. The deck area is attractive because it can enhance

safety when carrying out operation and maintenance work, and there is potential to support

infrastructure for other functions such as wind generation, ocean energy generation, solar

panels, hydrogen generation, desalination plants etc. There have already been some studies in

Asia investigating the retrofitting of a conventional catamaran vessel into a tidal energy

platform (Qasim et al. 2018), (Junianto et al. 2020), (Brown et al. 2021). Yet there has been

little to no public research on the modification of a catamaran for FOWT application. This

presents an opportunity for novel research, and in relation to this and the other factors

mentioned above, the primary incentive for this work is established.

4.2   The round bilge hull form

There are a variety of catamaran and other twin-hull concepts currently in existence, some

of which include displacement and semi-displacement, Small Waterplane Area Twin Hull

(SWATH), wave-piercing, and foil-assisted. Displacement catamarans are a commonly used

design for applications which require sufficient excess buoyancy. The seakeeping performance

and dynamic flow characteristics around the vessel are heavily dependent on the geometry of

these hulls. There are different hull forms available for displacement-type catamarans with the

most common hull form design being the Round Bilge hull form. This design has been

prominently used over many years in the design of monohull naval craft and multihull vessels.

The Round Bilge catamaran concept is essentially a "U-Shaped" hull form geometry (**Figure**

4-2) (Bashir 2014). The simplicity in its geometry is an advantage for FOWT application. This

hull form was chosen for the catamaran-type FOWT which is presented in the next section.
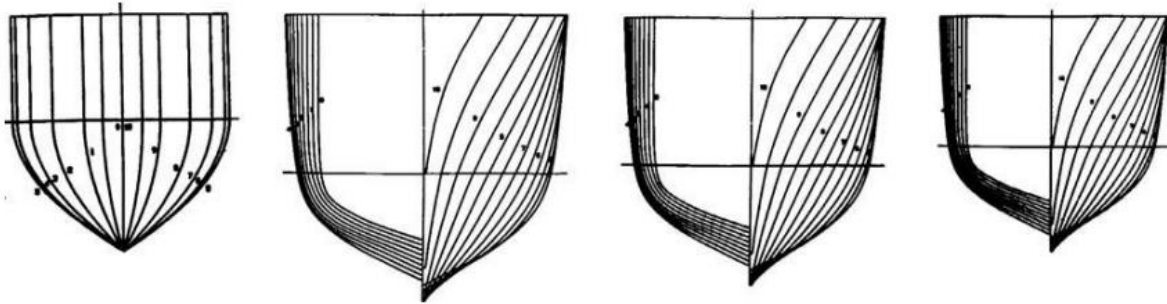
Figure 4-2. Round Bilge hull form (Bashir 2014).

4.3   The catamaran FOWT concept

The proposed concept in this work is inspired by a generic catamaran vessel with a with a

large deck mounted atop two equally spaced demi-hulls with a round bilge hull form. The wind

turbine is situated in the middle of the platform so that the tower centreline and platform

centreline align and pass through the origin (0, 0, 0). **Figure 4-3** shows the catamaran FOWT

concept labelled with relevant dimensions. The main components of the FOWT system are the

following: (1) wind turbine, (2) floating platform, and (3) mooring system.
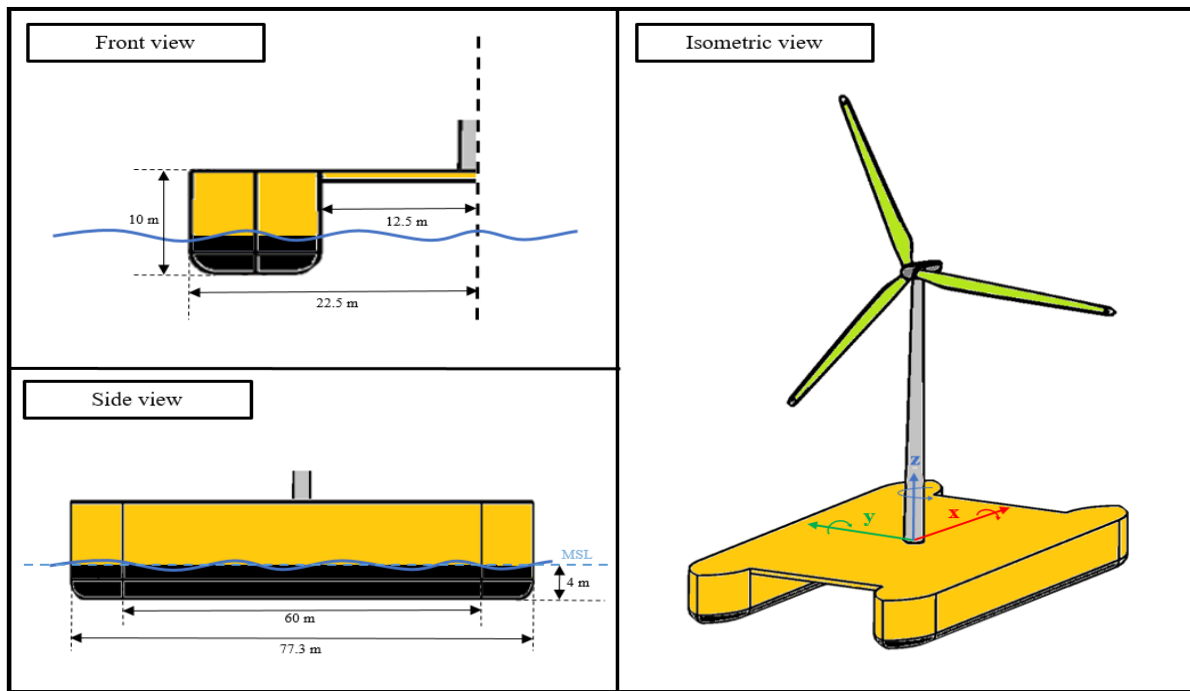
Figure 4-3. Preliminary catamaran FOWT concept schematics.

The model wind turbine in this work is the NREL 5 MW reference wind turbine (properties given in **Table 4-1**) which is used to assess the capacity of the proposed concept to function as a FOWT. The wind turbine is a conventional three-bladed horizontal-axis, upwind variable-speed wind turbine and comprises of blades, hub, nacelle, and tower.

Table 4-1. Properties of NREL 5MW reference wind turbine.

Parameter (Units)	Value
Rated Power (MW)	5
Rotor & hub diameter (m)	126 & 3
Cut-in, rated, cut-out wind speed (m·s^{-1})	3, 11.4, 25
Hub height (from the bottom of the tower) (m)	90
CM (Centre of Mass) location (from bottom of the tower) (m)	64
Rotor mass (kg)	110,000
Nacelle mass (kg)	240,000
Tower mass (kg)	347,460
Total mass (including tower) (kg)	697,460

As a preliminary design, the dimensions of the catamaran platform were selected so that the geometry, mass, and inertia properties of the platform were similar to that of a conventional

barge FOWT. Any improvement or deterioration in performance can be attributable to the platform design. The barge concept that was used as a comparison was the ITI Energy barge, a preliminary barge concept developed by the Universities of Glasgow and Strathclyde, and ITI Energy. Further details of the platform can be found in (Jonkman 2007). Additionally, the barge FOWT is also used for benchmarking, validation, and verification of catamaran concept. To prevent drifting from installed location, each floating platform is moored by a system of eight slack, catenary lines. For both platforms, at every bottom corner two mooring lines connect to the platform separated by a 45° angle. The mooring system properties are given in **Table 4-3. Figure 4-4** shows the mooring system configurations of both platforms created in ANSYS AQWA.

Table 4-2. Platform properties.

	Catamaran	ITI Energy barge
Diameter or width ×length (m),	45 × 60,	40 × 40
(LOA = length overall) (m)	(LOA = 77.3)	
Space between demi-hulls (m)	25	-
Draught (m)	4	4
Elevation to platform top (tower base) above SWL (m)	6	6
Total volume (m^3)	15,684	16,000
Water displacement (m^3)	5,480	6,400
Mass (kg)	4,901,080	5,452,000
CM location (m)	(0, 0, 1.51)	(0, 0, -0.2818)
Roll inertia about CM (kg m^2)	4,672,683,194	726,900,000
Pitch inertia about CM (kg m^2)	6,800,310,371	726,900,000
Yaw inertia about CM (kg m^2)	11,190,569,096	1,454,000,000

Table 4-3. Mooring system properties.

	Catamaran	Barge
Number of mooring lines	8	8
Depth to fairleads & anchors (m)	4 & 150	4 & 150
Radius to fairleads & anchors (m)	42.436, 429.095 & 439.566	28.28 & 423.4
Section length (m)	474.1	473.4
Mooring line diameter (m)	0.0809	0.0809
Line mass density (kg m^{-1})	130.4	130.4
Line extensional stiffness, EA (N)	589,000,000	589,000,000
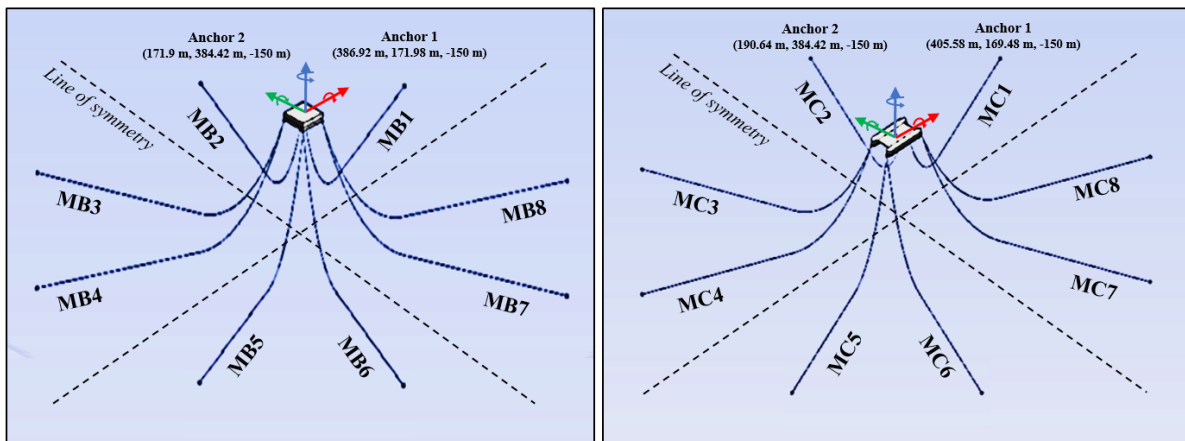
Figure 4-4. Mooring system configurations in ANSYS AQWA: barge (left),

catamaran(right).

4.4   Simulation

4.4.1   *Load cases and environment*

Table 4-4 details the preliminary tests performed using the developed numerical model in F2A and Load Cases (LCs) simulated. The first set of analyses focus on system identification, including frequency-domain analysis to obtain hydrodynamic coefficients, free-decay simulations to find natural frequencies, hydro-elastic response with regular waves in absence of wind, and RAOs for a complete assessment of hydrodynamic characteristics. The next set of simulations are fully coupled aero-hydro-servo-elastic time-domain simulations used to investigate the performance of the catamaran floating wind turbine system under combined wind and wave excitation. For these simulations, the Metocean data used is from a site located off the north coast of Scotland which has a water depth of 150m. LC 1 – 7 are defined in accordance with IEC 61400-3 where U_w is the locations' turbulent wind speed, measured at FOWT's hub-height (m/s), H_s is the significant wave height (m) and T_p is the spectral peak period (s). The wind characteristics of the selected site are modelled as three-dimensional turbulent wind fields based on the Kaimal turbulence model for IEC Class C and using

TurbSim, a sub-program in FAST (Jonkman and Buhl Jr 2006). The site wave conditions are modelled as irregular waves using the Pierson-Moskowitz wave spectrum in AQWA. Furthermore, the length of each simulation is 4,600s, with the first 1,000s discarded to remove transient effects potentially interfering with final results.

Table 4-4. Load cases.

LC	Description	U_w [m/s]	H_s [m]	T_p [s]
HDC	Frequency-domain analysis to obtain hydrodynamic coefficients	-	-	-
FD	Free decay analysis	-	-	-
RW	Regular wave	-	2.1155	5.2555
RAO	Response amplitude operators (White-noise wave)	-	2	10
WO	Wind only (steady)	3 - 25	-	-
1	Cut-in	4	1.6146	3.4985
2	Below rated	8	1.8037	4.2657
3	Rated	11.4	2.1155	5.2555
4	Above rated	18	2.9585	7.1203
5	Cut-out	25	4.0257	8.8897
6	Rated (Wave Dir 30°)	11.4	2.1155	5.2555
7	Rated (Wave Dir 90°)	11.4	2.1155	5.2555

4.4.2 Validation

The novelty of the catamaran FOWT concept means that no experimental or numerical data, or benchmark model is available in public domain, yet the numerical model requires verification and validation for results to attain credibility. Consequently, the methodology used to verify the catamaran is based on a comparison of results of the ITI Energy barge model with published research. Good agreement between the results of the barge numerical model and published research reassures the credibility of this new concept by verifying the procedure to obtain the results. Following verification, the behaviour of the catamaran model is validated through comparisons with published results of similar models.

4.5 Assessment of hydrodynamic characteristics

4.5.1 Hydrodynamic coefficients

The hydrodynamic coefficients of the catamaran and barge are calculated using ANSYS AQWA and presented in **Figure 4-5** and **Figure 4-6**. The coefficients are obtained in six degrees-of-freedom for a wave frequency range of 0.05 – 4.0rad/s at intervals of 0.05rad/s and incident angles varying between 0 – 90° at intervals of 30°. The calculated hydrodynamic coefficients of the barge platform were validated against the results published by (Olondriz et al. 2018). Overall, there is good agreement between the results which ensures the 3D analysis method used to obtain the hydrodynamic coefficients for both platforms is accurate and reliable. However, there is some discrepancy for heave and yaw radiation damping coefficients. Concerning heave damping coefficient, the plots follow a similar trend, however the peak amplitude of the present numerical model occurs at a higher frequency to the published results and concerning yaw, the plots follow an identical trend however the curve does not fall as sharply as frequency increases. Next, the trend of the hydrodynamic coefficient plots of the catamaran follows a similar pattern to the hydrodynamic coefficients plots of three catamarans modelled by (Fang 1996) and one catamaran modelled by (Wellicome et al. 1995). The successive occurrence of peaks at discrete frequencies is inherently a characteristic of catamaran vessels. The similarity in results provides additional reassurance that the model is behaving as expected.

Catamarans experience a phenomenon known as dynamic amplification which is caused by entrapped wave action between its demi-hulls. This phenomenon can lead to enhanced motion behaviours. A series of characteristic frequencies, ω_r , exist where demi-hull oscillation strongly excites the motion of the entrapped fluid; these frequencies can be identified by the following formula:

Symmetric interaction: $\qquad \omega_r = \sqrt{2n\pi g/d_r}$ for n = 1, 2, 3 … [82]

Antisymmetric interaction: $\qquad \omega_r = \sqrt{(2n-1)\pi g/d_r}$ for n = 1, 2, 3 … [83]

where d_r is the demi-hull separation (m) and n is the characteristic frequency ordering.

The characteristic frequencies can be either separated into symmetric or antisymmetric interaction. Symmetric interaction affects the vertical plane motions (surge, heave, pitch) and antisymmetric interaction affects the horizontal plane motions (sway, roll, yaw). These frequencies are analogous to the resonant modes of a standing wave between two vertical walls (Fang 1996). Moreover, the fact that catamarans have negative added mass in a stationary condition suggests that the effect of hydrodynamic interaction between the demi-hulls is strong. The frequency of the standing wave depends on the distance between the demi-hulls. The wider the distance is between the demi-hulls, the lower the frequency at which the phenomenon occurs (Dabssi et al. 2008).

In **Figure 4-5 & Figure 4-6**, the characteristic frequencies are distinct. Using Equation 83 and Equation 84 to calculate the characteristic frequencies, for heave and pitch plots of added mass and radiation damping coefficients, small peaks occur at 1.57rad/s due to symmetric interaction. For the added mass coefficients, a smaller peak can be seen at a frequency of 2.22rad/s. Peaks also exist for surge mode, however due to the scaling of the axis, they are not visible.

For horizontal plane motions, peak responses occur at 1.11, 1.92, 2.48, 2.93, 3.33 and 3.68rad/s due to antisymmetric interaction between the demi-hulls. Only the first two frequencies are dominant for the added mass and radiation damping coefficients of sway, roll, and yaw motions. Similar to pitch, a small peak occurs before the first characteristic frequency for roll. This peak corresponds to the roll resonant frequency.

Comparison of hydrodynamic coefficients show that the catamaran exhibits lower surge and heave, and higher sway, roll, pitch, and yaw added mass and damping coefficients. This observation suggests that the platform has lower hydrodynamic restoring stiffness and potential damping for surge and heave modes. At the same time, hydrodynamic restoring stiffness and damping for sway, roll, pitch, and yaw modes are higher. Moreover, it is expected that the barge platform will be more sensitive to aerodynamic loading due to smaller pitch coefficients, whilst the catamaran will be more sensitive to wave loading as a result of smaller surge coefficients.
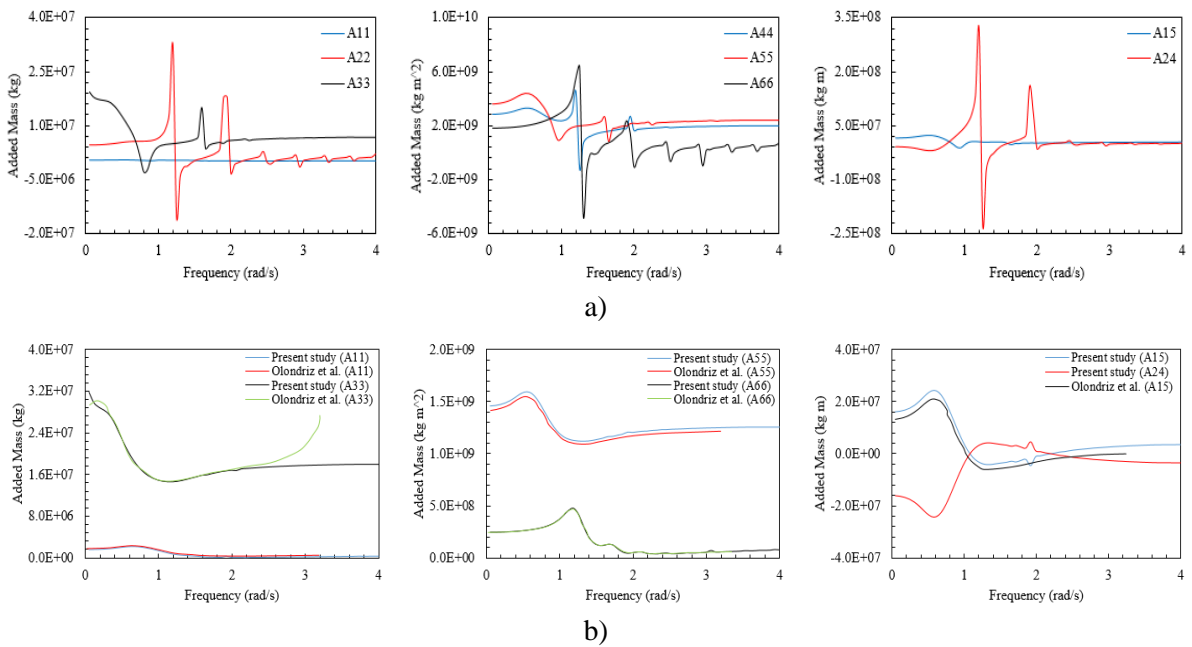
Figure 4-5. Hydrodynamic added mass coefficients a) catamaran b) barge.

a)

b)
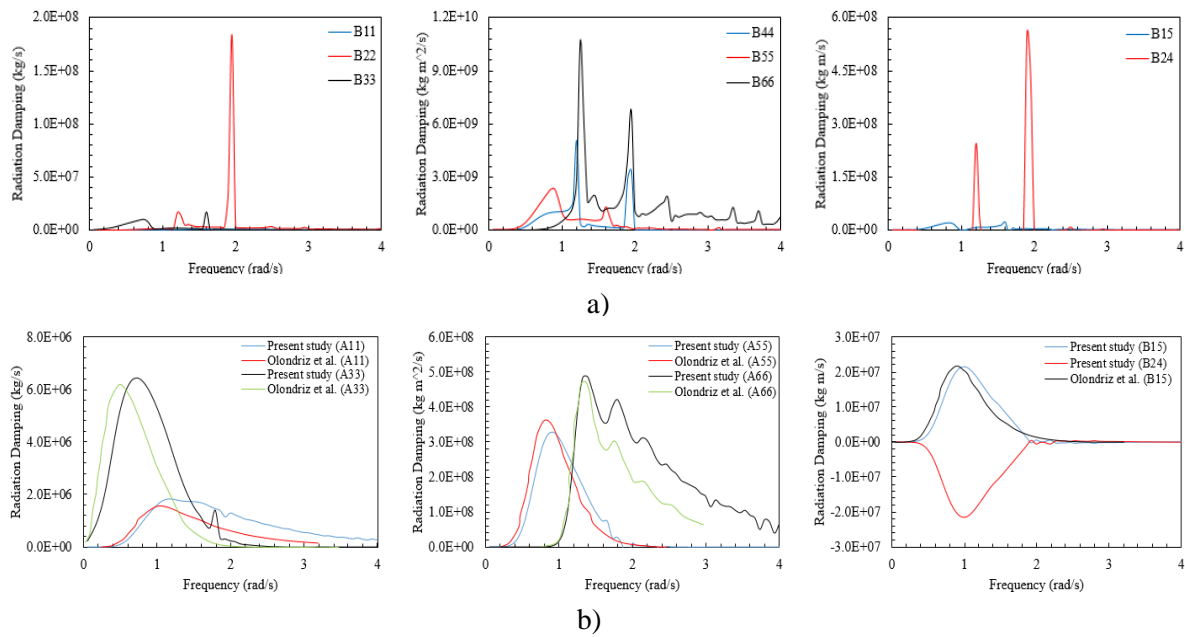
Figure 4-6. Hydrodynamic radiation damping coefficients a) catamaran b) barge.

4.5.2 Free decay

A free decay analysis was conducted for both platforms in six degrees of freedom. The natural periods of the platforms are presented in **Table 4-4** and plotted graphically in **Figure 4-7**. Typically, the first step in performing a dynamic analysis is determining the natural frequencies and mode shapes of the structure with damping neglected. These results characterize the basic dynamic behaviour of the structure and are an indication of how the structure will respond to dynamic loading. The natural frequencies of a structure are the frequencies at which the structure naturally tends to vibrate if it is subjected to a disturbance. The deformed shape of the structure at a specific natural frequency of vibration is termed its normal mode of vibration. Each mode shape is associated with a specific natural frequency. Natural frequencies and mode shapes are functions of the structural properties and boundary conditions. There are many reasons to compute the natural frequencies and mode shapes of a structure. One reason is to assess the dynamic interaction between a component and its supporting structure. Another is decisions regarding subsequent dynamic analyses can be based on the results of a natural frequency analysis. Also, the results of the dynamic analyses are

sometimes comparable to physical test results. All of these reasons are based on the fact that real eigenvalue analysis is the basis for many types of dynamic response analysis. Therefore, an overall understanding of normal modes analysis as well as knowledge of the natural frequencies and mode shapes for your particular structure is important for all types of dynamic analysis.

Table 4-5. Natural periods (s) of the FOWT systems.

	Surge	Sway	Heave	Roll	Pitch	Yaw
Catamaran	121.6	157.1	5.4	10.6	9.8	109.5
Barge	137.7	137.7	7.1	11.8	11.8	52.5
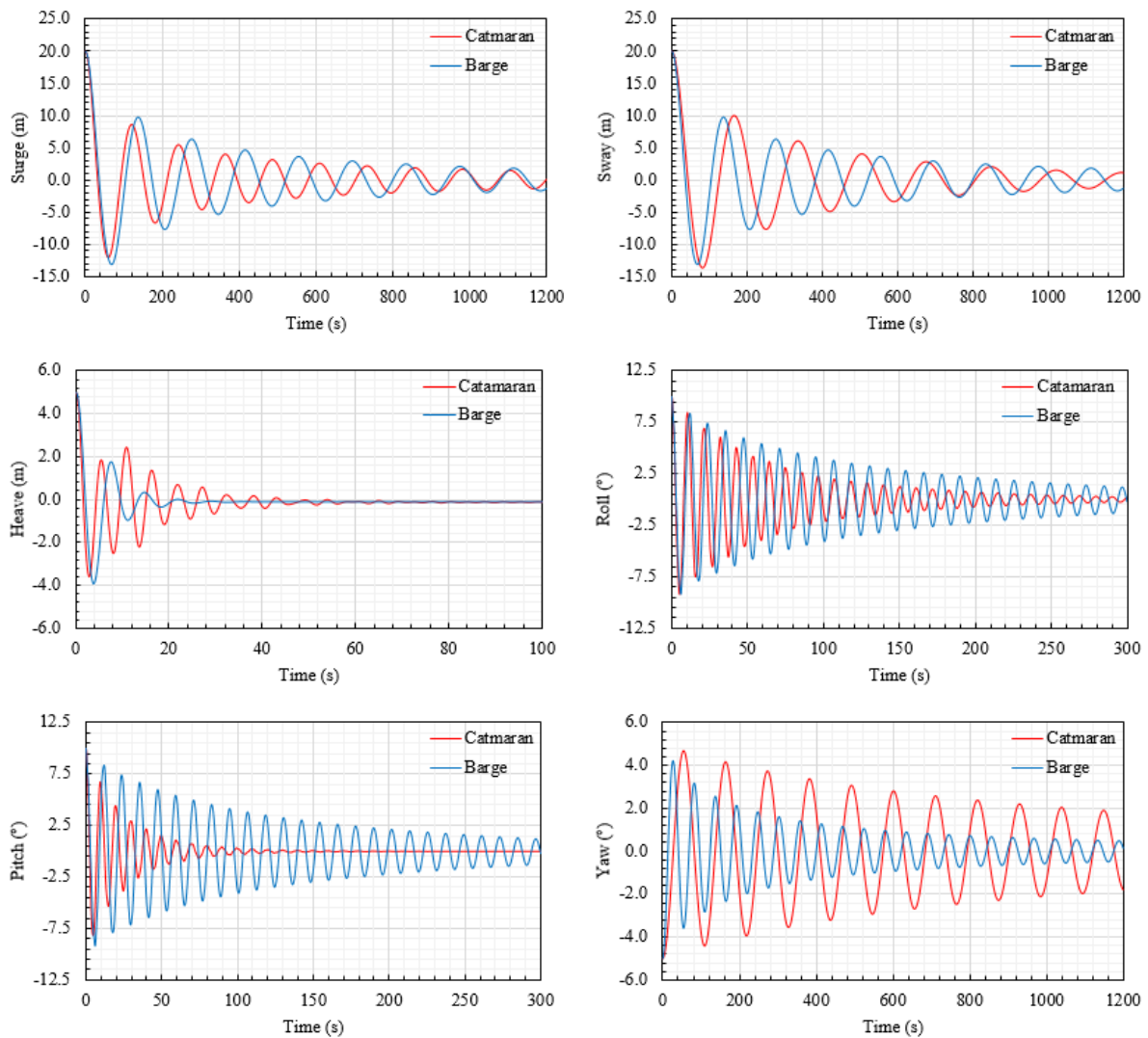
Figure 4-7. Free decay results.

4.5.3 *Hydro-elastic response under regular waves*

Figure 4-8 shows the time histories of platform surge, heave and pitch displacements, tower-top fore-aft displacement, tower-base force in the x-direction, and fairlead tensions (MB4/MC4) of both platforms subject to a regular wave with properties H = 2.1155m and T = 5.2555s. The results show the barge exhibits greater surge and pitch displacement, tower-top fore-aft displacement, tower-base force, and mooring line tension, whilst the catamaran has greater heave displacement.
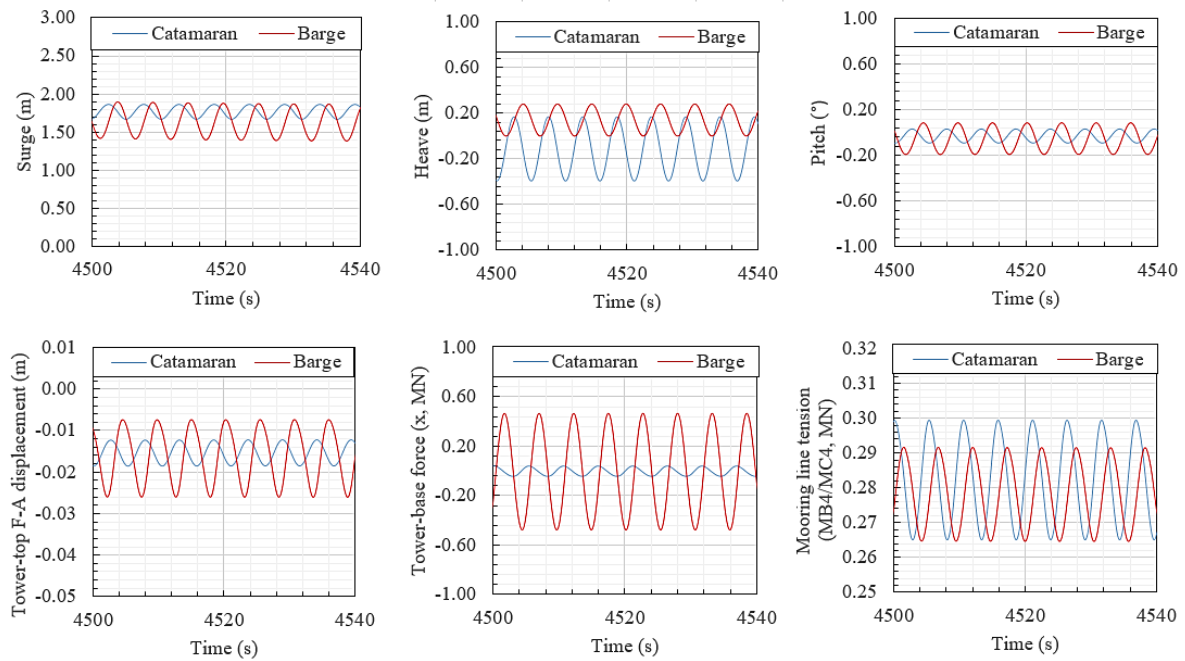
Figure 4-8. Hydro-elastic response with regular wave in absence of wind.

4.5.4 *Response amplitude operators*

RAOs are used in hydrodynamic analysis to initially assess the frequency-domain linear wave response of floating platforms (Robertson et al. 2014b). In FOWT design, the hydrodynamic loads coupled with wind induced aerodynamics, structural dynamics, and servo-controller dynamics must be accounted in order to quantify their contribution and effects on platform responses (Aboutalebi et al. 2021). Simulations to predict the RAOs were performed in OpenFAST (National Renewable Energy Laboratory (NREL) 2021) with the process described in (Ramachandran et al. 2013) and (Aboutalebi et al. 2021). The RAOs for both catamaran and barge platforms are plotted in **Figure 4-9**. Similar to the methodology adopted in validating hydrodynamic coefficients, published numerical results for the RAOs of the barge exist; these have been used for validation. The RAO outputs in this study for the barge FOWT agree with the results published by (Aboutalebi et al. 2021).

RAOs are plotted for a frequency range of 0.1 – 1.25rad/s and they show considerable excitation in surge, heave, and pitch modes. Since only wave response in a zero-degree heading

was simulated, the responses for sway, roll and yaw are considerably less in magnitude due to the wave heading and absence of wind forcing.

When considering the surge mode, there is a shift in peaks from 0.52rad/s to 0.62rad/s. These peaks are attributable to the pitch resonant frequency of the corresponding platform. Furthermore, the catamaran RAO is slightly lower which suggests it is less responsive than the barge. The actual surge resonant frequency of both platforms occurs at a much lower frequency, hence why as frequency decreases the RAOs increase.

The heave RAO plots of both platforms are identical in the lower frequency range and follow the incident wave until approximately 0.4rad/s. The RAO of the catamaran in the higher frequency range falls more sharply than the barge. However, at approximately 1.0rad/s the barge RAO begins to level out whereas the catamaran experiences another peak. This peak corresponds to the frequency of the standing wave created by the catamaran's demi-hulls.

For pitch mode, it is observed that the catamaran exhibits close to a 50% reduction in response compared to the barge. As mentioned above, the pitch resonance frequency of the catamaran is higher than the barge. Also, the peak response of the catamaran has a wider band compared to the barge, which means the catamaran is more responsive to a greater frequency range, whereas for the barge the peak rises and falls more sharply.
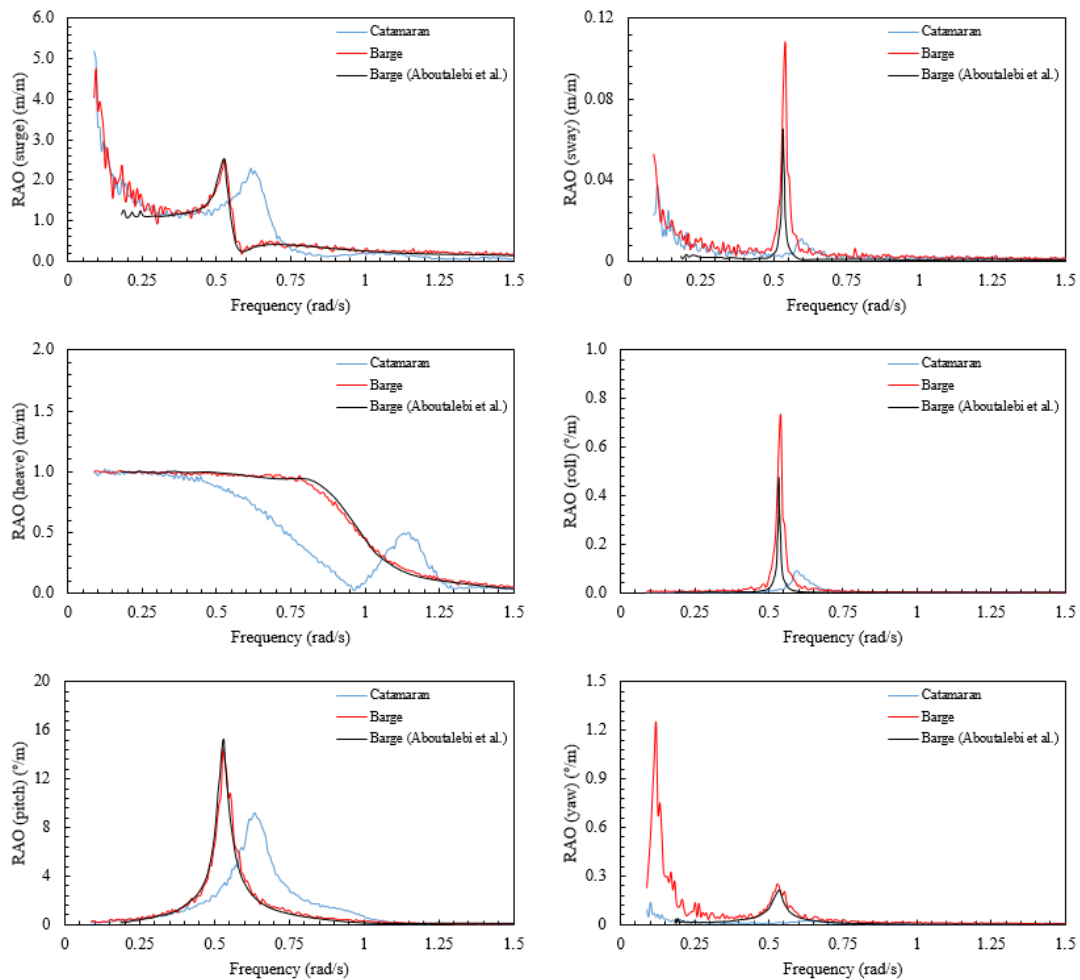
Figure 4-9. RAOs for 6 degrees of freedom of catamaran and barge platforms.

4.5.4.1 Varying angle of incidence wave

The RAOs of the catamaran platform for varying angles of incident wave are plotted in **Figure 4-10.** These results aim to provide a better understanding into the behaviour of the platform subject to wave misalignment.

The response of the platform in surge and sway are similar in magnitude of peaks and shape. The largest response occurs in wave heading angles parallel to the direction of motion i.e., 0° for surge and 90° for sway, and the smallest response occurs in wave heading angles perpendicular to the direction of motion i.e., 90° for surge and 0° for sway. For sway mode, a

small peak occurs at approximately 1.3rad/s for a wave heading angle of 90 °, this response is due to standing wave phenomenon between the demi-hulls.

Considering the heave mode, in the frequency range 0.85 – 1.25rad/s hydrodynamic interference caused by the entrapment of wave between the two demi-hulls is prevalent. For a wave heading angle of 90°, this phenomenon is most significant and has a maximum response of 1.8m/m. At approximately 1.6rad/s, another peak occurs which corresponds to the characteristic frequency for vertical plane motions due to symmetric interaction.

Similarly, to surge and sway, roll and pitch follow the trend that the largest response occurs in wave heading angles parallel to the direction of motion i.e., 0° for pitch and 90° for roll, and the smallest response occurs in wave heading angles perpendicular to the direction of motion i.e., 90° for pitch and 0° for roll. One major difference is that the roll maximum amplitude is three times that of pitch; this is because the catamaran is vessel-shaped and when exposed to oblique waves significant rolling can be induced.

Considering yaw mode, for wave heading angles 0° and 90° there is insignificant response, and for 30° and 60° one peak and two peaks occur, respectively, explained by the characteristic frequencies for horizontal plane motion due to antisymmetric interaction.
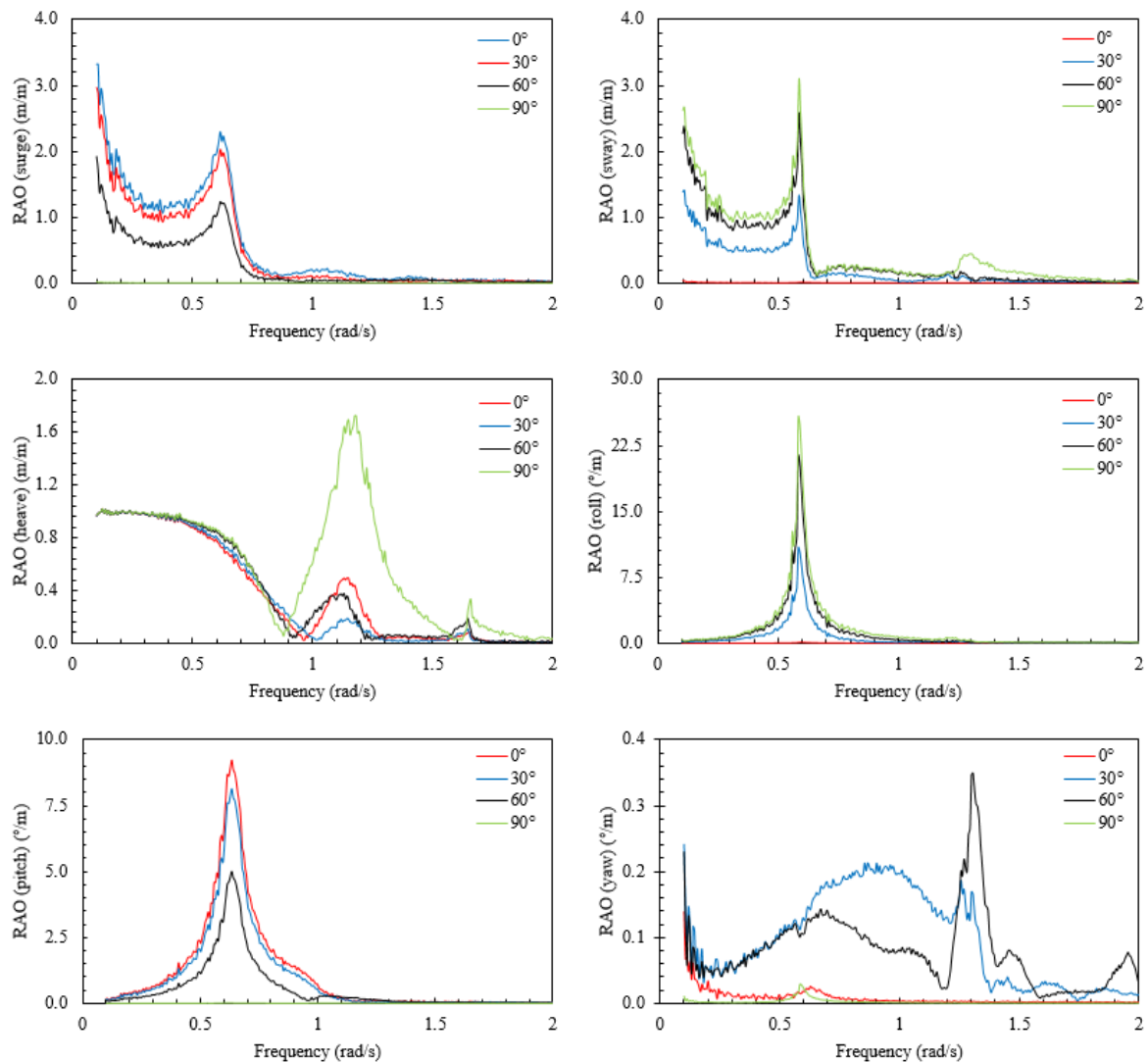
Figure 4-10. RAOs of catamaran for varying angle of incidence.

4.6 Steady wind

A series of steady wind only simulations were run to identify wind turbine characteristics and peak loads in a steady-state, and to ensure the numerical model is behaving as expected. A wind speed step of 1m/s was used for the whole wind turbine operating window (3 – 25m/s). The simulation length for each wind step was 300s, but only the last 50s of data was used to ensure steady state condition has been reached. **Figure 4-11** shows the main wind turbine characteristics under steady-state wind conditions including rotor thrust, speed and torque in addition to generator power and blade pitch angle. The rotor thrust reaches a peak thrust of

0.8MN at approximately 11.4m/s which is the rated wind speed of the turbine. The blade pitch control becomes active once the wind speed reaches the rated condition. The wind turbine maintains rated power as wind speed increases beyond the rated wind speed through pitching of the wind turbine blades. The generator power is maintained at 5MW whilst the rated rotor torque is approximately 40MN.

Figure 4-12 shows the responses of the blade-root and tower-base bending moments under steady-state wind conditions. The peak loads are observed at rated wind speed; for the flap-wise blade-root bending moment and F-A tower-base bending moment, the mean peak loads are 10MN·m and 60MN·m, respectively. For the edgewise blade-root bending moment and S-S tower-base bending moment, the trend is different. The edgewise blade-root bending moment reaches peak value at rated wind speed but then the load is relatively constant as the wind speed continues to increase remaining at a value of 1.6MN·m. For the S-S tower-base bending moment, the value steadily rises as wind speed increases. The peak S-S tower-base bending moment is approximately 8MN·m at a wind speed of 25m/s.
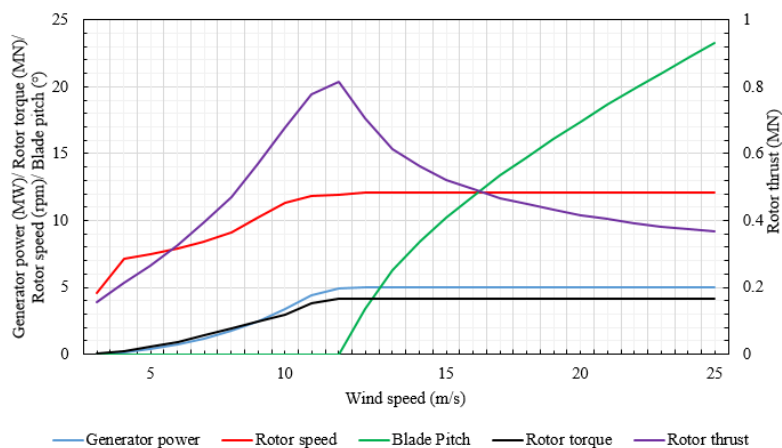
Figure 4-11. Wind turbine characteristics under steady-state wind conditions.
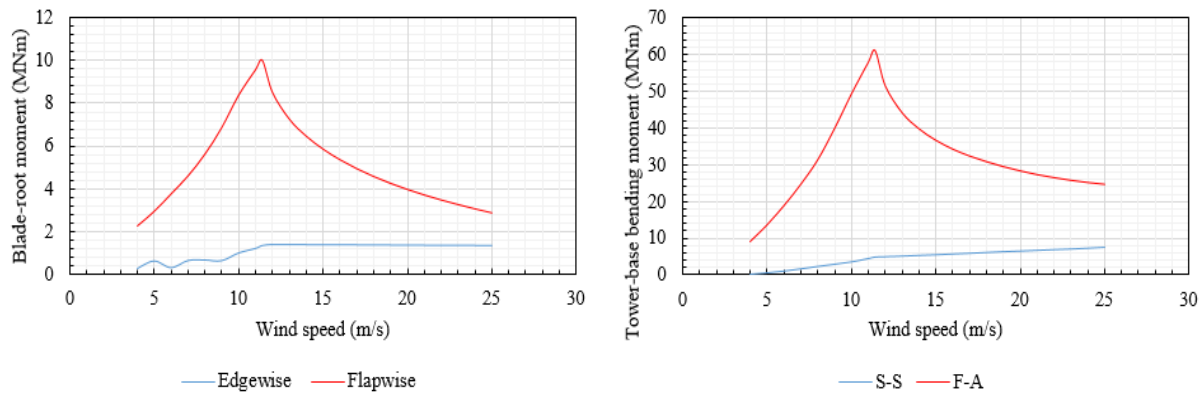
Figure 4-12. Blade-root and tower-base bending moments under steady-state wind conditions.

4.7 Dynamic responses

4.7.1 Platform motions

4.7.1.1 Statistical results

The statistical motions of the two platforms are presented in **Table 4-6**. For LC1 and LC2, the surge statistics are almost identical. Under LC3, some differences are observed, it is predicted the catamaran has a smaller mean surge with greater fluctuation and a greater maximum surge. The highest mean surge for both platforms was predicted under LC3, corresponding to the rated wind speed condition. A wind turbine operating at rated wind speed produces maximum rotor thrust (approx. 800kN for 5MW wind turbine), which significantly influences the surge of FOWTs. Under LC4 and LC5, the catamaran has a greater mean and maximum surge and increased fluctuation compared to the barge. Both platforms experience their greatest maximum surge under LC5 because of the largest wave loads. For all five LCs, the heave statistics of the two platforms are indistinguishable apart from the maximum responses for the last 3 LCs. This was expected due to the comparable dimensions of the water plane areas. Considering pitch, for all LCs the catamaran platform has the smallest mean. The elongated geometry of the catamaran compared to the barge provides a greater restoring

moment about the y-axis. The highest mean pitch response for both FOWTs is observed under

LC3. The fluctuation of the catamaran under LC4 is noticeably greater compared to the barge.

This is most likely due to combined wind and wave loading exciting the catamaran at its natural

pitch period, nonetheless performance of the catamaran is good with a predicted mean pitch of

0.2° and maximum pitch of 8.52°.

Table 4-6. Statistical results of platform motion responses (1000 – 4600s).

LC	Type	Surge (m)		Heave (m)		Rel. Pitch (°)	
		Catamaran	Barge	Catamaran	Barge	Catamaran	Barge
	Max	16.96	**16.35**	**0.066**	0.300	**0.314**	1.025
1	Mean	8.343	8.490	-0.125	**0.123**	**0.067**	0.328
	Std.dev	2.734	3.198	**0.059**	**0.059**	**0.080**	0.179
	Max	34.68	**33.35**	**0.456**	0.645	**1.581**	2.153
2	Mean	22.25	22.32	**-0.115**	**0.115**	**0.295**	1.094
	Std.dev	3.809	**3.674**	**0.114**	0.156	0.312	**0.226**
	Max	48.14	**45.52**	**0.410**	1.149	**2.936**	3.826
3	Mean	27.18	29.29	-0.143	**0.108**	**0.370**	1.726
	Std.dev	11.31	**7.050**	**0.151**	0.308	0.712	**0.545**
	Max	44.41	**30.08**	**1.720**	2.148	8.519	**4.243**
4	Mean	21.92	**19.30**	-0.134	**0.118**	**0.200**	0.997
	Std.dev	8.046	**4.298**	**0.398**	0.593	2.492	**1.026**
	Max	50.03	**37.19**	**2.727**	3.352	12.770	**12.190**
5	Mean	20.60	**8.583**	**-0.104**	0.122	**0.179**	0.862
	Std.dev	**10.78**	11.53	**0.733**	0.895	4.046	**3.775**

*(**BOLD** = minimum)*

4.7.1.2 Time- & Frequency-domain results

The time- and frequency-domain platform responses of both models under LC3 are

presented in **Figure 4-13** and **Figure 4-14**. Considering time-domain platform responses, it is

obvious the catamaran has increased fluctuation from mean surge compared to barge. The

mooring system is mainly responsible for surge stability, therefore in future research the

mooring system is one aspect that will be further investigated. Considering heave, the stability

of the catamaran is excellent, whilst the barge experiences greater fluctuation. The mean pitch

of the catamaran is smaller compared to the barge; however greater variation is observed. Even with increased fluctuation, the maximum pitch of the catamaran does not exceed ±3°.

Considering frequency-domain platform responses, the amplitude of surge response in frequency-domain for the catamaran and barge platforms is dominant near 0.06rad/s, corresponding to the resonant frequency of this mode for both platforms. Smaller peaks are observed at approximately 0.4rad/s and 0.54rad/s for the barge and catamaran, respectively, which equate to the pitch natural frequency of each platform. The response suggests the coupling between surge-pitch for both platforms is somewhat small. When considering heave, there is a limited response in lower frequency region. Peaks occur at 0.80rad/s and 1.14rad/s, for the barge and catamaran, respectively, which is due to the heave natural frequency of the respective platform. Considering pitch, an obvious peak can be seen at approximately 0.4rad/s, which corresponds pitch resonant frequency of the barge platform. The pitch resonant frequency of the catamaran platform is approximately 0.54rad/s and the amplitude of the peak is slightly higher compared to the peak at resonant frequency of the barge.
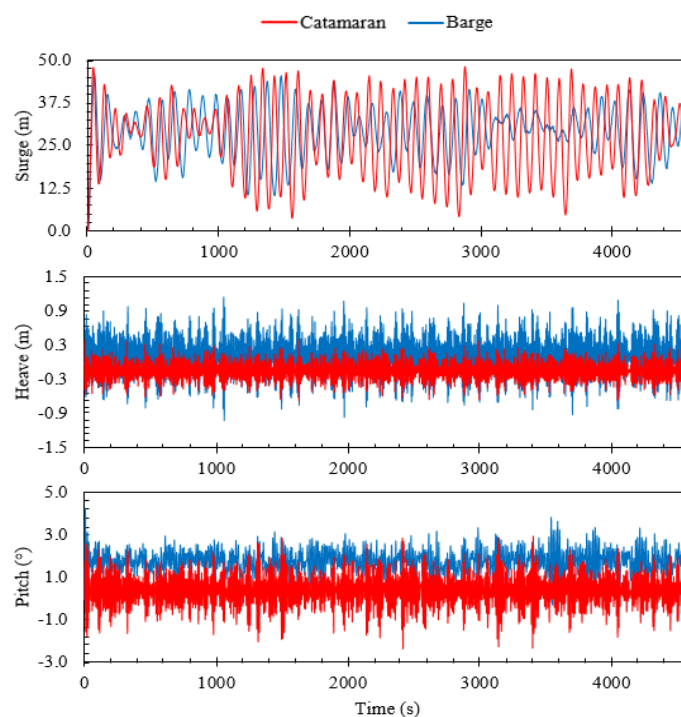
Figure 4-13. Time-domain responses of FOWT concepts under LC3 (rated wind speed).
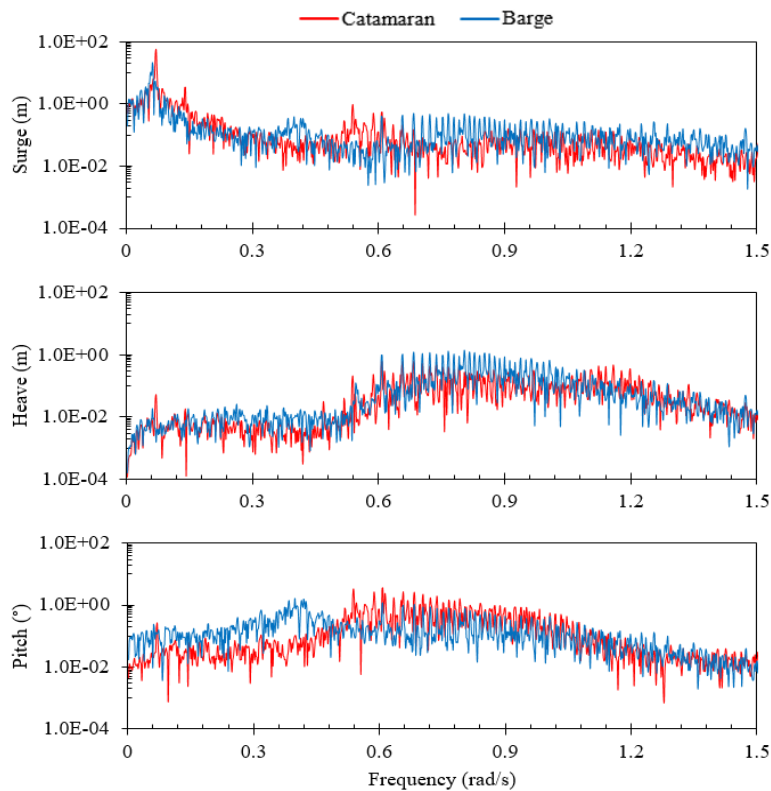
Figure 4-14. Frequency-domain (spectral) responses of FOWT concepts under LC3 (rated wind speed).

4.7.2 *Mooring line responses*

Figure 4-15 presents the mean and maximum fairlead tensions of the two FOWTs. Both mooring system configurations use eight catenary lines to keep the platform in position. The symmetric nature of the mooring systems requires only certain mooring lines to be examined. Therefore, four mooring lines of the barge (MB1, MB3, MB5, MB7) and catamaran (MC1, MC3, MC5, MC7) mooring systems are selected. Due to incident waves, prevailing wind and rotor thrust all acting or travelling downstream, the fairleads upstream of the origin will experience the greatest tension. This is because such external forces cause the platform to drift downstream. As this happens, the mooring lines upstream will stretch increasing tension in the lines, in order to prevent drifting, whilst the mooring lines downstream will slack.

Consequently, MB5 and MC5, exhibit the greatest tension. The barge and catamaran mooring lines have similar mean tensions under all LCs, except for mooring line MC5 in LC4 and LC5 where MC5 is fractionally higher than MB5. Under these two LCs, the maximum tension of mooring line MC5 is approximately 1.5 times the tension of MB5 under LC4 and 2 times the tension under LC5. This can be explained by the large surge response of the catamaran platform under these two LCs.
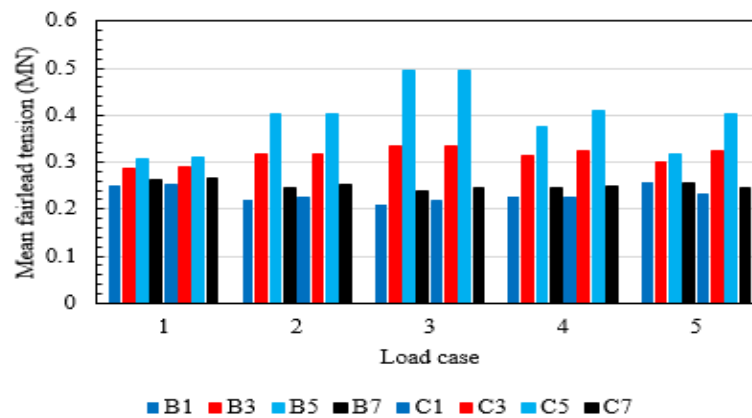
a) Mean fairlead tension.
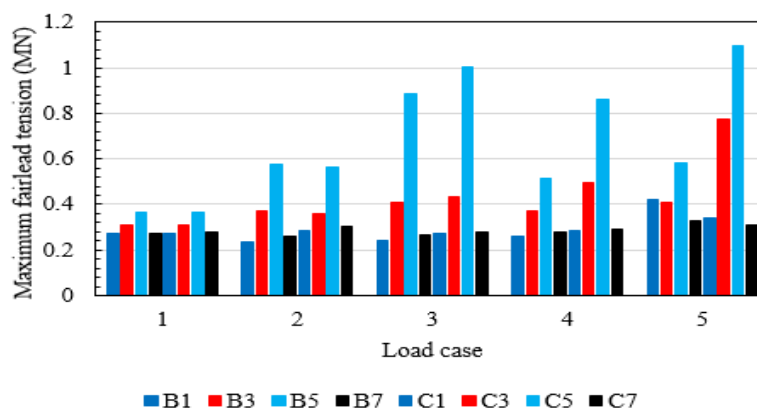
b) Maximum fairlead tension.

Figure 4-15. Fairlead tension (MB1 = barge line 1, MC1 = catamaran line 1).

4.7.3 Power production

The generator power statistics for LCs 1 - 5 are charted in **Figure 4-16** and the time-domain generator power under LC3 is presented in **Figure 4-17**. For LC1 and LC2, the results are incomparable. Under LCs 3 - 5, the catamaran has greater maximum generator power but larger standard deviation, whilst the barge has greater minimum and mean generator power. In **Figure 4-17**, it can be seen both FOWTs follow similar trends for the entire simulation, however the barge has better quality power because of less fluctuation.
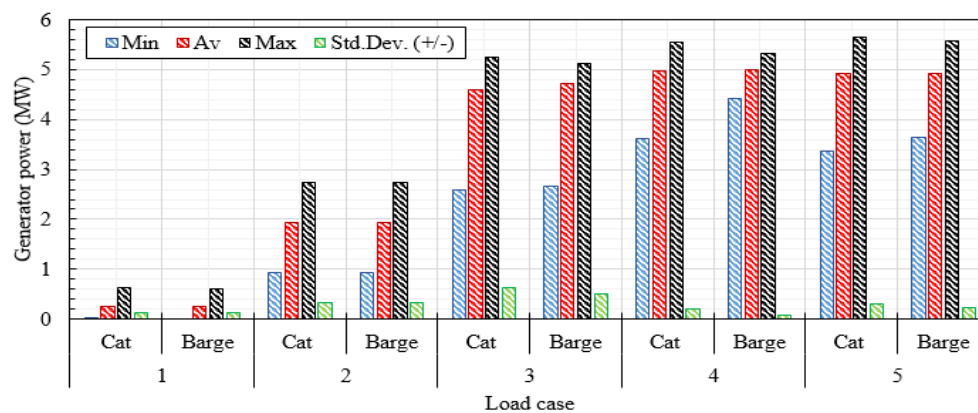
Figure 4-16. Comparison of generated power between catamaran and barge FOWTs.
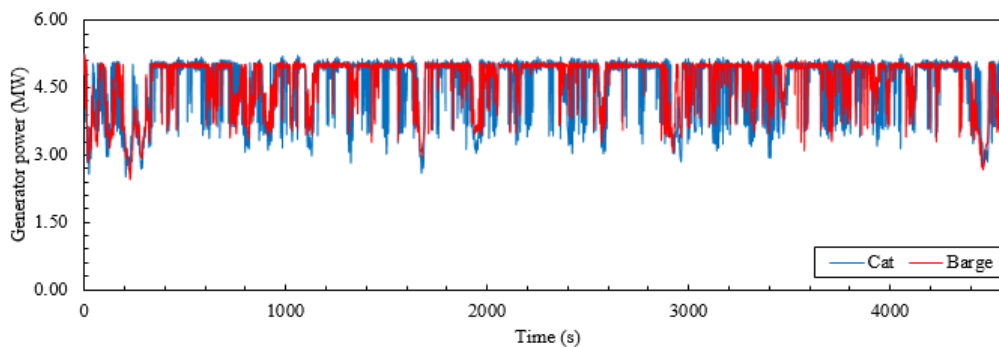
Figure 4-17. Generator power of the catamaran and barge FOWTs under LC3.

4.7.4 Blade, rotor, and tower responses

Figure 4-18 and **Figure 4-19** plot the rotor thrust, Out-of-Plane (O-o-P) blade-tip deflection and tower-base bending moments of both platforms. Rotor thrust, O-o-P blade-tip

deflection and Fore-Aft (F-A) tower-base moment all follow a similar trend because of the direct and indirect influence of the incoming wind. The rotor thrust, being the axial force, is applied by the wind kinematics on the wind turbine rotor and it is the dominant load acting on each FOWT. The O-o-P blade-tip deflection is the result of wind-induced force on the wind turbine blades. The F-A tower-base bending moment is mainly caused by the rotor thrust and has the most prominent influence on stress at the tower base. The peak thrust acting on both wind turbine rotors occur under LC3. This is also true for peak F-A tower-base bending moment and O-o-P blade-tip deflection. Comparing the two FOWTs, for all LCs, the barge platform has higher rotor thrust. Under LC3, the barge and catamaran platforms have an approximate mean rotor thrust of 750kN, and 700kN, respectively, which is a difference of 7%. The maximum rotor thrust of the barge and catamaran is 1066kN and 1123kN, respectively. The mean F-A tower-base bending moment is 64MN·m and 52MN·m for the barge and catamaran, respectively, representing a difference of 23%. The maximum F-A tower-base bending moment is 140MN·m and 104MN·m for the barge and catamaran, respectively. The mean O-o-P blade-tip deflection of both concepts for all LCs is similar. For LC4 and LC5, the standard deviation is higher for the catamaran compared to the barge. For all LCs, the barge has the greatest S-S tower-base bending moment, which stems from the tangential forces, or aerodynamic drag, that tend to bend the blades and tower in the rotor plane. Comparing the two platforms, the differences in the first two LCs are insignificant. For LCs 3 - 5, there is

approximately a 15% difference between the S-S tower-base bending moments of the barge and catamaran platforms.
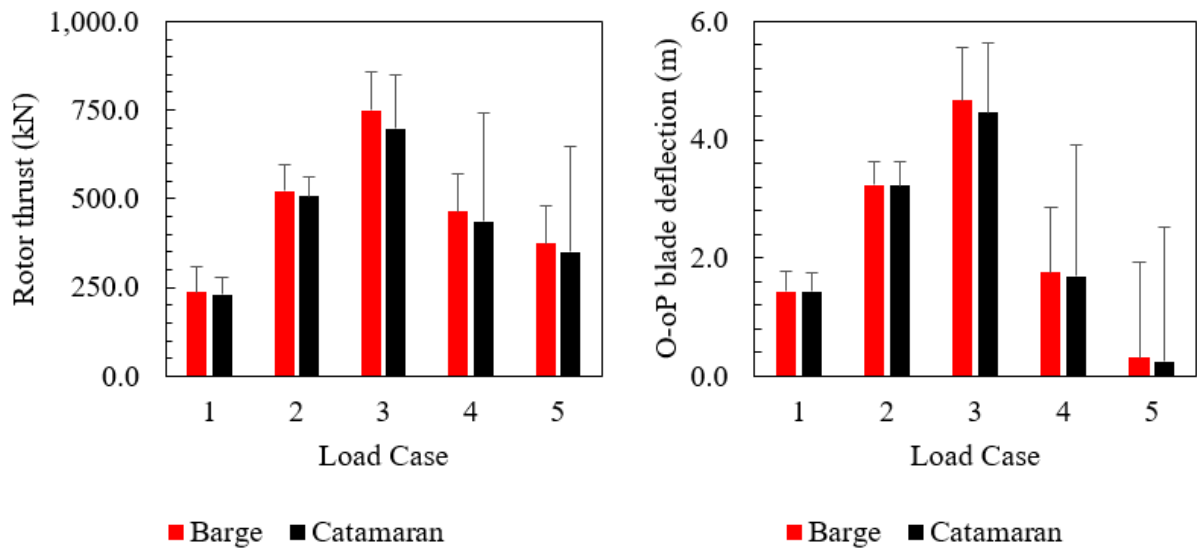
Figure 4-18. Comparison of mean rotor thrust and blade-tip deflection.
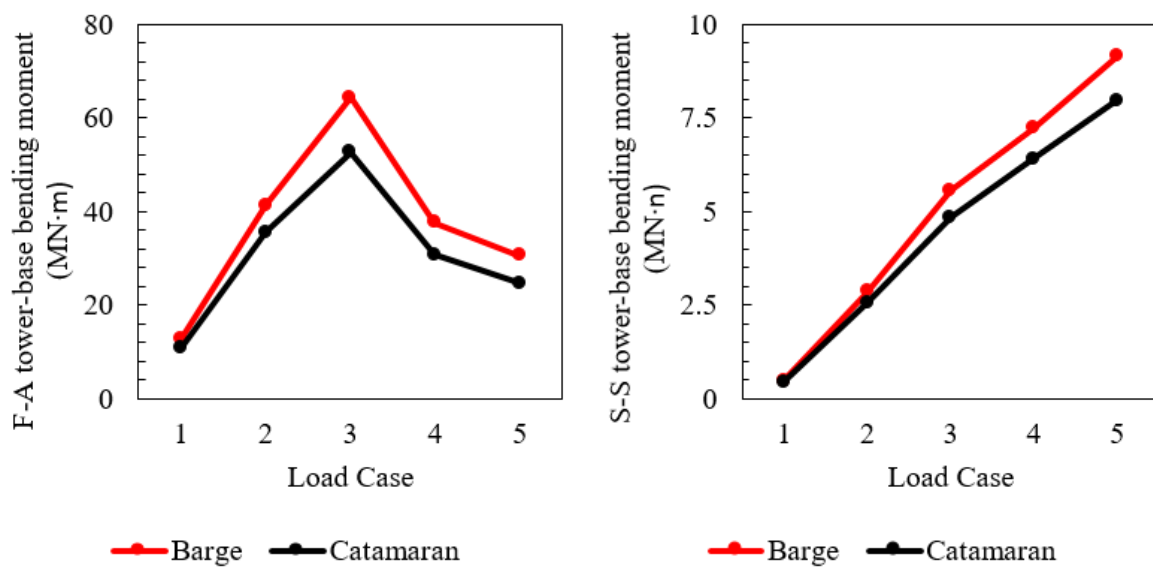
Figure 4-19. Comparison of barge and catamaran tower-base bending moments.

4.7.5   *Incident wave angle at 30° and 90°*

This next section presents and discusses the results of LC6 and LC7 which were simulated to investigate the dynamic responses, in terms of platform motions, mooring line tensions,

produced power and tower-base bending moments, of the two FOWTs when the alignment between the incoming wind and waves change.

4.7.5.1 Platform motions

Figure 4-20 charts the platform motion statistics and **Figure 4-21** and **Figure 4-22** compare the platform motion time histories of the two platforms under LC6 and LC7. Considering surge, the mean of both platforms is similar for all wave headings which is approximately a 25-30m offset. As the wave heading angle goes around the compass, the variation in surge of the catamaran reduces whereas for the barge it increases. For sway mode, this is mirrored with the catamaran fluctuating more compared to the barge. However, the amplitude of catamaran sway when the waves are incoming at 90° is reasonable with a maximum amplitude of 15m. The heave response of the barge is similar for all wave headings, meanwhile the variation in heave response of the catamaran noticeably increases when the waves are incoming perpendicular to wind inflow. This is due to entrapped water between the demi-hulls amplifying the heave response as discussed in the previous sections. A maximum heave of 1.5m is observed which means the effect of this dynamic amplification is insignificant. For roll and pitch motion of the catamaran similar but opposite trends occur. The roll response increases whilst pitch response decreases as the wave heading angle increases towards 90°. The roll behaviour of the barge is similar to the catamaran; however, the pitch behaviour is slightly different in that the response is nearly identical for varying wave headings. This suggests the pitch response of the barge is dominated by wind loading whilst the catamarans pitch response is dependent on wave loading. The yaw response of the catamaran when the wave heading is 90° is much larger compared to the barge. This is because the catamaran is much longer which means it will tend to yaw with incident waves perpendicular to the x-axis. **Figure 4-23** and **Figure 4-24** show the effect of yawing on power generation for the catamaran. When the platform is positioned directly facing the incoming wind, the power produced is 4.9MW. This

is the maximum power the turbine can produce given its efficiency. When the platform is yawed 5°, 10°, and 15°, the produced power is 4.85MW, 4.71MW, and 4.50MW, equating to a reduction of 1%, 3.82%, and 8% in generated power, respectively. Therefore, it can be said that if the platform does not yaw more than 15°, then reduction in power cannot exceed 8%, and for 10°, 3.82% and for 5°, 1%. Under LC7, the catamaran only experiences a maximum yaw of 6° during the one-hour simulation for a brief period of time which means that the produced power is not significantly affected.
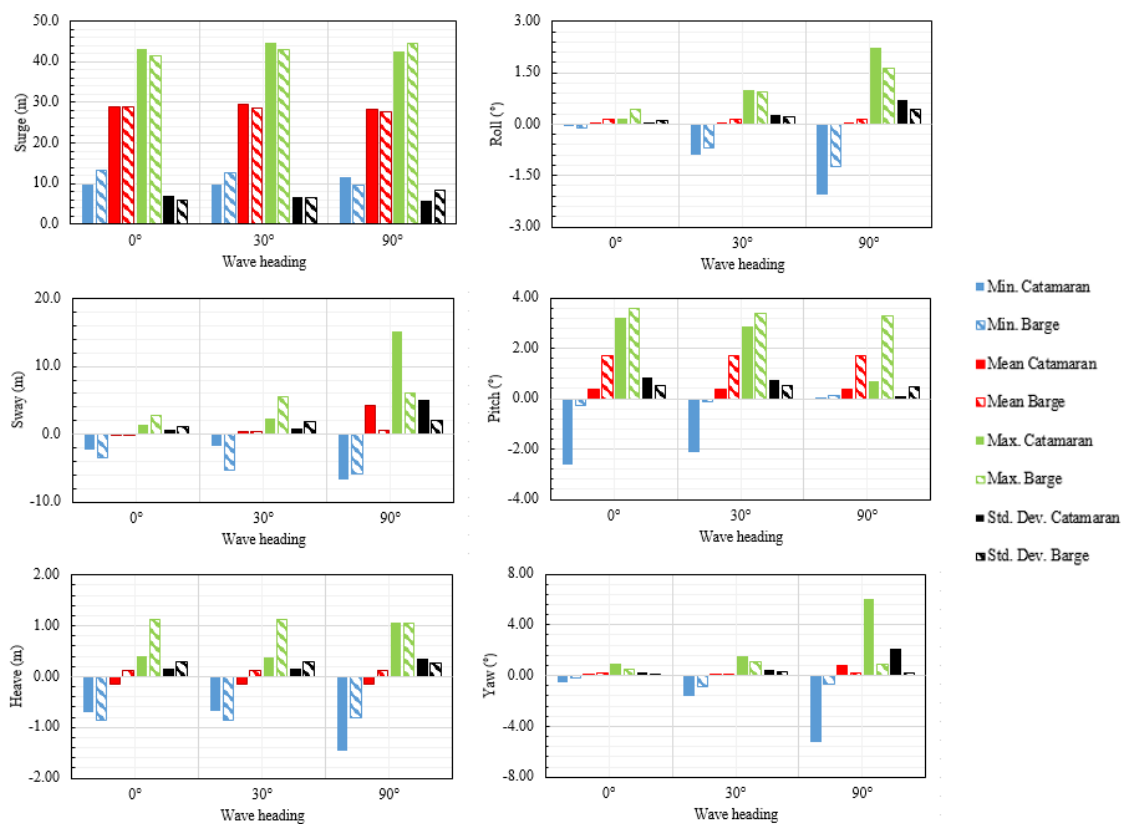
Figure 4-20. Platform statistics for varying angle of wave incidence.
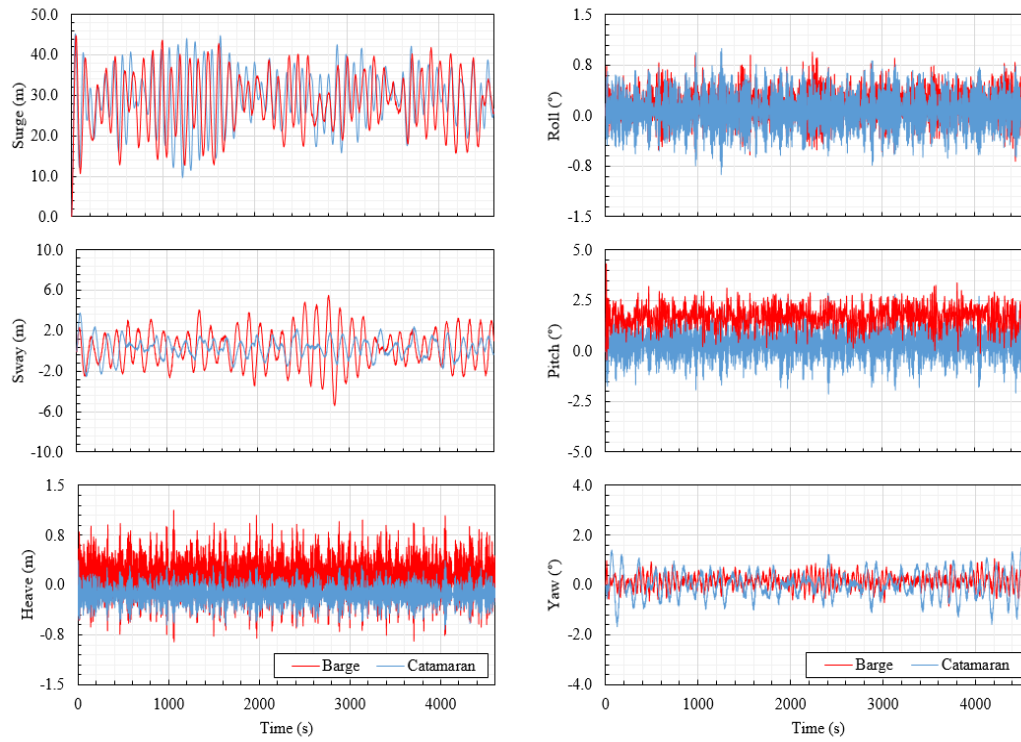
Figure 4-21. Time-domain platform motions under LC6.
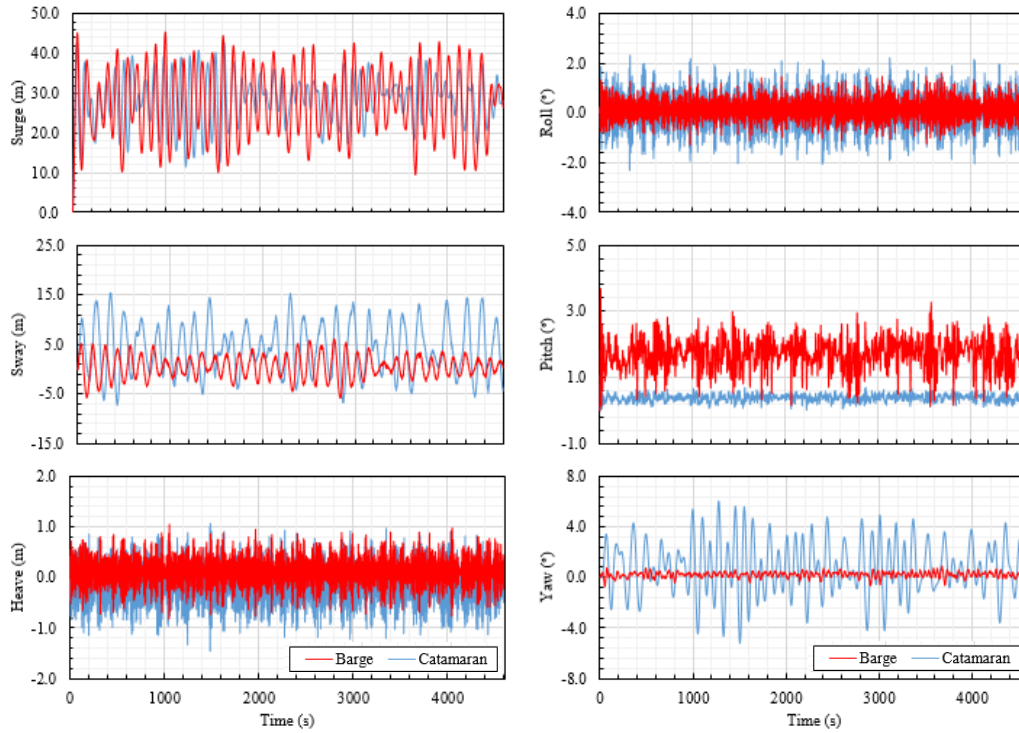
Figure 4-22. Time-domain platform motions under LC7.
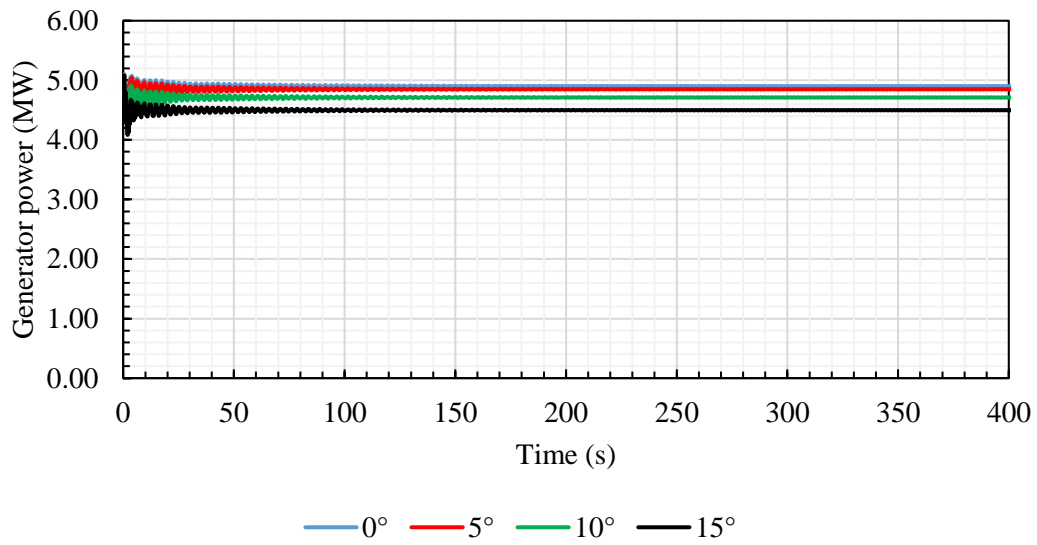
Figure 4-23. Effect of yawing on power generation.
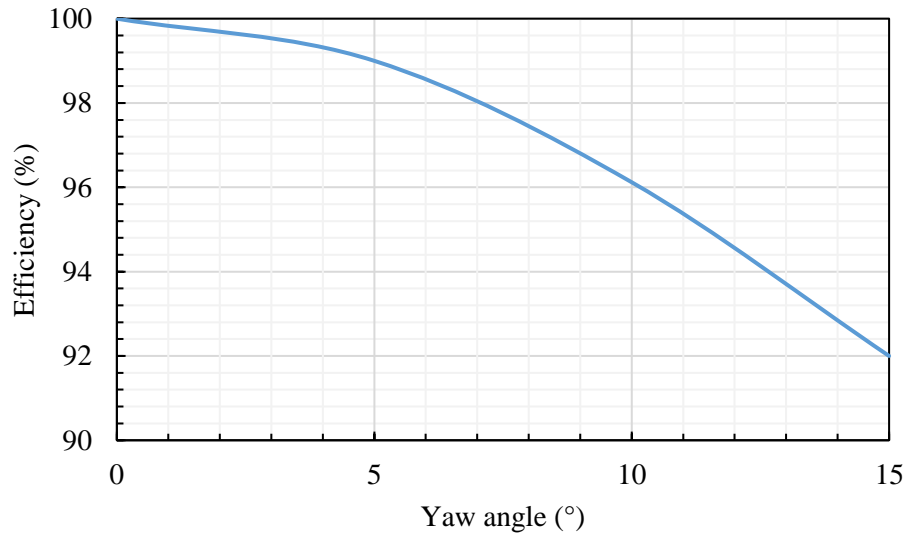
Figure 4-24. Wind turbine efficiency vs platform yawing.

4.7.5.2   *Mooring tensions*

Figure 4-25 compares the time-domain fairlead tensions of both platforms under LC6 and LC7. When considering LC6, there are negligible differences in the fairlead tension of all mooring lines between both platforms. The maximum fairlead tension is approximately 0.84MN. Under LC7, the waves are incoming perpendicular to the direction of wind flow. The surge response for the catamaran under this load case reduces. As a result, the predicted maximum fairlead tension is lower. Conversely, the surge response of the barge is similar for both load cases and the mooring line tension follows a similar trend in both simulations.
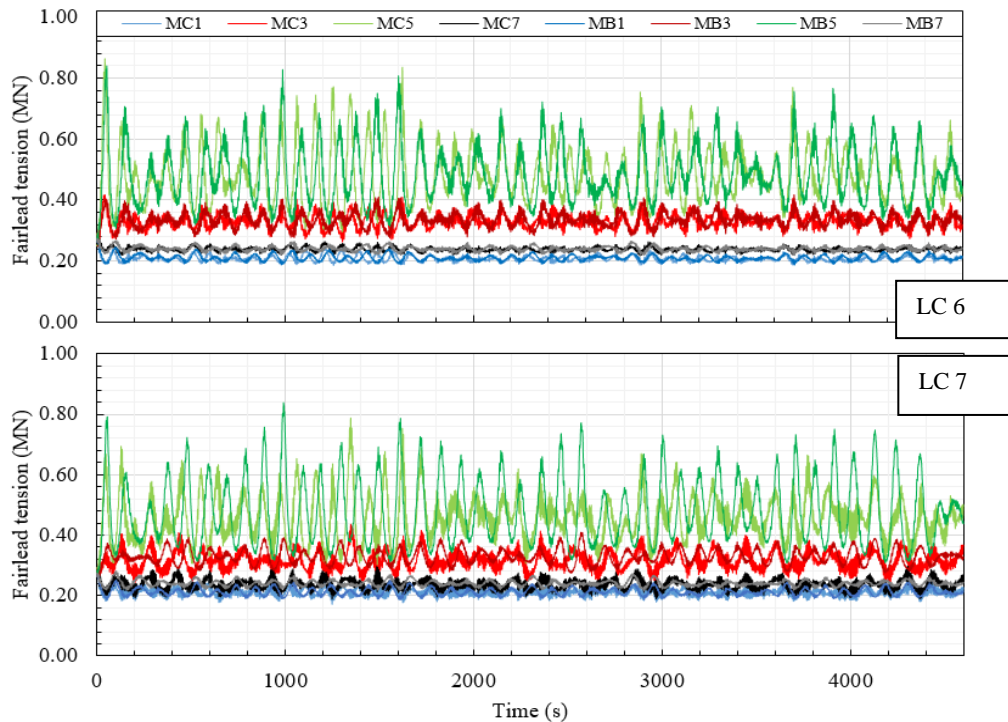
Figure 4-25. Time-domain fairlead tensions under LC6 and LC7.

4.7.5.3   Power production

Table 4-7 tabulates the power production statistics under LC6 and LC7, whilst **Figure 4-26** graphs the generator power time histories of both platforms. From **Table 4-7**, it can be said that the quality of power produced by the catamaran improves as the misalignment between the incoming wind and waves increases up to 90°. This is because the minimum and mean power produced increases whilst the standard deviation decreases. The maximum produced power also decreases however, this is by a small amount. On the other hand, the quality of power produced by the wind turbine supported by the barge is constant for all wave heading angles. Subject to LC6, **Figure 4-26** shows the produced power by the wind turbines supported by operate similarly. Under LC7, the power generated by the wind turbines follow a similar trend, however the power produced by the wind turbine supported by the catamaran platform is of better-quality power due to less fluctuation.

Table 4-7. Power production of both platforms under varying wave headings.

	0°		30°		90°	
	Catamaran	Barge	Catamaran	Barge	Catamaran	Barge
Min.	1.961	1.967	1.955	1.933	2.007	1.917
Mean	4.507389	4.52403	4.520281	4.523217	4.542581	4.518437
Max.	5.184	5.125	5.18	5.111	5.085	5.09
Std. Dev.	0.711707	0.673443	0.694152	0.672026	0.648891	0.674523
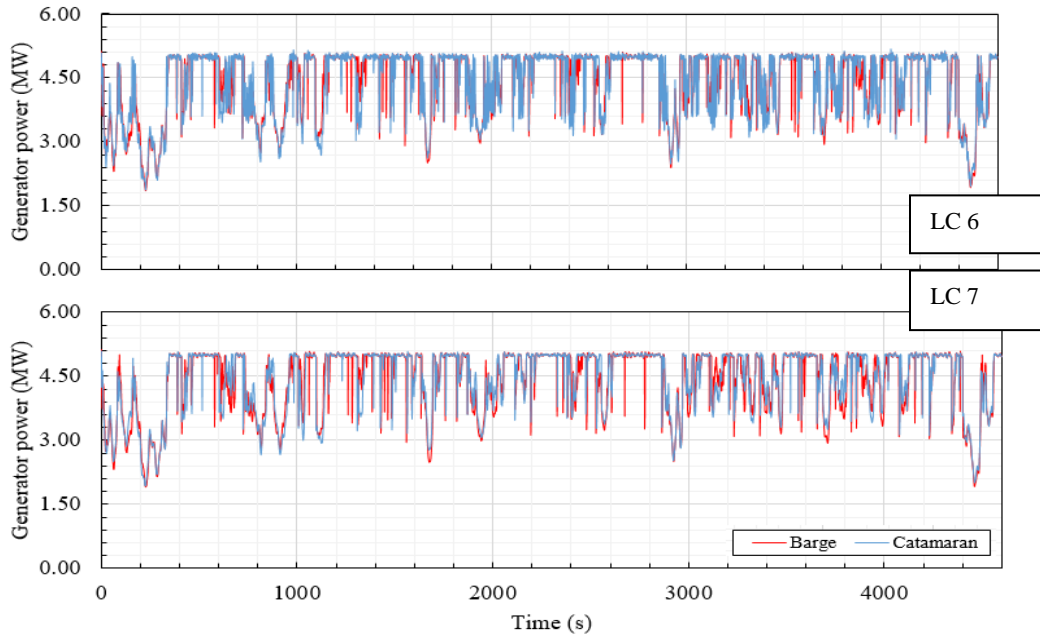
Figure 4-26. Time-domain generator power of both platforms under LC6 and LC7.

4.7.5.4   Tower-base bending moments

Figure 4-27 presents the tower-base bending moments about the x- and y-axis of both platforms for 30° and 90° wave headings. The results show that the bending moments at the tower-base of the wind turbine supported by the catamaran are smaller and experience less fluctuation compared to the barge for both wave headings. In addition, as the misalignment between the incoming wind and waves increase, the bending moment about the y-axis decreases whilst the bending moment about the x-axis increases for both platforms. This as expected as the wave hydrodynamic loading is the dominant loading.
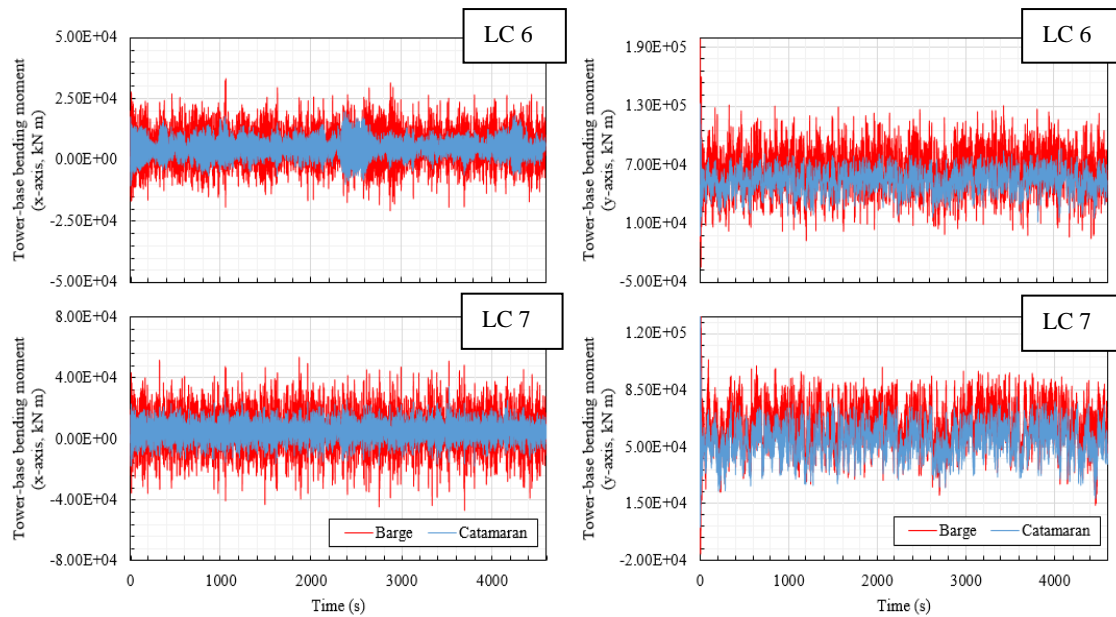
Figure 4-27. Time-domain tower-base bending moments of both platforms under LC6 and LC7.

4.8 Chapter summary and conclusions

This chapter has presented the development of a novel catamaran-type FOWT concept. The hydrodynamic characteristics and dynamic responses of the catamaran-type FOWT is assessed in intermediate water depth in common operational conditions. The results are compared with a well-known barge-type FOWT, the ITI Energy barge. The FOWTs are modelled using OpenFAST and ANSYS AQWA numerical tools coupled via a DLL, namely F2A, to conduct efficient fully coupled aero-hydro-elastic-servo simulations.

The results of the current research have revealed advantages which a catamaran-type floater has over a conventional barge-type floater:

- The catamaran has a large deck area; this can be used for other functions such as marine power generation, solar panels, or hydrogen conversion. If utilised properly the additional functionality could lead to cost reductions e.g., through increased power generation.

- Evaluation of hydrodynamic characteristics has shown that the catamaran has better hydrodynamic performance over the barge. The catamaran platform has higher sway, roll, pitch, and yaw hydrodynamic coefficients compared to the barge. This means the catamaran floater has increased hydrodynamic restoring stiffness and damping for these modes of motion.

- The catamaran platform responds distinctively at certain frequencies for vertical and horizontal plane motions due to symmetric or antisymmetric interaction, respectively. These frequencies are analogous to the resonant modes of a standing wave between two vertical walls. Moreover, the frequencies are characteristic to the individual platform and depend on demi-hull separation.

- Findings from the free decay results show that the catamaran floater has increased natural damping in the system for roll and pitch modes compared to the barge floater. This was especially the case for pitch, where observed damping was increased considerably. This was confirmed in the RAO analysis; the amplitude observed at the pitch natural frequency of the catamaran floater was reduced by 50% compared to amplitude observed at the pitch natural frequency of the barge.

- The time-domain simulations showed the response of both platforms were similar for simulated load cases, which meant the expected improvement in pitch stability was not necessarily reflected. The reason for this was that the simulated wave periods coincided with the natural pitch period of the catamaran which amplified the platform's dynamic response. Nevertheless, the pitch response of the catamaran was similar to that of the barge. The fact that the catamaran behaves similarly to the barge whilst being excited at its natural frequency highlights the platform's good hydrodynamic performance. One future avenue for research could be how the geometric characteristics of the catamaran floater affect its pitch natural period.

- The results of this study also showed that the catamaran floater had reduced tower-base bending moments (both F-A and S-S) for all simulated conditions. For rated wind speed (LC 3) and corresponding wave condition, the F-A tower-base bending moment was reduced by 22%.

Considering this research was a preliminary investigation into catamaran-type floaters and the design was a first iteration, there is unambiguous evidence that a catamaran floater has advantages over a conventional barge. With optimization and advanced concept development, it would be anticipated that the performance can be further enhanced which makes this a promising concept to support a wind turbine in intermediate water depths.

The next chapter represents the second stage of this project, which is the development, integration, and testing of two marine renewable energy system types with the catamaran-type FOWT individually. The first half of the chapter is the development of separate numerical models of the marine renewable energy systems, and the second half of the chapter is the integration of these numerical models into the numerical model of the catamaran-type FOWT developed in F2A.

Chapter 5.   Tidal and wave energy system numerical model development and integration

This chapter presents the second stage of this project which is the numerical model development and integration of tidal and wave energy systems. The chapter is organised into two parts: Section 5.1 is the numerical model development of the tidal and wave energy systems, and Section 5.2 is the numerical model integration with the numerical model of the catamaran-type FOWT. In Section 5.1, numerical models of the tidal turbine system (Section 5.1.1) and wave energy converter system (Section 5.1.2) are built within the appropriate tools. The models are validated against available experimental or numerical data. Section 5.2 develops: (1) a model of the catamaran FOWT integrated with tidal turbines (CTT) and (2) a model of the catamaran FOWT integrated with a WEC system (CWEC). Section 5.2.1 and Section 5.2.2 is dedicated to the CTT concept and CWEC concept, respectively. These models are used to improve understanding on the coupled dynamics of the catamaran FOWT when separately integrated with two different types of ocean energy systems. Specifically, the numerical models are used to study the overall platform motion and structural component responses in addition to total generated power. Additionally, any possible negative effects arising from the presence of the ocean energy systems will also be reported. The results of will be beneficial in understanding the coupled dynamics of the final model of the triple integrated CFOES. Section 5.2.3 presents a summary of the chapter and conclusions drawn from the obtained results.

5.1 Numerical model development of marine renewable energy systems

5.1.1 Tidal turbine

The tidal turbine system is a reference model design (RM1) developed by a consortium led by Sandia National Laboratories (Neary et al. 2014). The RM1 device is a dual variable-speed variable-pitch axial-flow tidal turbine device. The turbines were originally designed to be mounted onto a monopile foundation via a cross-arm assembly. The cross-arm assembly is nearly neutrally buoyant which eases maintenance operations. The dimensions of the RM1 device are provided in **Figure 5-1** and the main properties are listed in **Table 5-1**. Each rotor has a diameter of 20m, and they are offset by 28m from each rotor centreline. The hub depth is 20m which reduces cavitation potential. The controller is based on the NREL 5 MW reference wind turbine controller developed by Jonkman (Yang et al. 2020b).
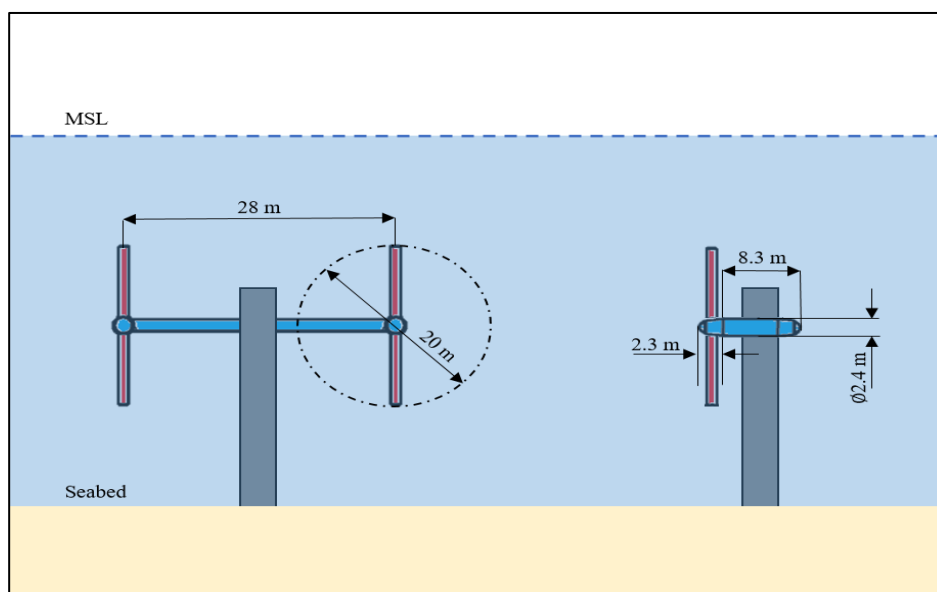
Figure 5-1. RM1 device dimensions.

Table 5-1. Design properties of tidal turbines.

Property (Unit)	Specification
Rated power per rotor/ total rated power (MW)	0.55/ 1.1
Rated current velocity (m/s)	2.0
Operational current velocities (m/s)	0.5 – 3.0

Hub diameter (m)	2.0
Total mass per turbine (kg)	61,300

5.1.1.1   *Verification and validation of numerical model*

Steady current simulations were run to test the numerical model of the tidal turbines for known inflow conditions. The turbines were examined for the full turbine operating window and the inflow current was increased in steps of 0.1m/s. The rotor speed and generator power were measured for each step in current speed. **Figure 5-2** presents the results and compares them to the results published by Yang et al. (Yang et al. 2020b). There is good agreement between the results of the present numerical model and the published results. The agreement verifies the numerical model can produce adequate results and that the tidal turbine controller is working as expected.
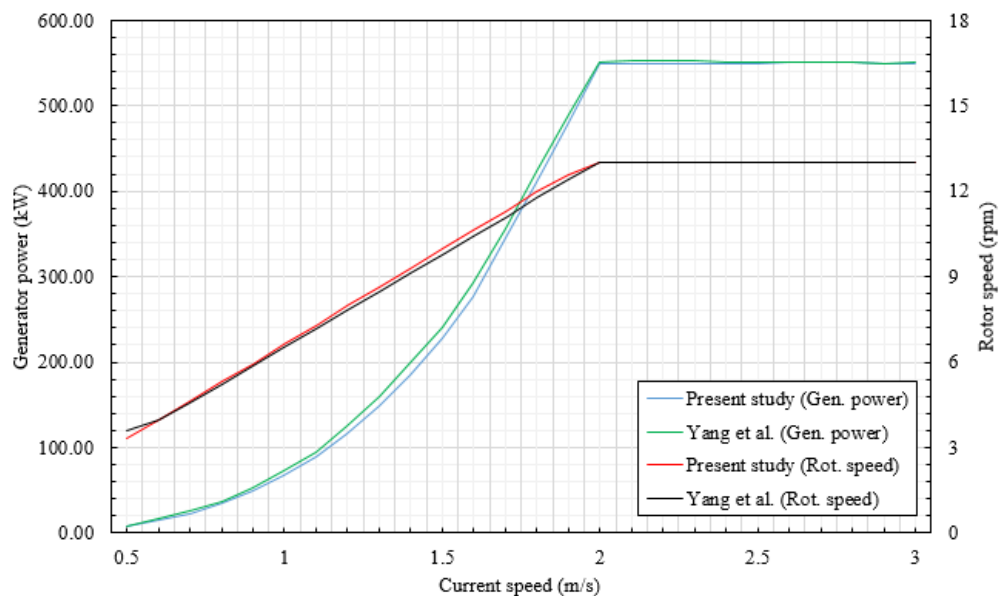
Figure 5-2. Comparison of rotor speed and generator power under steady conditions.

In addition to the steady current tests, simulations were run which varied the tidal turbine rotor speed under steady current of constant velocity. Such tests provide insight into the optimum performance of the tidal turbines. **Figure 5-3** plots the power coefficient against the

tip-speed ratio. The calculated performance curve of the tidal turbine rotors from the numerical model are compared to the experimental performance curves of the tidal turbine rotors published by Hill et al. (Hill et al. 2020). Hill et al. physically modelled the RM1 device in the Main Channel facility at St. Anthony Falls Laboratory at the University of Minnesota. It is noted that Hill et al. modified the blade profile of the RM1 device to cope with low Reynolds numbers during experiments. Moreover, only one performance curve is plotted from the numerical model because the tidal turbines are identically modelled.
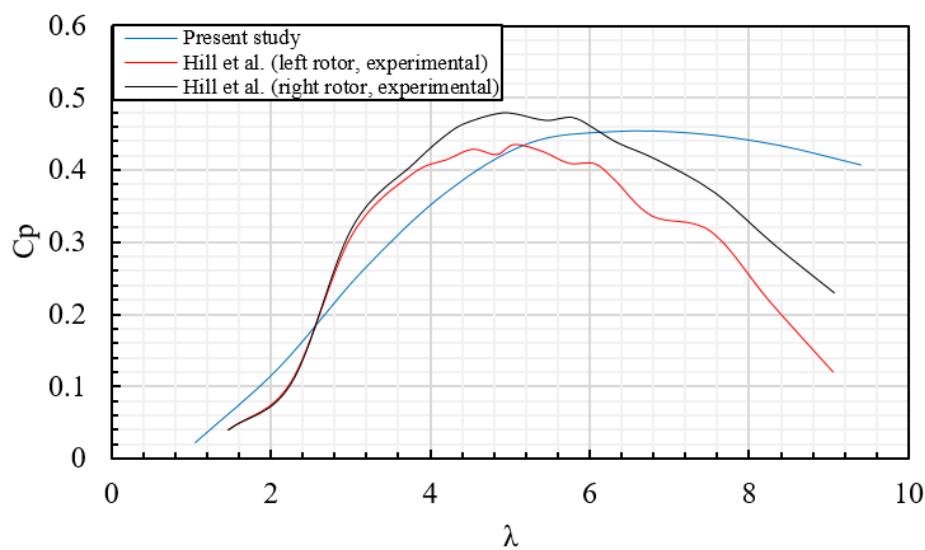
Figure 5-3. Calculated C_p vs λ (coefficient of power vs tip-speed ratio).

The comparison to experimental data offers opportunity to validate the numerical model as long as satisfactory agreement is observed between the results of the numerical model and experimental model. The maximum power coefficient of the tidal turbines predicted by the numerical model is 0.45, whereas the maximum power coefficients of the physical model are 0.43 and 0.48 for the left and right tidal turbine, respectively. There are some differences between the numerical and experimental datasets which include the tip-speed ratio at which the maximum power coefficients are observed and the rate at which the power coefficient falls as tip-speed ratio increases. For the present study, maximum C_p occurs when $\lambda = 6$, whilst for the physical model the maximum C_p is observed when $\lambda = 5$. This means that the numerical model

is predicting the optimum performance of the tidal turbines for slightly higher rotor speeds. The reason for this is because in order to achieve a rated power of 550kW under the rated current speed of 2m/s, the rotor speed was increased from 11.5rpm to 13rpm. The second difference was the rate at which the power coefficient decreases as the tip-speed ratio increases. In the present study, the performance curve does not decrease as sharply compared to the performance curves calculated from the experimental model. It is expected that the modifications in turbine blade profile have marginally altered the performance of the tidal turbines. Generally, the performance curves show satisfactory agreement across the tip-speed ratio range and there is good agreement in the magnitude of maximum $C_p \approx 0.45$. The combination of these two factors provides assurance that the numerical model of the RM1 tidal turbine system is satisfactory.

5.1.2   *Wave energy converter*

The WEC system is a series of point-absorbers which are collectively known as the Wavestar concept (**Figure 5-4**). An individual Wavestar unit is a partially submerged hemispherical buoy which is rigidly connected to an arm that is attached to the main structure via a hinge. Each float can rotate about the pivot point with the action of the waves. The relative motion between the floats and pivot points motivates hydraulic PTO pistons which in turn produce electrical power. Whilst a single Wavestar unit is a point-absorber WEC, the collective Wavestar system can also be considered as an attenuator WEC. This means when the wave propagates through the system each float is worked one after the other. Therefore, the system should be aligned with the dominant wave direction to maximize energy conversion. The advantages of this are that the produced power is smoother compared to other point-absorber WECs.
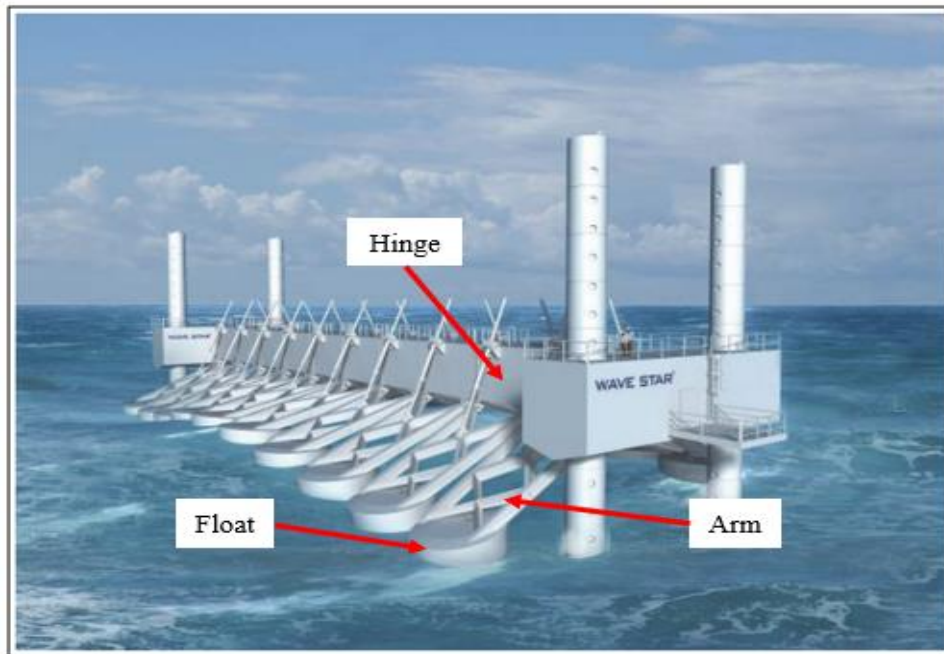
Figure 5-4. Wavestar concept (adapted from (Kramer et al. 2011)).

A single Wavestar unit is illustrated in **Figure 5-5** with main geometric dimensions given at 1/5 scale using Froude scaling laws. The inertial properties of the Wavestar at both 1/5 scale and full scale are given in **Table 5-2**. At full scale, each float has a dimeter of 5m which is rigidly connected to an arm at 1.6m above MSL. The arm is connected to the hinge situated 8.425m above the MSL. A 500kW rated Wavestar system would contain 20 floats with the same diameter, therefore one float can be assumed to have a rated power of approximately 25kW (Babarit et al. 2011). It must be noted though this is an assumption or "average" because in reality units at the end of the system will have a lower power output than the units at the front of the system. An additional linear damping value of 35,769 $N/(m/s)$ in heave was augmented to the model to account for viscous effects. For verification and validation of the numerical model, results are compared to the data measured during a tank test campaign at the Coastal, Ocean and Sediment Transport (COaST) Ocean Wave Basin at Plymouth University when an experimental model of the Wavestar system was tested at 1:5 scale and to published numerical results from a study conducted by Ghafari et al. (Ghafari et al. 2021). Ghafari et al.

integrated the Wavestar WEC system into a spar FOWT system. The validation and verification

exercise are presented in Section 5.1.2.1.2 and the results are converted to full-scale.
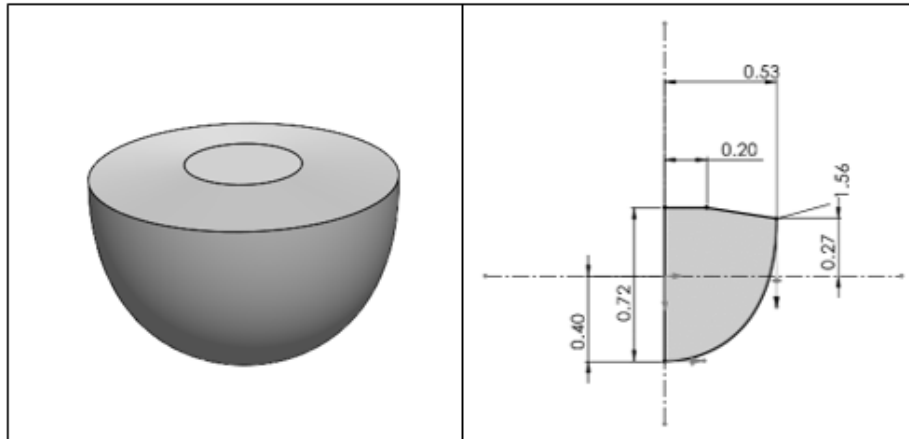
Figure 5-5. Wavestar float created in Solidworks (scaled model 1:5).

Table 5-2. Wavestar inertial properties.

Property (Unit)	1/5 (Froude scaling)	Full Scale
Mass (float and arm, kg)	220	27,500
Mass moment of inertia (kg m^2)	124	387,500
Centre of mass (CM) (m)	(0.18, 0,0.355)	(0.9, 0, 1.775)
Additional heave linear damping N/(m/s)	-	35769

5.1.2.1.1 PTO System

The mechanical power generated by the rotation of each float is converted into electrical

power by means of a hydraulic cylinder. In AQWA, to model a hydraulics PTO piston, a hinge

joint can be used. A rotational damping coefficient (B_{PTO}) is specified and the PTO force

(F_{PTO}) and power (P_{PTO}) can be determined by the following equations:

$$F_{PTO} = -B_{PTO}\dot{\theta} \tag{84}$$

$$P_{PTO} = -\dot{\theta}F_{PTO} \tag{85}$$

where $\dot{\theta}$ is angular velocity.

Figure 5-6 is a simple schematic of the hinge location, arm attachment point and centre of mass location of a single Wavestar unit. The presence of the arm means that the centre of mass location is slightly off-centre.
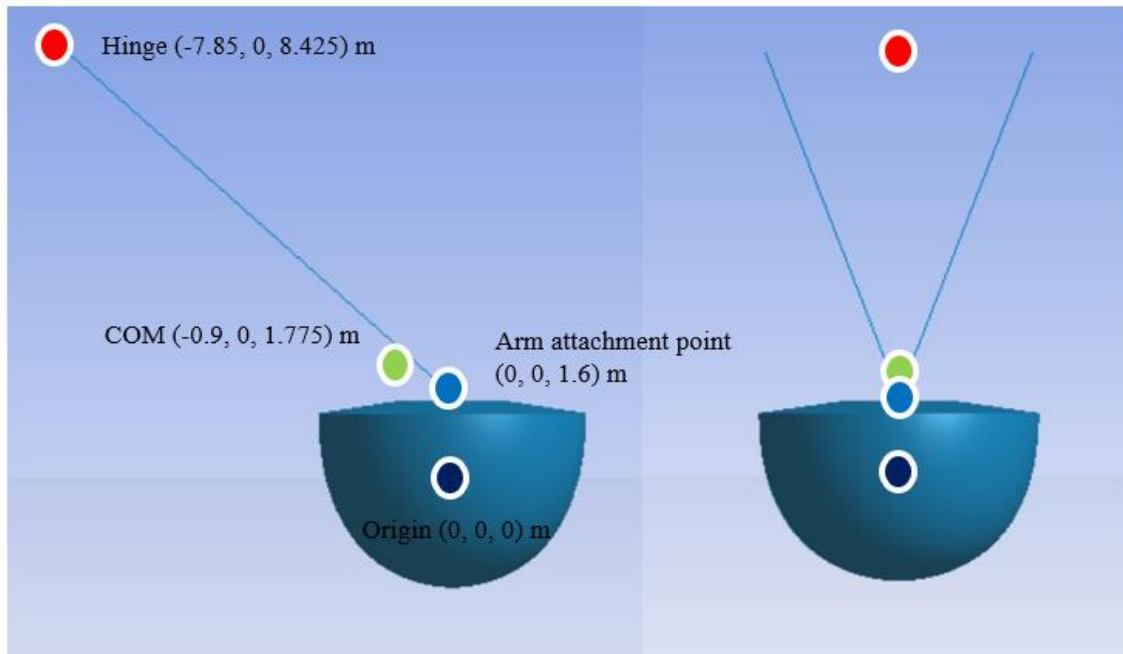
Figure 5-6. Hinge and arm connection of a single Wavestar unit.

5.1.2.1.2   Verification and validation of numerical model

Figure 5-7 shows time histories of heave displacement and heave velocity for varying PTO damping coefficients and presents a comparison of the kinematics between the present numerical model, the numerical results published by (Ghafari et al. 2021), and the experimental results recorded at COaST Ocean Wave Basin at Plymouth University. The results were obtained from a regular wave test ($H = 0.1$m, $T = 1.4$s) and presented in full-scale after applying Froude scaling laws. There is good agreement between the three data sets which verifies and validates the present numerical model of the Wavestar WEC system. The results show a clear trend; as the damping coefficient increases, the heave position and velocity amplitude decrease.
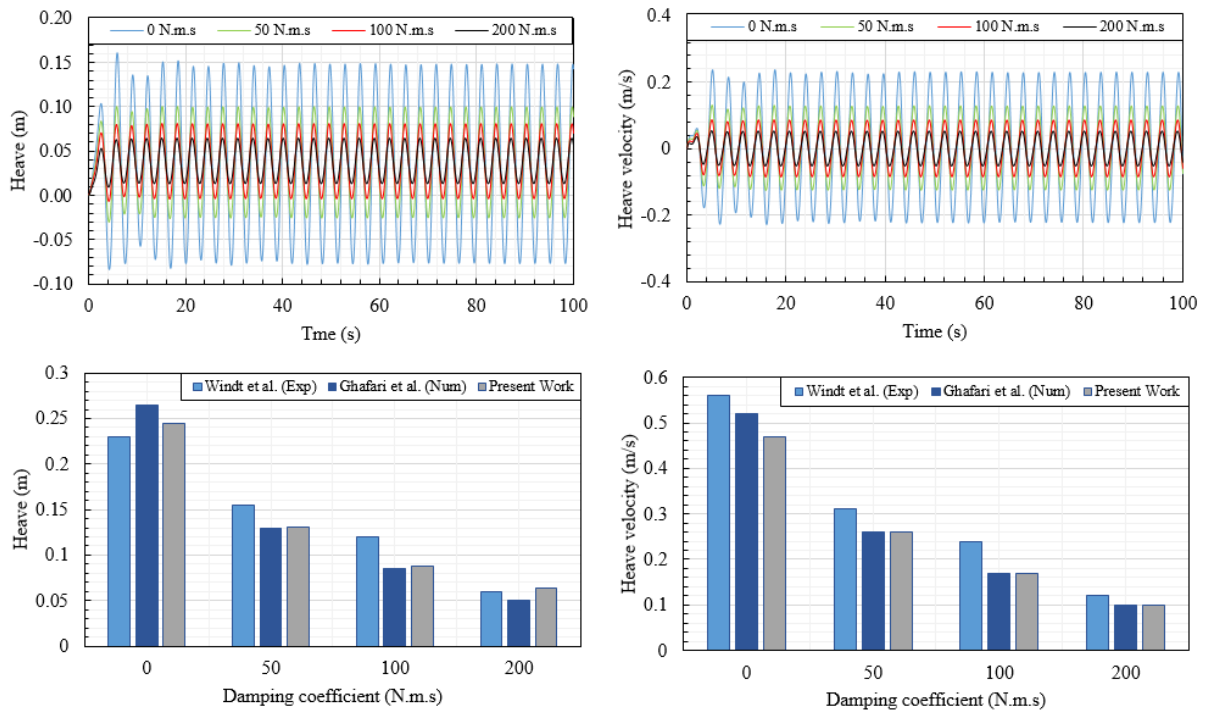
Figure 5-7. Validation of Wavestar kinematics against varying damping coefficients.

5.1.2.1.3   RAOs

Figure 5-8 show the heave and pitch motion RAOs of the single Wavestar unit. These were obtained from a frequency-domain analysis in ANSYS AQWA. RAOs are plotted for a frequency range of 0.05 – 6rad/s for a wave heading angle of 0°. A broad peak can be observed at frequency 1.2rad/s in the pitch RAO which corresponds to the pitch resonance frequency. The amplitude of motion at the resonance frequency is approximately 1.25°/m.
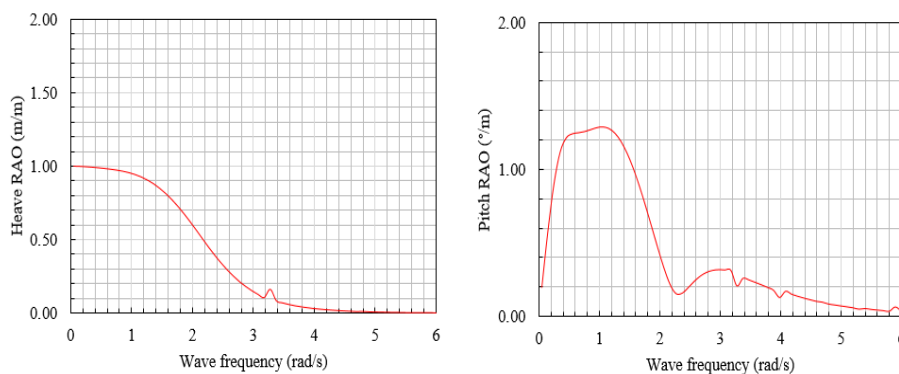
Figure 5-8. Pitch RAO of single Wavestar unit computed with frequency-domain model.

5.1.2.1.4   Free decay

A free decay analysis was conducted for pitch mode only. A 10° rotation is applied and then the Wavestar is released and allowed to come to rest. **Figure 5-9** shows the pitch response of the single Wavestar unit. The free decay test shows the natural period is approximately 4.3s which corresponds to a natural frequency of 1.46rad/s.
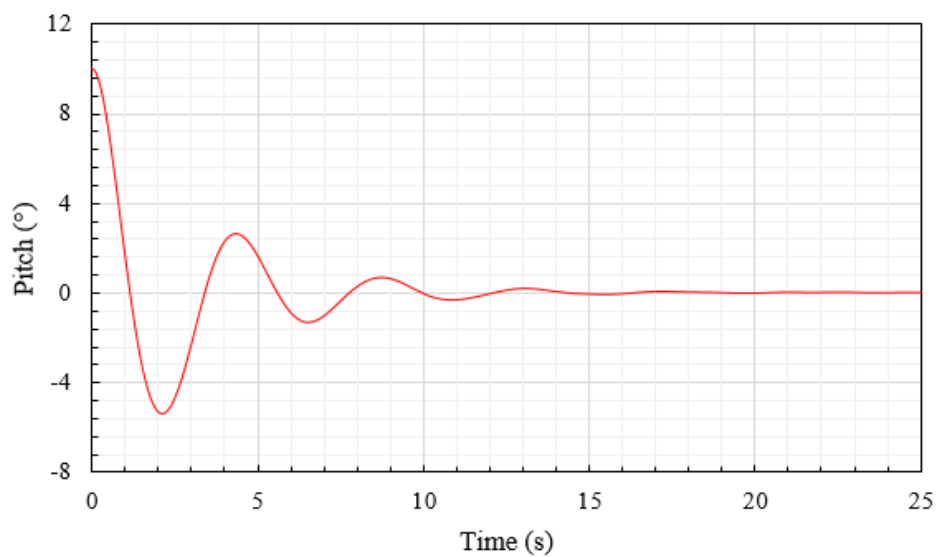
Figure 5-9. Pitch free decay of single Wavestar unit attached to hinge.

5.2   Coupling of numerical models of marine renewable energy systems with numerical model of catamaran FOWT

The second part of this chapter is dedicated to the coupling of the numerical models of the marine renewable energy systems with the numerical model of the catamaran-type FOWT. The result is two numerical models: (1) a numerical model of catamaran with tidal turbines, and (2) a numerical model of catamaran with WEC system. Section 5.2.1 describes the development of model 1 and Section 5.2.2 describes the development of model 2. Then, using the integrated models, simulations are conducted to provide insight into the behaviour of the catamaran-type FOWT combined with the marine renewable energy systems.

5.2.1   Catamaran with tidal turbines

Figure 5-10 is a schematic of the catamaran with tidal turbines (CTT) concept. Considering the tidal turbine system, one tidal turbine is installed to the keel of each demi-hull of the catamaran support platform in place of the monopile foundation and cross-arm assembly. The rotor centrelines remain submerged 20m below the mean seawater level to minimize cavitation potential and the rotors are offset by 35.2m from each rotor centreline. The presence of the turbines increases the platform mass by 2.5%. The support platform is also the foundation for the wind turbine, and it is held in position by an eight-line spread catenary mooring system configuration.
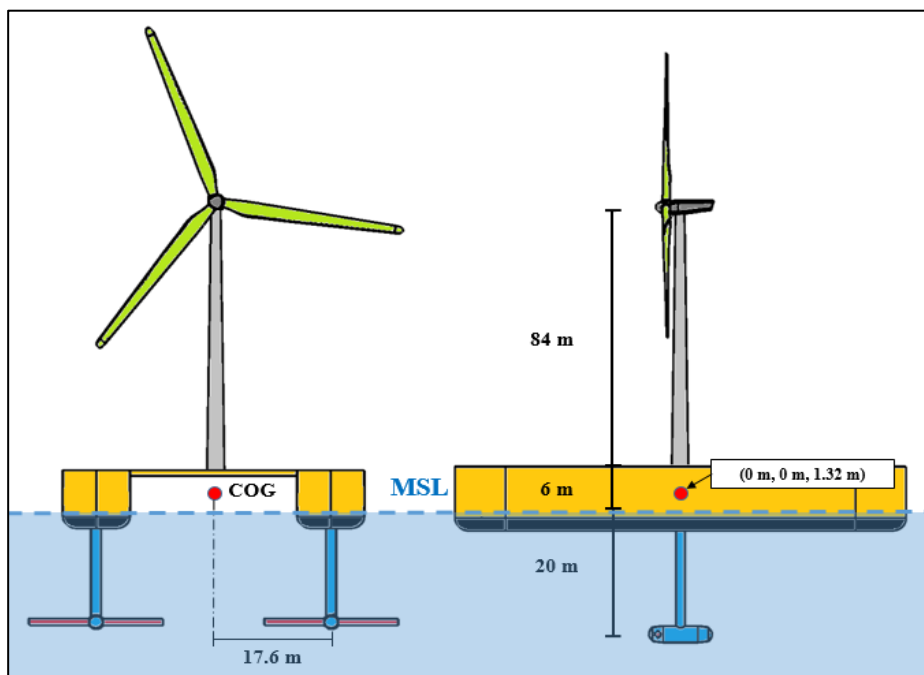
Figure 5-10. Schematic of CTT concept.

The NREL 5MW reference wind turbine, the catamaran support platform and the station-keeping system remain identical to the numerical model presented in Chapter 4 which means the only difference is the integration of the numerical model of the tidal turbines. **Table 5-3**

compares mass and inertia properties of the pure catamaran FOWT and CTT concept. **Figure 5-11** shows the CAD model of the CTT concept developed in Solidworks.

Table 5-3. Properties of the CTT concept.

	Catamaran	CTT
Mass (kg)	4,901,080	5,023,680
CM location (m)	(0, 0, 1.51)	(-0.01, 0, 1.32)
Roll inertia about CM (kg m^2)	4,672,683,194	4,781,318,142
Ixy (kg m^2)	0	-618
Ixz (kg m^2)	0	2,353,966
Pitch inertia about CM (kg m^2)	6,800,310,371	6,861,694,688
Iyz(kg m^2)	0	-33
Yaw inertia about CM (kg m^2)	11,190,569,096	11,240,002,086
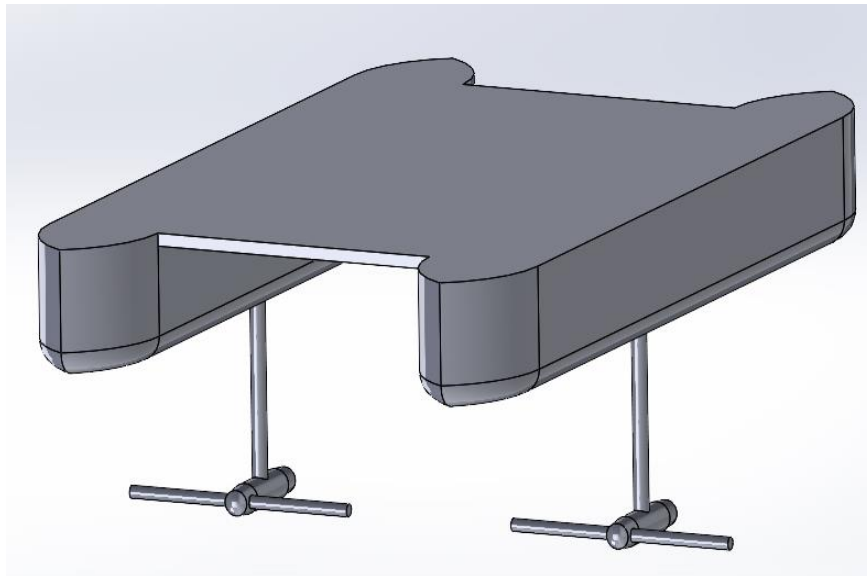
Figure 5-11. CAD model of CTT concept.

Similarly, F2A is used evaluate the performance of the CTT concept. An additional module is implemented within the engineering tool to calculate the hydrodynamic loading of the tidal turbines considering the dynamic inflow effects which arise because of platform motions.

5.2.1.1   Simulation

5.2.1.1.1   Testing of the coupled model

Since the numerical model of the catamaran-type FOWT was validated in Chapter 4 (Cutler et al. 2022) and the numerical model of the tidal turbines has been validated in Section 5.1.1.1. The numerical model of the CTT concept has been validated through partial validation of the two integrated numerical models, then, providing the coupled numerical model can produce a set of expected results from known conditions, the coupling of numerical models can be proven successful. To demonstrate this, results of the coupled numerical model is compared to a similar concept which previously integrated the same tidal turbine system. This concept is the Integrated Floating Energy System (IFES) concept presented in (Yang et al. 2020b). However, the IFES concept features a spar-type platform rather than a catamaran-type platform. So before direct comparisons can be made with the IFES concept, some small adjustments to the CTT numerical model are applied. The first adjustment to the CTT numerical model was to increase the water depth from 150m to 320m in order to model the same water depth in both models. As a result, a change in the position of the anchors and mooring line section length is applied to reflect the increase in water depth. The third adjustment was to the hub depth of the tidal turbines in the CTT numerical model: the depth of the turbines was increased from 20.2 to 46.5m. These modifications to the CTT numerical model permit a comparison to the results obtained from numerical model of the IFES concept. In essence, these changes mean that the tidal turbine system is positioned at exactly the same position in the water column but supported by different platforms. Two current only simulations were run to test the performance of the coupled numerical model. The first simulation run disabled platform motions in all degrees of freedom. By disabling platform motions the effects from platform dynamics on the tidal turbine responses are eliminated. This

was important because of the different support platform types which cannot be easily compared. Therefore, the performance of the tidal turbines can be evaluated fairly, and the results should be similar. The second simulation permitted platform motions to provide insight into the influence of platform dynamics on the performance of the tidal turbines. **Figure 5-12** compares the tidal turbine responses between the CTT concept and IFES concept when platform motions are disabled, and **Figure 5-13** compares the tidal turbine responses when platform motions are enabled. **Figure 5-12** shows that there is no difference in tidal turbines responses when mounted on either the catamaran- or spar-type platform when platform motions are disabled. The strong agreement in the results infer that the tidal turbine numerical model has been coupled appropriately in the present study. **Figure 5-13** shows the tidal turbines responses when platform motions are enabled. As expected, the different floating wind turbine platforms influence the tidal turbine responses. The time histories show the mean rotor speed, rotor thrust, and generated power is similar between the two concepts. However, the variability is somewhat different. The tidal turbines installed to the catamaran support platform exhibit greater fluctuations as a result of increased platform motions.
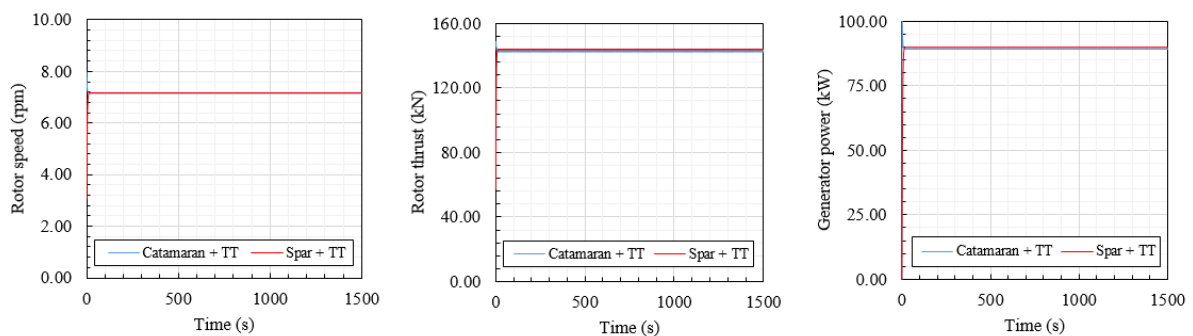
Figure 5-12. Comparison of tidal turbine responses between CTT concept and IFES concept when platform motions are disabled.
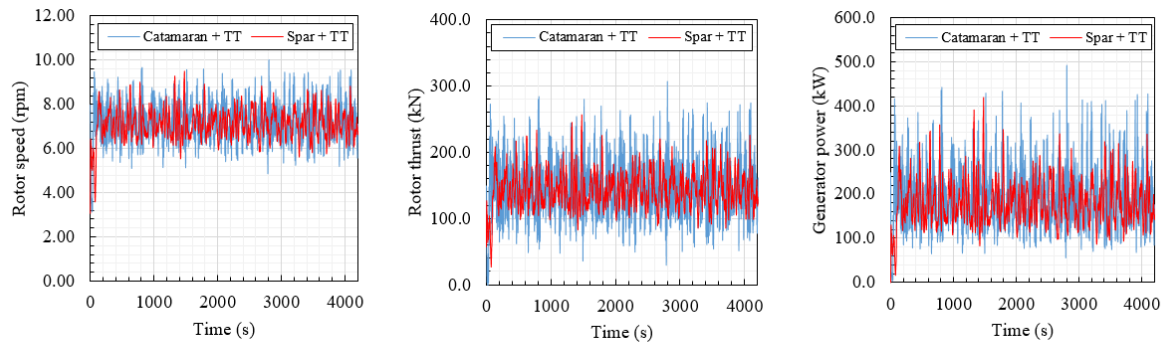
Figure 5-13. Comparison of tidal turbine responses between CTT concept and IFES concept when platform motions are enabled.

5.2.1.1.2   Tidal turbine hub depth study

A study was conducted to investigate the influence of tidal turbine hub depth on power production and global platform motions. **Figure 5-14** and **Figure 5-15** show the results of this study. As turbine hub depth increases, the inflow current velocity decreases because of the profile of the current velocity. Consequently, the amount of power produced by the turbines also reduces with depth. Therefore, with the aim to maximize power production from the tidal turbines, a tidal turbine hub depth of 20m was optimum for the catamaran-type platform. The position of the tidal turbines also had negligible effect on the global platform motions.
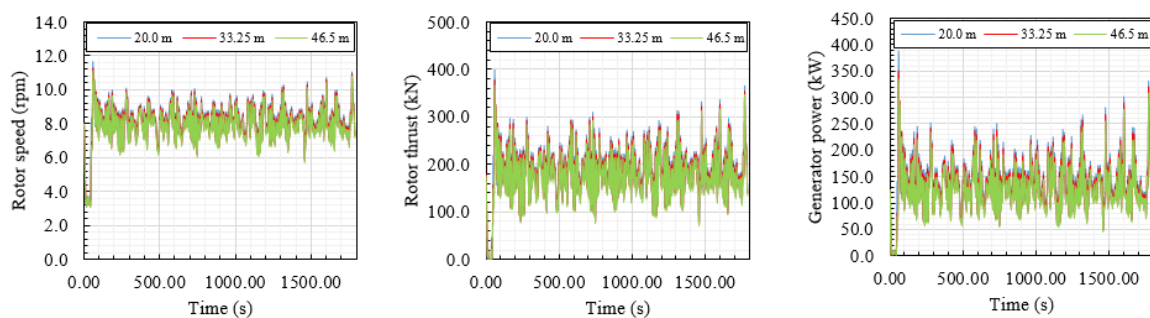
Figure 5-14. The influence of tidal turbine hub depth on tidal turbine responses.
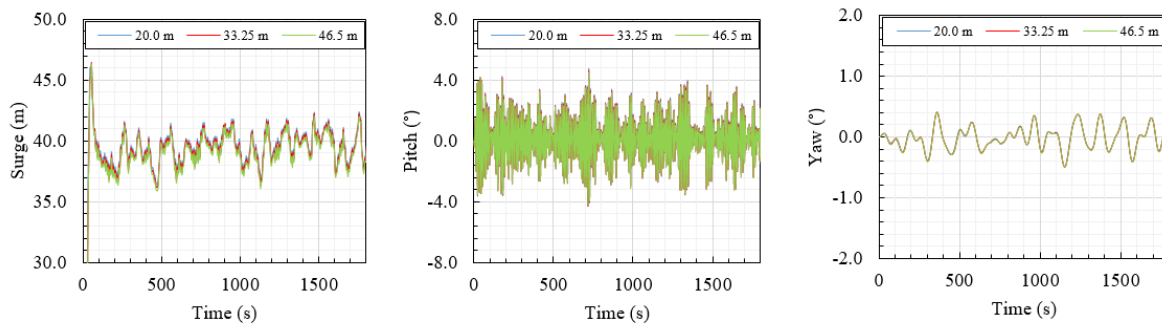
Figure 5-15. The influence of tidal turbine hub depth on global platform motions of

catamaran-type FOWT.

5.2.1.1.3   Free decay

A numerical free decay analysis was carried out to determine if the tidal turbines impact

the natural periods of global platform motions when in stand-still condition. The results of the

free decay analysis are presented in **Figure 5-16**. When the tidal turbines are in stand-still, the

effect on the platform natural periods of the system for all degrees of freedom is negligible. It

can be implied that when there no current or extreme current occurs, thus, the tidal turbines are

in stand-still condition, the responses of the CTT concept would be similar to that of a pure

catamaran FOWT.
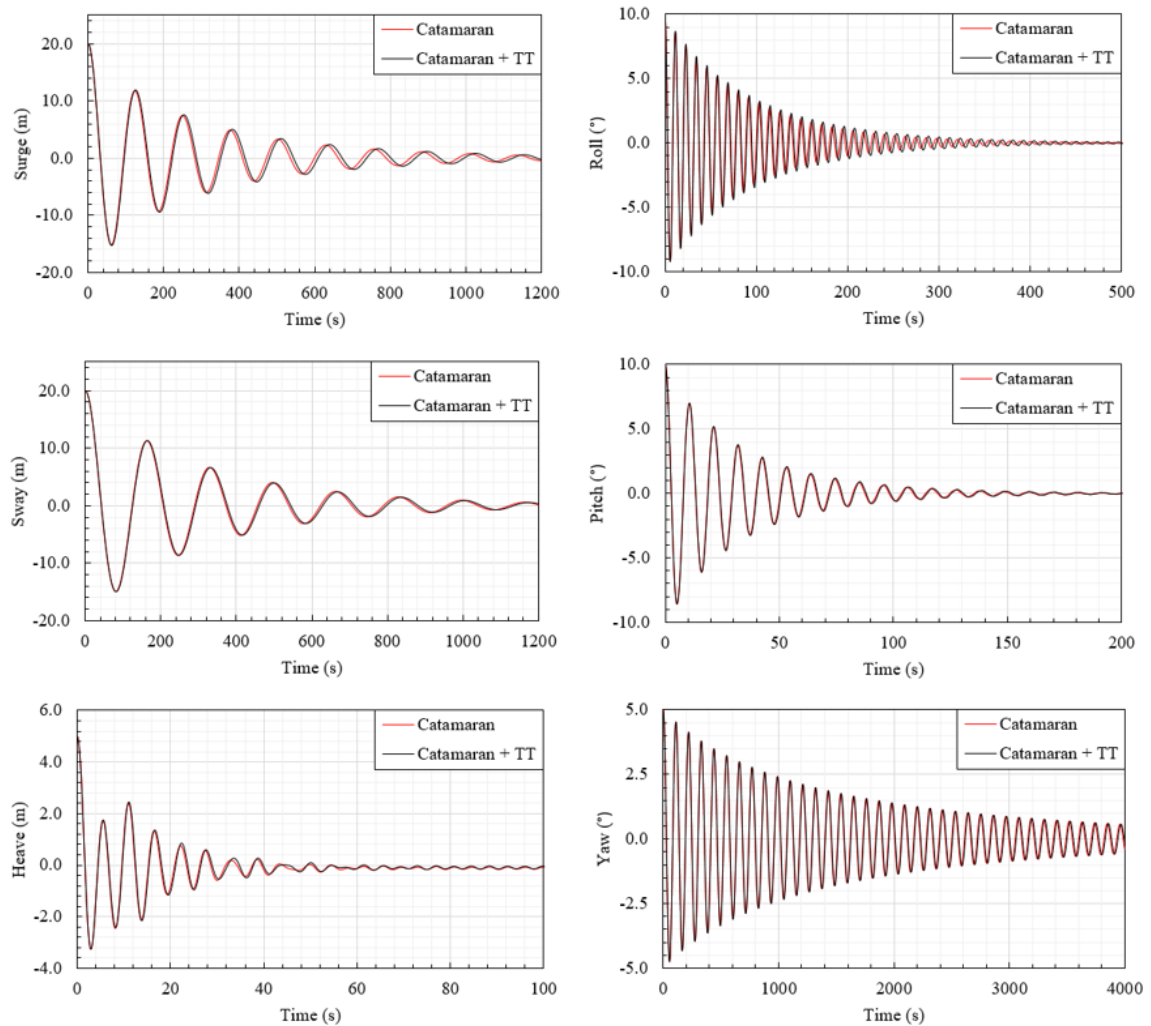
Figure 5-16. Free decay analysis of CTT concept and comparison against pure catamaran FOWT.

5.2.1.1.4 Operational conditions

The power production, wind turbine rotor and tower, support platform, mooring system, and tidal turbine rotor responses of the CTT concept are assessed and compared against a pure catamaran FOWT for three operating conditions: below-rated, rated, and above-rated. Analysis of these responses will provide insight into the behaviour of a floating wind and tidal turbine system when both energy systems are functioning. **Table 5-4** defines the operational load cases.

Table 5-4. Load cases for analysis of CTT concept in operational conditions.

Load Case	Turbulent wind velocity (m/s)	Significant wave height (m)	Spectral wave period (s)	Current velocity at MWL (m/s)
1	8.0	1.316	8.006	1.14
2	11.4	1.836	7.441	1.25
3	16.0	2.598	7.643	1.37

5.2.1.1.4.1 Rotor responses

Figure 5-17 presents the time-domain wind turbine rotor responses including rotor speed, rotor thrust, and rotor torque under LC2. The time-domain tidal turbine rotor responses are presented in **Figure 5-18**. Comparing against the responses of a pure catamaran FOWT system, insignificant differences are observed in the rotor responses for rated wind speed condition. The results show that the addition of the tidal turbines has negligible effect on the wind turbine aerodynamic performance. Similarly, it is noted that the cumulative hydrodynamic thrust produced by the tidal turbines is of a similar magnitude to the aerodynamic thrust produced by the wind turbine rotor.
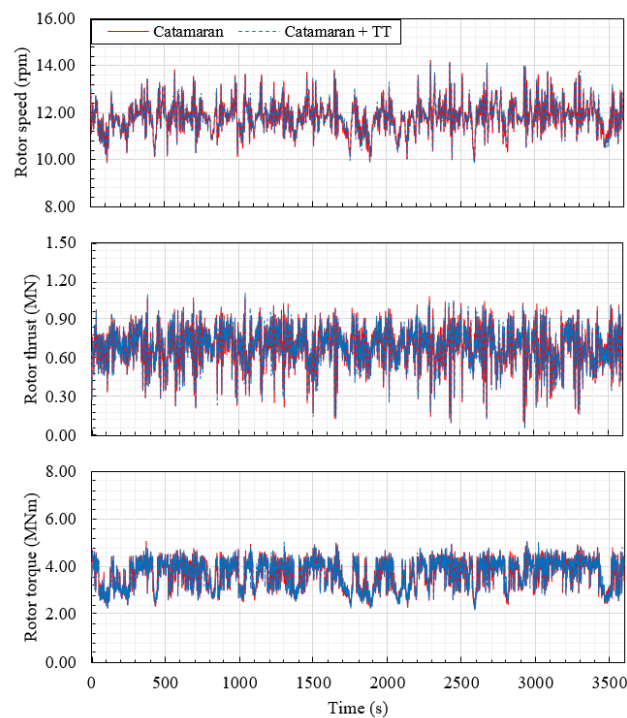
Figure 5-17. Comparison of wind turbine rotor responses between CTT concept and catamaran FOWT concept subject to LC2.
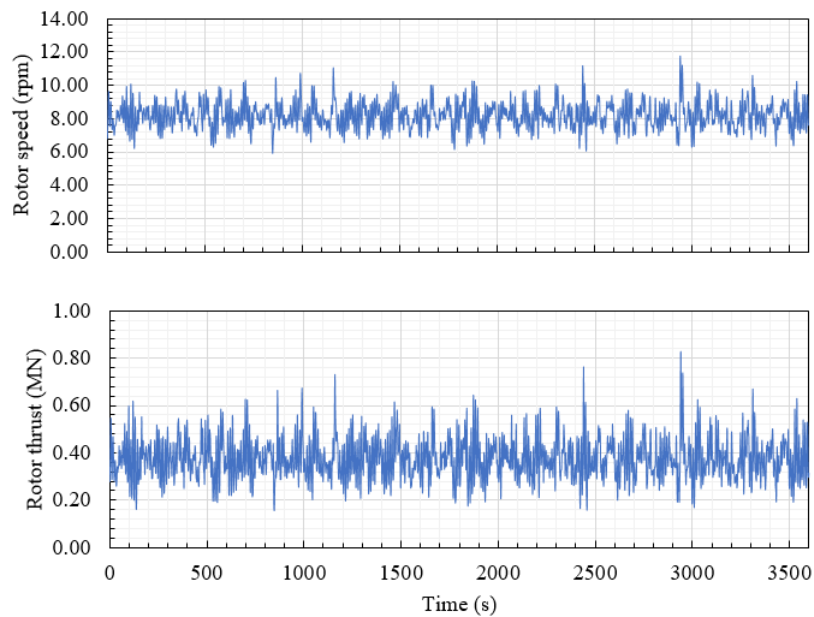
Figure 5-18. Tidal turbine rotor responses under LC2.

The wind turbine rotor response statistics are given in **Table 5-5** and the tidal turbine rotor response statistics are given in **Table 5-6**. There are some differences in the rotor responses, but these are minor and do not exceed 3% difference. This confirms that the tidal turbine system has weak influence on the wind turbine rotor dynamic responses.

Table 5-5. Statistical wind turbine rotor responses of the two concepts under operational load cases.

		LC 1		LC 2		LC 3	
		Catamaran	Catamaran + TT	Catamaran	Catamaran + TT	Catamaran	Catamaran + TT
Rotor speed (rpm)	Min.	7.51	7.47	9.86	9.85	8.99	9.08
	Mean	9.48	9.48	11.82	11.83	12.10	12.10
	Max.	12.92	12.87	14.23	14.14	15.58	15.57
	Std. Dev.	0.99	1.00	0.64	0.64	1.00	0.99
Rotor thrust (MN)	Min.	0.19	0.18	0.06	0.06	-0.18	-0.18
	Mean	0.50	0.50	0.69	0.68	0.48	0.48
	Max.	0.98	0.96	1.08	1.11	1.09	1.08
	Std. Dev.	0.11	0.11	0.15	0.14	0.21	0.20
Rotor Torque (MNm)	Min.	0.54	0.52	2.25	2.20	2.53	2.45
	Mean	2.04	2.04	3.69	3.70	4.18	4.18
	Max.	4.48	4.60	5.08	5.09	5.60	5.71
	Std. Dev.	0.59	0.60	0.57	0.57	0.47	0.46

Table 5-6. Statistical tidal turbine rotor responses under operational load cases.

		LC 1	LC 2	LC 3
	Min.	3.03	5.91	5.05
Rotor speed (rpm)	Mean	7.42	8.19	8.24
	Max.	9.75	11.77	12.97
	Std. Dev.	0.75	0.76	1.00
	Min.	-0.03	0.08	0.04
Rotor thrust (MN)	Mean	0.31	0.38	0.38
	Max.	0.28	0.41	0.50
	Std. Dev.	0.04	0.04	0.06

5.2.1.1.4.2 Tower responses

Figure 5-19 presents the time histories of the wind turbine tower-top F-A displacement and tower-base force in the x-direction for LC2. A histogram plot of the mean values for both variables is also presented for all LCs. The CTT concept has a slightly reduced response in both tower-top displacement and tower-base force compared to the catamaran concept. The reduction in displacement and force infers the tidal turbine system has fractionally improved the stability of the platform.
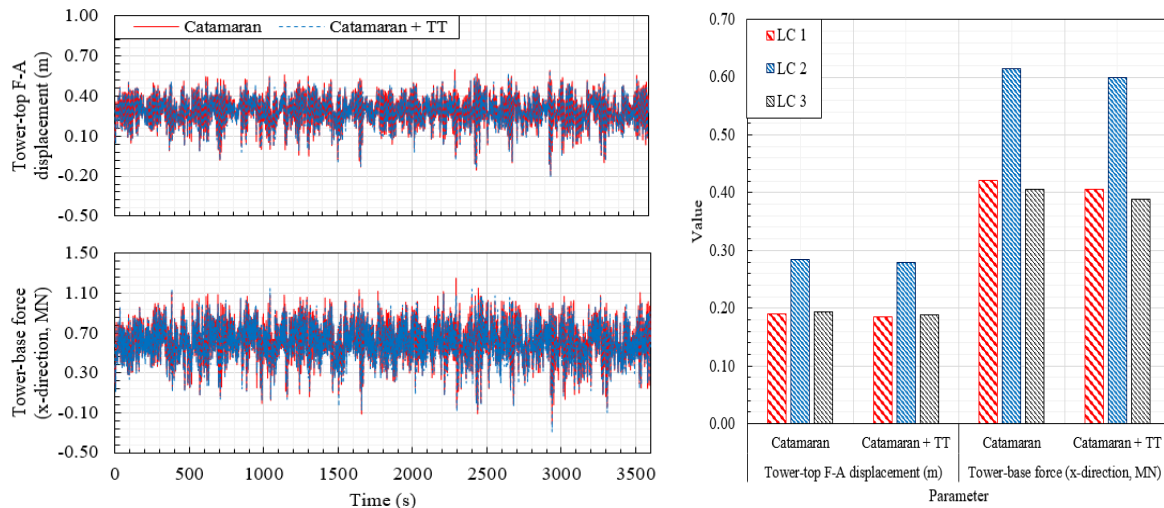
Figure 5-19. Comparison of time-domain tower-top F-A displacement and tower-base force in x-direction under LC 2 and comparison of statistics for all LCs between CTT concept and catamaran FOWT.

5.2.1.1.4.3   Platform motion responses

The time-domain platform motions of the CTT concept and the pure catamaran FOWT is shown in **Figure 5-20**. In addition, the platform motion statistics for both concepts for all LCs are presented. The integration of the tidal turbines affects the surge response of the global system. The extra hydrodynamic thrust exerted on the platform due to turbine operation increases the mean surge of the CTT concept. However, compared to the pure catamaran FOWT, the variation in surge has significantly improved. The tidal turbines produce hydrodynamic damping which makes the CTT concept more stable. The heave and pitch response of the CTT concept are more similar to the pure catamaran FOWT. The pitch response of the CTT concept has marginally improved which is as a result of the hydrodynamic thrust reducing the moment of the aerodynamic thrust. However, the overall results show that these platform degrees of freedom are not notably impacted when the tidal turbines are operating.
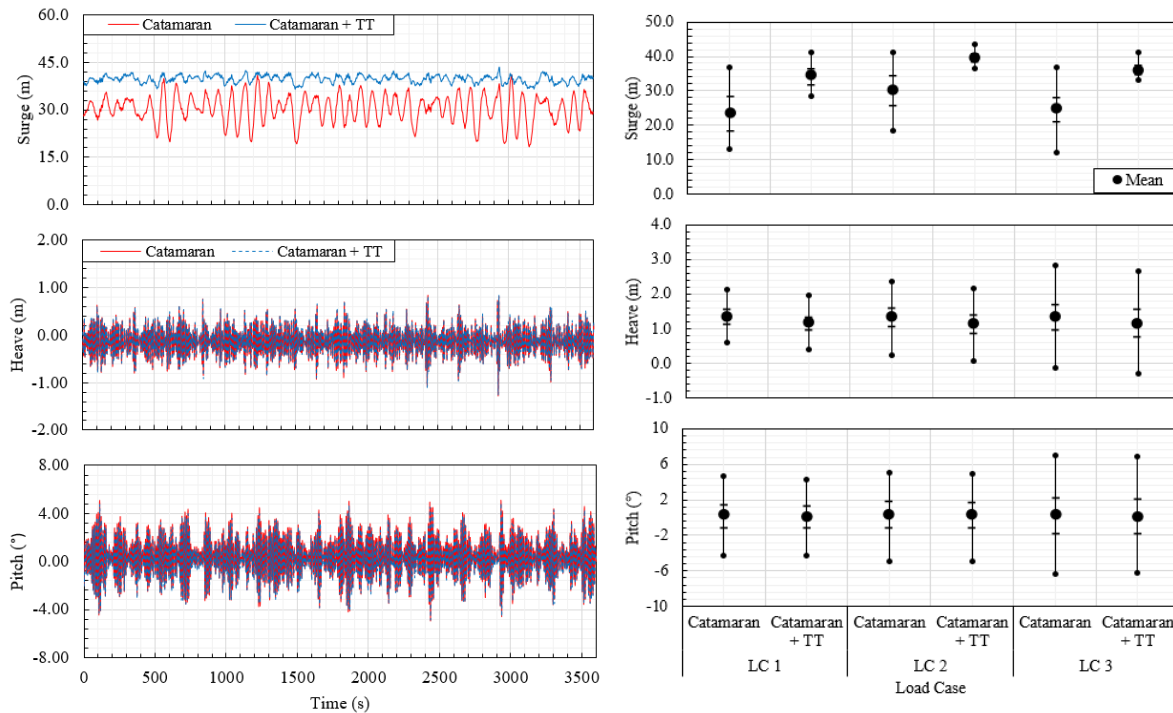
Figure 5-20. Comparison of time-domain platform motions under LC2 and comparison of platform motion statistics between CTT concept and catamaran FOWT.

The platform motion spectral responses for LC2 are presented in **Figure 5-21**. It can be clearly observed that the tidal turbines have had an effect on the surge response. The red curve (catamaran) has a distinct peak at a frequency of 0.1rad/s which corresponds to the surge natural frequency. Conversely, the blue curve (CTT concept) does not have a peak in this region. This peak has been damped by the operation of the tidal turbines. For the other two modes of motion, there are insignificant differences in the spectral responses. For all three modes, there is significant energy content between 0.5 – 0.7 rad/s which is the wave spectrum frequency range.
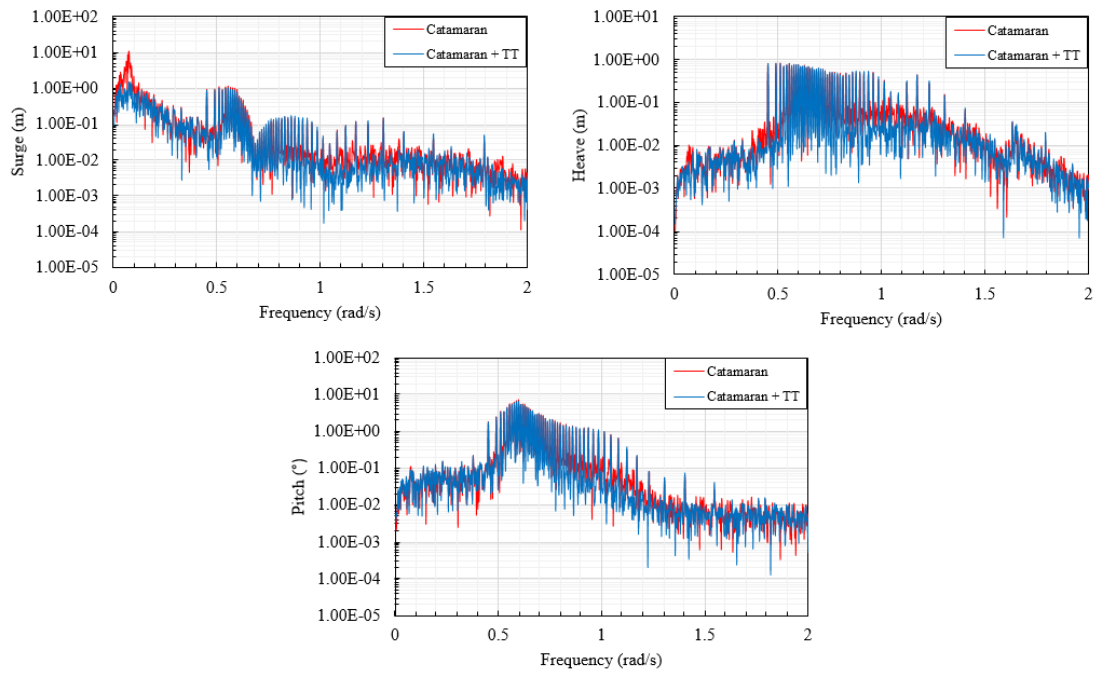
Figure 5-21. Comparison of spectral amplitudes of platform motions subject to LC2.

5.2.1.1.4.4 Mooring lines responses

Figure 5-22 plots the time-domain mooring line tensions under LC2. The major differences are observed in the upwind mooring lines (ML3 and ML4). It was expected due to the increased surge displacement that the upwind mooring lines of the CTT concept would be larger compared to the catamaran. The maximum tension recorded in ML4 of the CTT concept is approximately 0.9MN whereas the maximum tension in the equivalent mooring line of the pure catamaran concept is 0.7MN. On the other hand, a positive is that as a result of the hydrodynamic thrust, the variation in the mooring line tension has reduced.
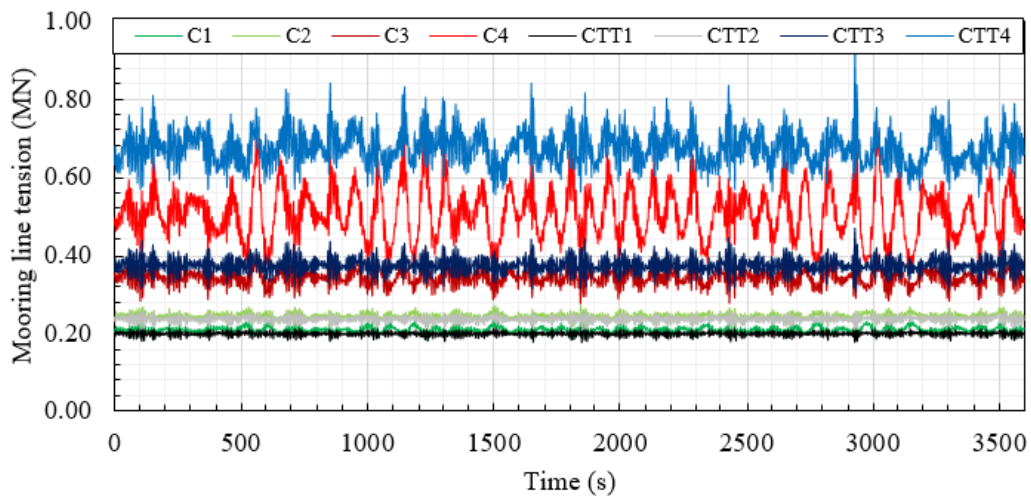
Figure 5-22. Comparison of tension in mooring lines between CTT concept and catamaran

(C) under LC2.

Figure 5-23 is a comparison of spectral amplitudes of mooring lines tension between the two concepts under LC2. The frequency-domain mooring line tension was analysed to show the impact of the hydrodynamic thrust generated by the tidal turbines. This impact is evident when observing the surge resonant frequency which is approximately 0.1rad/s. The operation of the turbines is damping the energy content at this frequency for the CTT concept.
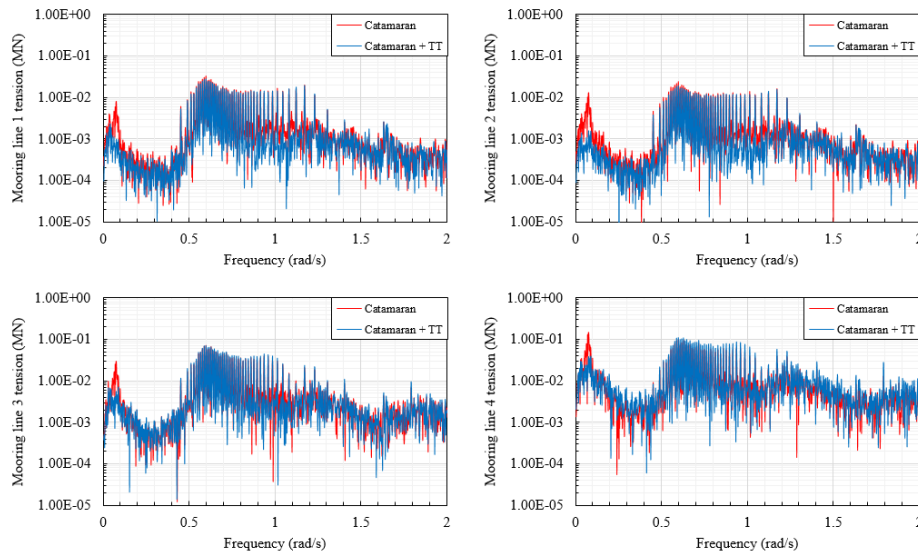
Figure 5-23. Comparison of spectral amplitudes of mooring line tension between the two

concepts under LC2.

5.2.1.1.4.5 Power generation

Figure 5-24 presents the generated power from the wind turbine and tidal turbine systems. The figure provides good insight into one of the main advantages of the CTT concept, which is the generation of additional electrical power from the tidal turbines. The extra mean power generated by the tidal turbines is 0.21, 0.28, and 0.29MW, respectively for each LC. This equates to an increase in electrical power of 10.1, 6.0, and 5.6%, respectively for each LC, compared to the pure catamaran FOWT. In sites where there is a good current resource, the additional power generated by the tidal turbines could be a substantial addition to the overall system power output. Furthermore, the simulated current velocity was considered below rated for the tidal turbine system. If there was a stronger current, then the increase in electrical power would be substantially higher.
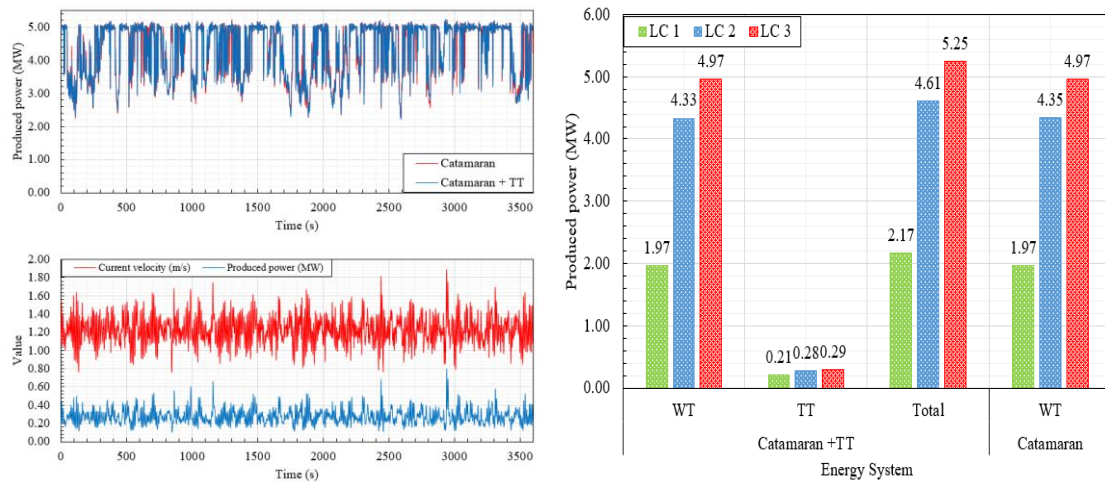
Figure 5-24. Comparison of the time-histories of the electrical power produced by the wind

turbines and the time-domain history of total power produced by the tidal turbines under

LC2, and a statistical comparison of the total power generated under all LCs.

5.2.2 *Catamaran with WEC system*

Figure 5-25 shows the hydrodynamic model constructed in ANSYS AQWA of the

catamaran with WEC system (CWS) concept. The figure is labelled with appropriate

dimensions to illustrate the integration of the WEC system onto the support platform of the

FOWT. Eighteen Wavestar units have been installed to the superstructure; six units each on

the port and starboard sides, and three units each installed to the fore and aft of the platform.

Each WEC unit is offset by 7m from the adjacent WEC unit(s). Wave power is generated

through relative displacement between the Wavestar units and catamaran platform. Each WEC

PTO system is located on the superstructure of the catamaran platform outside of the water at

a height of 8.425m. This is a strong advantage compared to other types of WEC as it eases

routine operation and maintenance. The model of the wind turbine, the catamaran support

platform, and the station-keeping system remain identical to the numerical model presented in

Chapter 4. Therefore, the only difference is the addition of the WEC system model. The WEC

system model has been validated at the start of this chapter, as such no further validation work

is required for the CWS concept. F2A is used to study the technical feasibility of the CWS concept. Multibody hydrodynamic interaction is a complex task which concerns the influence of one body's flow field on another's (ANSYS 2020). The significance of the interaction will depend on both the relative sizes of the bodies and the separation distances between them. F2A has excellent capabilities for numerical analysis of multibody offshore structures because ANSYS AQWA is the underlying hydrodynamic code. ANSYS AQWA accounts for the wave radiation coupling and shielding affects in the hydrodynamic interaction. A number of numerical simulations are performed to thoroughly assess the CWS concept. The hydrodynamic interaction between the catamaran support platform and WEC system will be studied through hydrodynamic coefficients. Several numerical models are developed, each one progressively becoming more complicated in terms of the number of structures present. It will be obvious to see the effect of hydrodynamic interaction in this manner. Then, to determine if the integration of the WEC system affects the catamaran support platforms natural periods a free decay analysis is completed. Regular wave studies are conducted to find the optimum damping coefficient for the WEC PTO system, to observe the amount of produced power as a function of wave period and to observe the dynamic responses of the combined structure for a regular wave. Irregular wave simulations are carried out to test the CWS concept in realistic wave conditions in the absence of wind. The performance of the CWS concept is assessed through an evaluation of platform motions, tower-top displacement, tower-base force, and mooring line tension.
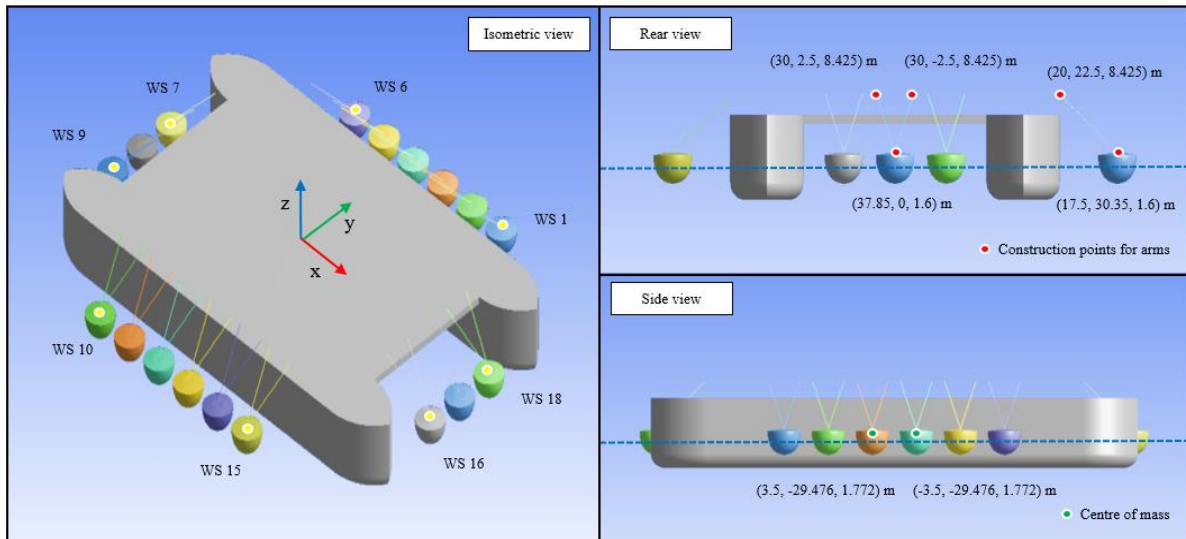
Figure 5-25. CWS concept developed in AQWA.

5.2.2.1   *Simulation*

5.2.2.1.1   Multibody hydrodynamic interaction

Hydrodynamic interacting structures will have altered hydrodynamic coefficients as a result of changes in radiation and diffraction forces due to the presence and influence of the other structure(s). To gain an understanding of the hydrodynamic interaction between the catamaran support platform and the WEC system, an investigation into the hydrodynamic coefficients was conducted. Several models are developed: (1) single Wavestar unit only, (2) catamaran support platform and single Wavestar unit installed to the fore of the platform, (3) catamaran support platform and single Wavestar unit installed to the port side of the platform, and (4) the complete CWS concept. Initially, the size difference between the two systems indicates the dominant influence the catamaran will have upon the WEC units. The influence of the full WEC system on the catamaran support platform and the influence of adjacent WEC units will also be of interest. Hydrodynamic diffraction analyses are performed in ANSYS AQWA to calculate the hydrodynamic coefficients. The frequency range is 0.05 - 4.0rad/s with

an interval frequency of 0.05rad/s, thus the hydrodynamic coefficients are calculated for a total of 80 wave frequencies.

5.2.2.1.1.1   Single Wavestar unit

The hydrodynamic added mass and radiation damping coefficients of a single Wavestar unit without the presence of the catamaran support platform are presented in **Figure 5-26**. There is a distinct peak at approximately 3.3rad/s for heave and pitch radiation damping coefficients corresponding to the heave natural frequency of the structure. Generally, the curves are smooth as there is no interaction from other structures.
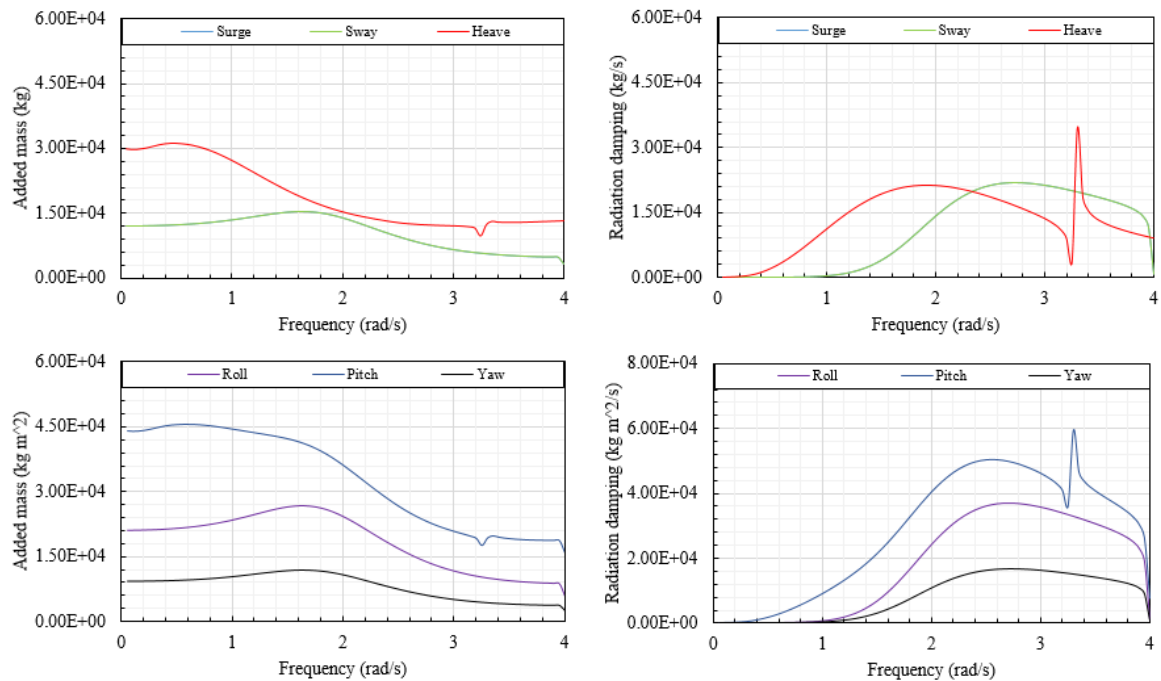
Figure 5-26. Hydrodynamic added mass and radiation damping coefficients of a single Wavestar unit.

5.2.2.1.1.2   Catamaran and single Wavestar unit attached to the fore of the platform.

Next, the hydrodynamic coefficients are calculated for a single Wavestar unit mounted to the fore of the catamaran support platform as shown in **Figure 5-27** and the results are

presented in **Figure 5-28**. A comparison is made to the hydrodynamic coefficients of the single Wavestar (e.g., WS A11). The hydrodynamic interaction between the Wavestar unit and catamaran support platform is obvious. There are numerous peaks which have appeared in the hydrodynamic coefficient curves throughout the analysed frequency range. These peaks follow the catamaran's resonant frequencies caused by entrapped wave action between its demi-hulls (see Section 4.5.1). The results show the catamaran's hydrodynamic behaviour strongly influences the hydrodynamic behaviour of a Wavestar unit positioned at the fore (or aft) of the platform. This is confirmed in **Figure 5-29** where the hydrodynamic coefficients have been grouped to highlight the symmetric and antisymmetric interaction, a behaviour unique to catamarans. The hydrodynamic coefficients of the Wavestar at the fore of the platform is strongly affected by both symmetric and antisymmetric interaction.
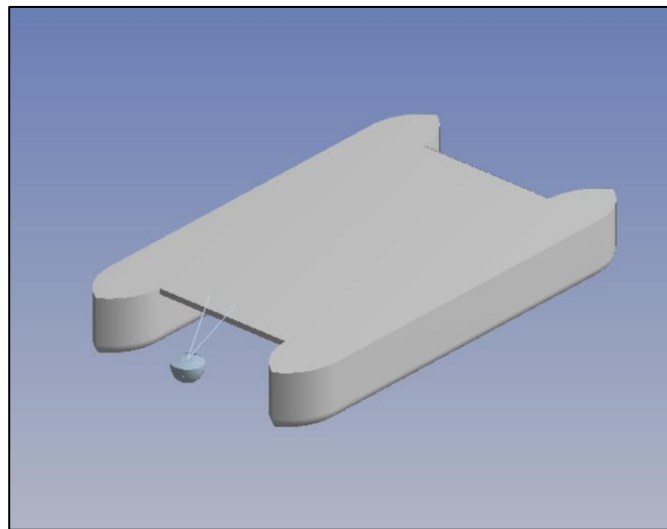
Figure 5-27. Catamaran support platform and single Wavestar unit installed to the fore of the platform.
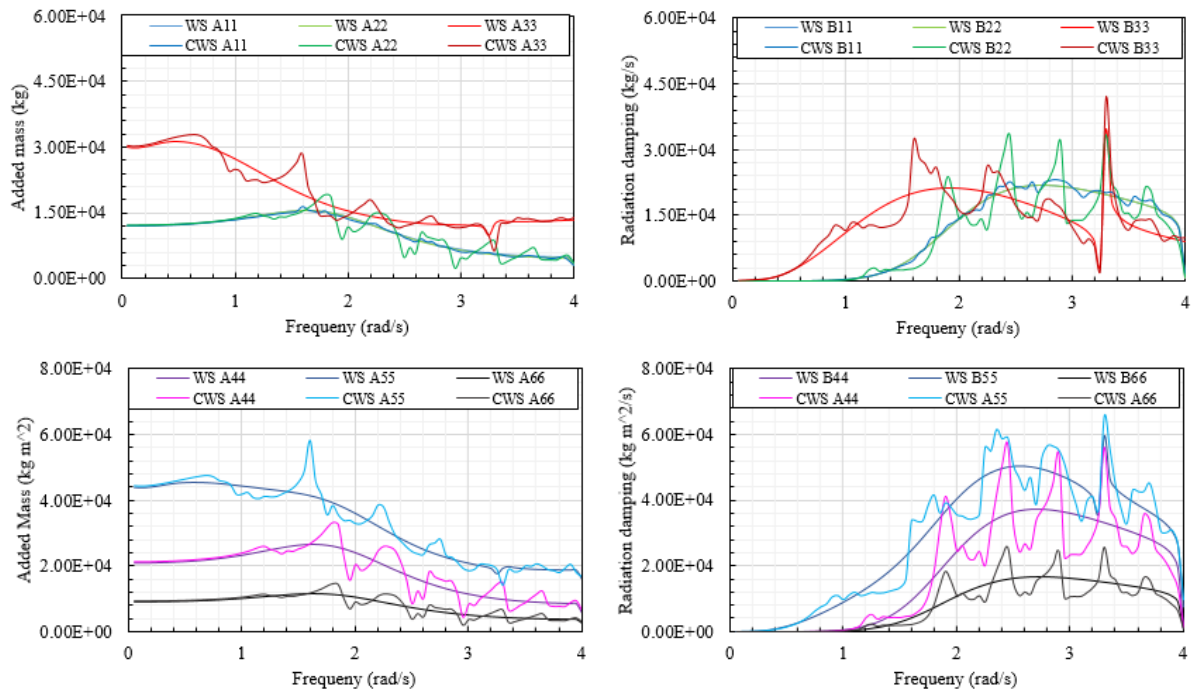
Figure 5-28. Comparison of hydrodynamic coefficients between single Wavestar and

Wavestar mounted to the fore of the catamaran support platform.
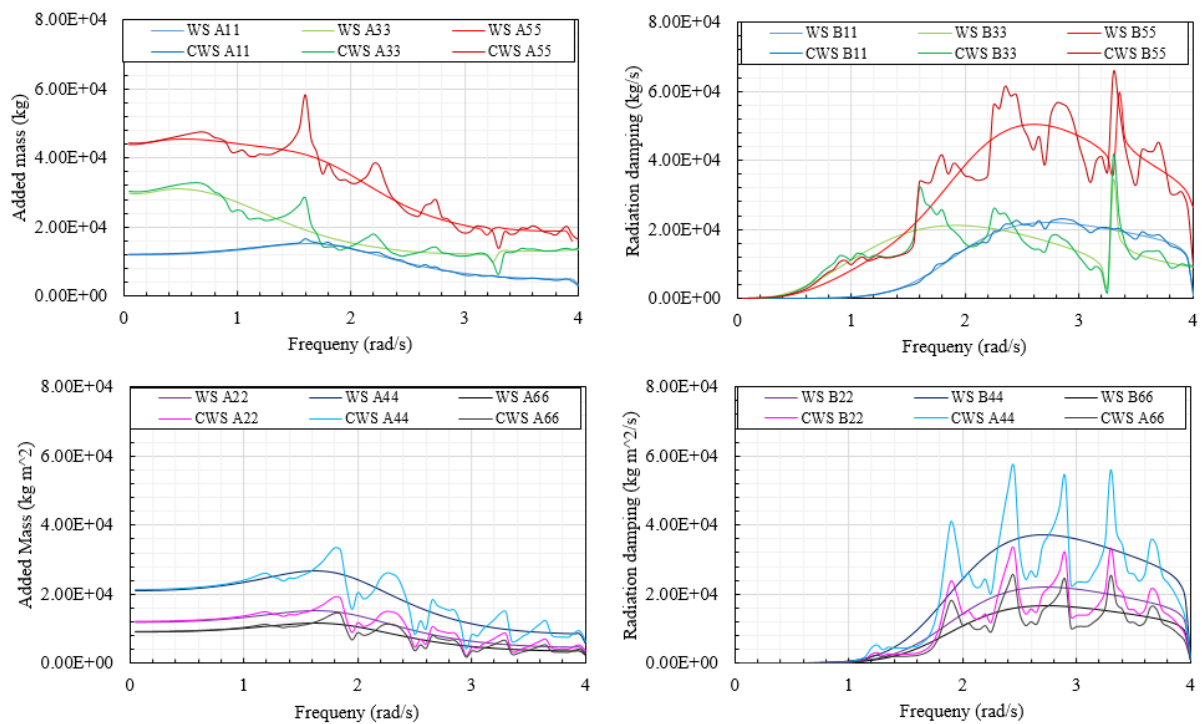
Figure 5-29. Symmetric vs antisymmetric interaction.

5.2.2.1.1.3   Catamaran and single Wavestar unit attached to the port side of the platform

The hydrodynamic coefficients are now calculated for a single Wavestar unit mounted to the port side of the catamaran support platform as shown in **Figure 5-30** and the results are presented in **Figure 5-31**. Compared to when the Wavestar unit is positioned at the fore of the platform, the roll added mass and radiation damping coefficients are distinctly different. As the catamaran rolls and waves radiate from the demi-hull, these waves will interact with the WEC unit. For horizontal plane motions, peak responses occur at 1.11, 1.92, 2.48, 2.93, 3.33 and 3.68rad/s due to antisymmetric interaction between the demi-hulls. This has caused large peaks to be present in the hydrodynamic coefficients at some of these frequencies reflecting this interaction. This behaviour is also observed in sway radiation damping curve. On the other hand, when the Wavestar unit is positioned on the port side and in line with the y-axis, symmetric interaction (surge, heave, pitch) does not have a strong effect.
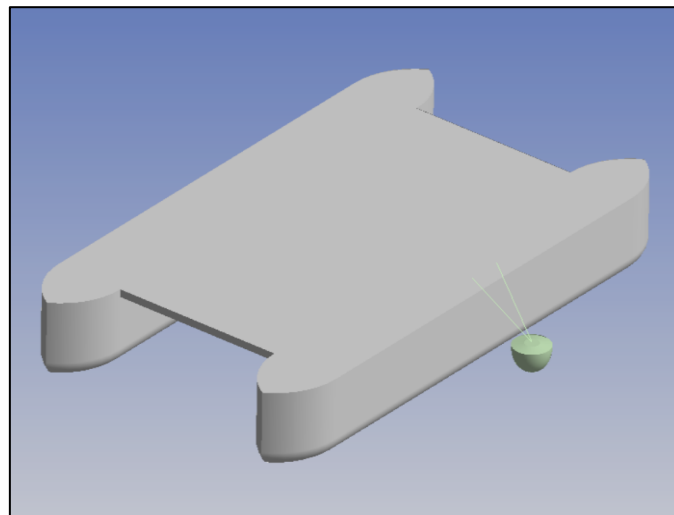
Figure 5-30. Catamaran support platform and single Wavestar unit installed to the port side of the platform.
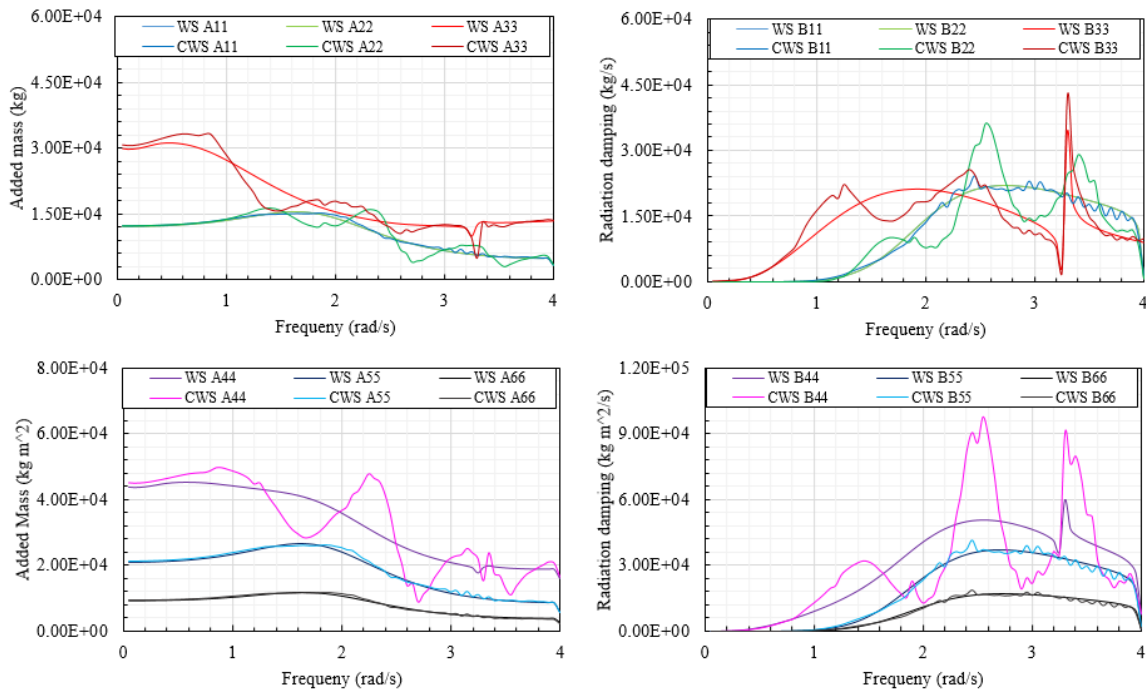
Figure 5-31. Comparison of hydrodynamic coefficients between single Wavestar and Wavestar mounted to the port side of the catamaran support platform.

5.2.2.1.1.4 Catamaran and WEC system

Finally, the hydrodynamic coefficients of the full WEC system mounted to the catamaran support platform are calculated. Using this model, the hydrodynamic interaction effect on the catamaran support platform from the full WEC system and the effect of adjacent Wavestar units can be investigated. **Figure 5-32** presents the catamaran support platform hydrodynamic coefficients in the CWS concept and compares them to a pure catamaran support platform. The sway added mass and radiation damping of the catamaran noticeably increases at 1.9rad/s. Similarly, the roll added mass and radiation damping also significantly increases at this frequency as a result of the WEC system. The WEC system has improved the hydrodynamic performance of the catamaran support platform for these two modes of motion. **Figure 5-33** and **Figure 5-34** present the hydrodynamic coefficients of the Wavestar units when considered in the full CWS concept. Considering the hydrodynamic coefficients of the Wavestar positioned at the fore of the platform, the effect of the adjacent Wavestar units becomes

apparent. The behaviour is no longer dominated by the catamaran, instead, there are many small peaks which shows the shielding effect of the two adjacent units. Considering the hydrodynamic coefficients of the Wavestar positioned at the port side of the platform, the roll hydrodynamic coefficients have increased significantly in magnitude and because of the adjacent Wavestar units, there are now peaks in the surge, heave, and pitch radiation damping curves. However, these peaks still follow the characteristic hydrodynamic behaviour of the catamaran support platform signifying the hydrodynamic dominance of the support platform in the CWS concept.
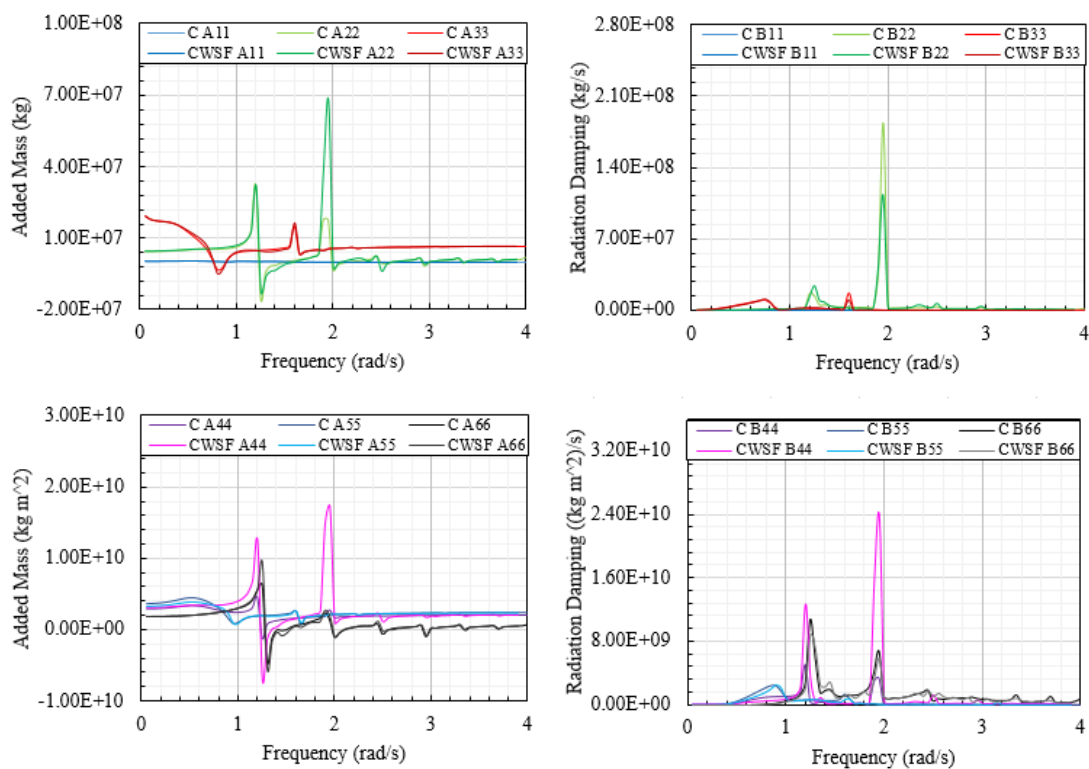
Figure 5-32. Comparison of hydrodynamic coefficients between catamaran as part of CWS concept and pure catamaran support platform.
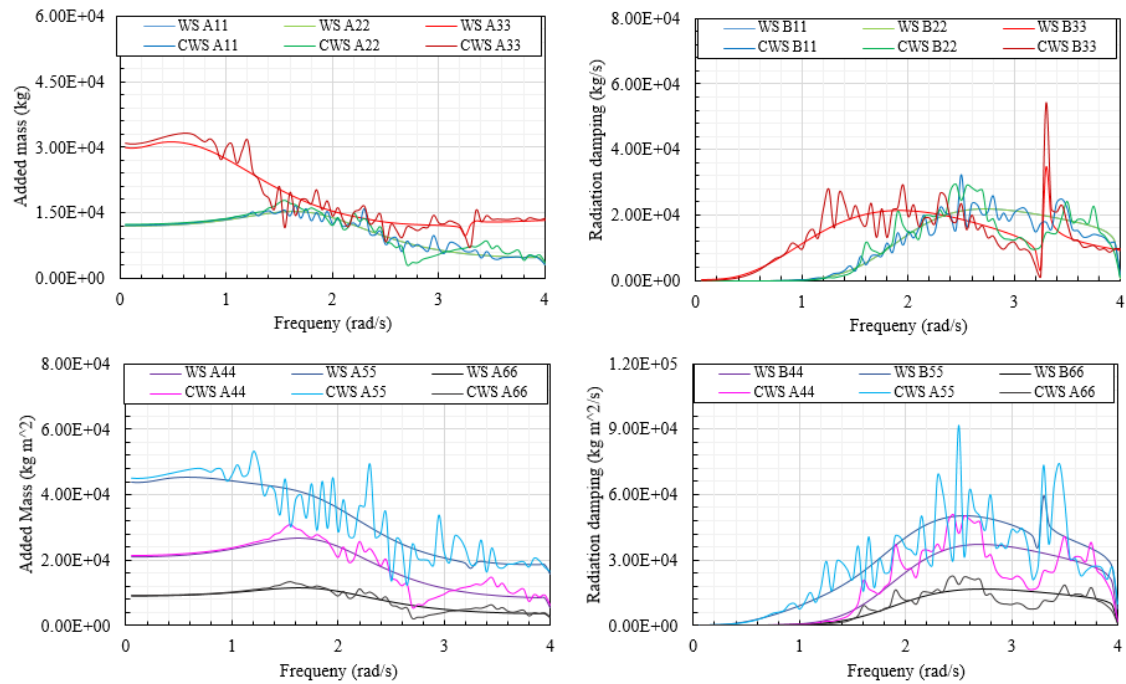
Figure 5-33. Comparison of hydrodynamic coefficients between single Wavestar and Wavestar mounted to the fore of the catamaran support platform (full CWS concept).
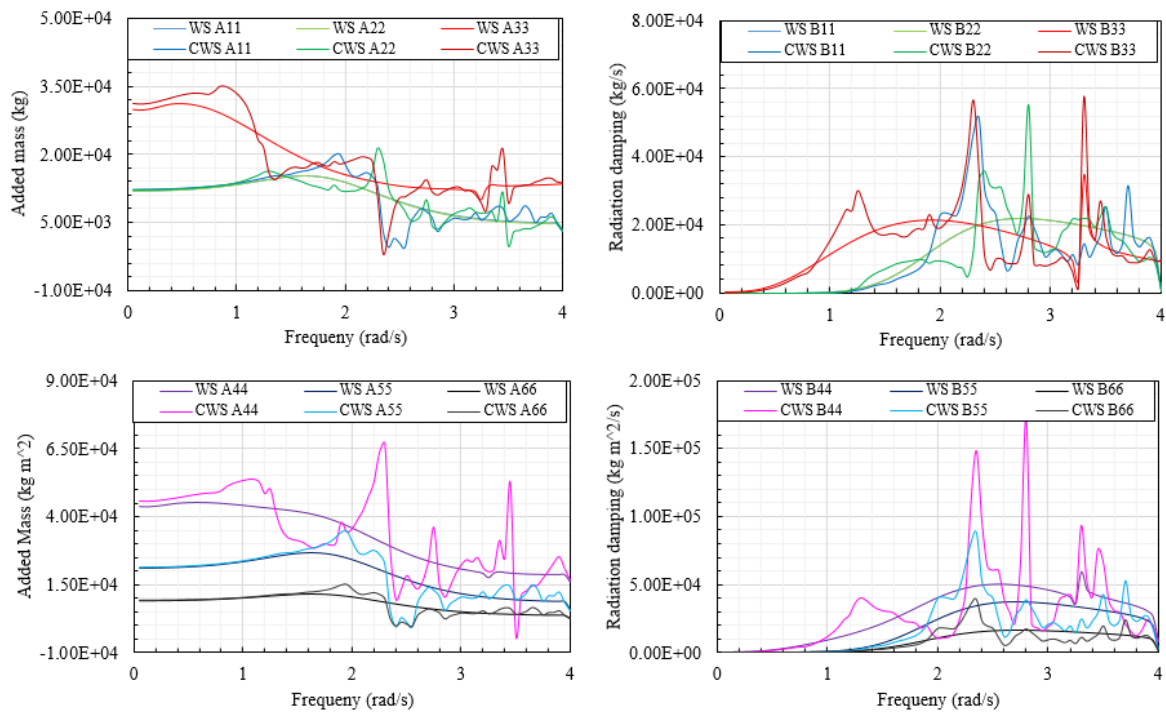
**Figure 5-34.** Comparison of hydrodynamic coefficients between single Wavestar and Wavestar mounted to the port side of the catamaran support platform (full CWS concept).

5.2.2.1.2   Free decay analysis

The natural periods of the catamaran FOWT system will be affected by the integration of the WEC system. Therefore, a free decay analysis was conducted to assess the significance. In the free decay tests, the WEC units are free to rotate about their individual hinge axis relative to the position attached to the platform. This means that hydrodynamic interactions and mechanical couplings are considered. **Figure 5-35** presents the results of the free decay analysis of the CWS concept and a comparison to a pure catamaran FOWT system. For surge and sway modes, the response of the CWS concept is similar to the pure catamaran FOWT. The addition of the WEC system slightly increases the surge and sway natural period of the platform. Considering heave mode, the natural period remains unchanged but the presence of the WEC system provides additional damping in this mode. This is also the same for roll and pitch modes, particularly roll mode where significant additional damping is observed. For yaw mode, the WEC system does not affect the natural period nor damping. The effect of combining the WEC system with the catamaran FOWT on the platform natural periods and system damping is positive, particularly for heave, roll, and pitch modes.
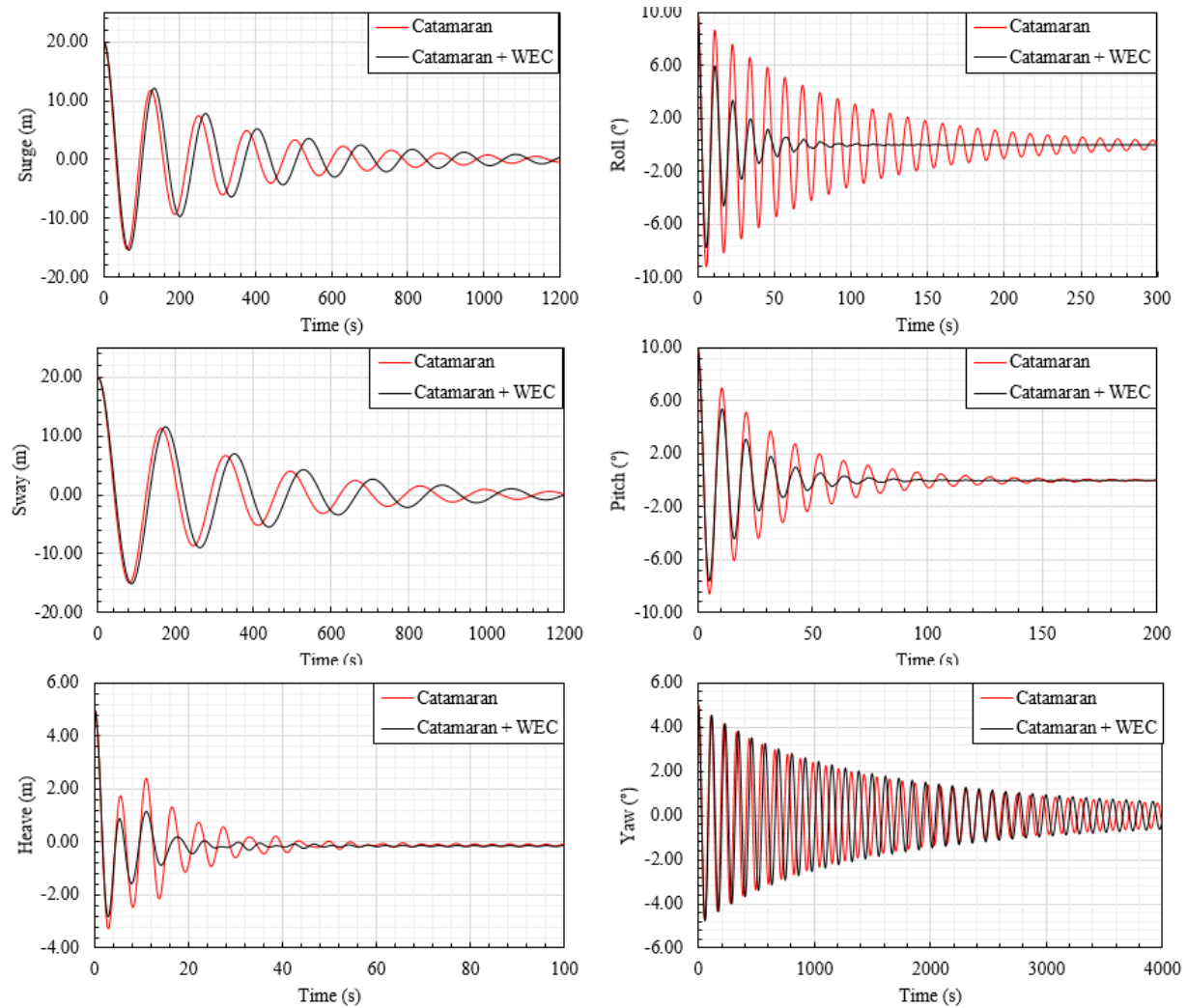
Figure 5-35. Free decay analysis of CWS concept and comparison against catamaran FOWT.

5.2.2.1.3   Regular wave analysis

5.2.2.1.3.1 Optimum PTO damping

To determine the optimum PTO damping coefficient in the context of power production, the CWS concept was subject to regular wave (H = 1.8m and T = 8s) whilst the PTO damping coefficient was varied. The PTO stiffness was zero for the regular wave simulations. From **Figure 5-36**, it can be observed that the maximum power generated from a Wavestar unit for the given incident regular wave is 20.8kW for when the damping coefficient is

7.50E+06kN·m/(rad/s). Therefore, this value is taken as the optimum damping coefficient for future simulations.
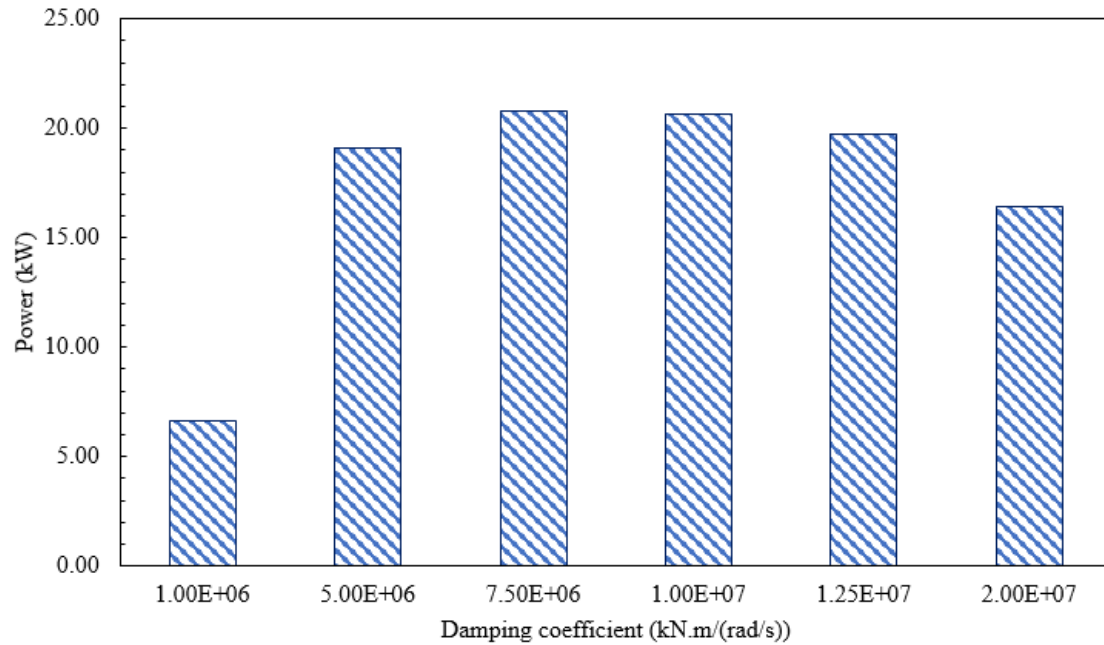
Figure 5-36. Power production of WEC8 for various PTO damping coefficients.

5.2.2.1.3.2 Mean power

For insight into the power production performance of the WEC system, a series of regular wave tests were simulated which varied the wave period whilst the incident wave height remained constant (H = 1.8m) for a wave direction of 0°. The wave period was increased incrementally in steps of 1s for a range of 3 – 16s. **Figure 5-37** presents the measured individual mean power of selected WEC units and **Figure 5-38** presents the total mean power of the WEC system. Only 10 WEC units needed to be measured due to system symmetry. WEC units 7 and 8 produce the most power in the WEC system. These two units produce a maximum mean power of 120kW for a wave period of 10s. The large quantity of power is as a result of the pitch natural period of the catamaran. As the catamaran pitches, the amount of power which the WEC units generate is amplified. This effect is also observed for the equivalent units at the

aft of the platform (WEC units 16 and 17). For the port and starboard side units, power is mainly produced for wave periods between 4 – 6s, with WEC units 5 and 6 generating the most. This is because these units are nearer to the fore of the platform. Power production ranges between 0 – 40kW for the port and starboard units. Looking at **Figure 5-38**, there are three regions where the total mean power has peaks: (1) for a wave period of 5s, (2) for a wave period of 7s, and (3) for a wave period of 10s. The peaks at 5 and 7 s are a combination of WEC unit natural period (4-5s) and the heave natural period of the catamaran (5.4s). The peak at 10s is due to the catamaran pitch natural period (9.8s). The maximum total mean power is approximately 680kW for a wave period of 10s. It is evident, a synergy between the WEC system and catamaran support platform exists in terms of power production due to the relative motion between the two systems.
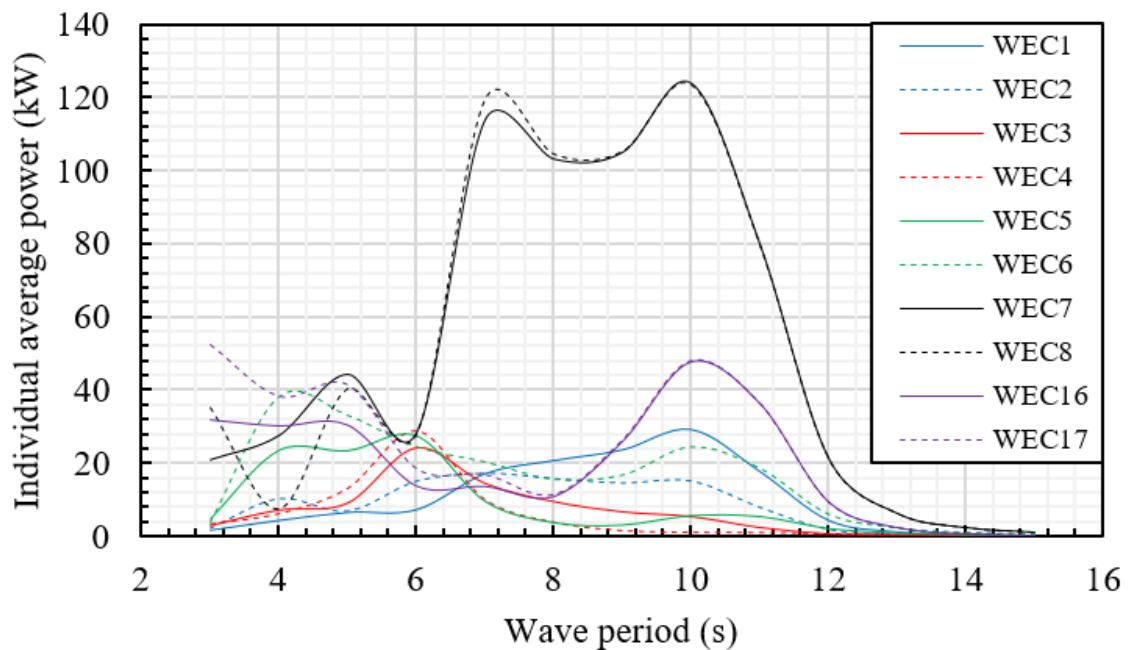
Figure 5-37. The effect of wave period on the average power of individual WEC units.
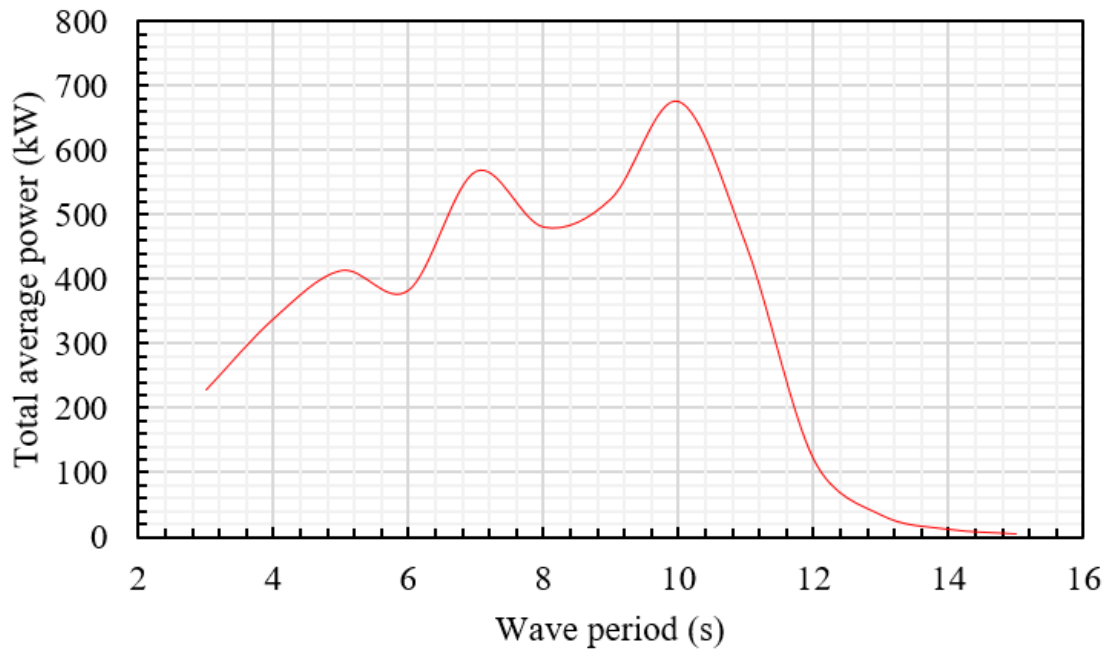
Figure 5-38. The effect of wave period on the total average power of the WEC system.

5.2.2.1.3.3 Regular wave

Figure 5-39 compares the platform surge, heave and pitch displacements, tower-top fore-aft displacement, tower-base force in the x-direction, and fairlead tensions (ML4), in the time-domain, between the CWS concept and the pure catamaran FOWT, subject to a regular wave which has the properties H = 2.1155m and T = 5.2555s. The results show the CWS concept travels further downwind, has a slightly larger tower-top F-A displacement, and larger mean mooring line tension in the upwind line, whilst the heave displacement has been reduced. The pitch displacement and tower-base force in the x-direction are indistinguishable between the two concepts.
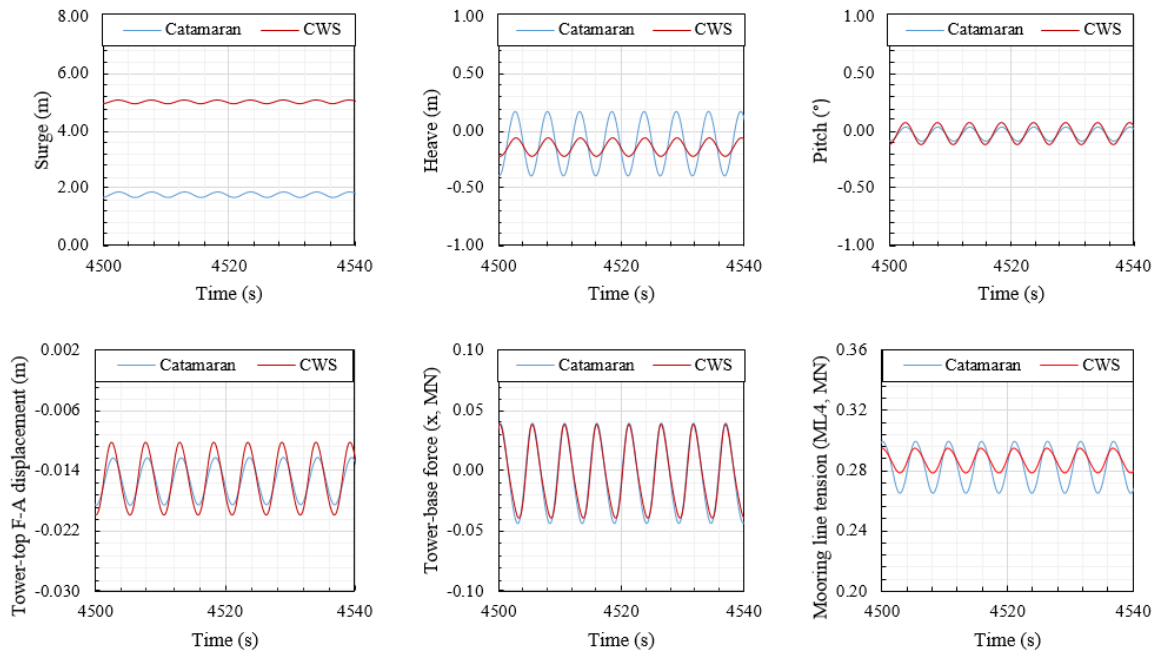
Figure 5-39. Comparison of hydro-elastic response between CWS concept and pure catamaran subject to regular wave in absence of wind.

5.2.2.1.4 Irregular wave analysis

5.2.2.1.4.1 Rated wave condition.

Figure 5-40 compares the platform surge, heave and pitch displacements, tower-top fore-aft displacement, tower-base force in the x-direction, and fairlead tensions (ML4), in the frequency-domain, between the CWS concept and the pure catamaran FOWT, subject to an irregular wave which has the properties H = 2.1155m and T = 5.2555s. The results show the CWS concept has reduced amplitudes compared to the pure catamaran concept for all analysed responses except for surge displacement.
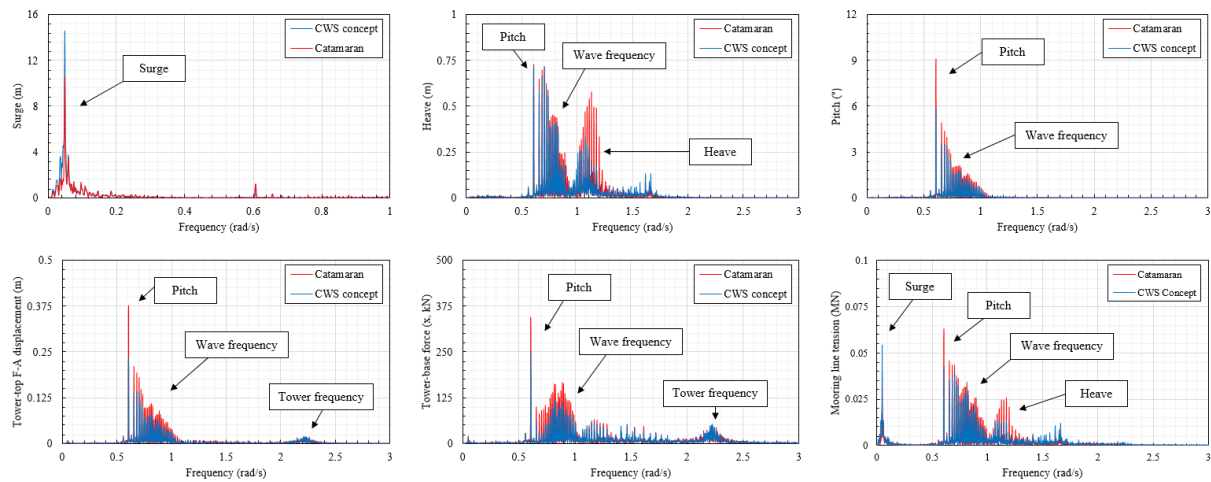
Figure 5-40. Comparison of spectral amplitudes of different structural responses between CWS concept and pure catamaran FOWT subject to irregular wave (rated).

5.2.2.1.4.2 Above-rated wave condition

Figure 5-41 compares the platform surge, heave and pitch displacements, tower-top fore-aft displacement, tower-base force in the x-direction, and fairlead tensions (ML4), in the frequency-domain, between the CWS concept and the pure catamaran FOWT, subject to an irregular wave which has the properties H = 2.9585m and T = 7.1203s. The results show the CWS concept has reduced amplitudes compared to the pure catamaran concept for all analysed responses except for surge displacement. For above-rated irregular wave condition, the surge and heave responses are more similar. The CWS concept has much better stability in pitch and consequently the tower responses exhibit a smaller response compared to the catamaran.
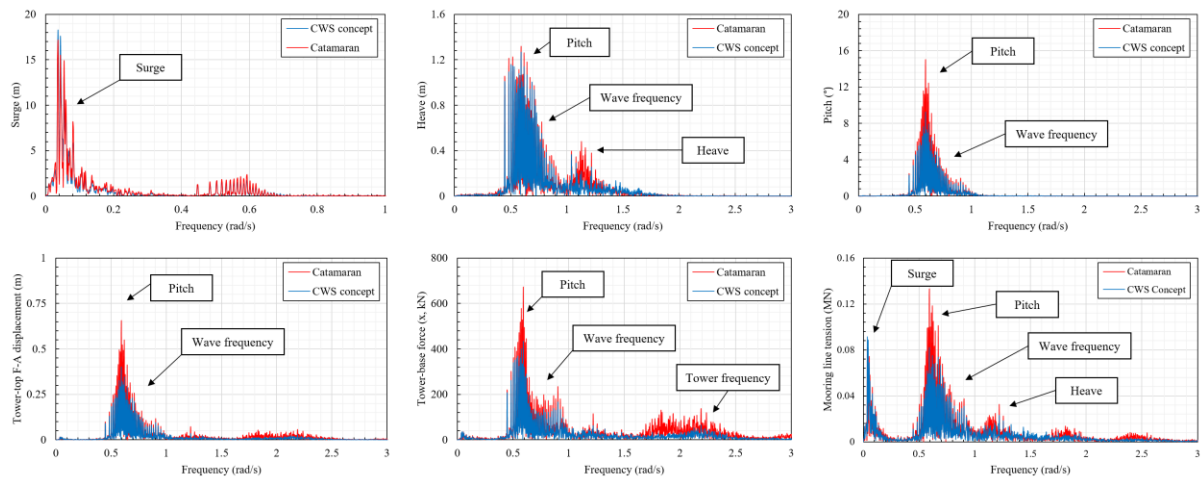
Figure 5-41. Comparison of spectral amplitudes of different structural responses between CWS concept and pure catamaran FOWT subject to irregular wave (above rated).

5.2.3   Chapter summary and conclusions

This chapter was dedicated to the development of numerical models of two types of marine renewable energy systems and integration into a numerical model of a catamaran-type FOWT. The two marine renewable energy systems were a tidal turbine system and a WEC system. The numerical model of the tidal turbines was constructed in AeroDyn and the numerical model of the WEC was constructed in AQWA. Then, the two numerical models were separately integrated into the numerical model of the catamaran-type FOWT. Using the newly integrated numerical models, the dynamic behaviour of the catamaran FOWT was studied with the addition of these marine renewable energy systems and the results were compared to the responses of a pure catamaran-type FOWT. The conclusions of this chapter are summarised in the following points:

For the CTT concept:

- The tidal turbines when positioned higher up in the water column produced more power. The position of the turbines had negligible effect on global platform motions.

- When the tidal turbines are in stand-still, they do not affect the platform motion natural periods.

- When operating, the turbines do not negatively affect the performance of the wind turbine. In fact, the tower-top displacement and tower-base force in the x-direction are slightly reduced. The hydrodynamic thrust reduces the moment produced by the aerodynamic thrust.

- The extra hydrodynamic thrust exerted on the platform due to turbine operation increases the mean surge of the CTT concept. However, the variation in surge has significantly reduced. The tidal turbines produce hydrodynamic damping which makes the CTT concept more stable.

- As a result of the increases surge displacement, the maximum mooring line tension in ML4 increases by approximately 28 %. The fluctuation though is much better.

- The extra mean power generated by the tidal turbines is 0.21, 0.28, and 0.29 MW, respectively, for the examined LCs. This equates to an increase in electrical power of 10.1, 6.0, and 5.6 %, respectively for each LC, compared to the pure catamaran FOWT.

For the CWS concept:

- Hydrodynamic interaction between the catamaran support platform and Wavestar units is strong. The hydrodynamic behaviour of the Wavestar units is governed by the characteristic hydrodynamic behaviour of the catamaran support platform. The integration of the WEC system increases the sway and roll radiation damping coefficients of the catamaran at its characteristic frequencies.

- The effect of combining the WEC system with the catamaran FOWT on the platform natural periods and system damping is positive, particularly for heave, roll, and pitch modes where additional hydrodynamic damping is observed.

- There is a synergy between the WEC system and catamaran support platform in terms of power production due to the relative motion between the two systems. The platform pitching of the catamaran support platform amplified the amount of the power the WEC system can produce.

- The CWS concept displays reduced amplitudes for the observed responses subject to regular and irregular wave except for surge displacement. The integration of the WEC system is beneficial due to the additional hydrodynamic damping provided by the system.

Chapter 6.   Integrated numerical model of a combined floating offshore energy system

This chapter presents the work and results from the final stage of this project which is to build an integrated numerical model of a CFOES comprised of three ORE systems. The novel system integrates a catamaran-type FOWT, a WEC system, and a tidal turbine system. The primary objective of combining three ORE systems using one floating platform is to increase the overall energy yield. However, the integration of the three systems needs to be harmonious and not result in the reduced performance or increased structural loading of the systems. Therefore, the constructed numerical model is used for integrated load analysis to evaluate the performance of the CFOES in typical operational and extreme conditions. The performance of the CFOES will be assessed in terms of total and individual system power production, rotor responses (wind and tidal), global platform motions, blade-root and tower-base loads of the wind turbine, and mooring line tensions. Comparisons of the key performance indicators are made to a pure catamaran FOWT system to determine the advantages and disadvantages of the hybrid concept.

In addition to the CFOES that features a catamaran-type support platform, another numerical model is built of a CFOES which comprises a braceless semisubmersible-type support platform which connects a 5MW wind turbine, a heave-type point absorber, and three tidal turbines. The development of this second numerical model demonstrates that the methodology devised in this project can be applied to other CFOES configurations with confidence for integrated loads analysis.

As such, this chapter is organised into the following sections: Section 6.1 presents the integrated numerical model of the CFOES and the results obtained from an integrated loads

analysis using the integrated numerical model. Section 6.1.1 describes the integrated numerical model of the CFOES and Section 6.1.2 presents and discusses the results for design load cases. Section 6.2 presents the second integrated numerical model of the BCFOES concept. Section 6.2.1 describes the approach to model the hydrodynamics of the concept and Section 6.2.2 describes the modelling of the WEC PTO system. Validation of the integrated numerical model is presented in Section 6.2.3 and the results of the coupled analysis are presented in Section 6.2.4. The chapter summary and conclusions are presented in Section 6.3.

6.1   Combined floating offshore energy system

6.1.1   Integrated numerical model

The main objective of a CFOES is to increase energy yield at the same location by exploiting more than one ORE source compared to a pure system which can only exploit one. However, with proper design there is an array of other synergies associated with CFOESs including better quality of power output, substantial cost reductions related to shared infrastructure, reduced platform motions and structural loading, and increasing sustainability. For a proposed CFOES concept to be successful, the systems need to be seamlessly integrated without affecting the operational or survival performance of the pure systems. The proposed CFOES concept is illustrated in **Figure 6-1** and the main components of the system include: (1) wind turbine, (2) floating platform, (3) mooring system, (4) WEC system, and (5) tidal turbine system. The advantages of the floating platform used in this CFOES concept were established in Chapter 4. The main advantages of using a catamaran support platform include inherent platform stability and a large usable deck area enabled by the cross-structure. Other FOWT concepts such as spars, semisubmersibles and TLPs do not have the deck area capability to use. This makes using a catamaran support platform in a CFOES attractive. For the proposed concept, the deck area permits the WEC PTO system to be mounted to the superstructure, thus,

easing operation and maintenance. In the CFOES concept, eighteen Wavestar units have been installed to the superstructure; six units each on the port and starboard sides, and three units each installed to the fore and aft of the platform. Additionally, one tidal turbine is installed to the keel of each demi-hull of the catamaran support platform. The proposed CFOES concept can exploit energy from wind, ocean waves, and underwater currents. **Table 6-1** presents the structural properties of the proposed CFOES concept. The total power rating of the proposed CFOES concept is 7MW; 5MW contribution is from the wind turbine and the tidal and WEC systems provide 1MW each. The addition of the tidal and WEC systems increase the power rating by 40% compared to a pure 5MW FOWT. Considering the numerical modelling of the CFOES, the final constructed integrated numerical model couples the numerical models presented in the previous chapters. These include the numerical model of the catamaran FOWT (Chapter 4), the tidal turbine system (Section 5.1.1), and the WEC system (Section 5.1.2). The coupling has been completed in the same manner as the CTT and CWEC concepts. However, rather than separate integration of the tidal turbine and WEC system with the FOWT system, all the models are coupled together to create the integrated numerical model of the CFOES concept. The numerical model constructed within F2A is used to perform integrated loads analysis on the CFOES concept in the context of normal operation and extreme conditions. The outputs of the numerical model are critically analysed in order to evaluate the performance of the CFOES. Comparisons are made against a pure catamaran FOWT to determine if the hybridization of ORE technologies is beneficial and the CFOES concept has merit.
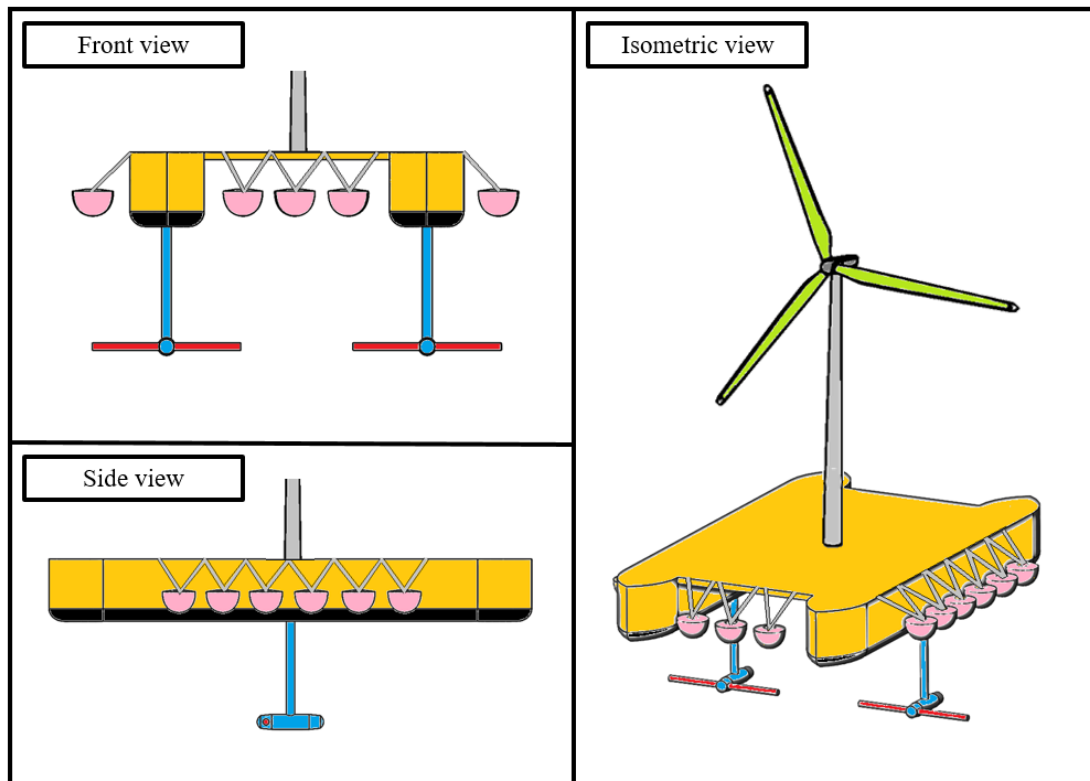
Figure 6-1. The CFOES concept.

Table 6-1. Properties of the CFOES concept.

	Property (Unit)	CFOES
FOWT and tidal turbines	Mass (kg)	5,023,680
	CM location (m)	(-0.01, 0, 1.32)
	Roll inertia about CM (kg m^2)	4,781,318,142
	Ixy (kg m^2)	-618
	Ixz (kg m^2)	2,353,966
	Pitch inertia about CM (kg m^2)	6,861,694,688
	Iyz(kg m^2)	-33
	Yaw inertia about CM (kg m^2)	11,240,002,086
WEC	Mass (float and arm, kg)	27,500
	Mass moment of inertia (kg m^2)	387,500
	Centre of mass (CM) (m)	(0.9, 0, 1.775)
	Additional heave linear damping N/(m/s)	35769

6.1.2   Results and discussion

Table 6-2 describes the simulated LCs to test the performance of the CFOES concept. The wind and wave energy resource design parameters have been obtained from a grid point close to Hywind Scotland [-1.5°E, 57.5°N], which is the site of the world's first floating offshore

wind farm. These site-specific LCs were created using published research whereby meteorological data from 1991 to 2020 was characterised using a cluster analysis and reduced into a computationally affordable number of simulation cases (Saenz-Aguirre et al. 2022). The LCs were selected in accordance with IEC 61400-3 to appropriately cover typical operational and extreme conditions for an adequate analysis of the CFOES concept.

Table 6-2. Load cases for CFOES.

LC	Description	U_w [m/s]	H_s [m]	T_p [s]	θ [°]	U_c [m/s]
1	Below rated	6	0.9	5.5	30	1.3
2	Rated	11.4	2.2	7.8	45	1.3
3	Above rated	20	3	8.3	75	1.3
4	Shutdown	27	3	8.3	0	-
5	Extreme	42.5	5.1	14.2	0	-

6.1.2.1   Below rated

LC1 reflects mild weather conditions simulating a below-rated wind speed (U_w = 6m/s) and benign sea state (H_s = 0.9m, T_p = 5.5s). The incident waves propagate with a 30° heading and a steady current flows at a speed of 1.3m/s. All three systems are in power production mode. **Figure 6-2** and **Figure 6-3** show the time-domain wind turbine generated power, rotor responses, and blade-root bending moments of the CFOES for LC1. The responses are compared to a pure catamaran FOWT system. The power produced by the wind turbines is indistinguishable and similar responses of the rotor and blade-root bending moments are observed. The performance of the wind turbine is not affected by the installation of either marine energy system for below rated wind conditions.
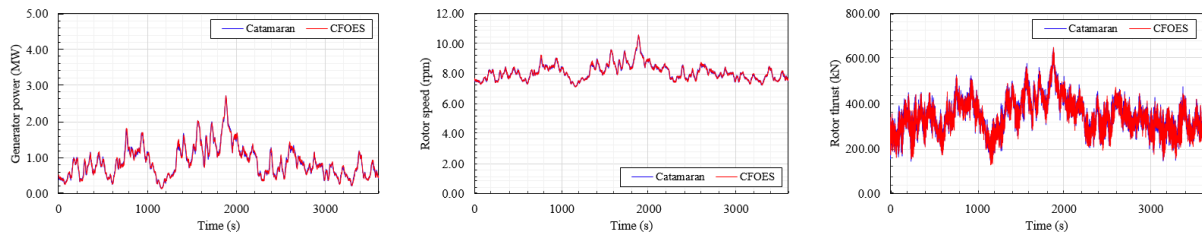
Figure 6-2. Comparison of wind turbine generated power and rotor responses under LC1.
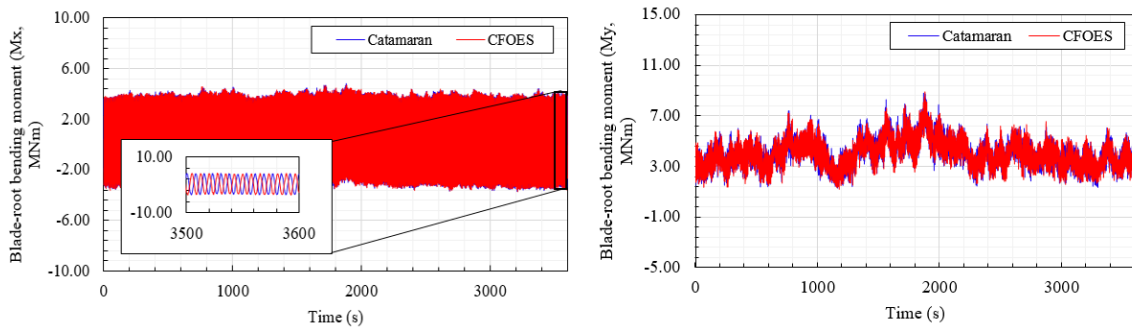
Figure 6-3. Comparison of wind turbine blade-root bending moments under LC1.

Figure 6-4 presents the time-domain wind turbine tower-base bending moments. The overall trend of the two curves for both bending moments is similar. There are points during the simulation where the CFOES appears to have a reduced side-side tower-base bending moment (e.g., 2,400-3,000s) compared to the catamaran concept. The presence of the WEC system increases the rolling stability of the platform, as a result the tower-base bending moment is reduced.
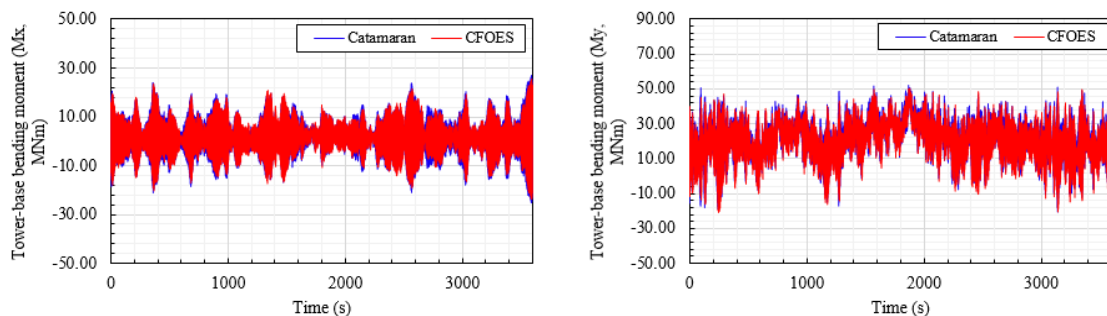
Figure 6-4. Comparison of wind turbine tower-base bending moments under LC1.

Figure 6-5 presents a comparison of the platform motions under LC1. For rigid body modes sway, heave, roll, and yaw, the responses of both concepts are similar. For surge and pitch motions, differences in responses between the CFOES and pure catamaran FOWT are observed. The differences are attributable to the operation of the tidal turbines. When the tidal turbines are in power production state, they produce a hydrodynamic thrust. Three effects arise because of this hydrodynamic thrust: (1) the additional force in the x-direction causes the CFOES to travel further downstream before finding equilibrium. Thus, the CFOES exhibits a greater surge response (approximately 32m), (2) the variability of surge is improved compared to the pure catamaran concept because of increased hydrodynamic damping, and (3) the total hydrodynamic thrust produced by the tidal turbines is approximately 400kN which is comparable in magnitude to the aerodynamic thrust produced by the wind turbine. The hydrodynamic thrust repels the overturning moment produced by the aerodynamic thrust, so the platform maintains an upright position. Consequently, the mean pitch is smaller for the CFOES compared to the pure catamaran concept.
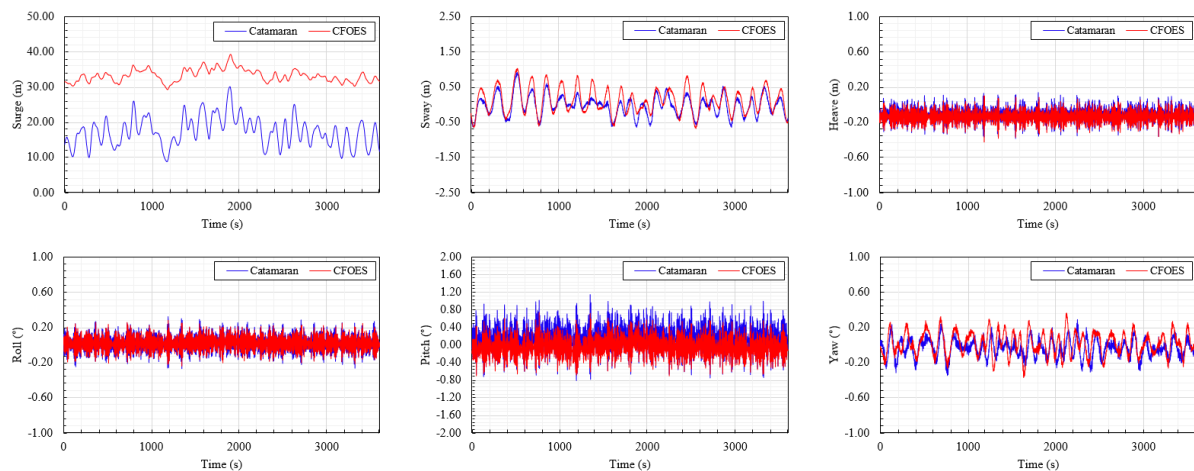
Figure 6-5. Comparison of platform motions under LC1.

Figure 6-6 presents a comparison of the mooring line tension time histories between the two concepts under LC1. A notable difference is observed in the upwind mooring line (ML4).

Naturally, the mooring line tension in the upwind line will increase with larger surge displacements downwind as the line stretches with the moving platform.
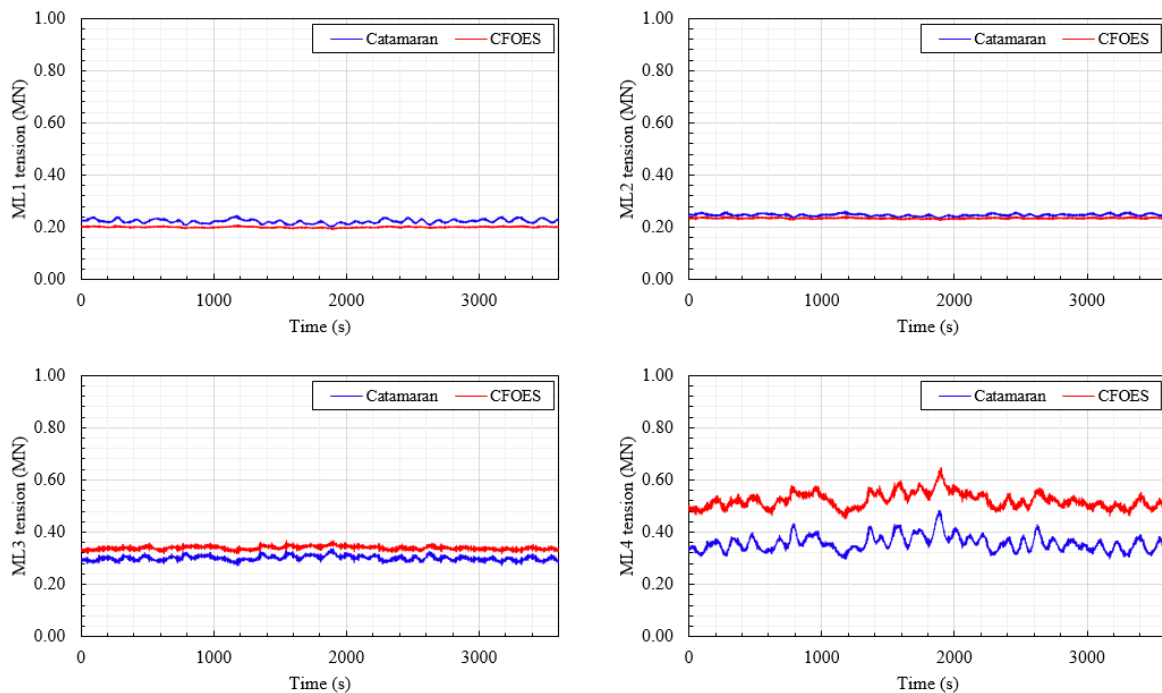
Figure 6-6. Comparison of mooring line tensions under LC1.

Figure 6-7 and **Figure 6-8** detail the power produced by the marine renewable energy systems. Concerning the WEC system, a small amount of power is produced which is due to the benign sea condition and the fact the sea is travelling with a 30° wave heading. The total additional electrical power produced by the WEC system is approximately 57kW. The main WEC units contributing to the total power are units 7, 8, 9, and 10 which are positioned fore of the platform and on the port side. Limited power is produced by units 1 - 6 as they are located on the starboard side of the platform and being shielded by the catamaran support platform. The mean total additional power produced by the tidal turbines is approximately 300kW. The power remains relatively stable during the simulation considering platform motions, which means the neither the wind turbine nor WEC system is negatively affecting the performance of the tidal turbine system. Therefore, an additional 355kW of mean power is produced by the

marine renewable energy systems under LC1. This represents an increase of 30% compared to the pure catamaran concept.
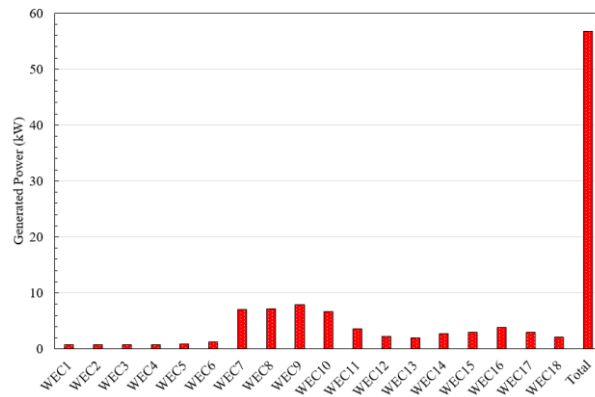
Figure 6-7. Generated power by the WEC system under LC1.
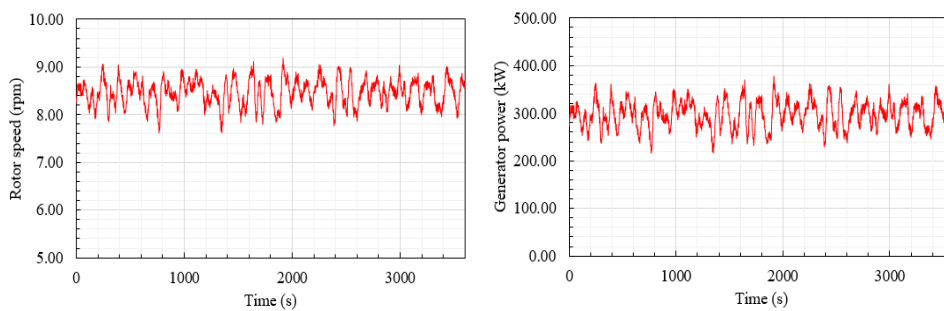
Figure 6-8. Tidal turbine rotor speed and generated power under LC1.

6.1.2.2   Rated

LC2 tests the performance of the CFOES under rated wind turbine conditions. For LC2, the wind speed at the hub height is 11.4m/s. The sea state is moderate with a wave height of 2.2m and a wave period of 7.8s. A steady current flows which has a velocity of 1.3m/s. The waves propagate with a heading of 45°, whilst the wind and current travel downwind in line with the x-axis. LC2 represents the wind condition that produces maximum aerodynamic thrust. At rated wind speed, the aerodynamic thrust is expected to fluctuate around 800kN; this load will transfer to key structural components such as the wind turbine blades and tower. **Figure 6-9** presents a comparison of the time-domain wind turbine generated power and rotor

responses between the CFOES and the pure catamaran-type FOWT under LC2. Visibly, the generator power and rotor responses of the CFOES vary less compared to the catamaran FOWT. The wind turbine on the catamaran support platform combined with the marine renewable energy system produces greater amounts of power and the output is smoother compared to the wind turbine supported by the catamaran platform only. Additionally, the wind turbine blades of the CFOES pitch less compared to the wind turbine blades of the catamaran FOWT. The marine energy systems in the CFOES improve overall platform stability and produce these positive effects for the wind turbine. Moreover, it can be suggested that for the full-service life of the wind turbine, the additional aerodynamic thrust, and blade rotation experienced by the pure catamaran FOWT, would lead to greater accumulated fatigue loading in structural components. This could cause the structure to fail earlier than the CFOES subject to the same conditions.
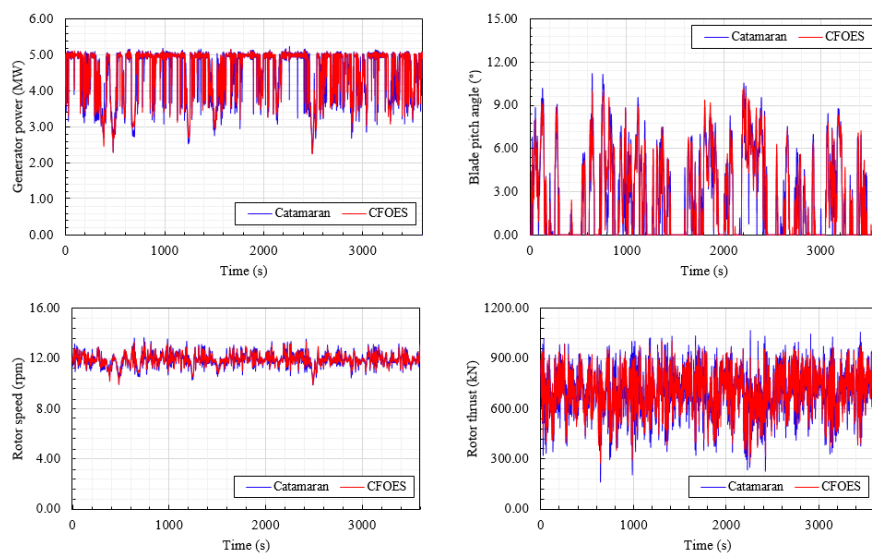

Figure 6-9. Comparison of wind turbine generated power and rotor responses under LC2.

Figure 6-10 shows the blade-root and tower-base bending moments for the two concepts under comparison when subject to LC2. No obvious differences are observed in the edgewise blade-root bending moment. For the flapwise blade-root bending moment, the response of

CFOES is more constant compared to the response of the catamaran FOWT. For the S-S tower-base bending moment, distinct differences are observed in the responses of the two concepts. The pure catamaran FOWT experiences greater response in its S-S bending moment compared to the CFOES concept. The maximum and minimum bending moment of the pure catamaran concept is approximately 35 and -20 MN·m, respectively. The maximum and minimum bending moment of the CFOES is approximately 22.5 and -12 MN·m, respectively. This is a reduction of 35% and 40% in the maximum and minimum S-S tower-base bending moment, respectively. The WEC system significantly dampens the rolling motion of the catamaran support platform when subjected to oblique waves.
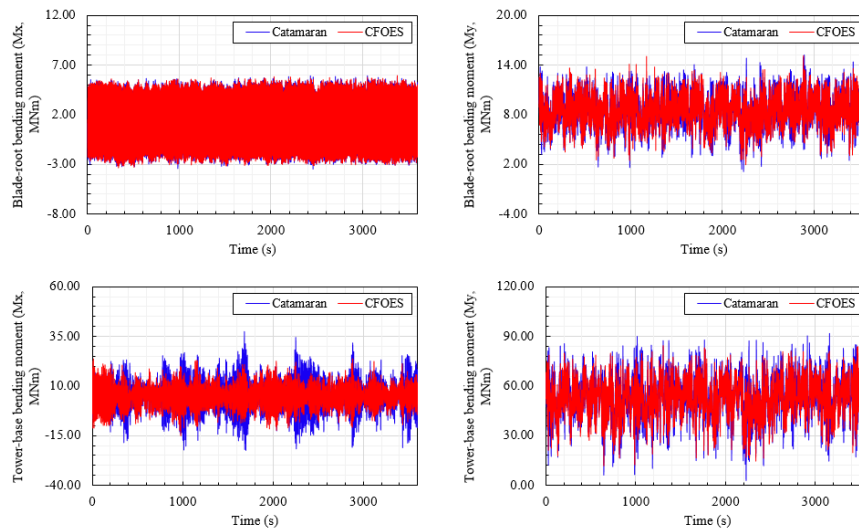
Figure 6-10. Comparison of wind turbine blade-root and tower-base bending moments under LC2.

The platform motions of the CFOES and pure catamaran FOWT under LC2 are presented and compared in **Figure 6-11**. For sway and heave degrees of freedom, relatively unimportant differences are observed. For surge, similar behaviour in LC1 is observed in LC2. For the other three degrees of freedom, the integration of the WEC system has reduced the motion amplitudes of the CFOES. Under LC2, the pure catamaran FOWT exhibits considerable rolling due to the 45° wave heading angle. The rolling range of the catamaran FOWT is 15°. The

advantage of integrating a catamaran-type FOWT with the proposed WEC system is clearly demonstrated here. The presence of the WEC system dampens the rolling of the platform via the PTO system generating electrical power in the process. The WEC system reduces the rolling range from 15° to approximately 5°, a reduction of 66%. For pitch and yaw modes, similar observations occur in that the CFOES has smaller motion amplitudes, but the effect is not as prevalent.
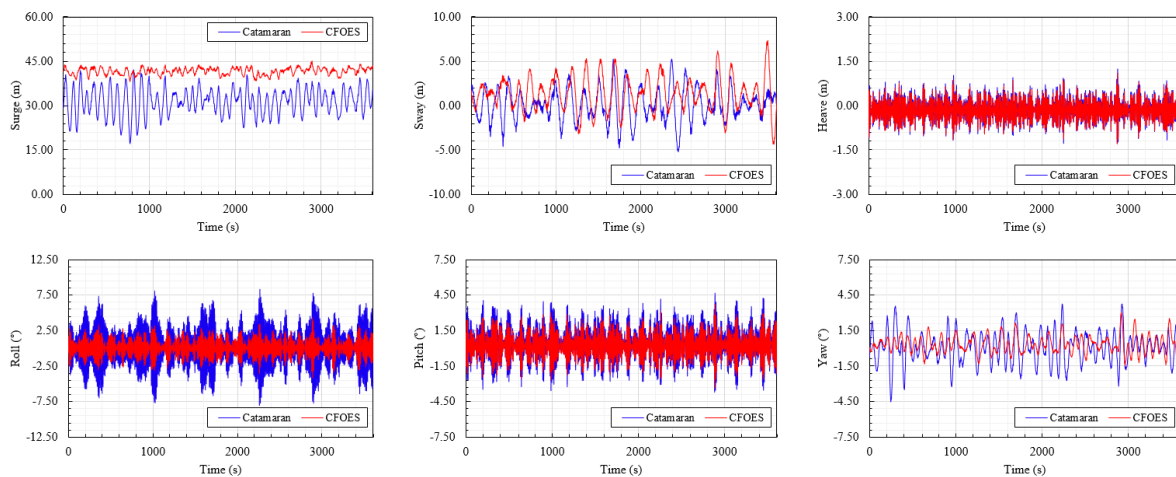
Figure 6-11. Comparison of platform motions under LC2.

The mooring line tension time histories of the two concepts under LC2 are presented in **Figure 6-12**. The tensions in ML3 and ML4 of the CFOES are higher than the tensions in the equivalent mooring lines of the catamaran FOWT concept. This is due to the operation of the tidal turbine system which increases the surge motion of the CFOES. The variability in the upwind mooring lines is reduced however due to the additional damping being created from the tidal turbines.
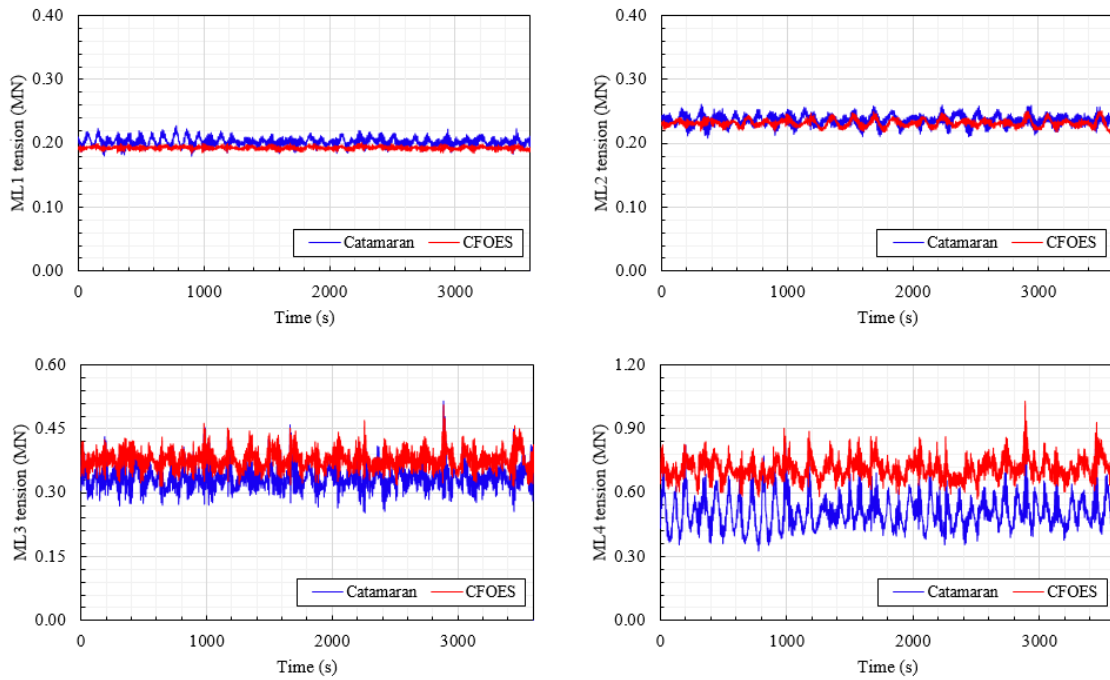
Figure 6-12. Comparison of mooring line tensions under LC2.

Figure 6-13 presents the power produced by the marine renewable energy systems under LC2. On average, an additional 300kW of electrical power is produced by both the WEC system and the tidal turbine system. At a few instances, the peak power produced by the tidal turbine system is approximately 625kW. The combined total average power produced by the marine renewable energy systems is approximately 600kW under LC2. Therefore, the CFOES can produce an extra 12% of additional electrical power compared to the pure catamaran FOWT.
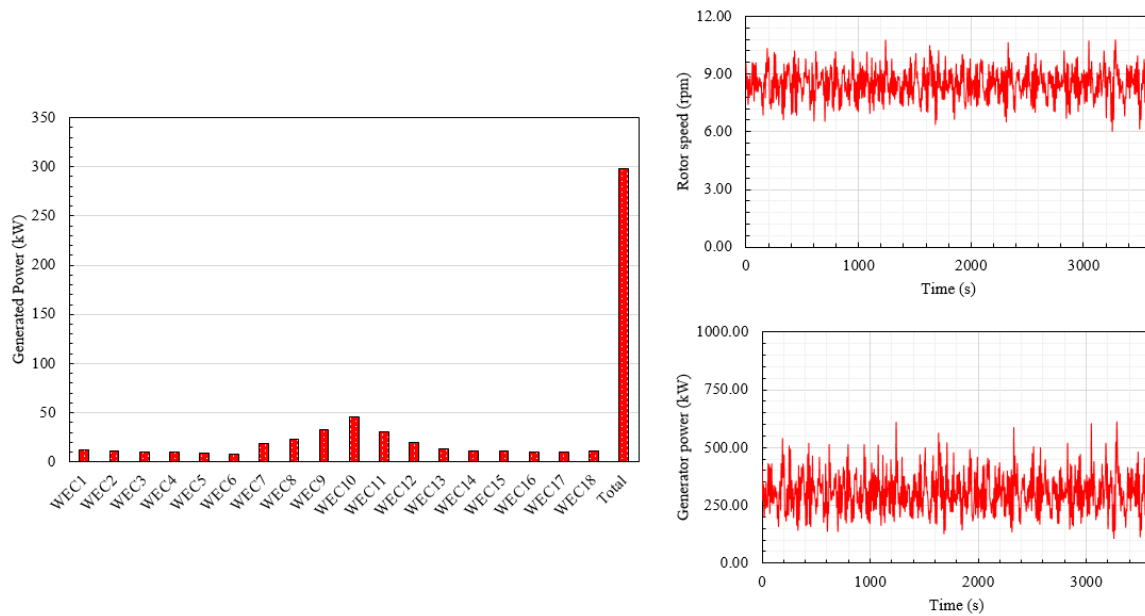
Figure 6-13. Generated power by the WEC system, and rotor response and generated power

of tidal turbines under LC2.

6.1.2.3   Above rated

LC3 tests the CFOES in above rated wind conditions; in this simulation the wind turbine

controller maintains rated power through adjustments in the blade pitch angle and rotor torque.

LC3 simulates the highest wind speed and roughest sea state out of the operational LCs (LC1-

3). The wind speed is 20m/s, and the irregular sea state has a significant wave height of 3m and

a peak wave period of 8.3s. The waves propagate with a heading of 75° which means the

behaviour of the CFOES in oblique seas can be appropriately examined. Additionally, a steady

current is present in the simulation which has a speed of 1.3m/s and flows downwind in line

with the wind and x-axis. The generator power and the rotor responses of the wind turbine of

the CFOES for LC3 are shown in **Figure 6-14**. It can be observed that the turbine maintains its

rated power of 5 MW throughout the simulation. The wind turbine blades have a pitch range

of approximately 12.5°. The blades of the CFOES pitch slightly less compared to the wind

turbine blades of the pure catamaran concept. Consequently, the quality of power produced by

the wind turbine in the CFOES is smoother compared to the power produced by the catamaran FOWT. The mean rotor thrust is similar between the two concepts which is approximately 375kN. However, the pure catamaran FOWT has a higher maximum thrust of approximately 800kN compared to the CFOES which has a maximum rotor thrust of 750kN.
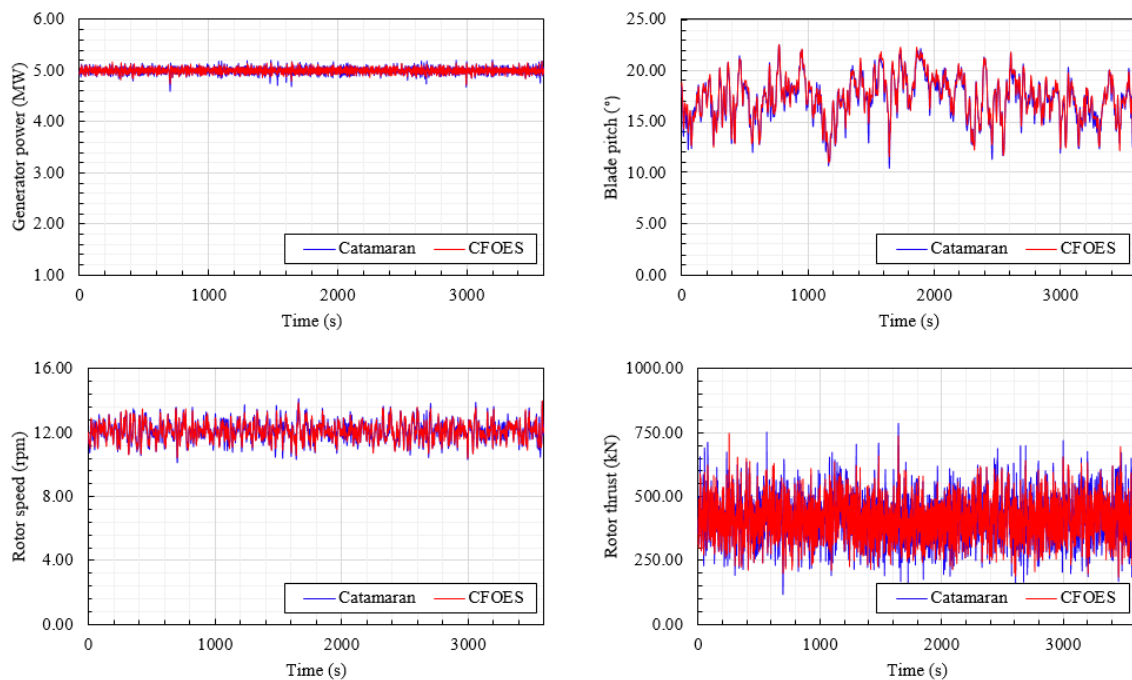
Figure 6-14. Comparison of wind turbine generated power and rotor responses under LC3.

The time-domain wind turbine blade-root and tower-base bending moments of the two concepts under LC3 are compared in **Figure 6-15**. The aerodynamic thrust produced by the wind turbine rotor directly affects the flapwise blade-root bending moment and the F-A tower-base bending moment. Consequently, the variation of these two responses of the CFOES is less compared to the catamaran FOWT. Similarly, to LC2, the S-S tower-base bending moment of the CFOES compared to the catamaran FOWT is much steadier due to the presence of the WEC system.
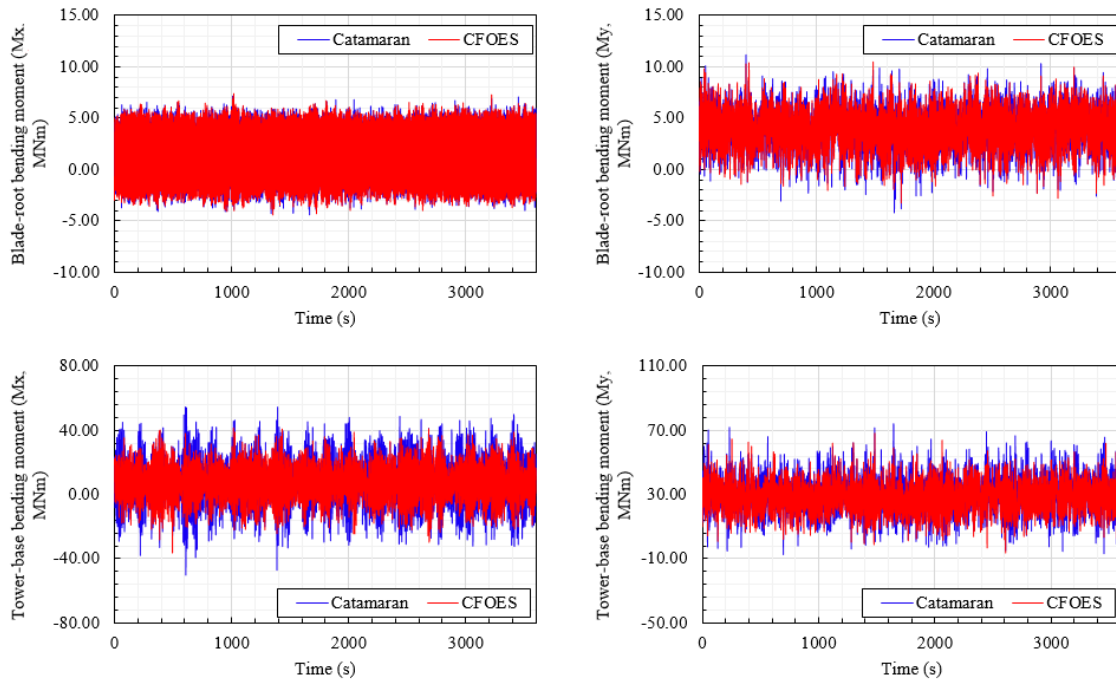
Figure 6-15. Comparison of wind turbine blade-root and tower-base bending moments under

LC3.

Figure 6-16 presents the platform motions of the two concepts subject to LC3. Considering surge mode, the tidal turbine system increases the mean surge due to the hydrodynamic thrust and reduces the deviation about the mean as a result of hydrodynamic damping. For sway and heave, the two concepts show a similar response. The rotational mode responses of the CFOES compared to the catamaran FOWT clearly demonstrate the advantages ORE hybridization. The roll and pitch response has been significantly improved owing to the presence of the WEC system which dampens the rolling and pitching motion of the platform. The mean yaw between the two concepts is similar, however, the standard deviation of the catamaran FOWT is much greater. The maximum and minimum yaw of the catamaran FOWT is 8 and -8°, respectively, whereas for the CFOES, these are approximately 6.4 and -4.8° respectively.
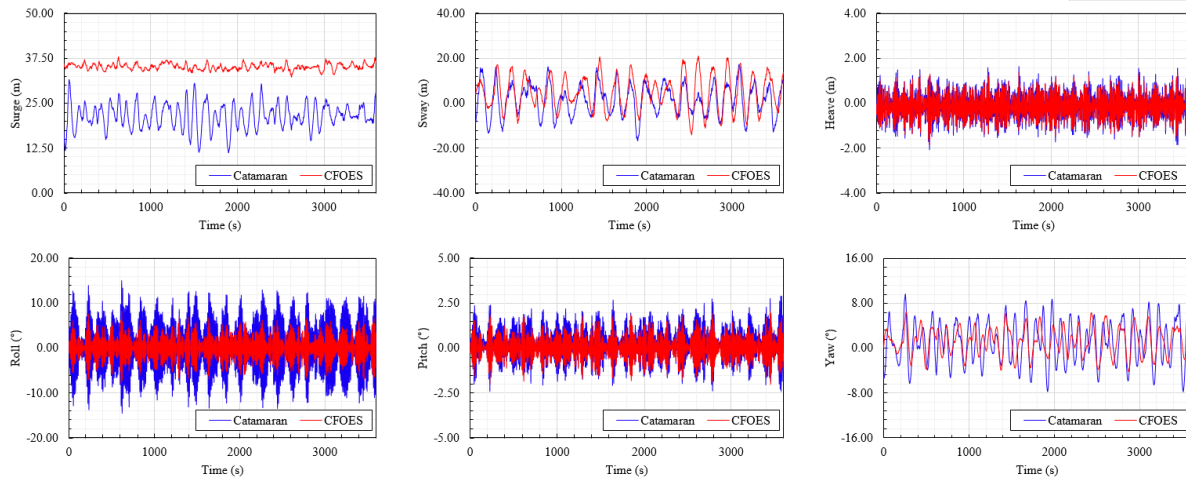
Figure 6-16. Comparison of platform motions under LC3.

The mooring line tensions of the two concepts under LC3 are plotted in **Figure 6-17**. The behaviour of fairlead tension is similar to that observed in LC1 and LC2, except that because of the larger hydrodynamic loading the tensions observed are somewhat higher. The peak tension in the upwind mooring line for the CFOES is approximately 0.875MN and the peak tension in the same mooring line for the pure catamaran concept is 0.625MN.
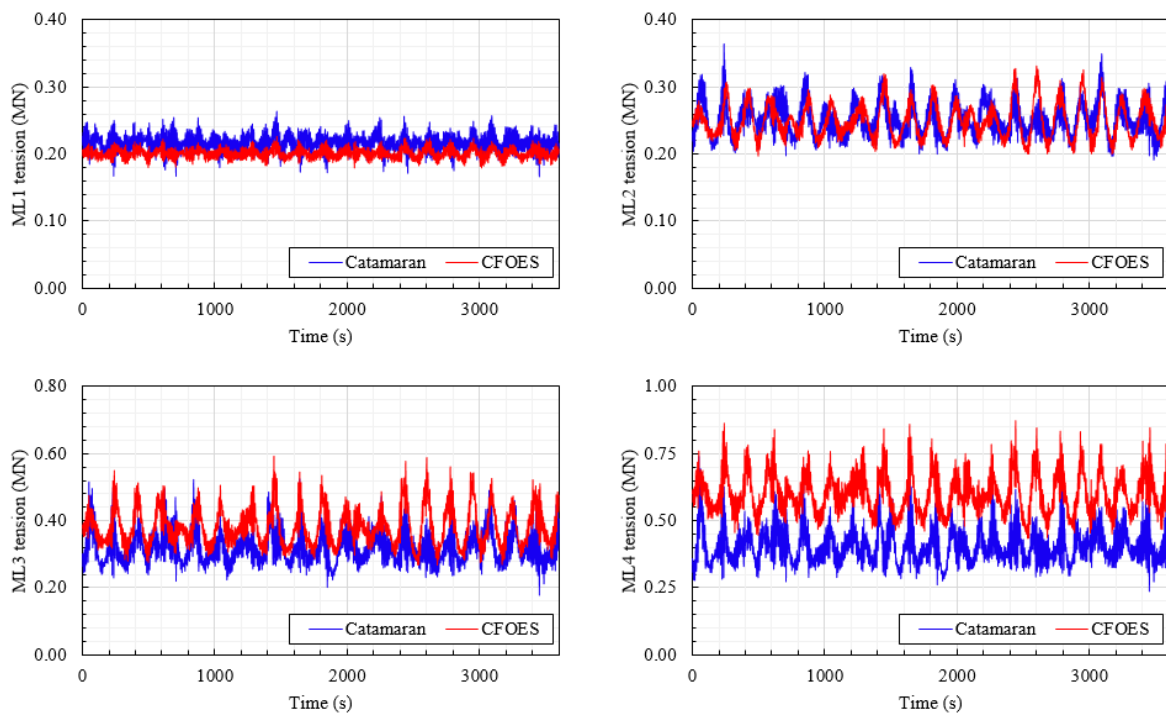
Figure 6-17. Comparison of mooring line tensions under LC3.

Figure 6-18 shows the power generated by the marine renewable energy systems under LC3. The WEC system achieves a mean power output of approximately 660kW under LC3. The Wavestar unit which produces the most power is WEC10 generating approximately 90kW of power. Considering the incident wave angle is 75°, the starboard units produce a reasonable amount of power, approximately 35-40kW, even though they are shielded by the catamaran demi-hull. The relative rolling motion between the platform and units is what creates this additional power. The tidal turbine system produces a mean power of approximately 300kW and the instantaneous maximum power is 500kW. This means that marine renewable energy systems within the CFOES can produce 1MW of additional mean power which represents a 20% increase compared to the pure catamaran FOWT system.
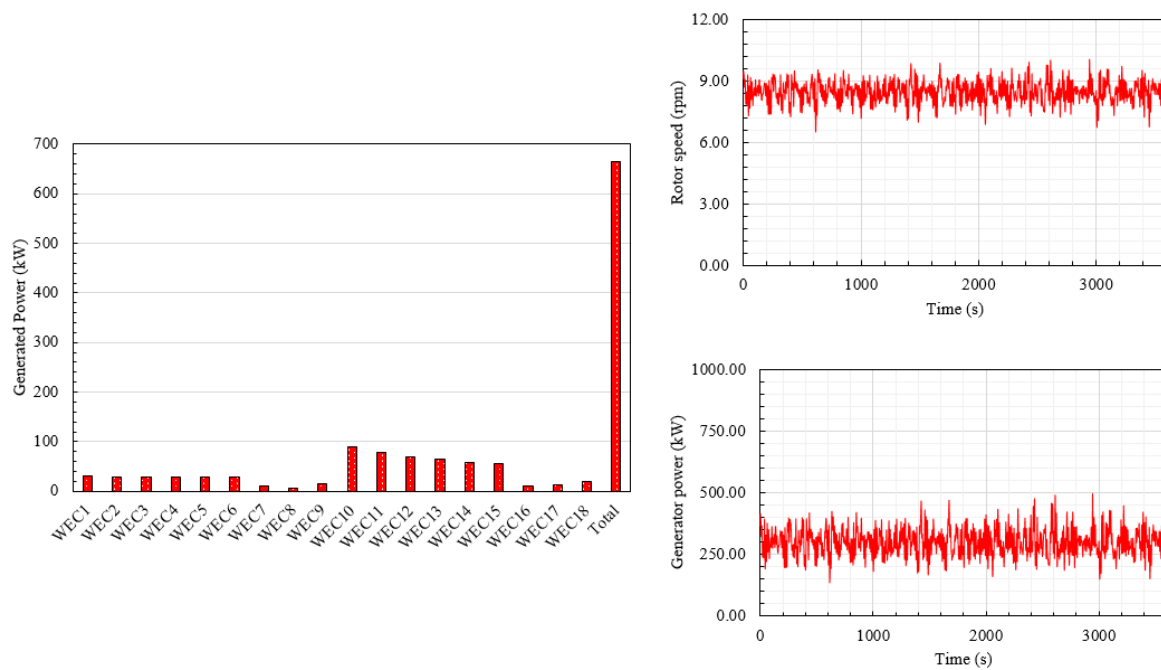
Figure 6-18. Generated power by the marine renewable energy systems under LC3.

6.1.2.4   Shutdown

LC4 tests the CFOES behaviour during a shutdown routine. The wind speed in this simulation is 27m/s which is above the maximum operating range of the NREL 5MW reference

wind turbine (> 25m/s). The sea state has significant wave height of 3m and a peak wave period of 8.3s. The wind and wave are co-aligned and travel along the x-axis. No current is present in this simulation; thus, the tidal turbines are in idling state during the shutdown of the wind turbine. The WEC system remains in operation and the shutdown of the wind turbine is initiated after 300s of simulation time. **Figure 6-19** presents generator power and rotor responses of the wind turbine under LC4. At 300s, the rotor speed is reduced to 0rpm, the blades begin to feather towards 90° (idling pitch angle) at a rate of 10°/s and the wind turbine stops generating power. There are negligible differences in the rotor responses of the two concepts after the shutdown is initiated. This is expected as the wind turbine controller is the same in the two concepts.
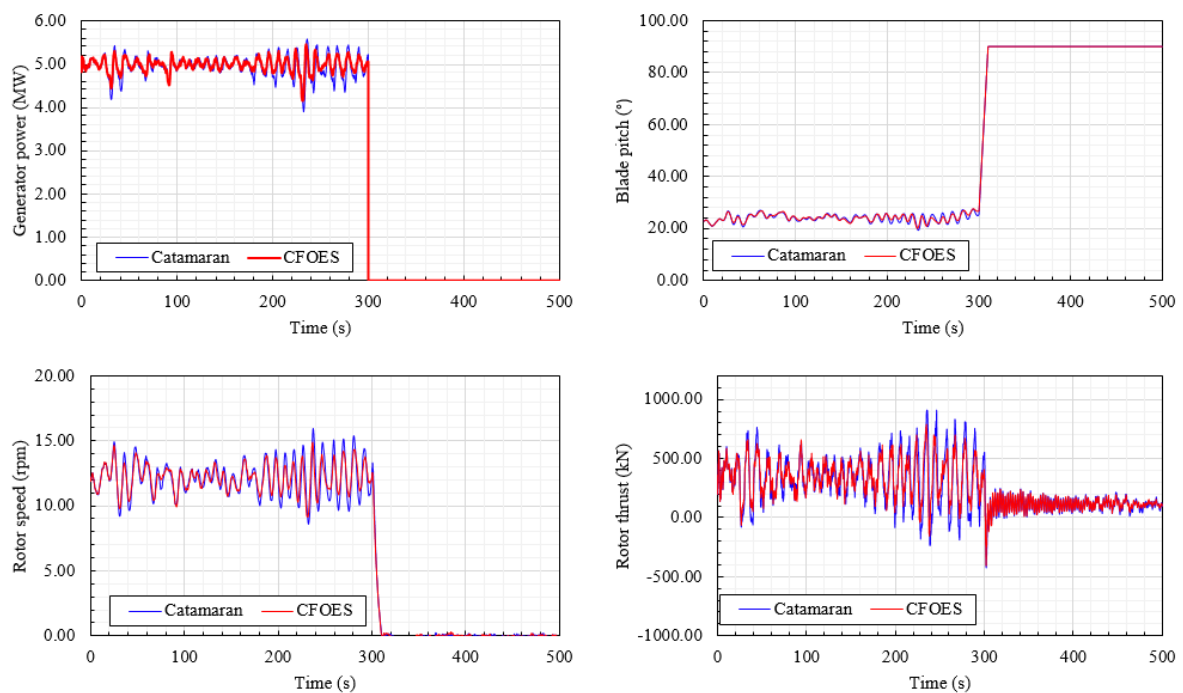
Figure 6-19. Comparison of wind turbine generated power and rotor responses under LC4.

Figure 6-20 shows the blade-root and tower-base bending moments for LC4. The CFOES and catamaran FOWT display similar responses for the I-P blade-root and F-A tower-base bending moments. However, different responses for the O-o-P blade-root and S-S tower-base bending moments are observed during the initial period after the shutdown routine. When the

turbine is shut down, aerodynamic thrust ceases. Then, the O-o-P blade-root bending moment will be influenced by platform pitching only. However, this will only be for a brief period as feathering of the blades is occurring. Once the blades are feathered, limited response is observed. In the period before the blades are fully feathered, the response of the CFOES is better compared to the catamaran FOWT. This is of consequence of the WEC system which improves platform stability. Also, when the turbine is shut down, rotor torque is no longer being applied to the shaft of the wind turbine. Rotor torque contributes to the S-S tower-base bending moment. Therefore, after the shut down the bending moment will reduce. However, there will still be a contribution from the platform rolling. The WEC system improves the S-S tower-base bending moment for the CFOES by damping the motion of the platform.
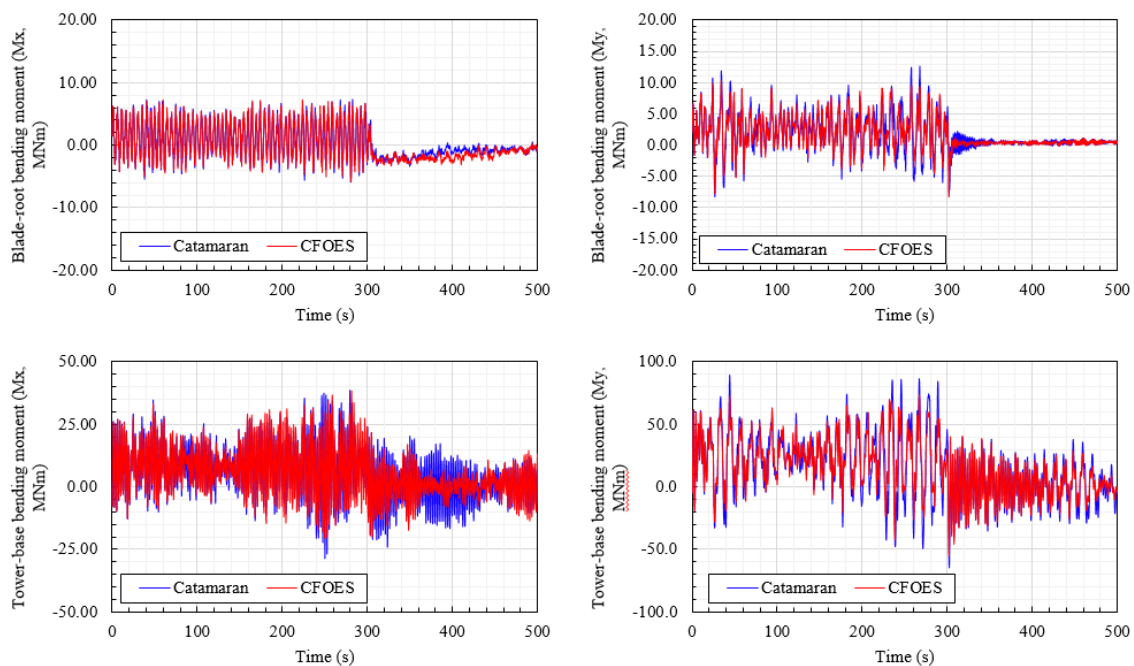
Figure 6-20. Comparison of wind turbine blade-root and tower-base bending moments under LC4.

**Figure 6-21** shows the time-domain platform responses of both concepts during the shutdown routine. The surge displacement of both concepts reduces as a result of aerodynamic thrust no longer being exerted on the rotor. The roll displacement also decreases due to rotor

torque no longer being applied. Compared to the pure catamaran concept, the WEC system dampens the rolling motion of the CFOES. Moreover, because aerodynamic damping is no longer present, the pitch displacement of both concepts is governed by the incident waves and noticeably increases compared to LC3. **Figure 6-22** shows the mooring line tensions and **Figure 6-23** shows the generated power by the WEC system under LC4, respectively. The surge displacements are somewhat similar between the concepts, consequently, the tension in the mooring lines is also similar. In the upwind mooring line of the pure catamaran concept, a high frequency component is more observable compared to the CFOES. This is because of the platform pitching. The CFOES has a reduced response because of the additional damping produced by the WEC system. The generated power by the WEC system is minor compared to other LCs, which suggests small relative motion between the catamaran support platform and WEC system.
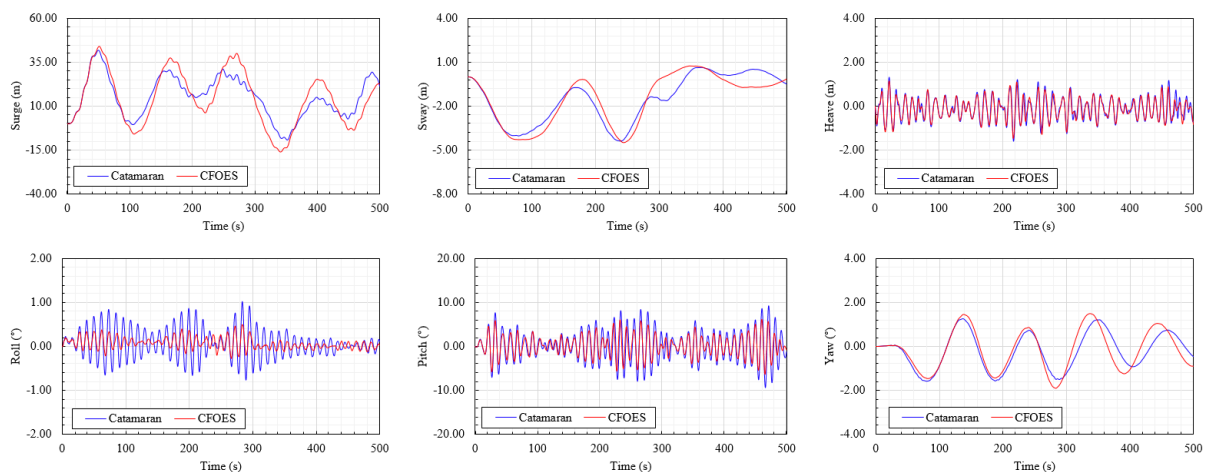
Figure 6-21. Comparison of platform motions under LC4.
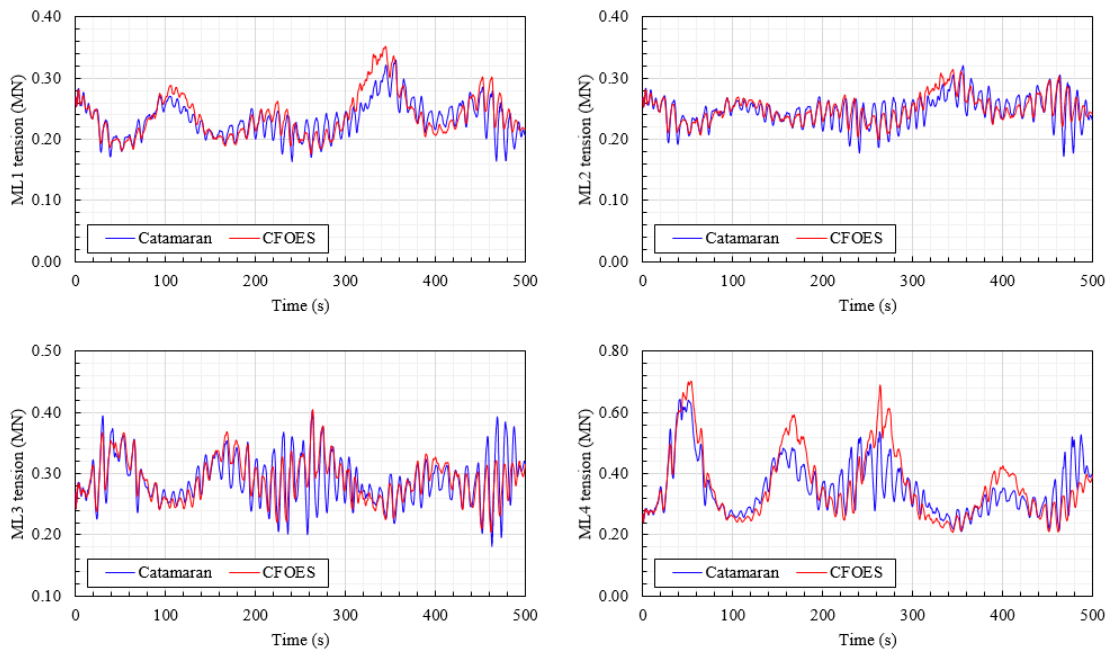
Figure 6-22. Comparison of mooring line tensions under LC4.
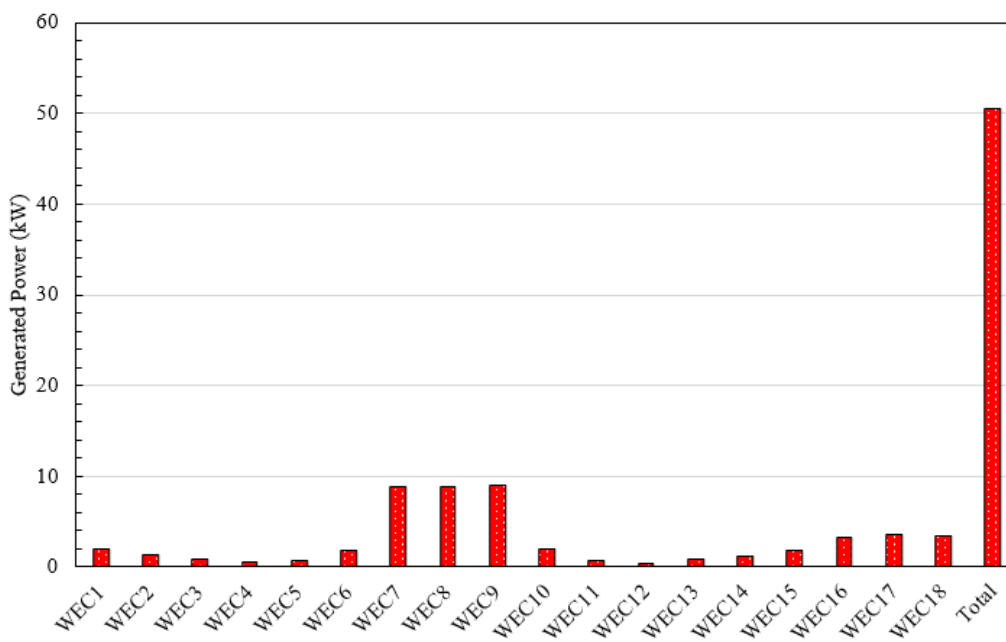
Figure 6-23. Generated power from the WEC system under LC4.

6.1.2.5   Extreme

LC5 examines the performance of the CFOES subject in extreme weather conditions. The wind speed recorded at the wind turbine hub height is 42.5m/s. The sea state is severe with a

wave height of 5.1m and a wave period of 14.2s. The wind and waves propagate in line with the x-axis and there is no sea current present. The wind turbine and tidal turbines are idling with blades feathered to 90°. **Figure 6-24** presents a comparison of the blade-root and tower-base bending moments, **Figure 6-25** presents a comparison of platform motions, and **Figure 6-26** shows the comparison of mooring line tensions under LC5, respectively. The responses between the two concepts are fairly similar which shows the presence of the marine renewable energy systems does not positively or negatively impact the catamaran FOWT in extreme conditions.
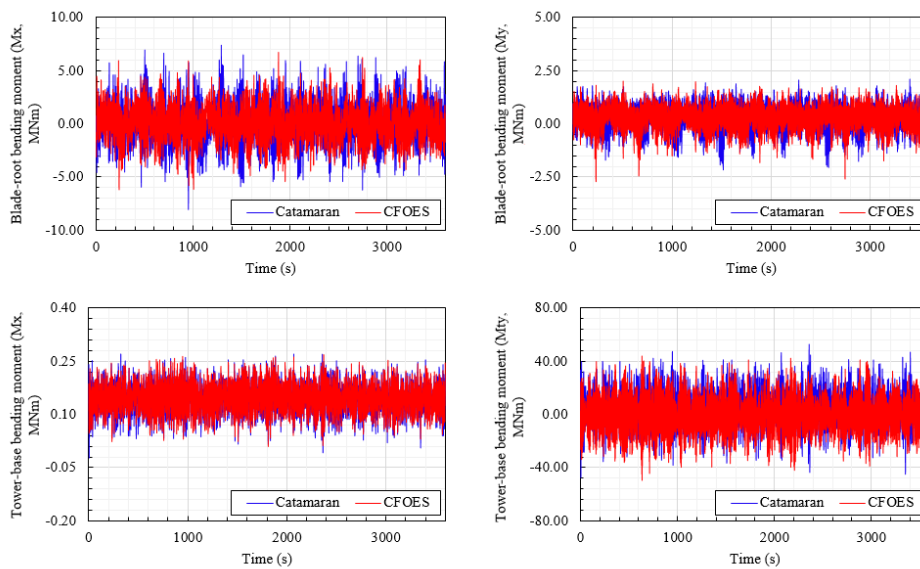
Figure 6-24. Comparison of blade-root and tower-base bending moments under LC5.
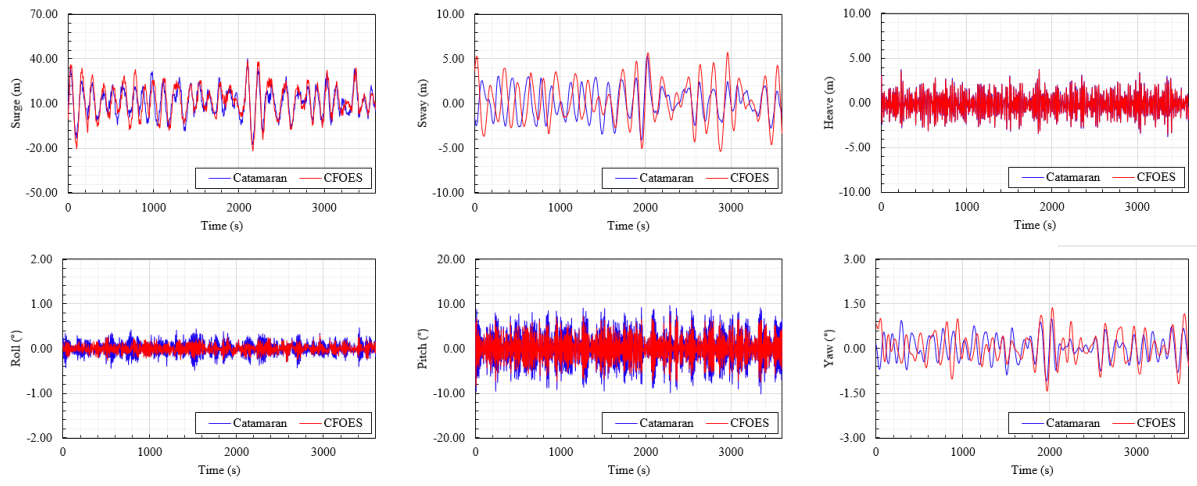
Figure 6-25. Comparison of platform motions under LC5.
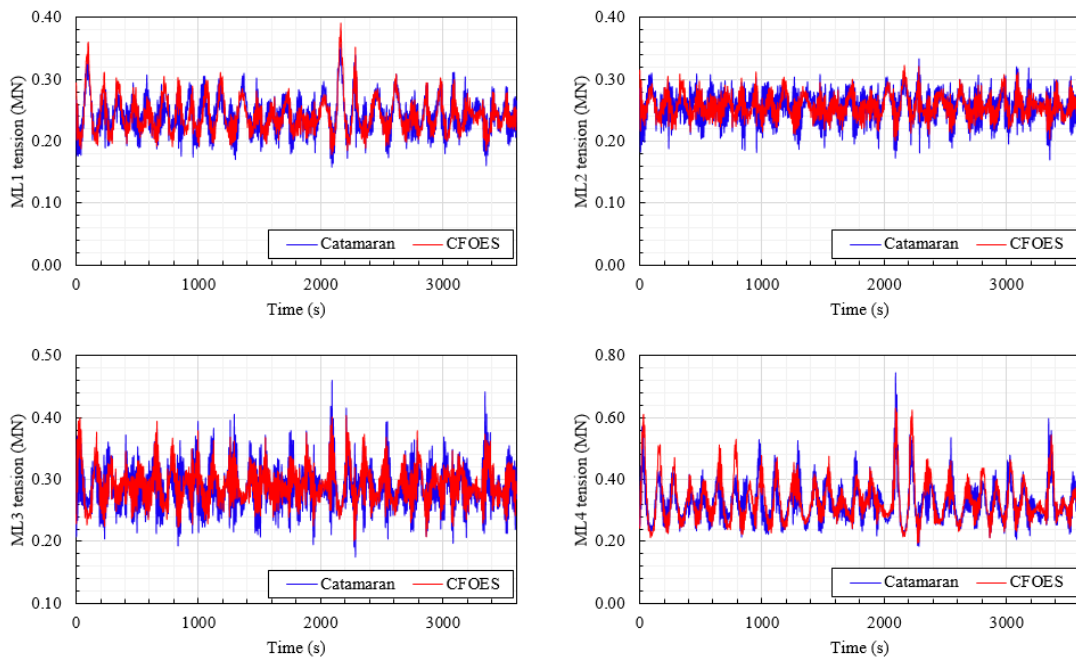
Figure 6-26. Comparison of mooring line tensions under LC5.

6.2   Braceless combined floating offshore energy system.

A second CFOES concept is introduced in this chapter which comprises a semisubmersible-type support platform as the common connection for three different ORE systems. The concept (see **Figure 6-27**), referred to as the Braceless Combined Floating Offshore Energy System (BCFOES), features a braceless 5-MW semisubmersible floating wind turbine (Luan et al., 2016) integrated with three tidal turbines and a point absorber WEC.

The support platform type is a braceless semisubmersible whereby 3 columns surround a central column separated by 120°, the distance between the centre and side columns is 41 m, all columns are 6.5m in diameter, the columns are supported by three pontoons which connect together at the centre, each pontoon is 9m wide, 6m high and has a radius of 45.5m. The wind turbine is the NREL 5 MW reference wind turbine which has a cut-in, rated, and cut-out speed of 3, 11.4 and 25m/s, respectively. The wind turbine is mounted on the floating platform's central column 10m above sea level. The mooring system is comprised of three mooring lines each separated by an angle of 120°. The fairleads are attached to the pontoons at a depth of 18m and the anchors have a radius of 1084.4m and depth of 200m. The WEC is attached to the central column and is free to translate up and down. All other degrees of freedom are constrained by a guide-roller system so that the WEC moves with the floating platform (see section 6.2.2). The three tidal turbines are reference model turbines designed by the Sandia National Laboratories (Yang et al. 2020b) and attached to the keel of the semisubmersible platform so that the hubs of the turbines are 43.5m below mean seawater level. The vertical axes of the support beams of the turbines are aligned with the vertical axes of the side columns of the platform. The tidal turbines have a cut-in, rated, and cut-out speed of 0.5, 2.0 and 3.0m/s, respectively. The tidal turbine controller is a variable-speed, variable-pitch controller based on the NREL 5MW reference wind turbine controller developed by Jonkman (Yang et al. 2020b).
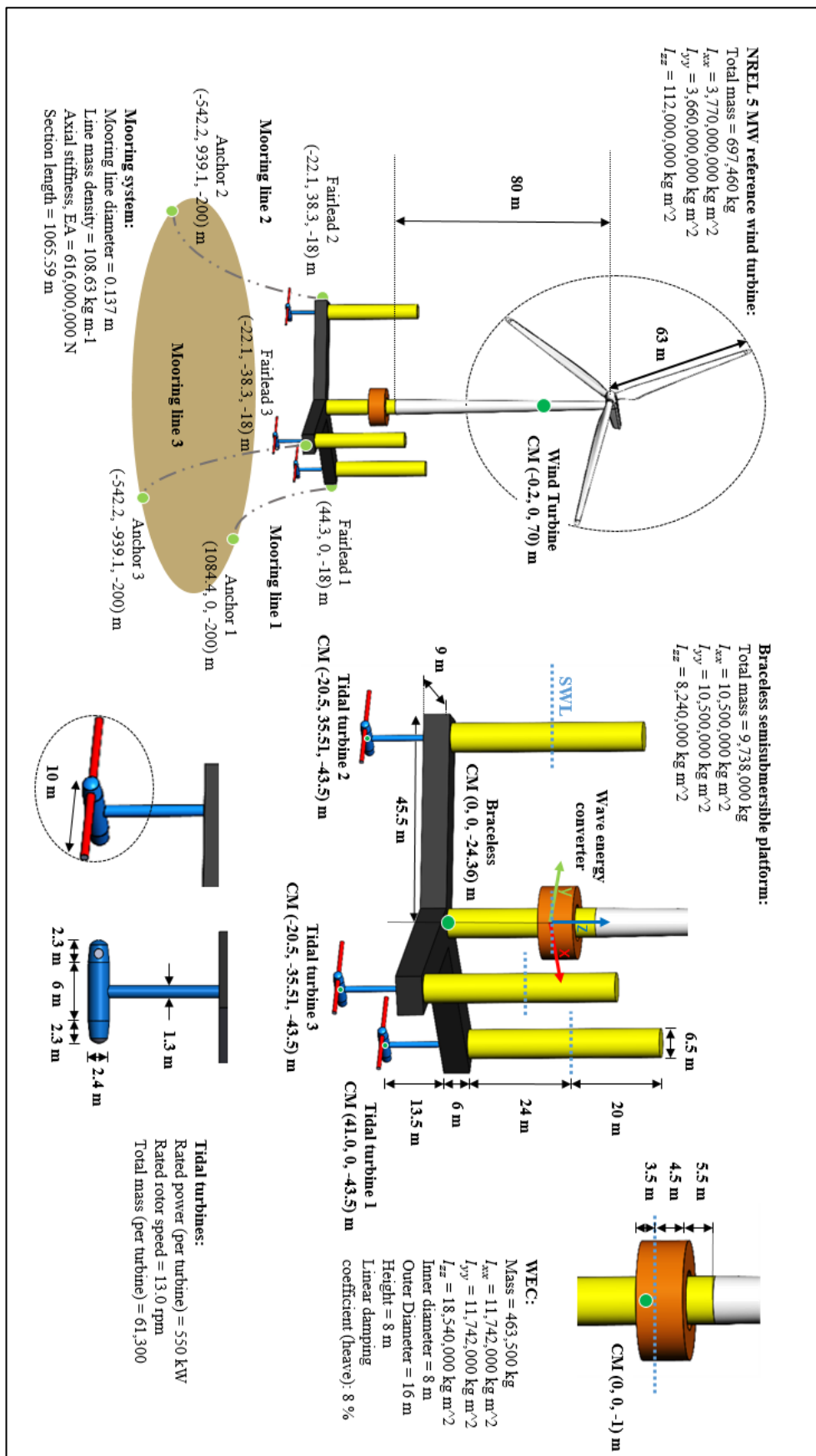
Figure 6-27. Schematic of the BCFOES.

6.2.1   Hydrodynamic modelling

The braceless semisubmersible is a large-volume structure with slender body components; in the developed numerical model a hybrid method is employed in ANSYS AQWA to calculate the hydrodynamic loads using diffracting panels for the pontoons and Morison elements for the columns (see **Figure 6-28**).
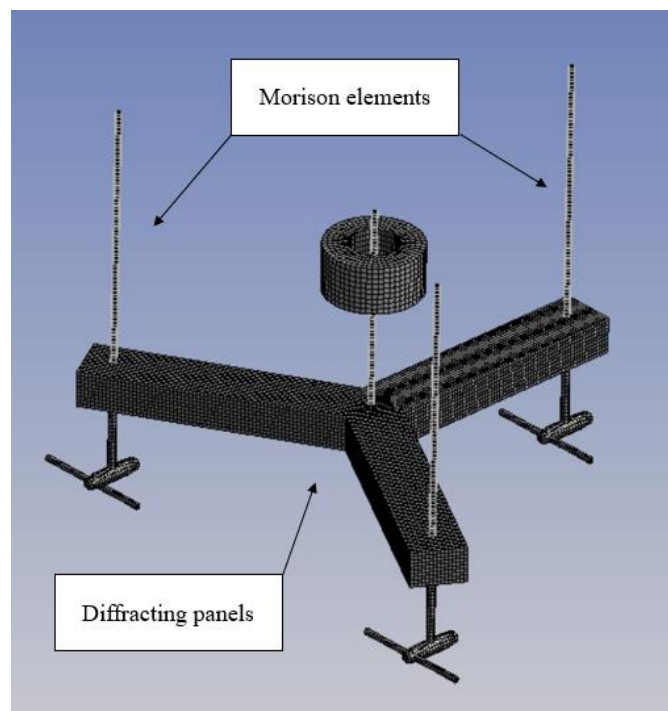
Figure 6-28. Mesh of BCFOES concept generated in ANSYS AQWA.

6.2.1.1   Morison element forces

Morison elements are used to model the columns of the braceless semisubmersible in the hybrid model. Morison's equation for the fluid forces exerted on a slender structural member is:

$$dF = \rho A C_M \dot{u}_f - \rho A (C_M - 1) \dot{u}_s + \frac{1}{2} \rho D C_D |u_f - u_s|(u_f - u_s)$$

$$= \rho A (1 + C_a) \dot{u}_f - \rho A C_a \dot{u}_s + \frac{1}{2} \rho D C_D |u_f - u_s|(u_f - u_s)$$

[86]

where C_D is the drag coefficient, D is the characteristic drag diameter, u_f is the transverse directional fluid particle velocity, u_s is the transverse directional structure velocity, $C_M = C_a + 1$ is the inertia coefficient where C_a is the added mass coefficient and A is the cross-sectional area. In this study, the values of the inertia coefficient and drag coefficients are 2.0 (or $C_a = 1.0$) and 1.2 respectively (ANSYS 2020).

6.2.2 Power-take-off system

The power-take-off (PTO) system (**Figure 6-29**) physically connects the semisubmersible platform and the WEC. The PTO system is simplified as a linear spring-damper system which is modelled in ANSYS AQWA using fender connections. Fenders allow the user to model material contact between two structures; the horizontal contact is also modelled using fenders. Depending on the relative positions of the structures and the fender positions on the structures, they create a varying force acting on the structure (WEC) which is added to the other forces used for computing the structures' motions. A contact plane, this is the plane which the fender will impact, and attachment point is defined for each fender. In this study, the fenders allow WEC heave motion up to 3m from resting position. To ensure consistent results and validation of results of this study, the damping and stiffness coefficients were kept identical with the work of Li et al (Li et al. 2021). These values were obtained from an optimization of the PTO system in the work of Wang et al (Wang et al. 2020).
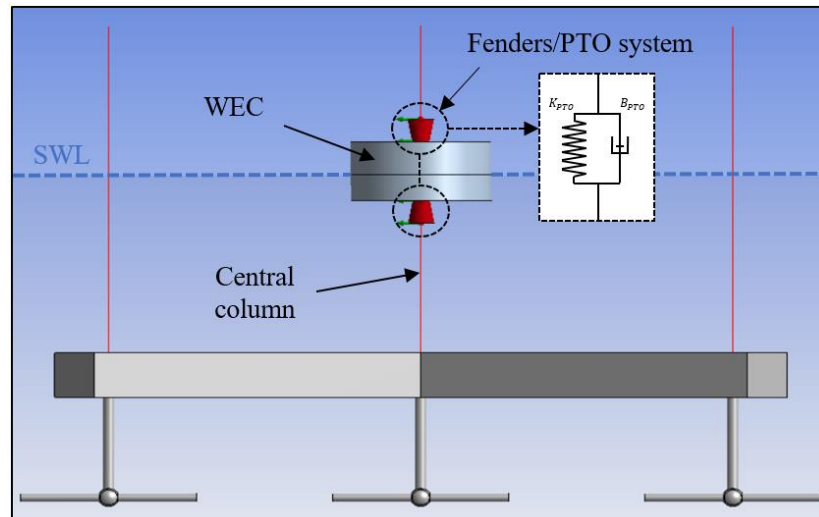
Figure 6-29. PTO system developed in ANSYS AQWA.

The force, F_{PTO}, and power, P_{PTO}, of the PTO system are found using the following equations:

$$F_{PTO} = B_{PTO}(V_{WEC} - V_{FOWT}) + K_{PTO}(x_{WEC} - x_{FOWT})$$

$$P_{PTO} = F_{PTO}(V_{WEC} - V_{FOWT})$$

[87]

where B_{PTO} is linear damping coefficient; K_{PTO} is the linear spring stiffness coefficient; V_{WEC} and V_{FOWT} is the heave velocity of the WEC and FOWT, respectively; and x_{WEC} x_{FOWT} is the heave displacement of the WEC and FOWT, respectively.

6.2.3   Validation

Similar to the CFOES concept, there is no numerical or experimental data available for the full BCFOES concept which means partial validation of independent systems is required to validate the numerical model. The tidal turbines have previously been validated in this thesis, they are positioned slightly lower down in the water column compared to the CFOES concept, however no further validation of this system is necessary. To validate the FOWT and WEC components, the work of Wang et al. (Wang et al. 2020) and Li et al (Li et al. 2021). is used as a means of comparison with the results from the present numerical model for a regular wave

simulation. The regular wave has a wave height of 2m and a wave period of 9s. The results of the simulation are presented in **Figure 6-30**. There is excellent agreement between the two data sets. There is slight discrepancy in the mooring line tensions, the differences however are small. These results confirm the FOWT and WEC coupling has been correctly modelled, and the numerical model can be used for advanced integrated loads analysis of the BCFOES concept.
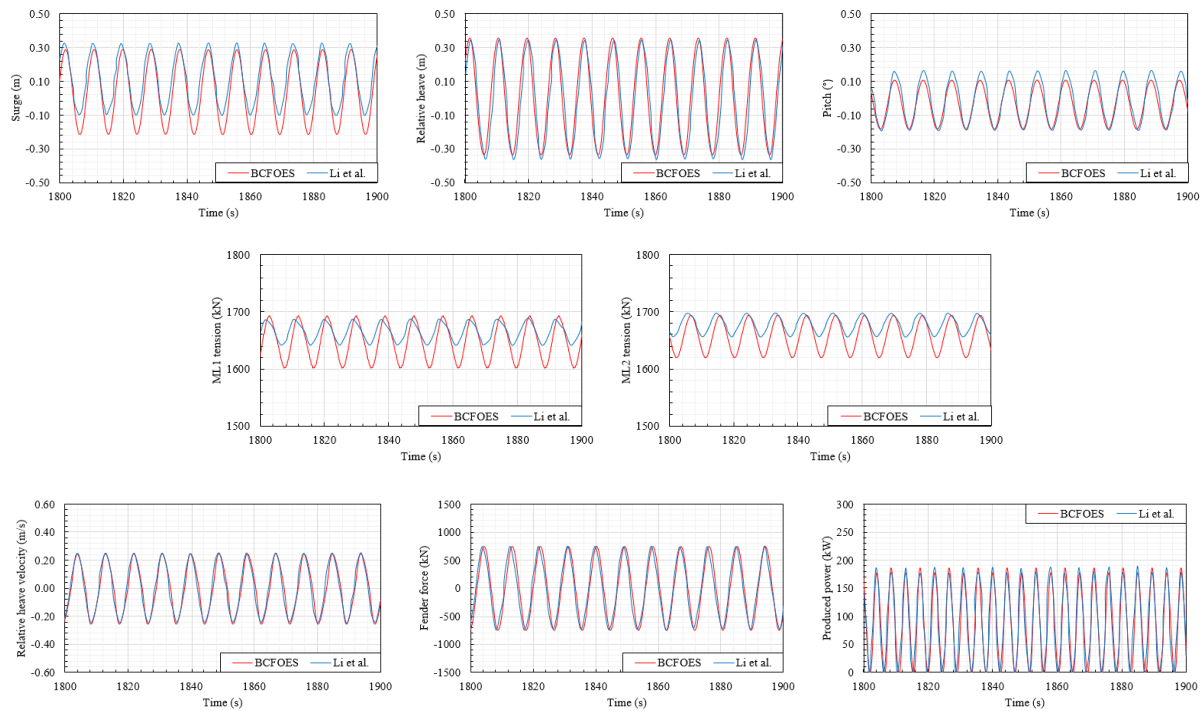
Figure 6-30. Validation of BCFOES numerical model - simulation of regular wave condition (H = 2m, T = 9s) and comparison against numerical results of Li et al (Li et al., 2021).

6.2.4   *Results and discussion*

Table 6-3 describes the LCs which have been simulated to test the performance of the BCFOES concept. This section then presents the numerical results which include free decay results and the responses of the BCFOES when subject to below-rated, rated and above-rated wind conditions. The findings are discussed and compared with respect to a pure braceless semisubmersible FOWT.

Table 6-3. Load cases for BCFOES.

LC	Description	U_w [m/s]	H_s [m]	T_p [s]	U_c [m/s]
FD	Free decay	-	-	-	-
1	Below rated	8	2.3	10	1.8
2	Rated	11.4	3.4	13.5	2.0
3	Above rated	16	5.3	17.7	2.2

6.2.4.1   Free decay analysis

A free decay analysis was conducted to observe the influence of the marine renewable energy systems on the platform natural periods of the BCFOES. Only free decay simulations for surge, heave, and pitch degree of freedoms were run. For sway and roll, the behaviour is similar to the surge and pitch, respectively, due to platform symmetry. For yaw, it is predicted the marine energy systems will not have a significant effect. Four configurations were run in the free decay analysis: (1) a pure braceless semisubmersible FOWT, (2) braceless semisubmersible FOWT and WEC, (3) braceless semisubmersible FOWT and three tidal turbines, and (4) BCFOES. The influence of the marine renewable energy systems on the platform natural periods will easily be identified in this manner. **Figure 6-30** presents the results of the free decay analysis and **Table 6-4** quantifies the natural periods of the four configurations and compares them to results presented across literature for the same configurations. Considering surge, the WEC slightly increases the surge natural period due to the increase in total mass, whilst the damping remains the same. For the present model, it seems that the mooring system is stiffer compared to other models in literature. The surge natural period for the present models is 70s whereas for published results it is 80s. For heave, the presence of the WEC has significant positive impact in terms of damping. Semisubmersibles are known to have limited inherent damping in heave within the system, so the integration of the WEC is a good damping mechanism solution. For configurations with the WEC, the system returns to equilibrium after approximately 125s whilst the other configurations without the

installed WEC oscillate for a significant amount of time after. On the other hand, the heave natural period is fractionally reduced for those configurations with a WEC. The heave natural period agrees well for all models. For pitch, the presence of the WEC has negligible effect on the pitch natural period but it does marginally increase damping. Instead, it can be observed that the tidal turbines increase the platform pitch natural period. There is generally a good agreement in pitch natural periods between the present models and published results. The agreement in results from the free decay analysis is another strong indicator that the present model has been adequately constructed.
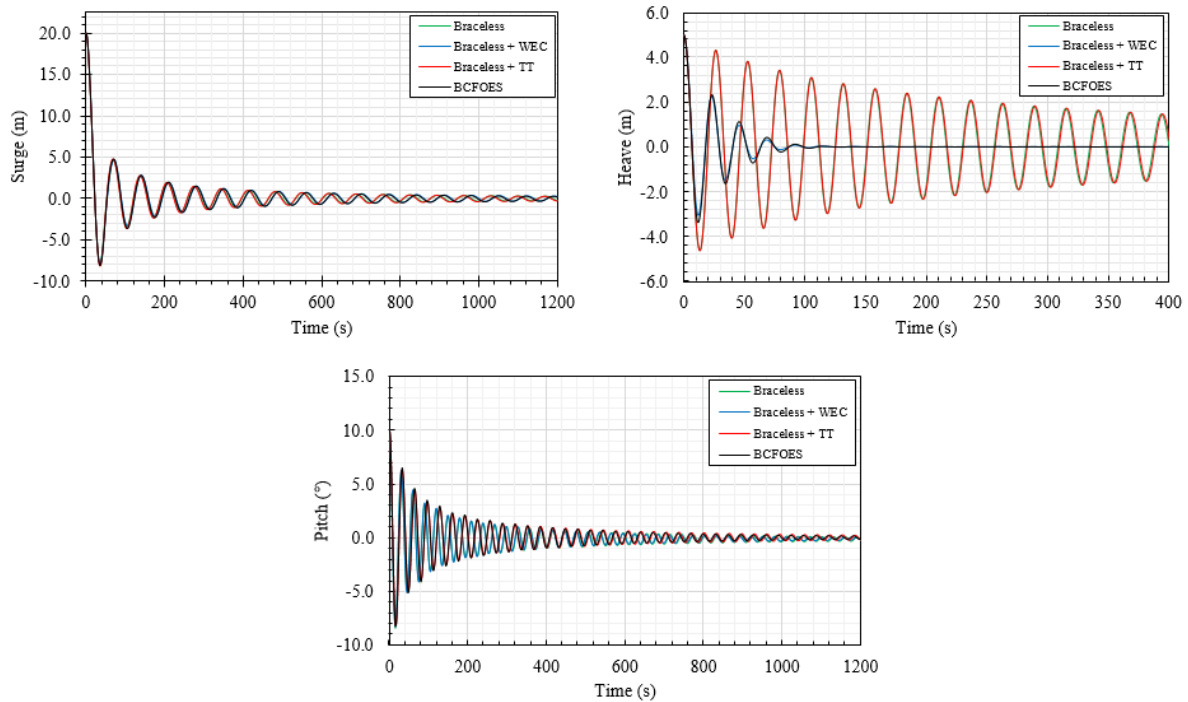
Figure 6-31. Free decay analysis of BCFOES.

Table 6-4. Natural periods of the four concepts: braceless semisubmersible, braceless + WEC, braceless + TT, and braceless + WEC + TT (triple) and comparison to available literature.

Numerical model	Surge (s)	Heave (s)	Pitch (s)
Braceless semisubmersible only	68.9	26.3	29.9

Braceless semisubmersible only (Luan et al. 2016)	79.5	25.8	31.32
Braceless + WEC	70.2	23.6	29.7
Braceless + WEC (F2A, (Li et al. 2021))	80.55	24.54	26.29
Braceless + WEC (AQWA, (Li et al. 2021))	80.55	24.54	29.91
Braceless + WEC (Wang et al. 2020)	83.78	24.74	29.77
Braceless + Tidal	68.8	26.4	32.1
BCFOES	70.2	23.8	31.8

6.2.4.2   Platform motions

The platform motion statistics of the BCFOES for all LCs are presented in **Figure 6-32** and compared to a pure braceless semisubmersible FOWT. Considering surge, the displacement of the BCFOES is greater compared to the pure FOWT equivalent. This increase is approximately 45%, 28%, and 20%, for below-rated, rated, and above-rated conditions respectively, and is as a result of the hydrodynamic thrust produced by the tidal turbines. The decreasing percentage suggests that for rougher environments i.e., greater wind speeds and larger waves, the impact of the tidal turbines on the surge displacement becomes less. An interesting find is that the variability of the BCFOES is greater than the pure FOWT system for rated and above-rated conditions. Results from the free decay analysis showed that the WEC increased damping in heave and thus reduced the heave response of the BCFOES. The statistical results display a similar trend; the range in heave of the BCFOES is smaller than the pure braceless semisubmersible for below-rated and above-rated conditions, 1.01 and 6.77m compared to 1.46 and 7.6m, respectively. For above-rated condition, the range in heave is reduced by 10%. For rated condition, the heave range is the same for both concepts, 2.8m. The wave period in this LC coincides with the WEC heave natural period which amplifies the response of both WEC and semisubmersible. However, even with this amplification the heave response is the same as the pure braceless semisubmersible FOWT. Considering pitch, the mean pitch of the BCFOES is smaller than the pure braceless equivalent for all LCs. The

hydrodynamic thrust being produced by the tidal turbines is of similar magnitude to the aerodynamic thrust produced by the wind turbine. Consequently, when the wind drops the opposing moment from the hydrodynamic thrust becomes the dominant moment which causes the platform to pitch forward into negative pitch. The tidal turbines increase the pitching range of the BCFOES in LCs 1, 2, and 3 by 27, 52, and 25%, respectively. On the other hand, the tidal turbines make the BCFOES more upright which increases the rotor area exposed to wind. Therefore, the wind turbine on the BCFOES will produce more power.
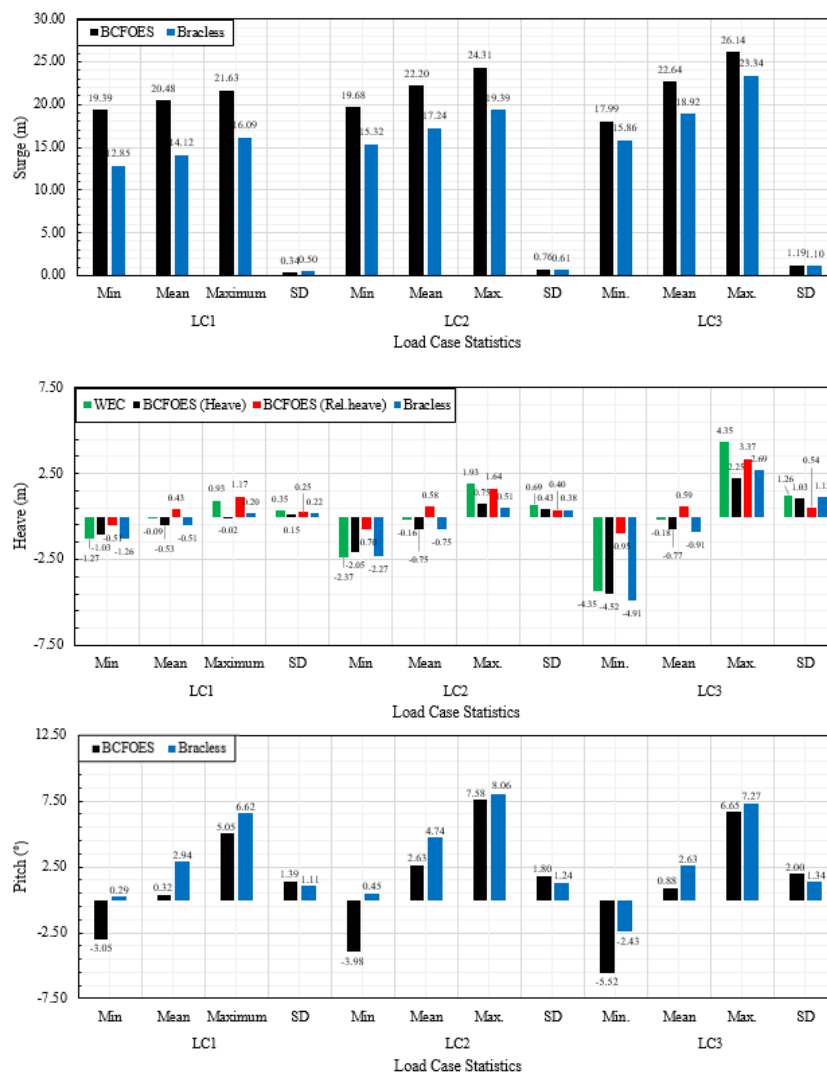
Figure 6-32. Comparison of platform motion statistics between BCFOES and pure braceless semisubmersible FOWT for LC1-3.

6.2.4.3   Mooring line tensions

The mooring line tensions of the BCFOES and braceless semisubmersible in the time-domain for all LCs are presented in **Figure 6-33**. It is clear that the hydrodynamic thrust of the tidal turbines increases the surge displacement. Consequently, the mooring line tension in the upwind line(s) will experience greater tension and the mooring line resists the platform motion. For LC1, ML2 of the braceless concept has an average tension just below 3MN. The BCFOES has an average tension of approximately 3.75MN. For LC2, ML2 of the braceless concept has an average tension of approximately 3.3N compared to an average tension of just below 4.5MN for the BCFOES concept. For LC3, ML2 of the braceless concept has an average tension of 3.75MN whereas the average tension in ML2 of the BCFOES concept is approximately 4.5MN. This represents an increase of 25, 36, and 20% in mooring line tension for LC1, LC2, and LC3, respectively, as a result of the integration of tidal turbines. Additionally, the variation in mooring line tension of ML2 the BCFOES is greater than the braceless concept. As an example, for LC3 it can be observed that the maximum mooring line tension experienced by ML2 restraining the BCFOES system is approximately 7.2MN. There is a point at the start of the simulation where the tension exceeds 7.5MN but this can be disregarded to account for transient effects. The maximum mooring line tension experienced by the same mooring line restraining the braceless concept is approximately 5MN.
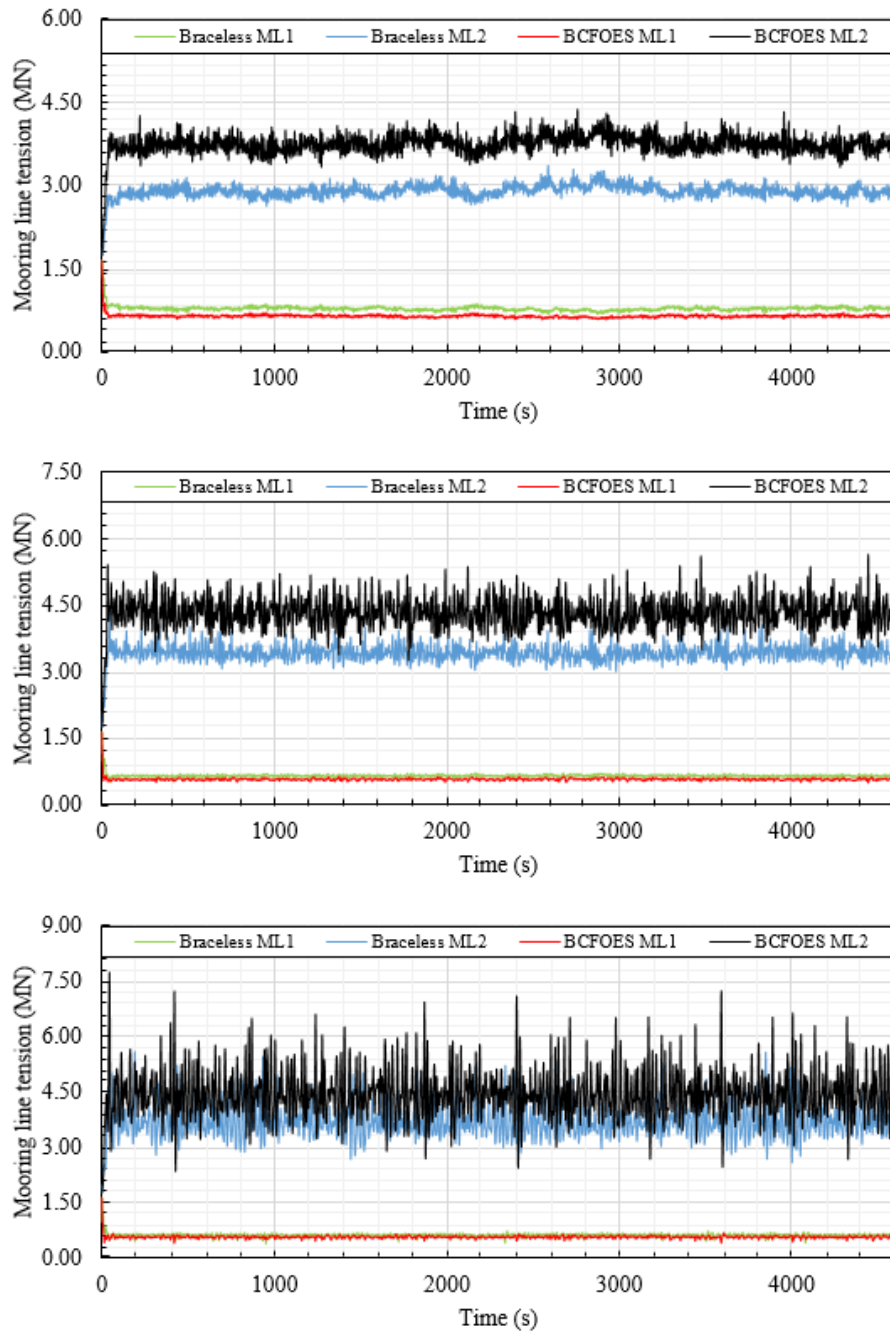
Figure 6-33. Mooring line tensions of BCFOES and pure braceless semisubmersible FOWT

for all LCs: LC1 (Top), LC2 (Middle), LC3 (Bottom).

6.2.4.4   Rotor responses

The statistics of rotor speed, rotor thrust, and rotor torque of the BCFOES are given in

Table 6-5 and the time-domain results are presented in **Figure 6-34**. The influence of the WEC

and tidal turbines on the performance of the wind turbine is minimal.

Table 6-5. Rotor response statistics of BCFOES for all LCs and comparison to braceless

semisubmersible FOWT.

		Rotor speed		Rotor thrust		Rotor torque	
		Braceless	BCFOES	Braceless	BCFOES	Braceless	BCFOES
LC1	Mean	9.21	9.28	0.53	0.49	1.92	1.97
	Maximum	12.06	12.11	0.99	0.98	4.26	4.29
	SD	1.34	1.35	0.13	0.14	0.60	0.61
LC2	Mean	11.85	11.89	0.80	0.75	3.71	3.75
	Maximum	14.60	14.67	1.06	1.08	6.40	6.40
	SD	0.72	0.77	0.11	0.13	0.55	0.53
LC3	Mean	12.10	12.10	0.55	0.51	4.18	4.18
	Maximum	15.48	15.91	1.03	1.11	6.33	6.34
	SD	1.06	1.09	0.12	0.13	0.15	0.15
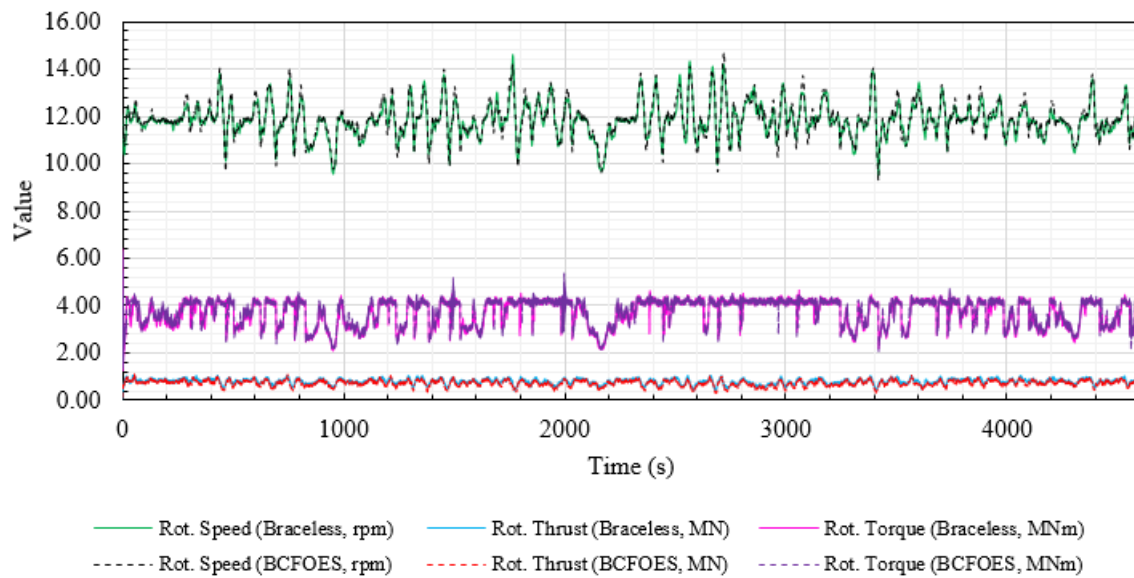
Figure 6-34. Time-domain rotor responses of BCFOES for all LCs and comparison to

braceless semisubmersible FOWT.

6.2.4.5 Power production

For all LCs, the power generated by the several energy systems within the BCFOES is

presented in **Figure 6-35**. The results are compared to the power production of a pure braceless

semisubmersible wind turbine. The collective tidal turbine system generates an additional total

mean power of 1.15, 1.38, and 1.44MW for LC1, LC2, and LC3, respectively. The WEC generates an additional total mean power of 0.04, 0.07, and 0.09MW for LC1, LC2, and LC3, respectively. The wind turbine in the BCFOES has improved power production performance compared to the wind turbine supported by the pure braceless semisubmersible. For LC1 and LC2, the wind turbine produces an additional 0.06MW. Therefore, the BCFOES produces 1.25, 1.51, and 1.53MW of additional power for LC1, LC2, and LC3, respectively. In percentages, this is an increase of 69, 35, and 31%. The advantage of combining different ORE systems in a single platform is obvious when considering the power production capabilities.
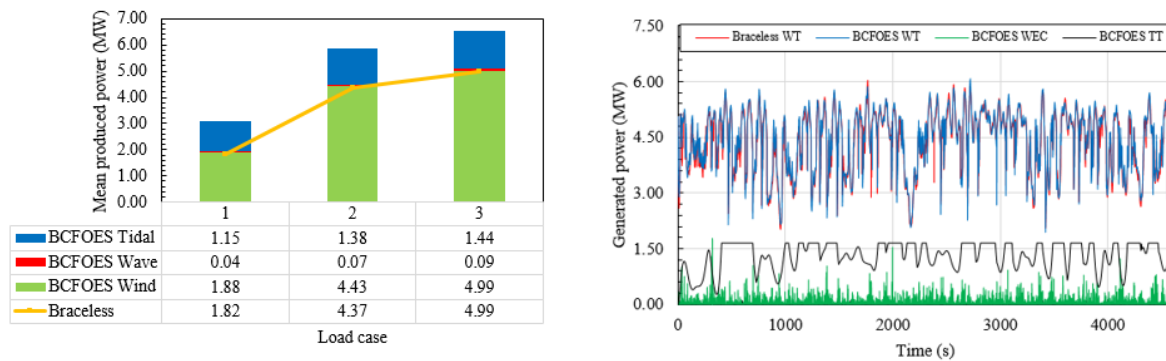
Figure 6-35. Power contributions of the BCFOES for all LCs and comparison against braceless semisubmersible FOWT.

6.3 Chapter summary and conclusions

This chapter presents the work from the final phase of this research project which is the development of a numerical model of a CFOES. The novel concept integrates three different types of ORE technologies: a catamaran-type FOWT, a WEC system, and tidal turbine system. The numerical model is used to evaluate the performance of the CFOES in operational and extreme conditions. The responses of the CFOES are compared to the responses of a pure catamaran FOWT. From the comparison, the advantages and disadvantages of ORE hybridization are determined. Additionally, a second numerical model of a CFOES is presented

in this chapter. The second CFOES concept is referred to as the BCFOES concept. The BCFOES comprises a braceless semisubmersible-type FOWT, heave-type point absorber, and three tidal turbines. The development of a second numerical model of a CFOES demonstrates the methodology can be applied to other CFOES configurations for integrated loads analysis. The conclusions of this chapter have been separated into two parts. The parts are based on the results of the respective numerical model. Conclusions are drawn from comparisons of the CFOES compared to the equivalent pure FOWT system. The conclusions are as follows:

(1) CFOES:

   (a) Wind turbine:

   - The performance of the wind turbine in below rated conditions is not affected by the addition of marine energy systems to the floating platform. In rated and above rated conditions, the performance of the wind turbine improves. The power output is greater and smoother and there is less variability in aerodynamic thrust, rotor torque and blade pitch.

   - The WEC system significantly reduces platform rolling and pitching more energetic sea states. Consequently, the tower-base bending moments are reduced. Under LC2, a reduction of 35% and 40% in the maximum and minimum S-S tower-base bending moment is observed. Under LC3, the S-S tower-base bending moment exhibits similar behaviour to LC2 and the F-A tower-base bending moment is steadier.

   - After a shutdown routine the rotor responses of the wind turbine are not impacted by the marine renewable energy systems. During the period after the shutdown routine, the O-o-P blade-root and S-S tower-base bending moment display a reduced response albeit a small reduction.

- In extreme conditions, the marine renewable energy systems do not positively or negatively impact the blade-root or tower-base bending moments.

(b) Platform motions:

- When the tidal turbines are in operation a hydrodynamic thrust is produced. Three main effects on global platform motions arise due to this hydrodynamic thrust: (1) the surge response is increased, (2) the variability about the mean surge is reduced because of hydrodynamic damping, and (3) the total hydrodynamic thrust produced by the two tidal turbines is approximately 400kN. For below rated conditions, this is comparable to the aerodynamic thrust which means the pitch displacement is reduced for the CFOES.

- The integration of the WEC system greatly increases the stability in roll and pitch for the CFOES. Under LC2, the WEC system reduces the rolling range from 15° to approximately 5°, a reduction of 66%.

- The tidal turbine system dampens platform yawing during operation.

- Without the tidal turbines operating, the surge and yaw response is similar to a pure catamaran FOWT.

- In extreme conditions, overall, the platform motions are similar to the global motion responses of the pure catamaran FOWT. The CFOES displays a reduced pitch response.

(c) Mooring line tensions:

- The tension in the upwind mooring lines increase due to greater surge displacement.

- The tidal turbines exert hydrodynamic damping which reduces the variability in the mooring line tensions for rated wind condition. In above rated wind condition, the variability appears to increase. This suggests the wave excitation force begins to dominate the mooring line responses.

- Without the tidal turbines operating, the mooring line tensions are similar.

- In extreme conditions, there is negligible differences in the mooring line tensions for all mooring lines.

(d) Generated power of marine energy systems:

- For LC1 the WEC system generates 57kW of additional power. The WEC units producing this power are the units that interact with the incident waves first. The generated power from the individual Wavestar units in the global system strongly depend on the position in relation to the incident wave direction. The tidal turbines produce 300kW of additional power. For LC1 the total generated power is increased by 30%.

- For LC2, the combined total average power produced by the marine energy systems is approximately 600kW, representing an increase of 12% additional generated power.

- For LC3, the WEC system produces a mean power output of 660kW. The Wavestar unit which produces the most power is WEC10 generating approximately 90kW of power. The tidal turbine system produces a mean power of approximately 300kW and the instantaneous maximum power is 500kW. This means that marine renewable energy systems within the CFOES can produce 1MW of additional mean power which represents a 20% increase compared to the pure catamaran FOWT system.

(2) BCFOES:

- The free-decay analysis shows surge and pitch are not affected by the integration of the marine renewable energy systems. The WEC positively impacts the heave response by damping the response significantly.

- For the simulated LCs, the surge displacement of the BCFOES is greater compared to the pure FOWT equivalent. This increase is approximately 45 %, 28 %, and 20 %, for below-rated, rated, and above-rated conditions respectively, and is as a result of the hydrodynamic thrust produced by the tidal turbines. For above-rated condition, the range in heave is reduced by 10 %. The tidal turbines increase the pitching range of the BCFOES in LCs 1, 2, and 3 by 27, 52, and 25 %, respectively. On the other hand, the tidal turbines make the BCFOES more upright which increases the rotor area exposed to wind. Therefore, the wind turbine on the BCFOES will produce more power.

- An increase of 25%, 36%, and 20% in mooring line tension is observed for the BCFOES for LC1, LC2, and LC3, respectively, as a result of the integration of tidal turbines.

- The influence of the WEC and tidal turbines on the performance of the wind turbine is minimal.

- The collective tidal turbine system generates an additional total mean power of 1.15, 1.38, and 1.44MW for LC1, LC2, and LC3, respectively. The WEC generates an additional total mean power of 0.04, 0.07, and 0.09MW for LC1, LC2, and LC3, respectively. Therefore, the BCFOES produces 1.25, 1.51, and 1.53MW of additional power for LC1, LC2, and LC3, respectively. In percentages, this is an increase of 69, 35, and 31%. The advantage of combining different ORE systems in a single platform is obvious when considering the power production capabilities.

Chapter 7.   Conclusions

This chapter presents an overall summary of the study and the main conclusions from the research on evaluating the performance of a CFOES in operational and extreme conditions. The chapter also discusses the limitations of the research and recommendation for future work.

This chapter is organised into the following sections: Section 7.1 presents the overall summary of the whole study. Section 7.2 presents the main conclusions of the research and Section 7.3 presents recommendations for future study.

7.1   Overall summary

The main aim of this thesis was to innovate and develop an CFOES concept that supported three different ORE technologies and to construct a numerical model in order to perform integrated loads analysis to assess concept performance under typical design load cases. The research presented in this thesis contributes to broadening knowledge depth on the coupled dynamic behaviour of ORE systems when integrated within a single floating platform.

The first chapter of this thesis gave an overview to the research, explained the motivation for the research and the engineering problem it tackles. The introduction provided initial background on the scientific topics ORE and CFOESs. The chapter stated the aims and objectives of the thesis. The first objective was to critically review the current state of knowledge on ORE and CFOESs. This objective was met through the material presented in Chapter 2.

The second thesis objective was to review design methods and numerical tools available for the design and analysis of a CFOES system. No tools exist explicitly for the design and analysis of CFOESs. Therefore, tools which were available for the advanced design and

analysis of pure ORE systems such as wind turbines or WECs were considered. Using these tools, a method was devised to couple the tools to accurately predict the coupled responses of the CFOES concept subject to design load cases. Chapter 3 was dedicated to this objective; the consideration was presented in the form of theoretical background of mathematical models underpinning the engineering tools.

The third objective of the thesis was to implement the methodology and construct a sophisticated numerical model of the CFOES in an engineering tool. The fourth objective was to subsequently validate the numerical model. The numerical model of the CFOES has been presented in Chapter 6. The model can be decomposed into three individual numerical models of the pure ORE systems (FOWT, WEC and tidal turbine). The separate development and validation of these numerical models have been presented in Chapter 4 and Chapter 5. Chapter 4 introduced the catamaran-type FOWT which is the central system in the CFOES concept. The numerical model of the FOWT was built within F2A. The validation of the numerical model was successful with results showing good agreement with published work. The numerical model was used to simulate a set of design load cases and the outputs from the model were presented and analysed in the chapter. Chapter 5 was dedicated to the development of the numerical models of the marine renewable energy systems. In the chapter, the results of the validations for both numerical models have been presented. The numerical models were separately integrated into the FOWT numerical model and used to investigate the coupled responses of the FOWT combined with a WEC system and a tidal turbine system. Finally, all three numerical models were coupled together to create the numerical model of the CFOES which has been presented in Chapter 6. The fact that CFOES are conceptual and extremely novel meant no numerical or experimental data exists. As such, validation of the numerical model of the CFOES was achieved through partial validation.

The fifth objective was to use the numerical model to perform coupled analysis on the CFOES concept so that the performance of the concept in the context of normal operation and extreme situation can be examined. The sixth objective was to critically analyse the dynamic responses of the CFOES to determine if the hybridization of ORE technologies in a single floating platform is beneficial and if the CFOES concept has merit. The results of the study on these objectives have been presented in Chapter 6. In addition, another CFOES was introduced in Chapter 6. The development of the BCFOES numerical model confirmed that the devised methodology can be implemented for other CFOES configurations.

The conclusions from the research in this thesis have been presented in this chapter. The conclusions are provided in both a general summary and the main findings that were made during the course of the research.

7.2   Main conclusions

The following are the main conclusions drawn from this thesis based on the calculated results and the observations made from the results.

7.2.1   Literature survey

A survey of literature was conducted on ORE and CFOESs and there was emphasis on combined concepts composed of a FOWT with either a WEC system, a tidal turbine system, or both. For each ORE industry, the literature survey reviewed information on the ORE resource, the types of machines used to convert the energy form into electricity, and the latest market and technology trends within the industry. The survey of literature progressed by establishing motives for ORE hybridization, defining a CFOES, and discussing main synergies of hybridization. An in-depth review of pre-commercial concepts and demonstrators, funded research programmes, and academic research on CFOESs was presented. Additionally, the

survey of literature covered theory, modelling and simulation of CFOESs. The survey of literature concluded the following main points:

- Floating wind turbines have 4 main types: barge, semisubmersible, spar and TLP. Barge-type floaters have advantages in construction and deployment, which could ease utility-scale production providing excessive pitching motion can be mitigated.

- WECs have a large spread of concepts but there is some industry consolidation towards the point absorber concept. This technology can absorb wave energy from all directions, and they have much smaller structural size compared to other concepts.

- Tidal turbine systems follow suit to the wind turbine industry with axial flow turbines as the most advanced technology.

- CFOES concepts that comprise FOWT combined with wave energy technology are more prevalent than CFOES concepts made up of FOWT combined with tidal energy technology. There are even some prototypes in development such as Floating Power Plant.

- Only one numerical model of, no experimental data for, and only one conceptualised commercial concept of a CFOES which integrates three or more ORE systems exist. There is an opportunity for research to significantly contribute to knowledge in the scientific area.

- At present, no numerical tools exist explicitly for modelling CFOES. This resulted in the integration of numerical tools that could model the independent ORE systems. The floating wind turbine is considered the central system (in terms of rated power capacity and structural size), so this was the basis for the numerical tool coupling i.e., numerical models of the marine renewable energy systems would be integrated into a numerical model of the FOWT.

- Software used to design and analyse FOWTs can be categorised based on the level of fidelity required by the numerical model. Engineering tools are considered mid-fidelity and are commonly used for loads analysis to examine concept designs for operational and extreme conditions. Thus, F2A was used to construct a numerical model of a CFOES.

- Engineering tools are comprised of computational modules that can numerically represent the offshore environment and structure. Offshore structures are exposed to a wide variety of external conditions. The main external conditions relevant to offshores structures are wind, ocean waves, and currents. Different mathematical models can be selected to represent the offshore environment to suit the needs of the analysis e.g., regular wave or wave spectrums which represent fully developed or developing seas.

- For each physical domain, similarly a range of models can be implemented to represent the applied load or system responses of a FOWT. The aerodynamics is commonly computed within engineering tools using BEMT theory. Corrections can be added to this model to capture other aerodynamic effects such as tip- and hub-losses, skewed wakes, and dynamic stall. Morison's equation or potential flow theory can be used to calculate the wave loading within engineering tools. The choice of model is dependent on size of the structure relative to incident wavelength. For commercial aero-elastic codes, FEM models and modal analysis methods are employed to model the structural dynamics of a FOWT. There are also multiple modelling options for the controller and mooring system. To simulate the coupled dynamics motion, Kane's method is employed in FAST to formulate an equation of motion for the entire system.

- WECs can be modelled in ANSYS AQWA owing to the software's excellent capabilities of calculating hydrodynamic loads and modelling complex multibody systems. Additionally, AQWA has 'joint' features which can be used to model the PTO system of some WECs. F2A uses AQWA as its core hydrodynamic module which meant coupling of FOWT numerical model and WEC numerical could be achieved. To model the tidal turbines, a module for calculating aerodynamic loads in FAST is repurposed to calculate the hydrodynamic loads of tidal turbines and integrated within the F2A via the external.dll.

7.2.2   *Development of catamaran FOWT numerical model*

A numerical study on using a catamaran vessel as a support platform for a FOWT was performed using OpenFAST and ANSYS AQWA numerical tools coupled via a DLL, namely F2A, to conduct efficient fully coupled aero-hydro-elastic-servo simulations. The results of the research revealed advantages of a catamaran-type platform compared to a conventional barge-type platform:

- The catamaran has a large deck area; this can be used for other functions such as marine power generation, solar panels, or hydrogen conversion. If utilised properly the additional functionality could lead to cost reductions e.g., through increased power generation.

- Evaluation of hydrodynamic characteristics has shown that the catamaran has better hydrodynamic performance over the barge. The catamaran platform has higher sway, roll, pitch, and yaw hydrodynamic coefficients compared to the barge. This means the catamaran floater has increased hydrodynamic restoring stiffness and damping for these modes of motion.

- The catamaran platform responds distinctively at certain frequencies for vertical and horizontal plane motions due to symmetric or antisymmetric interaction, respectively. These frequencies are analogous to the resonant modes of a standing wave between two vertical walls. Moreover, the frequencies are characteristic to the individual platform and depend on demi-hull separation.

- Findings from the free decay results show that the catamaran floater has increased natural damping in the system for roll and pitch modes compared to the barge floater. This was especially the case for pitch, where observed damping was increased considerably. This was confirmed in the RAO analysis; the amplitude observed at the pitch natural frequency of the catamaran floater was reduced by 50% compared to amplitude observed at the pitch natural frequency of the barge.

- The time-domain simulations showed the response of both platforms were similar for simulated load cases, which meant the expected improvement in pitch stability was not necessarily reflected. The reason for this was that the simulated wave periods coincided with the natural pitch period of the catamaran which amplified the platform's dynamic response. Nevertheless, the pitch response of the catamaran was similar to that of the barge. The fact that the catamaran behaves similarly to the barge whilst being excited at its natural frequency highlights the platform's good hydrodynamic performance. One future avenue for research could be how the geometric characteristics of the catamaran floater affect its pitch natural period.

- The results of this study also showed that the catamaran floater had reduced tower-base bending moments (both F-A and S-S) for all simulated conditions. For rated wind speed (LC3) and corresponding wave condition, the F-A tower-base bending moment was reduced by 22%.

7.2.3 *Marine renewable energy system numerical model development and integration*

A numerical study on combining a catamaran-type FOWT system with two different type of marine renewable energy systems separately was carried out. The two marine renewable energy systems were a tidal turbine system and a WEC system. Two numerical models were developed of the two types of marine renewable energy systems. The numerical model of the tidal turbines was constructed in AeroDyn and the numerical model of the WEC was constructed in AQWA. The two numerical models were separately integrated into a numerical model of a catamaran-type FOWT system. Using the two integrated numerical models, the dynamic behaviour of the catamaran FOWT was studied with the addition of the marine renewable energy systems. The results were compared to the responses of a pure catamaran-type FOWT. The main conclusions of the study are summarised in the following points:

For the CTT concept:

- The tidal turbines produce more power when positioned higher up in the water column. The tested hub heights had negligible effect on global platform motions.

- Platform motion natural frequencies are not affected when the tidal turbines are in stand-still.

- The turbines do not negatively affect the performance of the wind turbine when operating. In fact, the tower-top displacement and tower-base force in the x-direction are slightly reduced. The hydrodynamic thrust reduces the moment produced by the aerodynamic thrust.

- Hydrodynamic thrust is exerted on the platform due to tidal turbine operation. This increases the mean global surge of the CTT concept. However, the variation about the mean surge is reduced. The tidal turbines produce additional hydrodynamic damping.

- The maximum mooring line tension in the upwind mooring line of the CTT concept increases by approximately 28% compared to the pure catamaran concept.

- The mean power generated by the tidal turbines is 0.21, 0.28, and 0.29MW, respectively, for the examined LCs. This equates to a percentage increase in electrical power of 10.1, 6.0, and 5.6%, respectively for each LC, compared to the pure catamaran FOWT.

For the CWS concept:

- Hydrodynamic interaction between the catamaran support platform and Wavestar units is strong. The hydrodynamic behaviour of the Wavestar units is governed by the characteristic hydrodynamic behaviour of the catamaran support platform. The integration of the WEC system increases the sway and roll radiation damping coefficients of the catamaran at its characteristic frequencies.

- The effect of combining the WEC system with the catamaran FOWT on the platform natural periods and system damping is positive, particularly for heave, roll, and pitch modes where additional hydrodynamic damping is observed.

- There is a synergy between the WEC system and catamaran support platform in terms of power production due to the relative motion between the two systems. The platform pitching of the catamaran support platform amplifies the amount of the power the WEC system can produce.

- The CWS concept displays reduced amplitudes for the observed responses subject to regular and irregular wave except for surge displacement. The integration of the WEC system is beneficial due to the additional hydrodynamic damping provided by the system.

7.2.4 Development of CFOES numerical model

A numerical study was conducted to evaluate the performance of a CFOES. Three different types of ORE technologies are integrated within the novel concept: a catamaran-type FOWT system, a WEC system, and tidal turbine system. A numerical model was constructed using previously developed numerical models of the respective ORE system. The integrated numerical model was used to assess the CFOES in operational and extreme conditions. The responses of the CFOES are compared to the responses of a pure catamaran FOWT. The comparison determined the advantages and disadvantages of ORE hybridization. Additionally, a second numerical model of a CFOES was presented. The second CFOES concept was the BCFOES concept. The BCFOES comprises a braceless semisubmersible-type FOWT, heave-type point absorber, and three tidal turbines. The development of the BCFOES demonstrated the methodology can be applied to other CFOES configurations for integrated loads analysis. The conclusions are as follows:

For the CFOES concept:

a) Wind turbine:

- The performance of the wind turbine in below rated conditions is not affected by the addition of marine energy systems to the floating platform. In rated and above rated conditions, the performance of the wind turbine improves. The power output is greater and smoother and there is less variability in aerodynamic thrust, rotor torque and blade pitch.

- The WEC system significantly reduces platform rolling and pitching in more energetic sea states. Consequently, the tower-base bending moments are reduced. Under LC2, a reduction of 35% and 40% in the maximum and minimum S-S tower-

base bending moment is observed. Under LC3, the S-S tower-base bending moment exhibits similar behaviour to LC2 and the F-A tower-base bending moment is steadier.

- After a shutdown routine the rotor responses of the wind turbine are not impacted by the marine renewable energy systems. During the period after the shutdown routine, the O-o-P blade-root and S-S tower-base bending moment display a reduced response albeit a small reduction.

- In extreme conditions, the marine renewable energy systems do not positively or negatively impact the blade-root or tower-base bending moments.

b) Platform motions:

- When the tidal turbines are in operation a hydrodynamic thrust is produced. Three main effects on global platform motions arise due to this hydrodynamic thrust: (1) the surge response is increased, (2) the variability about the mean surge is reduced because of hydrodynamic damping, and (3) the total hydrodynamic thrust produced by the two tidal turbines is approximately 400kN. For below rated conditions, this is comparable to the aerodynamic thrust which means the pitch displacement is reduced for the CFOES.

- The integration of the WEC system greatly increases the stability in roll and pitch for the CFOES. Under LC2, the WEC system reduces the rolling range from 15° to approximately 5°, a reduction of 66%.

- The tidal turbine system dampens platform yawing during operation.

- Without the tidal turbines operating, the surge and yaw response is similar to a pure catamaran FOWT.

- In extreme conditions, overall, the platform motions are similar to the global motion responses of the pure catamaran FOWT. The CFOES displays a reduced pitch response.

c) Mooring line tensions:

- The tension in the upwind mooring lines increase due to greater surge displacement.

- The tidal turbines exert hydrodynamic damping which reduces the variability in the mooring line tensions for rated wind condition. In above rated wind condition, the variability appears to increase. This suggests the wave excitation force begins to dominate the mooring line responses.

- Without the tidal turbines operating, the mooring line tensions are similar.

- In extreme conditions, there is negligible differences in the mooring line tensions for all mooring lines.

d) Generated power of marine energy systems:

- For LC1 the WEC system generates 57kW of additional power. The WEC units producing this power are the units that interact with the incident waves first. The generated power from the individual Wavestar units in the global system strongly depend on the position in relation to the incident wave direction. The tidal turbines produce 300kW of additional power. For LC1 and the total generated power is increased by 30%.

- For LC2, the combined total average power produced by the marine energy systems is approximately 600kW, representing an increase of 12% additional generated power.

- For LC3, the WEC system produces a mean power output of 660kW. The Wavestar unit which produces the most power is WEC10 generating approximately 90kW of power. The tidal turbine system produces a mean power of approximately 300kW and the instantaneous maximum power is 500kW. This means that marine renewable energy systems within the CFOES can produce 1MW of additional mean power which represents a 20% increase compared to the pure catamaran FOWT system.

For the BCFOES concept:

- The free-decay analysis shows surge and pitch are not affected by the integration of the marine renewable energy systems. The WEC positively impacts the heave response by damping the response significantly.

- For the simulated LCs, the surge displacement of the BCFOES is greater compared to the pure FOWT equivalent. This increase is approximately 45%, 28%, and 20%, for below-rated, rated, and above-rated conditions respectively, and is as a result of the hydrodynamic thrust produced by the tidal turbines. For above-rated condition, the range in heave is reduced by 10%. The tidal turbines increase the pitching range of the BCFOES in LCs 1, 2, and 3 by 27, 52, and 25%, respectively. On the other hand, the tidal turbines make the BCFOES more upright which increases the rotor area exposed to wind. Therefore, the wind turbine on the BCFOES will produce more power.

- An increase of 25%, 36%, and 20% in mooring line tension is observed for the BCFOES for LC1, LC2, and LC3, respectively, as a result of the integration of tidal turbines.

- The influence of the WEC and tidal turbines on the performance of the wind turbine is minimal for examined load cases.

- The collective tidal turbine system generates an additional total mean power of 1.15, 1.38, and 1.44MW for LC1, LC2, and LC3, respectively. The WEC generates an additional total mean power of 0.04, 0.07, and 0.09MW for LC1, LC2, and LC3, respectively. Therefore, the BCFOES produces 1.25, 1.51, and 1.53MW of additional power for LC1, LC2, and LC3, respectively. In percentages, this is an increase of 69, 35, and 31%. The advantage of combining different ORE systems in a single platform is obvious when considering the power production capabilities.

7.3   Limitations of present study and recommendations for future research

CFOESs comprised of energy conversion systems which produce power from three different ORE sources remain conceptual. This study has revealed benefits of a triple CFOES including increased energy yield and reduced global platform motions. The study also demonstrated the advantages of using a catamaran-shaped support platform for offshore wind turbine application. However, there were limitations in the present study and aspects which require more understanding in order to develop the concept further. In light of this, each item below describes a limitation of the study or an area needing further understanding, and then a recommendation is provided for future work.

1. The dimensions of the catamaran-type platform were selected based on the geometry, mass, and inertia properties of a conventional barge FOWT. The reason for this was any improvement or deterioration in performance is attributable to the platform design. A limitation of the design was that it was not optimized. With optimization of platform design and further advanced conceptual development, it is expected that the performance can be

enhanced. Therefore, an investigation into the platform's hydrodynamic performance whilst varying parameters such as length, width and demi-hull separation is recommended.

2. The present study has developed a concept for a CFOES. The technology readiness level of the concept is between TRL 1-3 (fundamental research). As a result of the concept having a low TRL level, the levelised cost of energy of the concept has not been quantified in this study. A recommendation for future work is to investigate the economics of the concept.

3. Model testing is an essential compliment to numerical modelling. Model testing permits full validation of a certain aspects of a numerical model such as the hydrodynamic model. At the time of the study, no experimental data existed for the studied concept nor could a experimental campaign be conducted. As such, the developed model in this study is limited by unidentified hydrodynamic characteristics only obtainable through model testing such as damping coefficients. If a model testing campaign could be conducted, then this would allow for appropriate validation of the numerical model developed in this work.

4. To predict the rotor forces and electrical power of the tidal turbines, AeroDyn has been integrated into F2A numerical tool. At each time step, the platform response calculated by the AQWA solver in conjunction with the instantaneous relative current speed are used as input into AeroDyn. The AeroDyn code calculates the tidal turbine rotor force and power which are then fed back into F2A and included in the external force term. However, the AeroDyn model does not account for hydro-elasticity of the tidal turbine towers. In order to better understand the complete dynamics of the coupled system, a recommendation for future work is that the structural dynamics of the tidal turbine towers are included in the numerical model.

5. The numerical model developed in this study permits accurate calculation of the global platform motions and wave-induced load characteristics of the catamaran FOWT. However, no internal platform loads were calculated and thus the loads effects on the

structural integrity of the catamaran hull and superstructure were neglected. A recommendation for future work would be to conduct a structural analysis of the concept to assess the structural integrity of the support platform to the applied loads.

6. The arrangement of the WEC system was based on the assumption that more power can be generated with more units in the system (Ghafari et al. 2021). However, due to shielding effects, it was observed that the units at the end of the system may not generate optimum power. This was a limitation of the WEC arrangement. Therefore, a recommendation for future work would be to investigate the effect on power generation of the layout of the WEC system.

7. The PTO system of the WEC system is modelled as a linear PTO. For the CFOES. the linear PTO system was modelled using hinge features within AQWA. For the BCFOES, the linear PTO system was modelled using fender features. No implementation of wave energy control was included. Implementation of a control scheme for wave energy conversion could be considered for wave power optimisation.

References

Aboutalebi P, M'zoughi F, Garrido I, Garrido AJ (2021) Performance analysis on the use of oscillating water column in barge-based floating offshore wind turbines. Mathematics 9:1–22. https://doi.org/10.3390/math9050475

Aderinto T, Li H (2018) Ocean Wave energy converters: Status and challenges. Energies 11

Allseas (2021) Pioneering Spirit. https://allseas.com/equipment/pioneering-spirit/. Accessed 14 Sep 2021

ANSYS (2020) Aqwa Theory Manual

ANSYS (2012) AQWA Reference Manual Release 14.5. Canonsburg, USA

Arinaga RA, Cheung KF (2012) Atlas of global wave energy from 10 years of reanalysis and hindcast data. Renew Energy 39:49–64. https://doi.org/10.1016/j.renene.2011.06.039

Ashglaf M (2019) Development of Hybridization concept for horizontal axis wind / tidal systems using functional similarities and advanced real-time emulation methods. Normandie Universite

AW-Energy (2022) WaveRoller. https://aw-energy.com/waveroller/. Accessed 10 Oct 2022

Azcona J, Vittori F (2019) Mooring System Design for the 10MW Triple Spar Floating Wind Turbine at a 180 m Sea Depth Location. In: Journal of Physics: Conference Series. pp 0–10

Babarit A, Hals J, Kurniawan A, et al (2011) The NumWEC Project: Numerical Esitmation of Energy Delivery from a Selection of Wave Energy Converters. 1–317. https://doi.org/10.13140/RG.2.1.3807.8885

Bachynski EE, Moan T (2013) Point absorber design for a combined wind and wave energy converter on a tension-leg support structure. In: Proceedings of the ASME 2013 32nd International Conference on Ocean, Offshore and Arctic Engineering

Bae YH (2013) Coupled dynamic analysis of multiple unit floating offshore wind turbine. Texas A&M University

Bangga G (2018) Comparison of blade element method and CFD simulations of a 10 MW wind turbine. Fluids 3:. https://doi.org/10.3390/fluids3040073

Barltrop NDP (1988) Floating Structures: A Guide For Design And Analysis Vol 1. 1–630

Bashir MB (2014) Strength and Hydrodynamic Performance of a Multihull Vessel. Newcastle University

Ben Elghali SE, Benbouzid M, Charpentier J (2007) Marine Tidal Current Electric Power Generation Technology : State of the Art and Current Status. In: 2007 IEEE International Electric Machines & Drives Conference

Borg M, Bredmodes H (2015) LIFES50+ D4.4 Overview of the numerical models used in the consortium and their qualification

Borg M, Collu M, Kolios A (2014) Offshore floating vertical axis wind turbines, dynamics modelling state of the art. Part II: Mooring line and structural dynamics. Renew Sustain Energy Rev 39:1226–1234. https://doi.org/10.1016/j.rser.2014.07.122

Bosma B, Zhang Z, Brekken TKA, et al (2012) Wave energy converter modeling in the frequency domain: A design guide. 2012 IEEE Energy Convers Congr Expo ECCE 2012 2099–2106. https://doi.org/10.1109/ECCE.2012.6342553

Brommundt M, Krause L, Merz K, Muskulus M (2012) Mooring system optimization for

floating wind turbines using frequency domain analysis. Energy Procedia 24:289–296.

https://doi.org/10.1016/j.egypro.2012.06.111

Brown SA, Ransley EJ, Xie N, et al (2021) On the impact of motion-thrust coupling in

floating tidal energy applications. Appl Energy 282:116246.

https://doi.org/10.1016/j.apenergy.2020.116246

Burton T, Jenkins N, Sharpe D, Bossanyi E (2011) Wind Energy Handbook, 2nd Edition.

Wiley

Carbon Trust (2011) Accelerating Marine Energy

Carnegie (2022) CETO Technology. https://www.carnegiece.com/ceto-technology/.

Accessed 10 Oct 2022

Chen M, Xiao P, Zhou H, et al (2022) Fully Coupled Analysis of an Integrated Floating

Wind-Wave Power Generation Platform in Operational Sea-States. Front Energy Res

10:1–17. https://doi.org/10.3389/fenrg.2022.931057

Collu M, Borg M (2016) Design of floating offshore wind turbines. In: Offshore Wind

Farms: Technologies, Design and Operation. Elsevier Ltd, pp 359–385

CorPower Ocean (2022) Technology. https://corpowerocean.com/technology/. Accessed 10

Oct 2022

Cottura L, Caradonna R, Ghigo A, et al (2021) Dynamic modeling of an offshore floating

wind turbine for application in the mediterranean sea. Energies 14:.

https://doi.org/10.3390/en14010248

Coulling AJ, Goupee AJ, Robertson AN, et al (2013) Validation of a FAST semi-submersible floating wind turbine numerical model with DeepCwind test data. J Renew Sustain Energy 5:. https://doi.org/10.1063/1.4796197

Cutler J, Bashir M, Yang Y, et al (2022) Preliminary development of a novel catamaran floating offshore wind turbine platform and assessment of dynamic behaviours for intermediate water depth application. Ocean Eng 258:111769. https://doi.org/10.1016/j.oceaneng.2022.111769

Dabssi N, Chagdali M, Hémon A (2008) Hydrodynamic coefficients and forces on multihulls in shallow water with constant or variable depth. Transport 23:245–252. https://doi.org/10.3846/1648-4142.2008.23.245-252

Dahmani F, Sohn CH (2020) Effect of convergent duct geometry on the energy extraction performance of tandem oscillating hydrofoils system. J Fluids Struct 95:102949. https://doi.org/10.1016/j.jfluidstructs.2020.102949

Davidson J, Ringwood J V. (2017) Mathematical modelling of mooring systems for wave energy converters - A review. Energies 10:. https://doi.org/10.3390/en10050666

Ding S, Yan S, Han D, Ma Q (2015) Overview on Hybrid Wind-Wave Energy Systems. Proc 2015 Int Conf Appl Sci Eng Innov 12:502–507. https://doi.org/10.2991/asei-15.2015.101

Dong X, Li Y, Li D, et al (2022) A state-of-the-art review of the hybrid wind-wave energy converter Progress in Energy RECEIVED

Drassanes Dalmau (2021) 150 Passengers - ECO SLIM. https://www.dalmaushipyard.com/en/186380/ships/Passage/Passage-catamarans/150-

Passengers-ECO-SLIM.htm. Accessed 14 Sep 2021

Drew B, Plummer AR, Sahinkaya MN (2009) A review of wave energy converter technology. Proc Inst Mech Eng Part A J Power Energy 223:887–902. https://doi.org/10.1243/09576509JPE782

Eco Wave Power (2022) Our Technology - How it works. https://www.ecowavepower.com/our-technology/how-it-works/. Accessed 10 Oct 2022

Equinor (2020a) The future of offshore wind is afloat. https://www.equinor.com/en/what-we-do/floating-wind.html. Accessed 22 Sep 2021

Equinor (2020b) Hywind Scotland. https://www.equinor.com/en/what-we-do/floating-wind/hywind-scotland.html. Accessed 14 Jul 2021

Erselcan İÖ, Kükner A (2014) a Review of Power Take-Off Systems Employed in Wave Energy Converters. J Nav Sci Eng 10:32–44

Escaler X, Egusquiza E, Farhat M, et al (2006) Detection of cavitation in hydraulic turbines. Mech Syst Signal Process 20:983–1007. https://doi.org/10.1016/j.ymssp.2004.08.006

Esmaeilifar E, Hassan Djavareshkian M, Forouzi Feshalami B, Esmaeili A (2017) Hydrodynamic simulation of an oscillating hydrofoil near free surface in critical unsteady parameter. Ocean Eng 141:227–236. https://doi.org/10.1016/j.oceaneng.2017.06.037

European Commission (2023) Offshore renewable energy. https://energy.ec.europa.eu/topics/renewable-energy/offshore-renewable-energy_en. Accessed 26 May 2023

European Commission (2015a) Ocean Energy

European Commission (2014a) Final Report Summary - H2OCEAN (Development of a
    wind-wave power open-sea platform equipped for hydrogen generation with support for
    multiple users of energy) | FP7 | CORDIS.
    https://cordis.europa.eu/project/id/288145/reporting. Accessed 27 Sep 2022

European Commission (2014b) Final Report Summary - MARINA PLATFORM (Marine
    Renewable Integrated Application Platform) | FP7 | CORDIS.
    https://cordis.europa.eu/project/id/241402/reporting. Accessed 27 Sep 2022

European Commission (2015b) Final Report Summary - MERMAID (Innovative Multi-
    purpose off-shore platforms: planning, Design and operation) | FP7 | CORDIS.
    https://cordis.europa.eu/project/id/288710/reporting. Accessed 27 Sep 2022

European Commission (2011) Off-shore Renewable Energy Conversion platforms –
    Coordination Action | ORECCA Project | Fact Sheet | FP7 | CORDIS.
    https://cordis.europa.eu/project/id/241421. Accessed 27 Sep 2022

European Commission (2015c) Modular Multi-use Deep Water Offshore Platform
    Harnessing and Servicing Mediterranean, Subtropical and Tropical Marine and Maritime
    Resources | TROPOS Project | Fact Sheet | FP7 | CORDIS.
    https://cordis.europa.eu/project/id/288192. Accessed 27 Sep 2022

Excipio Energy (2022) Excipio Energy: About. https://excipioenergy.com/about/. Accessed
    18 Jan 2022

Falcão AFO, Henriques JCC, Gato LMC, Gomes RPF (2014) Air turbine choice and
    optimization for floating oscillating-water-column wave energy converter. Ocean Eng

75:148–156. https://doi.org/10.1016/j.oceaneng.2013.10.019

Falnes J (2007) A review of wave-energy extraction. Mar Struct 20:185–201.

   https://doi.org/10.1016/j.marstruc.2007.09.001

Fang C-C (1996) An Investigation of Motions of Catamarans in Regular Waves. University

   of Glasgow

Fang CC, Chan HS, Incecik A (1997) Investigation of motions of catamarans in regular

   waves - II. Ocean Eng 24:949–966. https://doi.org/10.1016/S0029-8018(97)00056-5

Floating Power Plant (2022) FPP Platform - Products & Services.

   https://www.floatingpowerplant.com/. Accessed 11 Dec 2021

Folley M (2017) The Wave Energy Resource (Chapter 3). In: A P, Kofoed JP (eds)

   Handbook of Ocean Wave Energy. pp 43–79

Gao Z, Moan T, Wan L, Michailides C (2016) Comparative numerical and experimental

   study of two combined wind and wave energy concepts. J Ocean Eng Sci 1:36–51.

   https://doi.org/10.1016/j.joes.2015.12.006

Ghafari HR, Neisi A, Ghassemi H, Iranmanesh M (2021) Power production of the hybrid

   Wavestar point absorber mounted around the Hywind spar platform and its dynamic

   response. J Renew Sustain Energy 13:1–15. https://doi.org/10.1063/5.0046590

Goupee AJ, Koo BJ, Kimball RW, et al (2014) Experimental comparison of three floating

   wind turbine concepts. J Offshore Mech Arct Eng 136:1–10.

   https://doi.org/10.1115/1.4025804

Gunn K, Stock-Williams C (2012) Quantifying the global wave power resource. Renew

Energy 44:296–304. https://doi.org/10.1016/j.renene.2012.01.101

Guo X, Yang J, Lu W, Li X (2018) Dynamic responses of a floating tidal turbine with 6-DOF
prescribed floater motions. Ocean Eng 165:426–437.
https://doi.org/10.1016/j.oceaneng.2018.07.017

Hall M, Buckham B, Crawford C (2014) Hydrodynamics-based floating wind turbine support
platform optimization: A basis function approach. Renew Energy 66:559–569.
https://doi.org/10.1016/j.renene.2013.12.035

Hallak TS, Gaspar JF, Kamarlouei M, et al (2018) Numerical and experimental analysis of a
hybrid wind-wave offshore floating platform's hull. Proc Int Conf Offshore Mech Arct
Eng - OMAE 11A: https://doi.org/10.1115/OMAE2018-78744

Hansen M (2008) Aerodynamics of wind turbines, Second Edi. Earthscan

Henderson R (2006) Design, simulation, and testing of a novel hydraulic power take-off
system for the Pelamis wave energy converter. Renew Energy 31:271–283.
https://doi.org/10.1016/j.renene.2005.08.021

Hill C, Neary VS, Guala M, Sotiropoulos F (2020) Performance and wake characterization of
a model hydrokinetic turbine: The reference model 1 (RM1) dual rotor tidal energy
converter. Energies 13:1–21. https://doi.org/10.3390/en13195145

Hu J, Zhou B, Vogel C, et al (2020) Optimal design and performance analysis of a hybrid
system combing a floating wind platform and wave energy converters. Appl Energy
269:114998. https://doi.org/10.1016/j.apenergy.2020.114998

Ideol (2020a) FLOATGEN. https://floatgen.eu/. Accessed 14 Jul 2021

Ideol (2020b) HIBIKI - Floating wind turbine solution | Japan offshore wind.
https://www.bw-ideol.com/en/japanese-demonstrator. Accessed 14 Jul 2021

International Electrotechnical Commission (IEC) (2009) IEC 61400-3: Wind Turbines part 3:
Design Requirements for Offshore Wind Turbines. Geneva

International Renewable Energy Agency (IRENA) (2020) Innovation outlook: Ocean energy
technologies

IRENA (2019) Future of Wind: Deployment, investment, technology, grid integration and
socio-economic aspects

Jonkman BJ (2009) TurbSim User's Guide : Version 1.50

Jonkman BJ, Buhl Jr ML (2006) TurbSim User's Guide - Technical Report NREL/TP-500-
39797

Jonkman J (2010) Definition of the Floating System for Phase IV of OC3

Jonkman J (2007) Dynamics modeling and loads analysis of an offshore floating wind
turbine, Ph.D. Thesis

Jonkman J, Matha D (2011) Dynamics of offshore floating wind turbines-analysis of three
concepts. Wind Energy 14:557–569. https://doi.org/10.1002/we.442

Jonkman J, Musial W (2010) Offshore Code Comparison Collaboration (OC3) for IEA Task
23 Offshore Wind Technology and Deployment

Jonkman JM, Buhl Jr ML (2005) FAST user's guide. Golden, USA

Junianto S, Mukhtasor, Prastianto RW, Wardhana W (2020) Motion Responses Analysis for
Tidal Current Energy Platform: Quad-Spar and Catamaran Types. China Ocean Eng

34:677–687. https://doi.org/10.1007/s13344-020-0061-1

Karimirad M (2012) Mechanical-dynamic loads. In: Comprehensive Renewable Energy. Elsevier Ltd., pp 243–268

Karimirad M (2014) Offshore Energy Structures: For Wind Power, Wave Energy and Hybrid Marine Platforms. Springer

Karimirad M, Koushan K (2017) WindWEC: Combining wind and wave energy inspired by hywind and wavestar. In: 2016 IEEE International Conference on Renewable Energy Research and Applications, ICRERA 2016. pp 96–101

Khan MJ, Bhuyan G, Iqbal MT, Quaicoe JE (2009) Hydrokinetic energy conversion systems and assessment of horizontal and vertical axis turbines for river and tidal applications: A technology status review. Appl Energy 86:1823–1835. https://doi.org/10.1016/j.apenergy.2009.02.017

Khan N, Kalair A, Abas N, Haider A (2017) Review of ocean tidal, wave and thermal energy technologies. Renew Sustain Energy Rev 72:590–604. https://doi.org/10.1016/j.rser.2017.01.079

Kinsey T, Dumas G (2010) Testing and analysis of an oscillating hydrofoils turbine concept. In: American Society of Mechanical Engineers, Fluids Engineering Division (Publication) FEDSM. pp 9–22

Konispoliatis DN, Manolas DI, Voutsinas SG, Mavrakos SA (2022) Coupled Dynamic Response of an Offshore Multi-Purpose Floating Structure Suitable for Wind and Wave Energy Exploitation. Front Energy Res 10:1–19. https://doi.org/10.3389/fenrg.2022.920151

Kramer M, Marquis L, Frigaard P (2011) Performance Evaluation of the Wavestar Protoype. Eng Environ Sci Phys

Laws ND, Epps BP (2016) Hydrokinetic energy conversion: Technology, research, and outlook. Renew Sustain Energy Rev 57:1245–1259. https://doi.org/10.1016/j.rser.2015.12.189

Le C, Zhang J, Ding H, et al (2020) Preliminary Design of a Submerged Support Structure for Floating Wind Turbines. J Ocean Univ China 19:1265–1282. https://doi.org/10.1007/s11802-020-4427-z

Lee D, Hodges DH, Patil MJ (2002) Multi-flexible-body Dynamic Analysis of Horizontal Axis Wind Turbines. Wind Energy 5:281–300. https://doi.org/10.1002/we.66

Lee H, Poguluri SK, Bae YH (2018) Performance analysis of multiplewave energy converters placed on a floating platform in the frequency domain. Energies 11:. https://doi.org/10.3390/en11020406

Lerch M, Garcia CC, Thys M, et al (2019) LIFES50+ D2.8 Qualification of innovative floating substructures for 10MW wind turbines and water depths greater than 50m

Li J, Shi W, Zhang L, et al (2021) Wind–wave coupling effect on the dynamic response of a combined wind–wave energy converter. J Mar Sci Eng 9:. https://doi.org/10.3390/jmse9101101

Li L, Gao Y, Yuan Z, et al (2018) Dynamic response and power production of a floating integrated wind, wave and tidal energy system. Renew Energy 116:412–422. https://doi.org/10.1016/j.renene.2017.09.080

Lin YH, Yang CH (2020) Hydrodynamic simulation of the semi-submersible wind float by

investigating mooring systems in irregular waves. Appl Sci 10:.
https://doi.org/10.3390/app10124267

Liu Q song, Miao W pao, Yue M nan, et al (2021) Dynamic Response of Offshore Wind
Turbine on 3×3 Barge Array Floating Platform under Extreme Sea Conditions. China
Ocean Eng 35:186–200. https://doi.org/10.1007/s13344-021-0017-0

Liu Y, Li S, Yi Q, Chen D (2016) Developments in semi-submersible floating foundations
supporting wind turbines: A comprehensive review. Renew Sustain Energy Rev 60:433–
449. https://doi.org/10.1016/j.rser.2016.01.109

Loughney S, Wang J, Bashir M, et al (2021) Development and application of a multiple-
attribute decision-analysis methodology for site selection of floating offshore wind
farms on the UK Continental Shelf. Sustain Energy Technol Assessments 47:.
https://doi.org/10.1016/j.seta.2021.101440

Luan C, Gao Z, Moan T (2016) Design and analysis of a braceless steel 5-mw semi-
submersible wind turbine. Proc Int Conf Offshore Mech Arct Eng - OMAE 6:.
https://doi.org/10.1115/OMAE2016-54848

Luan C, Michailides C, Gao Z, Moan T (2014) Modelling and analysis of a 5 MW
semisubmersible wind turbine combined with three flap-type wave energy converters.
In: Proceedings of the ASME 2014 33rd International Conference on Ocean, Offshore
and Arctic Engineering

Ma Y, Hu C, Zhou B, et al (2019) Hydrodynamic Analysis of a Semi-submersible Wind-
Tidal Combined Power Generation Device. J Mar Sci Appl 18:72–81.
https://doi.org/10.1007/s11804-019-00073-x

Madvar MD, Ahmadi F, Shirmohammadi R, Aslani A (2019) Forecasting of wind energy

    technology domains based on the technology life cycle approach. Energy Reports

    5:1236–1248. https://doi.org/10.1016/j.egyr.2019.08.069

Marine Power Systems (2022) Marine Power Systems: Technology.

    https://www.marinepowersystems.co.uk/technology/. Accessed 13 Jan 2022

Matsukuma H, Utsunomiya T (2008) Motion analysis of a floating offshore wind turbine

    considering rotor-rotation. IES J Part A Civ Struct Eng 1:268–279

Mattiazzo G (2019) State of the Art and Perspectives of Wave Energy in the Mediterranean

    Sea: Backstage of ISWEC. Front Energy Res 7:1–12.

    https://doi.org/10.3389/fenrg.2019.00114

McTiernan KL, Sharman KT (2020) Review of Hybrid Offshore Wind and Wave Energy

    Systems. J Phys Conf Ser 1452:. https://doi.org/10.1088/1742-6596/1452/1/012016

Meng L, He Y ping, Zhao Y sheng, et al (2020) Dynamic Response of 6MW Spar Type

    Floating Offshore Wind Turbine by Experiment and Numerical Analyses. China Ocean

    Eng 34:608–620. https://doi.org/10.1007/s13344-020-0055-z

Michailides C, Gao Z, Moan T (2016) Experimental study of the functionality of a

    semisubmersible wind turbine combined with flap-type Wave Energy Converters.

    Renew Energy 93:675–690. https://doi.org/10.1016/j.renene.2016.03.024

Michailides C, Luan C, Gao Z, Moan T (2014) Effect of flap type wave energy converters on

    the response of a semi-submersible wind turbine in operational conditions. Proc Int Conf

    Offshore Mech Arct Eng - OMAE 9B:1–10. https://doi.org/10.1115/OMAE2014-24065

Minesto (2022) Dragon Class – next generation marine energy power plants for commercial

up-scale. https://minesto.com/products. Accessed 15 Sep 2022

Mocean Energy (2022) Technology. https://www.mocean.energy/wave-energy-converter/.

Accessed 10 Oct 2022

Mofor L, Goldsmith J, Jones F (2014) Ocean Energy: Technology Readiness, Patents,

Deployment Status and Outlook. 76

Muliawan MJ, Karimirad M, Moan T (2013) Dynamic response and power performance of a

combined Spar-type floating wind turbine and coaxial floating wave energy converter.

Renew Energy 50:47–57. https://doi.org/10.1016/j.renene.2012.05.025

Murfet T, Abdussamie N (2019) Loads and response of a tension leg platform wind turbine

with non-rotating blades: An experimental study. J Mar Sci Eng 7:.

https://doi.org/10.3390/jmse7030056

National Renewable Energy Laboratory (NREL) (2022) OpenFAST v3.2.0 documentation.

https://openfast.readthedocs.io/en/main/. Accessed 31 Jul 2022

National Renewable Energy Laboratory (NREL) (2021) OpenFAST Documentation Release

v3.0.0

Neary VS, Previsic M, Jepsen RA, et al (2014) Methodology for Design and Economic

Analysis of Marine Energy Conversion (MEC) Technologies

Ocean Power Renewable Company (ORPC) (2022) RivGen Power System.

https://orpc.co/rivgen-power-system-integrated-microgrid-solutions/. Accessed 15 Sep

2022

OceanEnergy (2022) OceanEnergy: Home. https://oceanenergy.ie/. Accessed 10 Oct 2022

Olondriz J, Elorza I, Jugo J, et al (2018) An advanced control technique for floating offshore wind turbines based on more compact barge platforms. Energies 11:. https://doi.org/10.3390/en11051187

Orbital Marine Power (2022) Technology. https://orbitalmarine.com/technology/. Accessed 19 Jun 2022

Otter A, Murphy J, Pakrashi V, et al (2022) A review of modelling techniques for floating offshore wind turbines. Wind Energy 25:831–857. https://doi.org/10.1002/we.2701

Pérez-Collazo C, Greaves D, Iglesias G (2015) A review of combined wave and offshore wind energy. Renew Sustain Energy Rev 42:141–153. https://doi.org/10.1016/j.rser.2014.09.032

Petrini F, Li H, Bontempi F (2010) Basis of design and numerical modeling of offshore wind turbines. Struct Eng Mech 36:599–624. https://doi.org/10.12989/sem.2010.36.5.599

Principle Power (2020) WindFloat. https://www.principlepowerinc.com/en/windfloat. Accessed 16 Aug 2021

Qasim I, Gao L, Peng D, Liu B (2018) Catamaran or semi-submersible for floating platform - Selection of a better design. IOP Conf Ser Earth Environ Sci 121:0–7. https://doi.org/10.1088/1755-1315/121/5/052041

Quest Floating Wind Energy (2021) Global Floating Wind Market and Forecast Report

Ramachandran GKV, Robertson A, Jonkman JM, Masciola MD (2013) Investigation of response amplitude operators for floating offshore wind turbines. In: Proceedings of the International Offshore and Polar Engineering Conference. pp 369–376

Ren N, Ma Z, Shan B, et al (2020) Experimental and numerical study of dynamic responses of a new combined TLP type floating wind turbine and a wave energy converter under operational conditions. Renew Energy 151:966–974. https://doi.org/10.1016/j.renene.2019.11.095

Robertson A, Jonkman J, Masciola M, et al (2014a) Definition of the Semisubmersible Floating System for Phase II of OC4

Robertson A, Jonkman J, Vorpahl F, et al (2014b) Offshore code comparison collaboration continuation within IEA wind task 30: Phase II results regarding a floating semisubmersible wind system. In: Proceedings of the International Conference on Offshore Mechanics and Arctic Engineering - OMAE

Robertson AN, Jonkman JM (2011) Loads analysis of several offshore floating wind turbine concepts. In: Proceedings of the International Offshore and Polar Engineering Conference. pp 443–450

Roddier D, Banister K (2012) WindWaveFloat (WWF): Final Scientific Report

Rusu E, Onea F (2018) A review of the technologies for wave energy extraction. Clean Energy 2:10–19. https://doi.org/10.1093/ce/zky003

Saenz-Aguirre A, Ulazia A, Ibarra-Berastegi G, Saenz J (2022) Floating wind turbine energy and fatigue loads estimation according to climate period scaled wind and waves. Energy Convers Manag 271:. https://doi.org/10.1016/j.enconman.2022.116303

Sai KC, Patil AH, Karmakar D (2020) Motion response analysis of floating wind turbine combined with wave energy converter. APAC 2019 - Proc 10th Int Conf Asian Pacific Coasts 1099–1105. https://doi.org/10.1007/978-981-15-0291-0_150

Salehyar S, Li Y, Zhu Q (2017) Fully-coupled time-domain simulations of the response of a

floating wind turbine to non-periodic disturbances. Renew Energy 111:214–226.

https://doi.org/10.1016/j.renene.2017.04.017

Sanchez M, Carballo R, Ramos V, Iglesias G (2014) Energy production from tidal currents in

an estuary : A comparative study of fl oating and bottom- fi xed turbines. Energy

77:802–811. https://doi.org/10.1016/j.energy.2014.09.053

Sandberg AB, Klementsen E, Muller G, et al (2016) Critical factors influencing viability

ofwave energy converters in off-grid luxury resorts and small utilities. Sustain 8:1–22.

https://doi.org/10.3390/su8121274

Schupp MF, Bocci M, Depellegrin D, et al (2019) Toward a common understanding of ocean

multi-use. Front Mar Sci 6:1–12. https://doi.org/10.3389/fmars.2019.00165

Sea Power (2022) Seapower Platform. http://www.seapower.ie/our-technology/. Accessed 5

Mar 2022

Shaler K, Branlard E, Platt A, Jonkman J (2020) Preliminary Introduction of a Free Vortex

Wake Method into OpenFAST. J Phys Conf Ser 1452:1–9. https://doi.org/10.1088/1742-

6596/1452/1/012064

Shi W, Zhang L, Ning D, et al (2019) A comparative study on the dynamic response of three

semisubmersible floating offshore wind turbines. In: Proceedings of the International

Conference on Offshore Mechanics and Arctic Engineering - OMAE

Si Y, Chen Z, Zeng W, et al (2021) The influence of power-take-off control on the dynamic

response and power output of combined semi-submersible floating wind turbine and

point-absorber wave energy converters. Ocean Eng 227:108835.

https://doi.org/10.1016/j.oceaneng.2021.108835

SIMEC ATLANTIS ENERGY (2022) SAE secures funding from Scottish Enterprise. https://simecatlantis.com/sae-secures-funding-from-scottish-enterprise/. Accessed 19 Jun 2022

Sinn Power (2022) SOcean Floating Renewable Energy Hybrid Multipurpose Platform. https://www.sinnpower.com/socean. Accessed 7 Oct 2022

Skene DM, Sergiienko N, Ding B, Cazzolato B (2021) The Prospect of Combining a Point Absorber Wave Energy Converter with a Floating Offshore Wind Turbine. Energies 14:7385. https://doi.org/10.3390/en14217385

Sojo M, Auer G (2014) Marine Renewable Integrated Application Platform - Final Summary Report

Soleimani K, Ketabdari MJ, Khorasani F (2015) Feasibility study on tidal and wave energy conversion in Iranian seas. Sustain Energy Technol Assessments 11:77–86. https://doi.org/10.1016/j.seta.2015.03.006

Stewart G, Muskulus M (2016) A Review and Comparison of Floating Offshore Wind Turbine Model Experiments. Energy Procedia 94:227–231. https://doi.org/10.1016/j.egypro.2016.09.228

Subrata K. Chakrabarti (2005) Handbook of Offshore Engineering

Taboada J (2016) Comparative analysis review on Floating Offshore wind Foundations (FOWF). Ing Nav 75–87

Têtu A (2017) Power Take-Off Systems for WECs. In: Handbook of Ocean Wave Energy. pp

203–220

The Crown Estate (2012) UK Wave and Tidal Key Resource Areas Project - Summary
Report. 1–10

Thiagarajan KP, Dagher HJ (2014) A review of floating platform concepts for offshore wind
energy generation. J Offshore Mech Arct Eng 136:1–6.
https://doi.org/10.1115/1.4026607

Todalshaug JH (2017) Hydrodynamics of WECs. In: Handbook of Ocean Wave Energy. pp
139–158

U.S. Geological Survey (USGS) Water Science School (2019) How Much Water is There on
Earth? | U.S. Geological Survey. https://www.usgs.gov/special-topics/water-science-
school/science/how-much-water-there-earth. Accessed 25 May 2023

Uihlein A, Magagna D (2016) Wave and tidal current energy - A review of the current state
of research beyond technology. Renew. Sustain. Energy Rev. 58:1070–1081

UK Government (2021) HOME - UN Climate Change Conference (COP26) Glasgow.
https://ukcop26.org/. Accessed 9 Dec 2021

Van der Hoven I (1957) Power spectrum of horizontal wind speed in the frequency range
from 0.0007 to 900 cycles per hour. J Meteorol 14:160–164

van der Tempel J, Molenaar DP (2002) Wind turbine structural dynamics - A review of the
principles for modern power generation, onshore and offshore. Wind Eng 26:211–220.
https://doi.org/10.1260/030952402321039412

Walker S, Thies PR (2021) A review of component and system reliability in tidal turbine

deployments. Renew Sustain Energy Rev 151:111495.

https://doi.org/10.1016/j.rser.2021.111495

Walter M, Spitsen P, Beiter P, et al (2021) Offshore Wind Market Report: 2021 Edition

Wan L, Gao Z, Moan T (2015) Experimental and numerical study of hydrodynamic

responses of a combined wind and wave energy converter concept in survival modes.

Coast Eng 104:151–169. https://doi.org/10.1016/j.coastaleng.2015.07.001

Wang L, Sweetman B (2012) Simulation of large-amplitude motion of floating wind turbines

using conservation of momentum. Ocean Eng 42:155–164.

https://doi.org/10.1016/j.oceaneng.2011.12.004

Wang Y, Zhang L, Michailides C, et al (2020) Hydrodynamic response of a combined wind-

wave marine energy structure. J Mar Sci Eng 8:. https://doi.org/10.3390/JMSE8040253

Wavestar (2016) Concept. http://wavestarenergy.com/projects. Accessed 10 Oct 2022

Weiss CVC, Guanche R, Ondiviela B, et al (2018) Marine renewable energy potential: A

global perspective for offshore wind and wave exploitation. Energy Convers Manag

177:43–54. https://doi.org/10.1016/j.enconman.2018.09.059

Wellicome JF, Temarel P, Molland AF, Hudson DA (1995) Ship Science Report No.93

Theoretical Prediction of the Seakeeping Characteristics of Fast Displacement

Catamarans

Wendt FF, Robertson AN, Jonkman JM (2019) FAST model calibration and validation of the

OC5-deepcwind floating offshore wind system against wave tank test data. Int J

Offshore Polar Eng 29:15–23. https://doi.org/10.17736/ijope.2019.jc729

Wind Europe (2020) Offshore wind in Europe: Key trends and statistics 2019

Wind Europe (2017) Floating offshore wind energy: A policy blueprint for Europe

Yang Y (2020) F2A User Manual

Yang Y, Bashir M, Li C, Wang J (2021) Investigation on mooring breakage effects of a 5 MW barge-type floating offshore wind turbine using F2A. Ocean Eng 233:. https://doi.org/10.1016/j.oceaneng.2021.108887

Yang Y, Bashir M, Michailides C, et al (2020a) Development and application of an aero-hydro-servo-elastic coupling framework for analysis of floating offshore wind turbines. Renew Energy 161:606–625. https://doi.org/10.1016/j.renene.2020.07.134

Yang Y, Bashir M, Wang J, et al (2020b) Performance evaluation of an integrated floating energy system based on coupled analysis. Energy Convers Manag 223:113308. https://doi.org/10.1016/j.enconman.2020.113308

Yu Z, Hu Z, Zheng X, et al (2020) Aeroelastic performance analysis of wind turbine in the wake with a new elastic actuator line model. Water 12:. https://doi.org/10.3390/W12051233

Zhao Z, Shi W, Wang W, et al (2021) Dynamic analysis of a novel semi-submersible platform for a 10 MW wind turbine in intermediate water depth. Ocean Eng 237:109688. https://doi.org/10.1016/j.oceaneng.2021.109688

Zheng Z, Chen J, Liang H, et al (2020) Hydrodynamic responses of a 6 MW spar-type floating offshore wind turbine in regular waves and uniform current. Fluids 5:1–28. https://doi.org/10.3390/fluids5040187

Zhou M-R, Pan Y, Ren N-X, Zhu Y (2016) Operational Performance of a Combined TLP-
       type Floating Wind Turbine and Heave-type Floating Wave Energy Converter System.
       In: Advances in Engineering Research: 2nd International Conference on Sustainable
       Development (ICSD 2016). pp 341–345

Zhou Z, Benbouzid M, Charpentier J, Scuiller F (2017) Developments in large marine current
       turbine technologies – A review. Renew Sustain Energy Rev 71:852–858.
       https://doi.org/10.1016/j.rser.2016.12.113

Zhu H, Hu C (2016) A Study on Control of Wave Energy Converter for Motion Suppression
       of Semisubmersible. IFAC-PapersOnLine 49:380–385.
       https://doi.org/10.1016/j.ifacol.2016.10.434